

Turbulent Suspension and Sediment Grains Transport in Natural Flows

Submitted by

Imagbe Lucky Osaro

for the degree of Doctor of Philosophy

August 2018



Department of Earth Sciences

Declaration of Authorship

I hereby declare that no portion of this work referred to in this thesis has been submitted in support of an application for another degree or qualification of this or any university or other institute of learning.

Imagbe Lucky Osaro

Abstract

Sand grain entrainment and suspension in low-concentration flows is generally assumed to be controlled by the magnitude of the basal shear stress and the resulting flow velocity fluctuations. Basal shear stress and velocity fluctuations are key fundamentals of the classic “mixing-length” theories of turbulence developed by Reynolds, Prandtl, von Karman and others. However, concerns have been raised about discrepancies between estimates of basal shear stress obtained from the traditional methods of the Law-of-the-Wall and Reynolds stress decomposition which challenges the continued reliance on the turbulence-suspension theory as it applies to sediment grains transport.

This research uses state-of-the-art, high resolution (in space and time) velocity fluctuations data obtained from a flume tank experiment to re-examine and validate key assumptions of the turbulence-suspension theory and investigate how well the turbulence model support thin long run-out turbidity-current flows transporting sand into Agadir basin, offshore Morocco, Northwest Africa.

In validating the theory, six flow cases characterised by varying flow conditions including flow discharge rate, thicknesses of flow and bed roughness were measured in a clear water flume tank experiment instrumented with a Nortek II ADV flow velocity sampling instrument. A total of 45 flow experimental runs that generated over 30,000 instantaneous flow velocities with depth measurements for each run were undertaken.

Results and data analysis show a reasonable agreement between the measured flume-tank data with that predicted by the turbulence model with respect to the time-averaged velocity profile with depth as well as the estimates of basal shear stress from the Reynolds and Law- of-the-Wall methods. Thus, this widely used mathematical approximation of turbulent suspension remains supported by experimental evidence and can continue to be confidently utilized.

However, reported field observations and inferences of long run-out thin turbidity current flows transporting sand-sized sediments into the Agadir basin could not be replicated by a numerical flow model that is based solely on the turbulence-suspension theory. Instead, the flow model demonstrated that thicker mud-rich turbidity current flows can achieve long distance transport of sand in Agadir basin. Therefore, it is suggested that turbulence and other sediment grain support mechanisms such as hindered settling and grain-grain collisions not incorporated in the flow model may have significantly contributed to the long-distance transport of sand grains by thin turbidity current flows across the Agadir basin.

Acknowledgement

I specially thank my supervisor, Professor Dave Waltham, for his endless and immense help, advice, suggestions and support throughout the course of my PhD. I am also very grateful to Professor Margaret Collison and Dr Javier Hernandez-Molina for their help and encouragements towards the realisation of this academic stride.

I am very grateful to Nigerian Federal government and the management of Petroleum Technology Development Fund (**PTDF**) for granting me full scholarship to undertake this study overseas especially in one of the world's leading Earth Science departments. I also thank the University of Jos, Nigeria for granting me paid study leave for the entire period of my PhD.

Special thanks to the Sorby Fluid Laboratory team at the University of Leeds, especially Professor Jeffrey Peakall, Dr Gareth Keevil and Dr Robert Thomas, for allowing me access to their laboratory and their invaluable support while carrying out the flume experiments.

Many thanks also to my colleagues and friends (past and present) in Earth Science department, Royal Holloway University of London, for their wonderful companionship and encouragement. To all my office mates, Azad, Dilshad, Hongden, Nanpan, Sylvester, Awad and others, I say thanks for all your support, jokes and laughs.

I also wish to appreciate all my colleagues in Geology department, University of Jos, for their concern and prayers. Mr Nimchak and all members of staff of training, University of Jos are well appreciated.

Special thanks to Osaigbovo, Felix, Osamede, Odeh, Onyekachi, Pa Lexy, Amy, Wuruola and Bola as well as every other person who contributed to the successful realization of this thesis and my apologies that I could not mention everybody personally.

Finally, gratitude to my family for their patience, great support, prayers, love and encouragement. I say many thanks to my enduring and exceptional wife, Queen, for being both mother and daddy to my children while I was away. I also appreciate my wonderful children, Oghosa, Osayamen, Ofure and Osaheni for their understanding despite never failing to always ask "Daddy when are you coming back" anytime we have phone conversation.

Dedication

To my late mother, **Deaconess (Mrs) Anna Imagbe**, of blessed memory, for her encouragement and relentless support towards my education.

Table of Contents

Declaration of Authorship.....	2
Abstract.....	3
Acknowledgement	4
Dedication	5
List of Figures	11
List of Tables	14
1 Chapter One; General Introduction.....	15
1.1 Research Motivation.....	16
1.2 Aims and Objectives.....	19
1.3 Background	19
1.3.1 Transport of sediment grains.....	20
1.3.2 Turbulence in natural flows	22
1.3.3 Synopsis of the Mixing-length turbulence theory	24
1.3.4 Turbidity currents and river flows.....	27
1.3.5 Turbidity current flows.....	29
1.3.6 Synopsis of Numerical modelling of Turbidity Currents	33
1.4 Thesis Structure	36
2 Chapter Two; Review of Key Concepts:	38
2.1 Introduction	39
2.2 Nature and origin of sediments.....	39
2.2.1 Cohesive and non-cohesive sediments.....	39
2.3 Properties of individual sediment grains	40
2.3.1 Grain size.....	40
2.3.2 Grain shape	43
2.3.3 Composition and density	44
2.3.4 Bulk properties of sediments.....	45

2.4	Sediment grain entrainment.....	47
2.5	Approaches to predict sediment grain entrainment	48
2.5.1	Shields diagram	49
2.5.2	The Hjulstrom diagram	51
2.5.3	Influence of bed slope.....	53
2.5.4	Influence of bed roughness.....	54
2.6	Settling velocity of sediment grains	56
2.7	Hindered settling.....	58
2.8	Sediment grain transport.....	58
2.8.1	Bed load sediment transport	60
2.8.2	Suspended load transport.....	62
2.9	Chapter summary.....	64
3	Chapter Three; Character and Behaviour of turbulent flows	65
3.1	Introduction; Key terms	66
3.2	Laminar and Turbulent Flow Regimes; Reynolds number	66
3.3	Behaviour of turbulent flows	68
3.3.1	The flow boundary layer	68
3.3.2	Steady and Unsteady Flows	70
3.3.3	Uniform and non-uniform Flows	70
3.3.4	Froude Number.....	71
3.3.5	The Rouse Number	72
3.4	Shear Stress and Shear Velocity.....	73
3.5	Estimating Shear Stress.....	74
3.5.1	Bed Slope Method.....	74
3.5.2	The Logarithmic Profile Method	75
3.5.3	Reynolds Stress Method	77
3.5.4	Uncertainty in Shear stress estimation	78
3.6	Review of Governing Equations.....	78

3.6.1	Basal Reynolds Shear Stress.....	79
3.6.2	Slope Calculated Basal Stress.....	80
3.6.3	Mixing Length Theory; Basal Shear Stress	81
3.6.4	Flow Average Velocity.....	82
3.6.5	Chezy equation.....	83
3.6.6	Turbulent suspension of sediment grains.....	83
3.7	Chapter Summary	86
4	Chapter Four; Experimental Set-up, Instrumentation and Procedure	87
4.1	Introduction	88
4.2	Design and set-up of experiment.....	88
4.3	Instrumentation	92
4.3.1	The Acoustic Doppler Velocimetry.....	92
4.4	Experimental Procedure	95
4.5	Constraints of Experiment	98
4.6	Chapter Summary	100
5	Chapter Five; Results.....	101
5.1	Introduction	102
5.2	Flow Velocity Measurements	102
5.2.1	Experimental Conditions.....	102
5.2.2	Velocity-depth profiles.....	103
5.2.3	Instantaneous streamwise velocity- time series.....	103
5.3	Shear Stress Estimates	107
5.3.1	Bed slope method	107
5.3.2	Reynolds Shear Stress Method	107
5.3.3	The Logarithmic Profile Method	111
5.4	Comparing Measured Data with Model Predictions	118
5.4.1	Measured and Modelled Flow Velocities.....	118
5.4.2	Reynolds Stress Validation.....	118

5.4.3	Law-of-the-Wall Validation	119
5.5	Hydraulic slope estimates from Reynolds Stress	119
5.6	Floor Surface Roughness and Drag coefficient	120
5.6.1	Surface Roughness	120
5.6.2	Drag coefficient	121
5.7	Linking Turbulence and Sediment Grain Suspension	123
5.8	Chapter Summary	125
6	Chapter Six	126
6.1	Introduction	127
6.2	The late Quaternary Agadir Basin, Offshore NW African Margin	128
6.2.1	Introduction	128
6.2.2	Bathymetry	129
6.2.3	Agadir basin sedimentary facies	130
6.2.4	Why study Bed A5 flows?	132
6.3	The Numerical flow model	134
6.4	Method: <i>Sensitivity Analysis</i>	136
6.4.1	The default run	137
6.4.2	Coarse diameter doubled	137
6.4.3	Fine diameter doubled	138
6.4.4	Coarse concentration doubled	139
6.4.5	Fine concentration doubled	139
6.4.6	Inflow width doubled	140
6.4.7	Flow thickness doubled	141
6.4.8	Chezy coefficient doubled	142
6.4.9	Model run time doubled	142
6.4.10	Inflow time doubled	143
6.5	Model output	144
6.5.1	Modelled bathymetry and flow evolution of Agadir basin	144

6.5.2	Approximate fit to data; comparison to field evidence.....	146
6.5.3	Resulting maximum flow thickness; comparison to field evidence.....	148
6.5.4	Maximum suspended grain size in Bed A5 flow	149
6.6	Chapter summary.....	153
7	Chapter Seven.....	154
7.1	Validation of the turbulence-suspension theory.....	155
7.1.1	Comparison of bed shear stress estimates.....	155
7.1.2	Comparison of direct slope with Reynolds slope.....	158
7.1.3	Influence of roughness.....	159
7.2	Bed A5 flow: comparing flow model with field-scale data	160
7.2.1	Areal extent of deposit	160
7.2.2	Downstream grain-size trends	162
7.3	Variation of flow thickness.....	164
7.4	Evolution of Bed A5 flow.....	166
7.5	Implications of study.....	170
8	Chapter Eight: Summary	173
8.1	Summary and Conclusion	174
8.2	Future work.....	176
	APPENDIX.....	177
	A1. Glossary of notations.....	177
	A2. Key to graphic log on Bed A5 facies, Agadir basin (Fig 6.4)	179
	A3. Measured and modelled flow velocity data Case 1.....	180
	A4. Measured and modelled flow velocity data Case 2.....	181
	A5. Measured and modelled flow velocity data Case 3.....	182
	A6. Measured and modelled flow velocity data Case 4.....	183
	A7. Measured and modelled flow velocity data Case 5.....	184
	A8. Measured and modelled flow velocity data Case 6.....	185
	REFERENCES.....	186

List of Figures

Figure 1.1 Schematic diagram of sediment transport process	20
Figure 1.2 Forces acting on a stationary sediment grain resting on a bed	21
Figure 1.3a and b; Sketch diagram illustrating the mixing length theory	25
Figure 1.4 Sketch drawings, velocity profiles of turbidity current (a) and river flow (b).....	28
Figure 1.5 Conceptual velocity and concentration profiles of a turbidity current	28
Figure 1.6: The anatomy of a typical turbidity current.....	30
Figure 1.7: Schematic forces and processes affecting a turbidity current flow	31
Figure 2.1: The Original Shields diagram (Shields, 1936).....	50
Figure 2.2: The Hjulstrom diagram	52
Figure 2.3a and b: Schematic diagram hydraulic smooth and rough surfaces	54
Figure 2.4: Sketch of modes of sediment grain transport	62
Figure 3.1: Sketch diagram of a unidirectional flow	66
Figure 3.2: Sketch diagram showing the character of laminar and turbulent flows	67
Figure 3.3 : Velocity profile and boundary layers for turbulent flow	69
Figure 3.4: Basal shear stress estimation methods	75
Figure 4.1: Sketch diagram of the laboratory flume tank used in this research.....	89
Figure 4.2: Photograph of concrete slab floor of flume tank, flow cases 1 and 2	90
Figure 4.3: Photograph of gravel slab floor of flume tank, flow cases 3-6	90
Figure 4.4: Photograph of the Flume (Measurement and Observation section)	91
Figure 4.5: Nortek ADV probe with transducer, receiver, and sampling volume.....	93
Figure 4.6: The Four signal receiving beams of an ADV	93
Figure 4.7: Sketch diagram of how slope of flow was measured	97
Figure 5.1: Vertical velocity profiles relative to flow height for flow cases 1-6.....	103
Figure 5.2: Instantaneous velocity –time series for case 1(Concrete floor)	105
Figure 5.3: Instantaneous velocity –time series for case 1(Gravel floor)	106

Figure 5.4: Vertical profile of the Reynolds shear stress, $u'w'$, Case 1	108
Figure 5.5: Vertical profile of the Reynolds shear stress, $u'w'$, case 2.	108
Figure 5.6: Vertical profile of the Reynolds shear stress, $u'w'$, case 3	109
Figure 5.7: Vertical profile of the Reynolds shear stress, $u'w'$, case 4	109
Figure 5.8: Vertical profile of the Reynolds shear stress, $u'w'$, case 5	110
Figure 5.9: Vertical profile of the Reynolds shear stress, $u'w'$, case 6	110
Figure 5.10: Velocity profile for flow case 1 (Measured vs Modelled dataset)	111
Figure 5.11: Velocity profile for flow case 2 (Measured vs Modelled dataset)	112
Figure 5.12: Velocity profile for flow case 3 (Measured vs Modelled dataset)	112
Figure 5.13: Velocity profile for flow case 4 (Measured vs Modelled dataset)	113
Figure 5.14: Velocity profile for flow case 5 (Measured vs Modelled dataset)	113
Figure 5.15: Velocity profile for flow case 6 (Measured vs Modelled dataset)	114
Figure 5.16: Plot of average velocity, u vs log of height, $\ln(z)$, flow case 1	115
Figure 5.17: Plot of average velocity, u vs log of height, $\ln(z)$, flow case 2	115
Figure 5.18: Plot of average velocity, u vs log of height, $\ln(z)$, flow case 3	116
Figure 5.19: Plot of average velocity, u vs log of height, $\ln(z)$, flow case 4	116
Figure 5.20: Plot of average velocity, u vs log of height, $\ln(z)$, flow case 5	117
Figure 5.21: Plot of average velocity, u vs log of height, $\ln(z)$, flow case 6	117
Figure 5.22: Comparison of direct slope with Reynolds slope estimates	120
Figure 5.23: Comparison of roughness length (concrete and gravelly floors).....	121
Figure 5.24: Drag Coefficient estimates from Law-of-the-Wall.....	122
Figure 5.25: Drag coefficient estimates from Reynolds Stress	123
Figure 5.26: Comparison of vertical Reynolds normal stress, w'^2 , to $u'w'$	124
Figure 6.1: Location map of Agadir Basin showing the pathway of Bed A5 flow	128
Figure 6.2: Change in seafloor gradient (red line) along the axis of Agadir basin	129
Figure 6.3 Core photograph of turbidites from the Agadir basin	131

Figure 6.4: Bed A5 interpreted facies profile (from Stevenson et al., 2014).....	133
Figure 6.5: Default run of the Numerical flow model.....	137
Figure 6.6: Effect of increasing grains coarse diameter to 500 μ m.....	138
Figure 6.7: Effect of increasing the fine diameter to 100 μ m.....	138
Figure 6.8: Effect of increasing the coarse concentration to 3.0%.....	139
Figure 6.9: Effect of increasing the fine concentration to 7.0%.	140
Figure 6.10: Effect of flow width of the canyon to 30.0km	140
Figure 6.11: Effect of increasing the flow thickness to 400.0m.....	141
Figure 6.12: Effect of increasing Chezy co-efficient by a factor of two	142
Figure 6.13: Effect of increasing model run time by a factor of two	143
Figure 6.14: Effect of increasing inflow time by a factor of two.....	143
Figure 6.15: Modelled Bathymetric map of Agadir basin	144
Figure 6.16: Modelled flow evolution of Agadir basin.....	145
Figure 6.17: Flow model with approximate fit to data	147
Figure 6.18: Flow model showing the flow thicknesses with distance.....	148
Figure 7.1: Agreement between measured and modelled dataset.....	155
Figure 7.2: Similarity of velocity profile from measured and modelled dataset	156
Figure 7.3: Comparing basal shear stress estimates from LoW and RSS.....	157
Figure 7.4: Comparing direct slope estimates with that from Reynolds Stress.....	159
Figure 7.5: Areal extent of modelled (A) and mapped flow deposit (B).....	161
Figure 7.6: Downstream core locations (blue circles) for this study	163
Figure 7.7(A & B): Comparison of measured (b) and modelled (a) D_{50} grain sizes	163
Figure 7.8: Variation of flow thickness with run-out distances (A = 50.0m thick; B =100.0m thick; C = 150.0m thick; D = 200.0m thick;).....	165
Figure 7.9: Possible mechanisms for deposition of Bed A5.....	168

List of Tables

Table 2.1: Analytical methods for sediment grain size	41
Table 2.2: Millimetre and phi scale grain size ranges for sediments	42
Table 2.3: Sediment grains sorting values and their interpretation	47
Table 3.1: Froude number and the states of flow	71
Table 3.2: Froude number and the states of flow	72
Table 3.3: Some Flow Velocity measuring equipment	85
Table 4.1: Summary flow character for the six cases	91
Table 5.1: Summary of flume hydraulic data for all six experimental cases	102
Table 5.2: Descriptive statistics of measured velocity for all six flow cases	104
Table 5.3: Shear stress estimates using the bed slope method	107
Table 5.4: Shear stress estimates using the Reynolds Stress method	107
Table 5.5: Shear stress estimates using the Logarithmic Profile	111
Table 5.6: Summary of Regression statistics of velocity data for all six cases	118
Table 5.7: Comparison of calculated and predicted RSS estimates	119
Table 5.8: Estimates of direct and Reynolds slope with their uncertainties	120
Table 5.9: Estimates of roughness lengths for surfaces used in the experiment	121
Table 5.10: Estimates of basal shear stress from LoW and RSS (flume center)	122
Table 5.11: Comparison of CD estimates from LoW and Reynolds Stress	123
Table 6.1: Input variables used in the flow model	136
Table 6.2A: Key Bed A5 field data from Stevenson et al., (2014)	150
Table 6.3: Estimates of maximum suspended grain size for bed A5 flow	151

1 Chapter One; General Introduction

1.1 Research Motivation

Sediment grain transport is an intriguing area of research that has over the past decades attracted an increasing attention which resulted in theoretical hypothesis pioneered by notable researchers such as Reynolds, (1896), Prandtl, (1925), O'Brien, (1933), Shields, (1936), Rouse, (1939), as well as Bagnold, (1966), among several others. Following the enviable strides, focus over the years shifted to applying analytical flow models to gaining new insights and deeper understanding with regards to the intrinsic processes of sediment grains dislodgement from the parent bed, the grain motion, action of overlying flow, predicting sediment transport rates as well predicting flow properties.

Sediment grains are predominantly transported by turbulent fluid motion in the form of suspended load as well as grain-grain interaction with the bed which is usually less significant (Syvitski et al., 2003). Up until now, the actual physical processes of these two modes of sediment transport especially that by turbulent motion requiring the precise prediction of a threshold criterion for grain entrainment into a turbulent flow remains largely unclear (Frey and Church 2009).

The current use of experimental and numerical models to understand the turbulence characteristics of natural flows has largely been limited due to complexities in the principles of appropriate flow models (Sukhodolov et al., 1998). Most experimental models use time-averaged flow velocity fluctuations which are the most common flow property to characterise and quantify turbulence in natural flows. However, over the years, the lack of readily available fluctuating velocity measuring devices as well as the difficulty of deploying such instruments in natural flows has been a major challenge (Grant and Madsen, 1979; Soulsby, 2005). Also, measuring flow velocity at a single point has not adequately characterise the spatial variability of exchange in turbulent flow boundary layers (Offen and

Kline, 1974; Laufer, 1975), yet turbulence of natural flows has been characterised based on data obtained from single current meters which may not yield reliable outcomes.

It is established that sediment grains in low concentration flows only begin motion, when the grains are subjected to a flow force referred to as *bed shear stress* that is in excess of a threshold value (Shields, 1936, Bagnold 1966, Xie, 1981). Suspension of these grains in the flow are generally assumed to be supported by turbulence which largely depends on the basal shear stress. The mixing length theory of turbulence describes grain suspension in flows and predicts the corresponding flow force. Traditionally, three methods predominantly used to analyse this basal flow force and includes the Law-of-the-Wall (or *log-profile*); Reynolds decomposition (*Reynolds shear stress*) and the bed slope. However, variability in the results from recent experiments conducted by some researchers such as Kim et al., (2000); Biron et al., (2004); Sherwood et al., (2006); Noss et al., (2010); Lee and Baas, (2012); Bagherimiyab and Lemmin, (2013); Lee and Baas, (2016); Shivpure et al., (2016), raises questions with regards to the validity of the turbulence suspension theory and therefore necessitates its validation.

Previous attempts at validating this widely used turbulence-suspension theory since its initial formulation has been fraught with challenges. Prandtl, (1925), O'Brien, (1933) and Bagnold, 1966 conceded not being able to adequately validate the theory due to non-availability of flow adequate fluctuating velocity sampling devices.

With advancement in acoustic technology and availability of high resolution flow fluctuating velocity sampling equipment, such as the Laser Doppler Velocimeter, Particle-image Velocimeter, Hot-wire Anemometer as well as the 3-C high resolution Acoustic Doppler Velocimeter, it is now possible to fully test the assumptions and predictions of this theory. This research will attempt a validation of this sediment transport theory to ascertain its

relevance and suggest its future application or otherwise in solving sediment grain transport problems.

It is well known that natural turbidity currents can transport large volumes of sediments from the continent to the deep ocean with turbulence as the suspension mechanism. However, recently published work from the Agadir basin, offshore NW Africa by Tailing et al., (2007) and Stevenson et al., (2014), from observation and the analysis of sediment cores recovered from the Modern seafloor demonstrates that very large voluminous flows (apparently ten times more voluminous than the annual flux contributed by all rivers of the world), are responsible for the transport of sediments from the Moroccan margin into the Agadir basin. It was also reported that sand was transported only a few meters above the bed floor, which imply transport by a relatively thin flow, with thickness size of approximately 5 to 7 meters. It has remained arguable and unclear, how a thin flow can transport sand across the over 250 km wide Agadir basin without it depositing its load, leading to suggestions of additional mechanism, apart from turbulence, that act to suppress settling. This thesis will investigate this observation and inference by using a simple 2-D depth-averaged analytical model to show that sand grains can plausibly be suspended in flows of this thickness by turbulence alone. The 2-D analytical model to be used was developed by Waltham et al., (2008), using algorithms of Reynolds-Averaged Navier Stokes (RANS) as well as the Chezy equations and based solely on turbulence-suspension theory.

1.2 Aims and Objectives

This study investigates turbulence in natural flows and how it could support the transport of sediment grains in long run-out flows. It is a novel approach seeking to first, validate the widely used Mixing-length turbulence-suspension theory and then apply a numerical flow model based on the turbulence suspension theory to understand sediment transport in Agadir basin, offshore Morocco, NW Africa.

Pertinent questions to be addressed by this research include:

1. Can flow properties of long run-out oceanic turbidity currents be inferred based on relatively simple inputs using a depth-averaged numerical turbulence flow model?
2. How possible is it to re-create the extent and grain size trends of long run-out turbidity current flows that extend beyond the continental slope with a depth-averaged numerical flow model?
3. How well can measured experimental flow fluctuating velocity data and the resulting velocity profile compare with similar data obtained from the theoretical model of turbulence?
4. How possible is it to apply a 2D depth-averaged numerical flow model to understand how and why large volume, long run-out turbidity current flows only suspended sand a few meters from the bed floor?

1.3 Background

This section aims at providing a general background to the theme of the research which investigates the role of turbulence in supporting the transport of by natural flows such as turbidity currents. It introduces the key terms and concepts such as turbulence, turbidity currents as well as the mixing-length turbulence theory of sediment grains transport.

1.3.1 Transport of sediment grains

Huge volumes of terrestrially-derived sediments are transported annually from the continent by rivers to the shallow continental shelves and are further moved into deep oceans by turbidity currents (Milliman and Syvitski, 1992; McCool and Parsons, 2004).

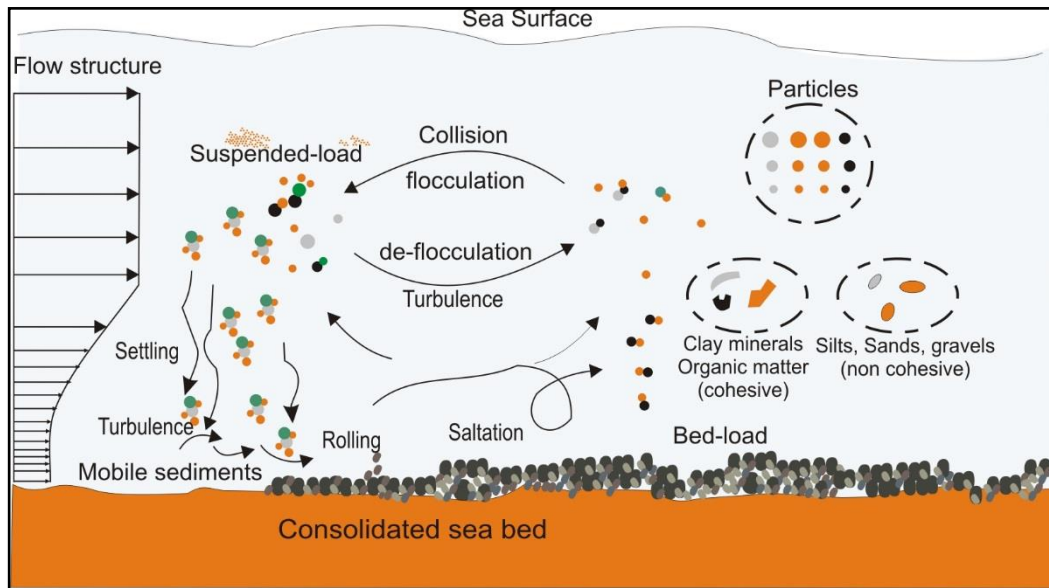


Figure 1.1 Schematic diagram of sediment transport process (Modified from Wang and Andutta, 2013)

The mode and pattern of sediment transport depends on the physical properties of the sediment grains such as grain size and density as well as the properties of the transporting medium such as density, viscosity of the fluid and whether the flow is laminar or turbulent. Two modes of sediment transport are commonly recognised, and these are bedload and suspension load. Bedload sediment grains transport typically involves movement of coarse grains along or close to the bed by rolling or scraping along the bed while suspended grains transport involves movement of relatively fine-grained sediments (clays, silts and fine sands) high above the bed in the flow (figure 1.1). According to Kneller et al., (2016), the velocity of

flow, the grain-grain interaction in the flow and the bed configuration considerably affect the extent to which sediment grain movement takes place.

To understand how sediments move from one location to another, knowledge of the forces acting on a sediment grain is very important. Figure 1.2 below is a sketch showing the multiplicity of forces acting on sediment grains at rest on the bed. These forces include force of gravity, F_G , lift (due to Bernoulli effect), F_L and drag forces, F_D (due to frictional forces which arise from the collision between the grains in motion and the flow boundary).

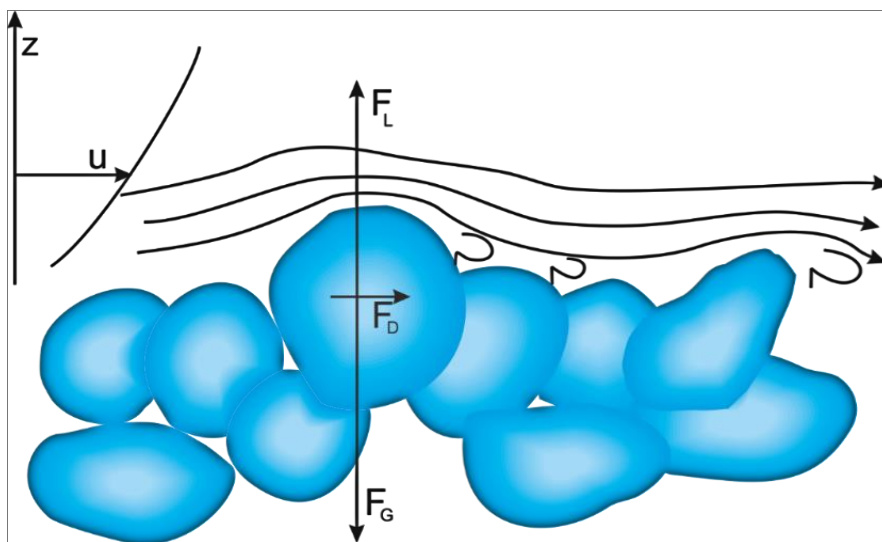


Figure 1.2 Forces acting on a stationary sediment grain resting on a bed

As modified from Wiberg and Smith (1987), Lamb et al. (2008). Here sediment grains are subjected to forces due to lift, F_L , gravity, F_G and drag, F_D . β is the bed slope angle and ϕ_0 is the frictional angle.

Sediment grains transport in natural flows is a very important aspect of sedimentology and have wide applications in geomorphology, environmental and civil engineering. Knowledge of sediment transport provide insights in improving current understanding of the processes of erosion and entrainment of sediment grains, as well as clues to predicting the timing and location where erosion or deposition/accumulation of sediments is anticipated. In particular, the reliable prediction of where clastic sediments such as sands accumulate subsea and their thicknesses remains a primary interest in hydrocarbon exploration.

Sediment transport study also helps to mitigate potential environmental and civil engineering problems such as pollution, erosion and flood control, local bed scouring, dredging as well as dam breaching flows among others (Dewals et al., 2010b; van Rijn 2007).

1.3.2 Turbulence in natural flows

Flow Turbulence is an intricate phenomenon describing a flow state with regards to how highly irregular and chaotic the flow could be. Turbulence is flow condition in which characteristic flow quantities show a random variation with time and space (Hinze, 1975). As defined by Tritton (1988), flow turbulence is the constant state of instability of a flow and usually occurs due to exchanges between fluid particles having varying velocities, density, temperature or pressure.

With regards to sediment grain transport, turbulence in natural flows is regarded as the main driving force responsible for the transport of terrestrially-derived sediments (Lapointe, 1992; Clifford and French, 1993; Best, 2005b; Van Maren et al., 2009; Shugar et al, 2010). According to Nichols (2009), turbulence facilitate the suspension and transport of sediment grains in natural flows.

Natural turbulent flows are usually three-dimensional, occurring at high Reynolds numbers and often expressed in a wide range of scales. The largest scale is expressed by periodic, wave-shaped anisotropic flow structures described as Kelvin-Helmholtz instabilities (Simpson, 1999) which result from shear between the turbidity current and the ambient fluid at the upper flow boundary. The smallest scales are usually fine-scale isotropic velocity fluctuations.

Turbulence as a property of flow could facilitate mixing arising from the rapid fluctuations in the flow velocity which creates microscopic instabilities (eddies) in the flow (Middleton and Southard, 1984). For example, ocean mixing due to turbulence is attributed to mean shear

produced by winds or tides as well as breaking surface waves (Burchard et al., 2008). For small-scale flows including laboratory flows, turbulence has been produced by fluctuations in flow speed which is significantly enhanced through the use of external devices such as high-powered shakers, impellers and vibrators.

However, irrespective of the turbulence generation mechanism, Bagnold (1954), from his study, noted that, the turbulence structure of a flow is bound to change if there is high volume of suspended sediment grains concentration in the flow. The mechanisms for suppressing turbulence in most flows is summarised in Balachandar and Eaton (2010). For low concentration flows, suppression of turbulence has been linked to an enhanced inertia, effective viscosity of the flow and rapid dissipation of due to sediment drag (Bennet et al., 2013). Wang and Larsen (1994), had demonstrated that high fine-grained sediment concentration above a threshold value could cause the electrostatic bonds existing between the fine grained (e.g. clay) sediments to suppress the turbulence of the flow. There are investigations, currently, on why small concentrations of fine sediments (<0.1% volume) could suppress turbulence in a flow as noted in decelerating flows especially at its final stage (Baas et al., 2009; Baas et al., 2011; Cantero et al., 2012b). High fine grained sediment concentration in turbulent flows has been noted to cause fast gravitational settling of the sediment grains which ultimately increase the near-bed concentration that results in damping in flows (Talling et al., 2015).

Turbulence in natural flows is quantified from the velocity fluctuations occurring at a relatively high temporal resolution (1-200Hz) in the flow. Many custom-made acoustic devices are currently available for undertaking flow velocity sampling and turbulence measurements. These devices include the Acoustic Doppler Velocimeter (ADV), Acoustic Doppler Velocity Profiler (ADVP), Laser Doppler Velocimeter (LDV), Ultra sound pulse Doppler velocimetry, hot-film probes, hot-wire anemometers as well as electromagnetic current meters (ECM). Details of these can be found in (Hurther and Lemmin, 2001, 2008), Kim et al.

(2000), Biron et al. (2004), García et al. (2005), Rowiński et al. (2005), Jaafar et al. (2009), Pope et al. (2006), Liu and Wu (2015), Shivpure et al. (2016). The choice and applicability of these measuring devices will depend on the need of the study and technical criteria such as interference with the flow, adaptability to measurement environment as well as ease of calibration frequency.

Measured instantaneous flow velocity vector usually comprise three components: the streamwise (U), the spanwise (W), and the vertical (V) velocity components. All three velocity components can further be statistically resolved into the mean velocity, for streamwise, \bar{u} and the fluctuating velocity, u' , according to the equation below:

$$u = \bar{u} + u' \quad (1.0)$$

Quantification of the magnitude of turbulence in a flow is of significant interest as it accounts for understanding flow competence with regards to the run-out distance of turbulent flows and the maximum sediment grain size that can be suspended by such flows.

1.3.3 Synopsis of the Mixing-length turbulence theory

As discussed in the last section, in most natural flows, the extent to which fine-grained sediments are moved by the flow significantly depend upon the degree of flow turbulence (as the frictional interaction with the underlying flow bed is greater when flow is turbulent). Thus, understanding turbulence and the average behaviour of the fluctuations of a flow is crucial for predicting sediment grain motion and their distributions.

Prandtl Ludwig, 1925 proposed the mixing-length theory to predict the evolution of velocity profiles down the flow path from an assumed initial condition and derived a formula for velocity distribution in a moving fluid. The theory was postulated based on comparison with the molecular motion of a gas in which the momentum of a moving fluid particle does not change until it has moved a distance referred to as the *mixing-length*. Thus, the mixing-length

refers to the average distance that a fluid particle can move freely without collision and momentum exchange. It also describes the flow height which characterise interchanges of fluid particles in a turbulent flow as well as the distance the particle could keep its original characteristics before assuming that of the surrounding fluid.

Prandtl expressed the fluctuating velocities, u' and v' as;

$$u' \propto l \frac{\partial \bar{u}}{\partial z} \quad (1.1)$$

$$v' \propto l \frac{\partial \bar{u}}{\partial z} \quad (1.2)$$

Where \bar{u} is the time-averaged velocity (streamwise direction), l is the mixing length ($l=\kappa z$) κ is the Von Karman Constant, which has been traditionally taken as 0.41.

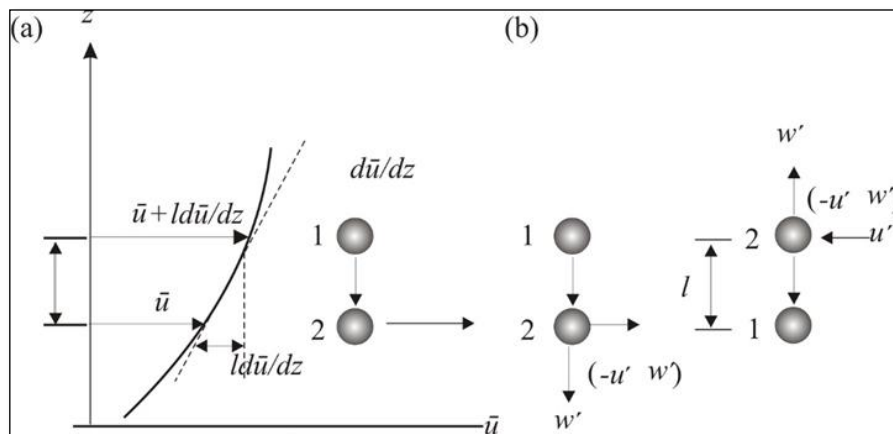


Figure 1.3a and b; Sketch diagram illustrating the mixing length theory

(Adapted from Subhasish, 2016)

Figure 1.3(a) schematically describes a fluid particle located at level 1 (higher) moving a distance l , at level 2 (Lower) due to eddy motion. The flow velocity at level 1, is still retained until it arrives level 2 and then decreases to the velocity at level 2 after exchanging the momentum with the surrounding fluids of level 2.

The basic assumption of the mixing-length theory is that each particle retains the original momentum during its vertical motion until it reaches its new position, where it mixes with

the surrounding fluid and takes on its character including the corresponding time-averaged velocity

Thus, in a typical turbulent shear flow, fluctuations in velocity culminating in the transfer of momentum by eddy viscosity are expressed by this concept to determine the amount of turbulence that could support the suspension and motion of sediment grains in a flow.

The instantaneous velocity of the flow at level z (fig 1.4) is given by the expression;

$$u' = \left(\bar{u} + l \frac{\partial \bar{u}}{\partial z} \right) - \bar{u} = l \frac{\partial \bar{u}}{\partial z} \dots\dots\dots (1.3)$$

l is the mixing length.

Three major assumptions made in the Mixing length theory of turbulence includes:

- That close to the base of bed, the shear stress is approximately equal to the bed shear stress ($\tau \approx \tau_0$)
- The mixing length increases linearly with distance from the bed. That is $l = \kappa z$
- depth profile of velocity is logarithmic (the law of the wall)

The mixing-length theory yields the log-law expression for determining the mean velocity distribution although it is yet to be fully validated in unsteady non-uniform flows. According to Yang and Chow (2008), the mixing-length theory cannot be used to express turbulence intensities directly due to equations 1.1 and 1.2, in which turbulence is expected to dissipate at points where $\frac{\partial \bar{u}}{\partial z}$ is equal to zero (at points of maximum velocity). This is contrary to expectations in non-uniform flows where turbulent mixing does not dissipate at points of maximum velocity.

The key prediction of the theory is that the depth profile of velocity is logarithmic (the law of the wall), i.e.

$$\bar{u} = \frac{u_*}{k} \ln \left(\frac{h}{z_0} \right) \dots\dots\dots (1.4)$$

where the “shearing velocity”, u_* , is related to basal shear stress by

$$\tau_{xz} = -\rho u_*^2 \quad (1.5)$$

and k is von Kármán’s constant.

An important parameter, z_0 , is the height where flow velocity is predicted to be zero, although, in practice, at this very small distance from the flow base the flow has become laminar and follows a simple linear profile.

1.3.4 Turbidity currents and river flows

Turbidity currents and open channel flows are the typical mainstream transport media for moving sediment grains from the continent to deep water. Oceanic turbidity currents and rivers are recognised most volumetrically important sediment transport processes on Earth and form very large deposits (Ingersoll et al., 2013). Open channel flows such as rivers and debris flow mainly transport sediment grains from the continental land mass to shallow coastal waters while turbidity currents (due to density contrast between the sediment grains and ambient water), move sediment grains from the shallow continental shelves to the deep ocean.

Turbidity currents should not be confused with river currents though both may have laminar and turbulent flow regimes, they are quite different in several ways. According to Middleton (1993), turbidity currents are sediment-gravity flows while river currents are fluid-gravity flows. The suspended sediment concentration of rivers may be considered negligible while that of turbidity currents is relatively significant (Fig 1.5). The ambient fluid of a river current is air while that of turbidity current is sea water. A typical velocity profile of river current shows a velocity maximum at or near water surface unlike that of turbidity current whose

velocity maximum is close to the bed with an upward decreasing velocity until near zero at the top (fig. 1.4).

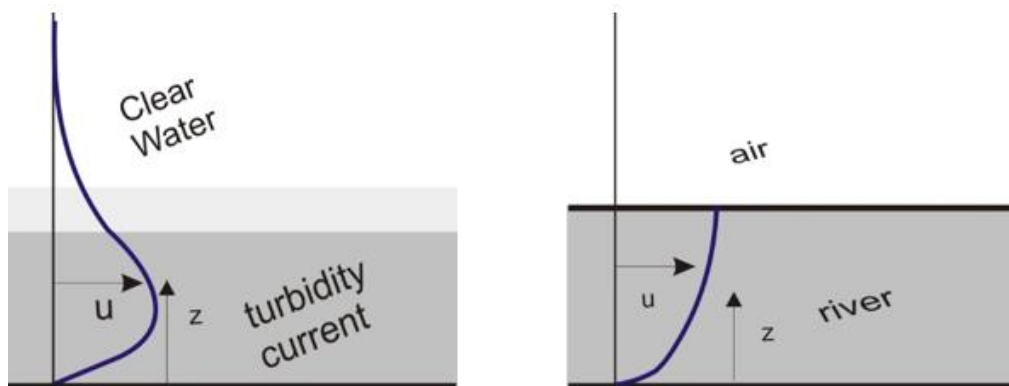


Figure 1.4 Sketch drawings, velocity profiles of turbidity current (a) and river flow (b)

In river currents, sand and gravel fractions are transported primarily by bed load (traction) mechanism while sands in natural turbidity currents are transported by suspended load. River deposits are characterised by cross bedding while sandy turbidites show a general lack of cross bedding but a characteristic normal grading (Shanmugam, 2001). River currents are the aqueous analogs of turbidity currents (Luchi et al., 2018).

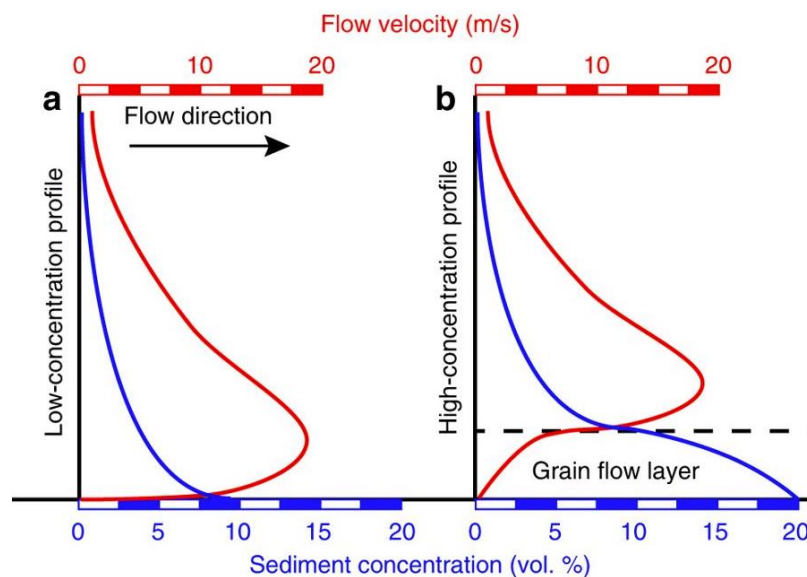


Figure 1.5 Conceptual velocity and concentration profiles of a turbidity current (Adapted from Stevenson et al., 2018)

Turbidity and river currents are also quite different from debris flows. Unlike turbidity currents and rivers, debris flows are strictly cohesive laminar flows that could transport sediments of various size range from clays to boulders. In debris flows, grain-to-grain contact is frequent while it is rare in turbidity currents. The velocity profile of a typical debris flow may be similar to that of a river current (Figure 1.4b), as the velocity maximum is at or near the surface of flow (Kaitna et al., 2014).

The link between rivers and oceanic turbidity currents and how changes in discharge from rivers affect the frequency and character of turbidity currents are well explained in Clare et al. (2016). This thesis will however dwell mainly on understanding turbulence and turbidity currents with respect to sediment transport. The section below reviews recent developments in understanding this subaqueous flow.

1.3.5 Turbidity current flows

Turbidity currents are a type of gravity currents that transport terrestrially-derived sediments over very long distances with small gradients into the deep sea (Talling et al., 2015; Kneller et al., 2016). Turbidity current flows usually move downslope under the action of gravity as well as the excess density contrast which may arise due to the presence of suspended sediment grains in the interstitial fluid (Middleton, 1993; Kneller and Buckee, 2000; Sequerios, 2000).

Natural turbidity currents are able to transport large volumes of sediments with flow thickness ranging up to several hundreds of metres (Piper et al., 1998; Sumner and Paull, 2014). According to Talling et al., (2007c), a single turbidity current flow transporting sediment grains into the oceans is approximately ten times the annual sediment flux from a combination of all rivers globally (Milliman and Syvitski, 1992). Turbidity currents are also

able to propagate for up to several hours or days (Xu et al., 2004). Evidences of these long run-out turbidity currents have been observed in the formation of giant clastic sediment accumulations such as the Bengal and Amazon Fans (Talling et al., 2015; Azpiroz-Zabala et al., 2017; Halsey et al 2017; Imran et al., 2017; Luchi et al., 2018), with majority of fans being host to hydrocarbon reservoirs (Kneller and Buckee, 2000; Sequerios et al., 2009).

Dispersed sediment grains and organic matter suspended within the interstitial fluids in a turbidity current are usually supported by the fluid turbulence. Although several other nomenclatures have been used to describe the sediment support mechanisms, (see Kueneen and Migliorini, 1950; Lowe (1982); Mutti (1992); Mutti et al., (2003, 2009); Shanmugam (1997, 2000, 2002), this work specifically adopts definition in which sediment suspension is by fluid turbulence and this will be used throughout this thesis.

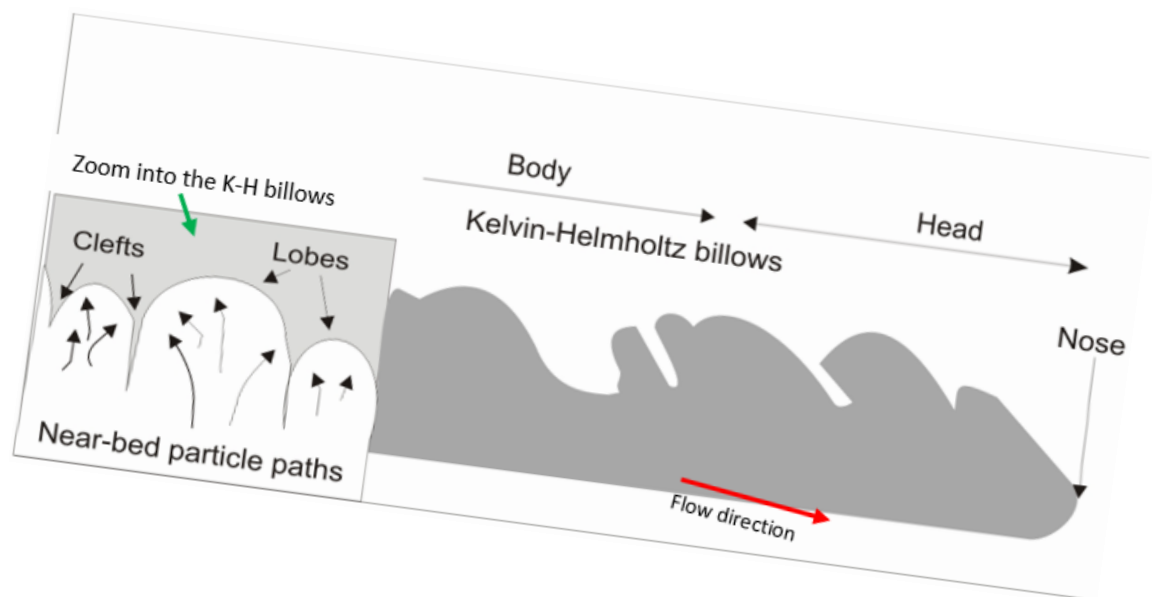


Figure 1.6: The anatomy of a typical turbidity current (Modified from Kneller and Buckee (2000)).

A turbidity current anatomy as described by Britter and Simpson, (1979), Kneller and Buckee (2000) shows complex flow dynamics, geometrically divided into three distinct parts; the head, body and tail (Fig1.6).

The head of a turbidity current, which is typically the frontal region and shaped like a semi-ellipse is relatively thicker and deeper than the body as well as tail regions due to the resistance to motion caused by the ambient fluid. The head characterise the zone of intense mixing and usually controls the current that follows behind. The overhanging nose-like structure of the head have been attributed to a no-slip condition characteristic of the base of the current as well as the frictional resistance typical at the top of the head.

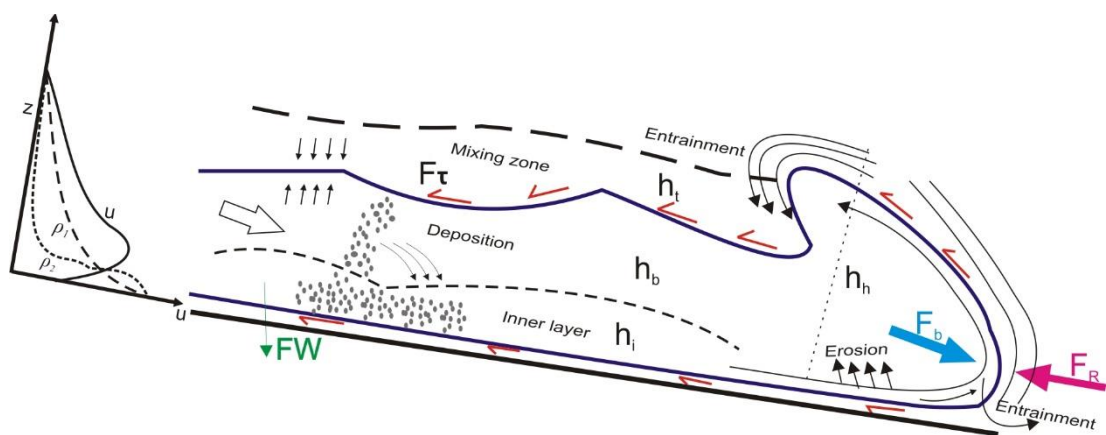


Figure 1.7: Schematic forces and processes affecting a turbidity current flow (Modified from Manica 2012).

The front of the head also consists of a pattern of complicated structure of *lobe and cleft*, identified as similar to the *Kelvin-Helmholtz-type billows* which are instabilities formed due to fluids being entrained or overrun at the base of flow (Simpson, 1972).

These series of transverse vortices forms at the interface between the current and the ambient fluid and attributed to density change (Britter and Simpson, 1979), (fig 1.5b). Just behind the head is the body of the flow which has been observed to travel faster by up to 30-40% than the head (Middleton 1966b, c; Kneller and Buckee, 2000). Middleton, (1966b) observed that minor changes in flow bed slope angles of less than 4% do not significantly affect the speed of the head of a moving turbidity current because of increase in the frictional resistance of the head of flow which balances the increased buoyancy.

The vertical profile of a turbidity current has been analysed in numerous researches and described by Parker et al., (1987), Altinakar et al., (1996), Stacey and Brown, (1988a); Kneller et al., (1999); Gray et al., (2006); Islam and Imran, (2010); Sequerios et al., (2010). The velocity maximum usually occurs close to the bed near the density maximum and an upwards decreasing velocity until near zero at the top (fig 1.4). The height of the maximum velocity is controlled by the ratio of the drag forces at the upper and lower boundaries (Kneller et al., 1997). The maximum flow velocity represents the velocity in the head of the turbidity current flow.

Subaqueous flow processes such as turbidity currents flows are till date yet to be fully understood. Although there are documented descriptions of turbidity currents deposits in numerous locations globally, only few direct observations and measurements beyond the continental shelf has been made. The occurrence of natural turbidity currents has remained very unpredictable and access challenges beyond the lower continental shelf, has made it difficult to directly observe and monitor its physical behaviour as well as measure the average sediment concentration (Talling et al., 2013). This has motivated researchers to seek alternate methods of its study such as identifying suitable analogs (fluvial sedimentary outcrops), (Konsoer et al., 2013) but the use of these analogs has also been limited due to significant variation in the governing physical mechanisms. Studies based on laboratory experiments and numerical modelling have become very relevant (Normark, 1970; Pirmez et al., 1997; Sequeiros et al., 2010; Cartigny et al., 2013; de Leeuw et al., 2016). In particular, laboratory experiments have successfully been used in testing and developing simplifying assumptions that are necessary in computational models (Kneller and Buckee, 2000). Laboratory flume experiments have over the last two decades deepened our insights from mere descriptions of turbidity current behaviour to understanding details of its turbulence structure (Kneller et al., 1997; Parsons 1998; Buckee et al., 2001). However, concerns with regards to scaling of laboratory turbidity currents have remained a limiting factor (Prandtl,

(1952); Middleton and Southard, (1984) and Talling et al. (2013). The large scale of natural turbidity current has been challenging to adequately reproduce on a one-to-one basis in the laboratory.

However, recent advances in technology with respect to availability of flow monitoring and measuring equipment have resulted in successful attempts at generating data in modern systems (Cooper et al., 2013; Clarke, 2016; Clare et al., 2016). These are however, currently limited to submarine canyons close to the shoreline, delta-fronts, freshwater lakes as well as reservoirs (Khripounoff et al 2003; Xu et al., 2004; Migeon et al., 2012; Mulder et al., 2012; Azpiroz-Zabala et al., 2017; Symons et al., 2017). It is however, still unclear how turbidity currents propagate beyond the continental slope (Clarke et al., 2012a).

Numerical models of turbidity current flow are now a significant tool for improving our understanding of the hydrodynamics of a turbidity current flow and validating assumptions of laboratory experiments normally constrained with field data. Currently, there are a number of numerical modelling methods applied to study turbidity current flows which has provided valuable findings and helped in understanding the turbulent flow process (Blanchette et al., 2006; Waltham, 2006; Heimsund, 2007; Cantero et al., 2009; An et al., 2012; El-Gawad et al., 2012; Hu et al., 2012; Janocko et al., 2013; Cao et al., 2014).

The next section below provides a brief introduction to some of the numerical modelling approaches for turbidity current flows.

1.3.6 Synopsis of Numerical modelling of Turbidity Currents

Numerical modelling of turbidity currents involves applying the relevant hydraulic equations from simple one-equation to highly detailed three-dimensional models to resolve all scales of motion of a flow and make predictions. Numerical flow models are generally classified based on their complexity such as the single equation model (Chezy-type equation), box

models, depth-averaged equation (shallow water) and full 3-D models. This review is not exhaustive as there are many more advanced numerical modelling approaches not discussed here but it is an introductory guide based on the relevance to this thesis.

1.3.6.1 *Single equation models*

This is the earliest as well as the simplest model expressing the hydraulic behaviour of turbidity current flow. Single equation models are based on the Chezy equation for steady uniform flow as derived from the Navier-Stokes equations. According to Kneller and Buckee (2000), a single equation model is expressed mathematically as;

$$\bar{u} = \sqrt{\frac{8g\rho' \sin(\alpha)h}{f_b + f_i}} \quad (1.4)$$

Where \bar{u} is the depth-averaged velocity, g is the acceleration due to gravity, ρ' is the density of the current relative to the ambient density, α is the slope of the sea bed over which the current is propagating, h is the height of the current, f_b and f_i are the friction coefficients for the lower and upper boundaries of the current.

Single equation models has been utilised in modelling the bulk flow properties of natural turbidity currents such as the Grand-Banks current (Kuenen, 1951; Mulder et al., 1997).

1.3.6.2 *Box models*

Box models mostly simulate low-concentration surge-type turbidity currents and unlike other modelling methods, they are not based on the Navier-Stokes equations. The modelling approach was developed by Dade and Huppert (1995) for a gravity current essentially initiated as a result of the intrusion of suspended particles over the current horizontal boundary into a deep and calm ambient (Harris et al., 2002). A major assumption of this model is that the current evolves in the form of constant area rectangles with uniform flow properties (speed, height and volume concentrations) in both the streamwise and vertical directions inside the current (Huppert, 1998). The implication of this is that there is no

ambient fluid entrainment into the current. The Box model is characteristically very simple as it can provide quick estimates of key flow characteristics such as the thickness, run-out distance and grain size.

Outcomes of box modelling technique have shown significant agreement when compared with data from experimental modelling for deposits of strongly depositional lock-exchange currents. However, the box models are yet to be validated against natural turbidity current deposits due to challenge in constraining the initial conditions (Kneller and Buckee, 2000).

A characteristic problem with depth-averaged models of this type is the assumption of uniform vertical sediment concentration arising from vertical mixing in the flow by turbulence.

1.3.6.3 *Shallow water models*

This is a more precise representation of sediment-laden current flows, essentially valid for currents whose length is significantly greater than their depths (Meiburg et al., 2015). The shallow water models are characterised by streamwise variation in current height and velocity while assumptions of proper mixing of the current accounts for the uniform vertical flow properties (density and velocity). Other key assumptions of the model include negligible viscous forces in the flow as well as minor vertical accelerations to ensure the vertical pressure gradient is hydrostatic.

The Shallow water model was first applied to investigate aspects of saline gravity currents produced in a lock-release experiment by Rottman and Simpson (1983). This was further extended later to particle-driven gravity currents by Bonnetcaze et al. (1993). Extensive literature on the Shallow water models as applied to gravity currents has been documented in Ungarish (2009).

Several forms of density current shallow water models have been proposed. Parker et al. (1986), suggested the 'four-equation' model, which though regarded as complex,

significantly account for sediment grain entrainment from the bed and the entrainment of ambient fluid (water) into the flow. The model has found usefulness in representing large scale turbidity current flows (Huang et al., 2005). Also, Doyle et al. (2010) applied similar model with some modifications to model the plumes generated by a dense pyroclastic flow.

1.4 Thesis Structure

This thesis comprises of eight chapters and an appendix.

Chapter two deals with the dynamics of sediment grain movement and includes key concepts of the research designed to give the reader a broad insight into the nature of sediments, sediment properties, modes of sediment transport as well as the physical processes which control and influence the transport of sediment grains.

Chapter three provides background literature and terms relating to the character and behaviour of turbulent flows, review of the governing equations and methods of estimating shear stress.

Chapter four is the experimental chapter which describes the rationale and details of the flume experiment conducted; the experimental set-up, instrumentation and procedures.

Chapter five is the result chapter which provides details of the analytical results generated from the flume experiment including the velocity profiles of the turbulent clear water flow, validation of the turbulence-suspension theory as well as comparing experimental mean flow velocities with estimated velocities obtained from the theoretical turbulence-suspension model.

Chapter six presents the application of numerical model to understand turbidity current flow in Agadir basin, offshore Morocco. A sensitivity analysis of the model to examine the response of model input parameters was also carried out.

Chapter seven is a general discussion on the implications of the research

Chapter eight summarises the key findings of the research and a short conclusion to the thesis. It also includes an outline of suggested possible future work.

2 Chapter Two; Review of Key Concepts:

Dynamics of Sediment Grain Movement in Turbulent Flows.

2.1 Introduction

This chapter is a concise review of relevant published literatures that provide background understanding of the nature and basic physical properties of sediment grains, the forces acting on sediment grains that cause motion as well as modes and patterns of their motion.

2.2 Nature and origin of sediments

Sediment is an aggregate of grains (or particles), either in loose or indurated form, formed by the physical and chemical disintegration of rocks from the earth's crust Van Rijn (1993); Selley (2000). Sediments on the earth surface consists of clay, silt, sand, gravel and cobbles. For the purpose of this study, focus will be given to sediment types based on the mutual interactions of the grains due to electrochemical forces such as van der Waals forces and electrostatic attraction (Pye, 1994; Righetti and Lucarelli, 2007). According to Partheniades (2009), differentiating between coarse and fine grained sediments is not only based on their size but also in the mutual interaction of the grains. Consequently, in addition to size discrimination, sediments will further be distinguished into the coarse non-cohesive and finer cohesive sediment classes (see table 2.2).

2.2.1 Cohesive and non-cohesive sediments

Generally, sediment grains with size greater than 0.01mm, such as coarse silts, sand, gravel and cobbles are described as non-cohesive. These are sediments characterised by very small electro-chemical attraction and grains are isolated during transport (transport is as individual grains rather than in flocs as in cohesive sediments). Non-cohesive medium-fine sediment grains do not normally require high shear stress for entrainment into the turbulent flow.

Sediment grains with size less than 0.01mm, such as clays and fine silt, with the potentials of attracting each other due to the electrochemical forces binding them together are generally

considered cohesive. However, with increase in concentration, there is more likelihood of the grains aggregating together to form a large floc.

Cohesion of sediment grains significantly contribute to the resistance of grains to shear and its influence on suspended grain transport has been discussed in Parker (1990), Raudkivi (1998), Jain and Kothiyari (2009). The cohesiveness and resistance of the grains to being dislodged during flow depends on the average grain size of the sediments as well as the mean velocity of flow. Thus there is a significant correlation between the grain size and the minimum flow velocity to cause entrainment of grains and its transport (Grabowski et al., 2011). Cohesive sediments grains form large aggregates called flocs which could influence the general flow pattern. With increase in the flocs size, their effective density decreases (Droppo et al., 2000; Van and Van Bang, 2013).

2.3 Properties of individual sediment grains

Sediment grains have a range of physical properties such as grain size, grain shape, mineralogy and density. The influence of these properties on flow will be briefly examined.

2.3.1 Grain size

Grain size is a key parameter in the sediment transport process. It directly influences the mode and pattern of sediment transport as well as the corresponding transport mechanism. Sediment grain size has been used to provide information about the sediment provenance as well as the grain's dynamic condition of its transport and deposition (Krumbein and Tisdell, 1940; Selley, 2000; Blott et al., 2004; Goossens, 2008; Buscombe and Masselink, 2009). According to Wilcock and Kenworthy (2002), grain size influences the transport of sediment grains in two ways. For flows over a homogenous bed, transport is controlled by the size of the grains with smaller grains being more mobile than the larger ones unless cohesion plays a major role or there is biologic mediation. But in conditions where the bed is heterogeneous,

the relative size of the grains affect the transport rates, in which the transport rate of the coarse sediment grain is increased with respect to the finer grains.

There are several methods for estimating the size of a sediment grain and these depend on the physical state. In the laboratory, two common traditional methods are well established in determining grain size and these are the sieving and sedimentation methods. Recent reviews can be found in (Blott et al., 2004; Syvitski, 2007).

Over the years, there has been developments in grain size analysis resulting in the use of automated counter devices such as electro-resistance particle counting (Coulter Counter), X-ray attenuation (Sedigraph), Laser diffractometry and photometrcal techniques (Hydrophotometer) as well as photon correlation spectroscopy (Singer et al., 1988; McCave and Syvitski, 1991; Tscharnuter, 2000; Gao et al., 2005; Blott and Pye, 2006; McCave et al., 2006; Warrick et al., 2009; Di Stefano et al., 2010; Blott and Pye, 2012; Polakowski et al., 2014), (table 2.1).

Table 2.1: Analytical methods for sediment grain size

Type of Sample	Sample class	Analytical method
Unconsolidated, loose sediments	Boulders, Cobbles, Pebbles	Manual measurement of individual clasts
	Granules, Sands, Silt	Sieving, settling tube analysis, image analysis
	Clays	Pipette analysis, Sedimentation balances, Photohydrometer, Sedigraph, Laser diffractometer, Electro-resistance (Coulter counter)
Lithified sediments	Boulder, Cobbles, Pebbles	Manual measurement of individual clasts
	Granules, Sand, Silt	Thin section measurement, image analysis
	Clays	Electron microscope

Classification of grain size in sediments dates back to 1898, pioneered by Udden and subsequently modified by Wentworth (1922) and Krumbein and Pettijohn (1938), describing the grade names and their lithified equivalents, followed by a further modification with the introduction of the phi (ϕ) scale (see table 2.2), which converts the grade boundaries into phi values by a logarithmic transform as below:

$$\phi = -\log_2 D_g \quad (2.1)$$

Where D_g is the grain average diameter.

Table 2.2: Millimetre and phi scale grain size ranges for sediments

Grain Size Class Mm	Phi scale	Description	Degree of Cohesion
<0.004	>8	Clay	Very cohesive
0.004 - 0.062	8 to 4	Silt	Cohesive
0.062 – 0.25	4 to 2	Fine Sand	Weakly cohesive
0.25 – 0.50	2 to 1	Medium sand	Cohesion increase with decreasing grain size
0.50 - 2.0	1 to -1	Coarse sand	Cohesionless
2.0 – 16.0	-1 to -4	Gravels	Cohesionless
16.0 – 64.0	-4 to -6	Pebbles	Cohesionless
64.0 – 256	-6 to -8	Cobbles	Cohesionless
>256	>-8	Boulders	Cohesionless

Modified from Udden and Wentworth, and Blair & McPherson (1999); Charlton (2006).

Numerous studies have also been carried out relating grain size to sediment transport. For clastics in particular, the grain size has been used excellently in predicting the relative amount of energy that is responsible for the final transport and deposition of a sediment grain and interpreting the depositional environments of ancient sedimentary rocks (Dashtgard et al., 2008; Wilson et al., 2008; Salarashayeri and Siosemarde, 2012; Miall, 2013).

The size of sediment grains could influence the fluid flow in sedimentary rocks and has been used as a reliable index for environmental characterisation (Sun et al., 2002; Owens et al., 2005). In addition, the hydraulic character of sediment grains is significantly influenced by its settling velocity which depends mainly on the grain size. According to Eggenhuisen et al.

(2017), from observation data, grain size is the primary control on sediment grain suspension as coarser grains tend to fall faster under the action of gravity in a stationary body of water. This has made it important to always incorporate settling velocities of grains in sediment transport studies considering the fluctuations and competency in flows. The observed decrease in grain size with distance of transport in most field studies being attributed to grain fracturing and abrasion is mainly related to the velocity of flow, mineralogy of the sediment grain as well as the initial grain size and the travel distance.

2.3.2 Grain shape

Grain shape and size together define the macroscopic appearance of a sediment grain. However, grain shape specifically describes the sediment grain's geometric form. From the shape of a sediment grain, valuable information such as the sediment depositional history as well as the behaviour of the transporting medium can be predicted (Kleesment, 2009). Quartz has been the standard mineral for grain shape analysis (Beal and Shepard, 1956; Griffiths, 1967; Blott and Pye, 2008).

The description of the shape of sediment grains is done with reference to how round or smooth a sediment grain is. For example, roundness reflects the degree of "smoothness" or "roughness" of the grain. Roundness is also described in relation to how well the rounding or angularity of the corners and edges are. Pettijohn (1975), explained that the roundness of a grain gives an account of its abrasion history. Sphericity on the other hand suggests how close a grain shape approximates to a sphere. Sphericity and roundness together, as a function of the sediment parent rock and original grain shape, have been noted to increase with long distance transport. Form has also been used to describe the overall appearance of a sediment grain and has been noted to affect the efficiency of grains transport.

Grain shape is a very significant factor in the hydrodynamic behaviour of sediments especially with regards to their transport. However, because of the limited understanding of its impact

in sediment transport, it is hardly included in most sediment transport formulas. Currently, there are data from a few investigations comprising both laboratory and field work, on the behaviour of various sediment grains in flow modelling. According to Komar and Li (1986), from the results of their experiments, elongate grains are more imbricated than spherical grains and thus less exposed to flow. Also, it was shown that the value of Shields number required for the initiation of motion of elongate grains was five to six times greater than that for spherical grains. Allen (1984), from his experiments on bivalves shells also hinted from his results that the drag increases with the elongation of the shells, thus reducing their transport capacity when compared to the spherical grains. Smith and Cheung (2004), also related the compelling impact of grain shape on fall velocity.

Cho et al. (2007), also suggested that though the shape of a sediment grain reflects the sediment transport history, which may not necessarily only relate the wear during transport, but it could also influence the grain susceptibility to transport. The more spherical a grain is, the easier it is to transport due to less friction. Sperry and Peirce (1995), emphasised the relevance of grain shape and its impact on the total surface area as well as the pore geometry which subsequently influences the hydraulic conductivity of the sediments.

2.3.3 Composition and density

The composition of sediment grains depends largely on the clastic sediment source. Most individual grains are mono-mineralic, having a single type of mineral such as quartz, while large grain accumulations, sourced from the breakdown of pre-existing rocks are mostly composed of a variety of minerals including quartz, feldspar, mica, pyroxene and hornblende. However, quartz and feldspar are the dominant minerals in most sediments with their specific gravity ranging from 2.60-2.72. The mineralogical composition of sediment grains is a well-established source of information from which the transport history can be inferred. Example, zircon, tourmaline and rutile are stable heavy minerals known to withstand several cycles of weathering, erosion and long distance transport (Bridge and Demicco, 2008). It

should be noted that the most common mineral present in the bed load of most river channels is quartz, and it originates mostly from igneous and metamorphic rocks (Bogárdi and Szilvássy, 1974).

The mass density of a sediment grain, describes the solid mass per unit volume. This naturally will depend on the sediment mineralogical composition which controls the relative ease with which the grains could be entrained in a flow and maintained in suspension.

2.3.4 Bulk properties of sediments

Sediments comprising grains of different sizes, shapes and mineral composition have bulk physical properties, known to influence the aggregate character of the sediment and affects grain entrainment and transport in flows. Some of these bulk properties include grain size distribution and porosity. Also, these bulk sediment characteristics influence the bulk density, permeability and shear strength of the sediments.

2.3.4.1 Grain size distribution

Sediments comprise a range of sediment grains with various sizes which holistically have a direct impact on the sediment hydraulic properties and this may be influenced by the magnitude of the electrochemical forces binding the grains together among other factors.

The size distribution of a sediment mixture, especially clastics, is commonly measured by the sieve analytical method. Results of these analysis are further statistically analysed using the Folk and Ward (1957) graphic method with further interpretations based on percentiles taken from the cumulative frequency curves. The mean grain size, sorting and standard deviation are derivatives of the process.

2.3.4.2 *Grain sorting and packing*

Sorting of sediment grains is a measure of the spread of grain sizes distributed on either side of an average or around a mean value in a sediment mixture. The degree of sorting, however, reflects the range of grain sizes in the sediment bed.

There are various descriptive terms associated with sorting and the corresponding graphic phi values and these are presented in table 2.4 below. However, more details on sorting can be found in Boggs (2009), Folk (1980) as well as Tucker (2009).

Sediment sorting is fundamental to understanding the impact of grain size on the porosity of a sediment as well as provide clue as to the effectiveness of the depositing flow to separate grain sizes of the various size range. Well-sorted sediment grains have a narrow range of sizes whereas poorly sorted sediment shows a wider range. In sediment transport, poorly sorted sediments with a wide range of grain sizes would require critical flow velocity of higher magnitude to entrain sediment grain into a flow than a well-sorted sediment.

Grain packing reflects the arrangement of the grains in a sediment and this largely depends on the grain size, shape as well as sorting. The way sediment grains are packed primarily influences the porosity and permeability of the sediment. Poorly sorted sediments have closer packing and porosity will be lower. However, the closer and tighter the packing arrangement, the greater the magnitude of shear stress required to entrain individual sediment grains from the bed.

Table 2.3: Sediment grains sorting values and their interpretation

Phi standard deviation	Sorting
<0.35	Very well sorted
0.35 to 0.50	Well sorted
0.50 to 0.70	Moderately well sorted
0.70 to 1.0	Moderately sorted
1.0 to 2.0	Poorly sorted
2.00 to 4.0	Very poorly sorted
>4.0	Extremely poorly sorted

Adapted from Folk and Ward (1957)

2.4 Sediment grain entrainment

Turbulent flows moving over a bed of sediment grains are able to pick up grains from the sediment bed and carry them into suspension in a flow. This character of a flow is described as “grain entrainment”. For well over a century, there has been research to gain more insights into the process of how sediment grains are dislodged from the parent bed, moved into suspension and transported by the overlying flow. Despite the long study which has resulted in several theoretical hypotheses, the actual physical process responsible for sediment grain entrainment and the precise prediction of a threshold criterion defining the flow conditions which account for grain entrainment is yet to be fully understood.

The entire entrainment process looks complex as the interactions between the flow and the parent bed may lead to the formation of bed forms which influence how easy sediment grains are likely to be entrained into a flow.

According to Sutherland (1967), sediment grain entrainment is a two-phase process involving the motion and intrusion of turbulent eddies into the thin laminar sublayer. The process is believed to prompt an increase in the mean flow velocity around the grains (to dislodge the

grains held within the sediment bed) as well as the mean bed stress to set the entrained grains in motion.

However, two kinds of theories have been developed on sediment grain entrainment. The first theory is primarily based on statistical methods and this has to do with the relation of near-bed flow turbulence to sediment grain entrainment. Near-bed flow turbulence is characterised by four events such as sweep, ejection, outward interaction and inward interaction events. All four events have varying influence on sediment grain transport modes and rate (Bridge and Bennett, 1992), which will be discussed later. The second theory was proposed by Shields (1936), in which (Wright and Parker, 2004a) a sediment grain entrainment criterion is set and this depends on the threshold bed shear stress. The assumptions of the mean flow velocity or the mean bed shear stress controlling the sediment grain entrainment process now formed the basis of later entrainment models (Garcia and Parker, 1991; Raudkivi, 1998; Elhakeem and Imran, 2011; Elhakeem and Sattar, 2015; Elhakeem et al., 2016).

A common feature of most of the sediment grain entrainment models is that the threshold conditions rely on the equilibrium of grain forces although some disparity in its elucidation is still observed with regard to which of the forces are relevant (for example, weight, buoyancy, drag and lift), how they could combine and most importantly, the forces parameterization (Papanicolaou et al., 2002; Hofland and Battjes, 2006; Schmeeckle et al., 2007).

The next section describes the forces acting on a sediment grain prior to entrainment and during flow.

2.5 Approaches to predict sediment grain entrainment

Defining sediment grain entrainment threshold is very crucial in sediment grain transport. Threshold conditions for grain entrainment have been defined based on the critical mean

flow velocity (from the cross-sectional average) or on the critical bed shear stress. For ease of understanding, it is expedient to define related terms as below;

- Shear Stress; this is expressed as a force per unit area of the bed. It is a measure of the frictional force from moving water and acting on the river or channel bed. It acts in the flow direction and is responsible for the entrainment of bed materials into flow. According to Biron et al. (2004), shear stress, τ_0 , is defined by

$$\tau_0 = \rho g h s \quad (2.7)$$

- Critical shear stress, τ_{crit} , is the magnitude of shear stress required to move sediment grains from the channel bed into flow.

$$\theta_{crit} = \frac{\tau_{crit}}{g(\rho_s - \rho)D} \quad (2.8)$$

- Grain Reynolds Number, R_{e^*} , this describes the degree of sediment bed roughness arising from grain packing. It is mathematically expressed as proportional to the ratio between the grain size and thickness of the laminar sublayer.

$$R_{e^*} = u^* \frac{D}{\nu} = \frac{11.6D}{\delta_{sub}} \quad (2.9)$$

Where θ_{crit} is the dimensionless critical shear stress (Shields parameter), τ_0 is the bed shear stress, τ_{crit} is the critical shear stress, ν is the kinematic viscosity, u^* is the shear velocity, D is the grain diameter and δ_{sub} is the thickness of the laminar sublayer.

2.5.1 Shields diagram

Shields (1936), was among the foremost researchers to describe how motion of sediment grains starts after considering the forces acting on the grains. Shields successfully derived a quantitative parameter, defined as a dimensionless critical bed shear stress, which predicts the threshold at which spherically shaped non-cohesive sediment grains are set in motion. The Shields parameter, (otherwise called the Shields entrainment function or Shields parameter) expresses the ratio between the applied bottom shear stress that tends to

destabilise the bed to free the grains and the stabilizing gravitational force. The Shields formula is:

$$\theta_{crit} = \frac{u_*^2}{g(S_s-1)D} = \frac{u_*^2}{\Delta g D} \quad (2.10)$$

Where $u_* = \sqrt{\tau/\rho}$ is shear velocity, τ is the bed shear stress, D is the grain diameter and g is the acceleration due to gravity. $S_s = \frac{\rho_s}{\rho}$; ρ_s is the sediment grain density, ρ is the water density.

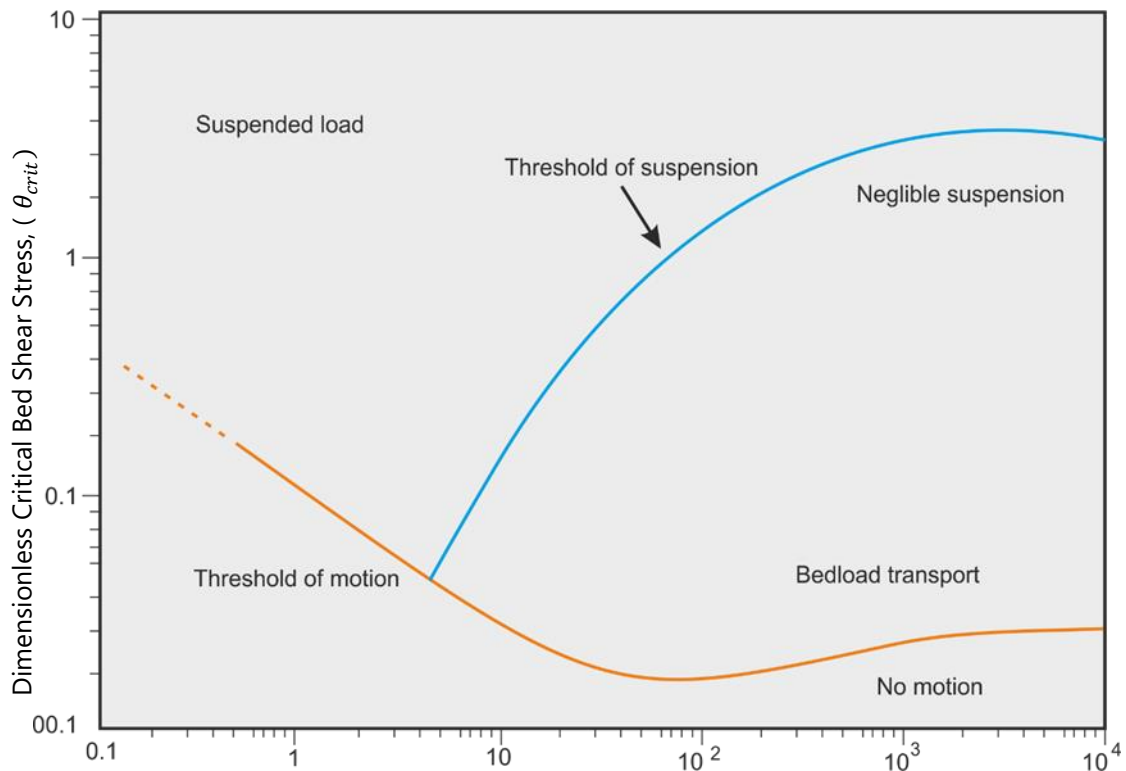


Figure 2.1: The Original Shields diagram (Shields, 1936).

Fig 2.1 above shows a sketch of the original Shields diagram in which sediment threshold conditions is displayed as a narrow band (orange-coloured band) with interpretation made in reference to this band. The diagram also shows that above this band, sediment grains will be set in motion, whereas, below it, due to insufficient shear stress, sediments grains are unable to be mobilised into flow for motion.

Consequently, three sediment transport zones can be distinguished from the Shields curve, namely No motion, Bed load and suspended load. According to Shield, when $Re^* > 1000$, (as the case of most rough and turbulent flows), the shields parameter or number will remain unchanged.

The Shields diagram, however, has lately come under criticisms with regard to its accuracy (Miller et al., 1977; Buffington and Montgomery, 1997; Buffington, 1999). Dissatisfactions as reported by Mantz (1977); Yalin and Karahan (1979); Buffington (1999) as well as Smith and Cheung (2004) were mainly from observed large scatters in sediment characteristics. These discrepancies have been attributed to be caused by the non-uniform flow conditions characterising natural flows. Consequently, several attempts were made by other researchers including Vanoni (1964), to modify the original Shields diagram to address some of the observed discrepancies.

These researchers also advocated the use of alternate plots for different flow cases such as Vanoni (1964); Yalin and Karahan (1979) and Paphitis (2001).

Similar predictions of bed critical threshold conditions in the field have been notably very challenging leading to the development of alternate Shield type equations and diagrams (Chien and Wan (1999), Paphitis (2001), Hager and Oliveto (2002), Cheng (2004) and Cao et al. (2006)). Essentially, despite all these several alternate contributions, Shields (1936) predictive equation and diagram still remain the most globally accepted standard method for determining the threshold for incipient motion conditions.

2.5.2 The Hjulstrom diagram

Despite the criticisms of the Shields curve described above, it remains a good technique for estimating entrainment thresholds for cohesionless grains. Cohesionless sediment grains, as

applied in this thesis, include sediment grains that are subject to the influence of drag and lift forces as well as turbulent velocities.

Hjulstrom (1935), based on results of a series of experiments published the first curve that describes the relationship between the sediment size and the flow velocity required for the sediment erosion, transportation and deposition.

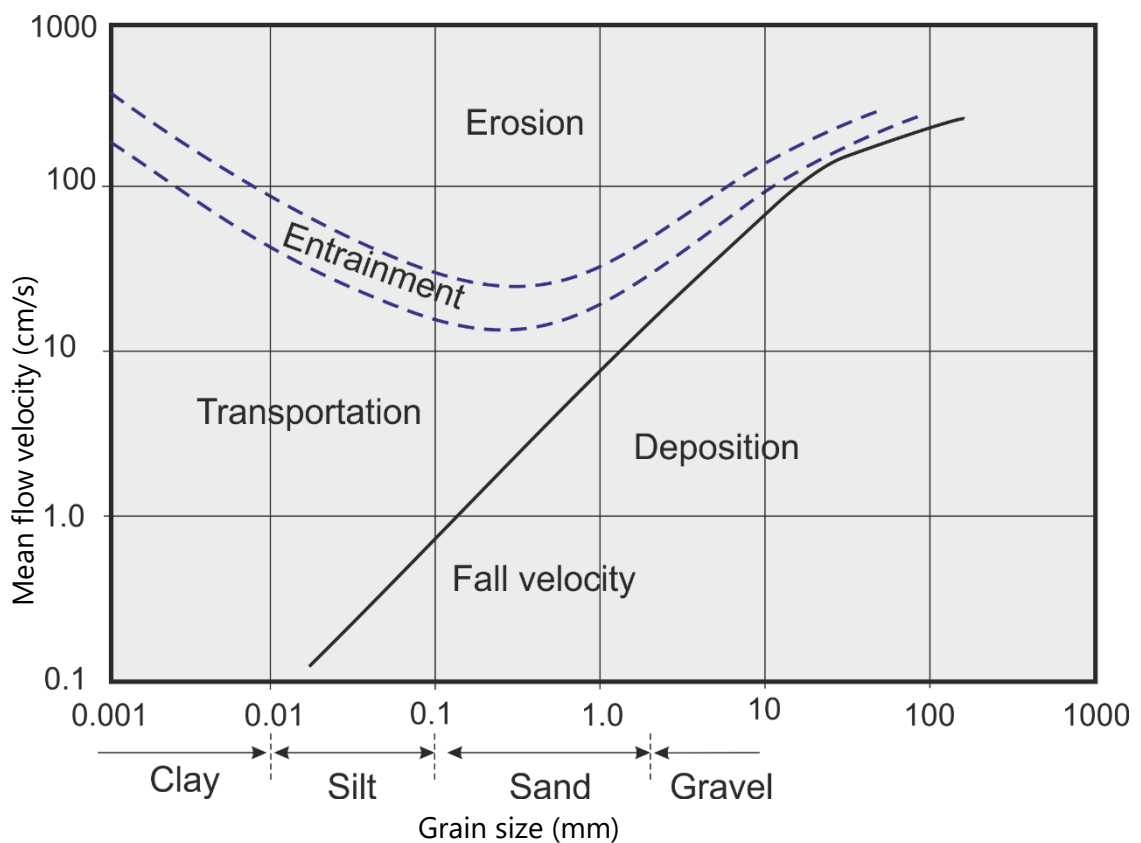


Figure 2.2: The Hjulstrom diagram

Essentially, the graph relates grain size to the flow velocity. However, for grain sizes coarser than 0.5mm, the flow velocity is observed to increase with the grain size, as the coarser the grains, the higher the velocity of flow required and similarly, for finer grains such as having mud or clays in the flow, a higher flow velocity is required to overcome the cohesive forces binding the finer sediment grains together.

The challenge with using Hjulstrom diagram is that all the forces that are required to move sediment grains are not only related to flow velocity. Boundary shear stress is a particularly important force which varies with flow depth. Hjulstrom diagram is used mainly to predict the mean velocity of flow that could reasonably entrain sediment grains into a flow.

2.5.3 Influence of bed slope

The influence of bed slope angle on incipient motion was first investigated by Shields (1936), although most of his work centred on nearly horizontal slopes. Since most natural flow channels do not have horizontal slopes especially in mountainous areas where there could be steep gradients, it is expedient to account for the influence of the downslope component of gravity on the initiation of sediment grain motion. Neill (1967), from a follow up model to Shields experiments confirmed that bed critical shear stress decreases with increasing channel slope. Later experimental works of Shvidchenko and Pender (2000) as well as Shvidchenko et al. (2001) also showed that incipient motion was slope dependent, even for very low angle slope values. With a higher bed shear stress, sediment grains therefore, are expected to become more mobile resulting from an increase in bed slope in addition to the effect of gravitational force acting in the downstream direction (Wiberg and Smith, 1987; Lamb et al., 2008).

Thus, sediment grain at the surface of a sloping bed will only begin to move when the force resisting the downstream motion is balanced by the drag force and the gravitational force.

Lamb et al. (2008), expressed the force balance on a sediment grain for a sloping bed as;

$$F_D + (F_G - F_L) \sin \beta = [(F_G - F_L) \cos \beta - F_L] \tan \phi_0 \quad (2.6)$$

Where ϕ_0 is called the grain angle of repose (or frictional angle) and β is the bed slope.

2.5.4 Influence of bed roughness

Bed roughness have been noted to be irregularities, relief structures or obstacles on the boundary (bed) of a flow which generate eddies that influence the magnitude of flow resistance, mean flow, turbulence and grain motion in a flow. It is produced by bedforms as well as individual sediment grains. Bed boundary roughness expresses the magnitude of the frictional resistance and effect that the underlying bed or boundary has on the flow. There are two main components of bed roughness and these includes the form roughness and sediment grain roughness. The sediment grain roughness relates the effect of frictional resistance to the grain size.

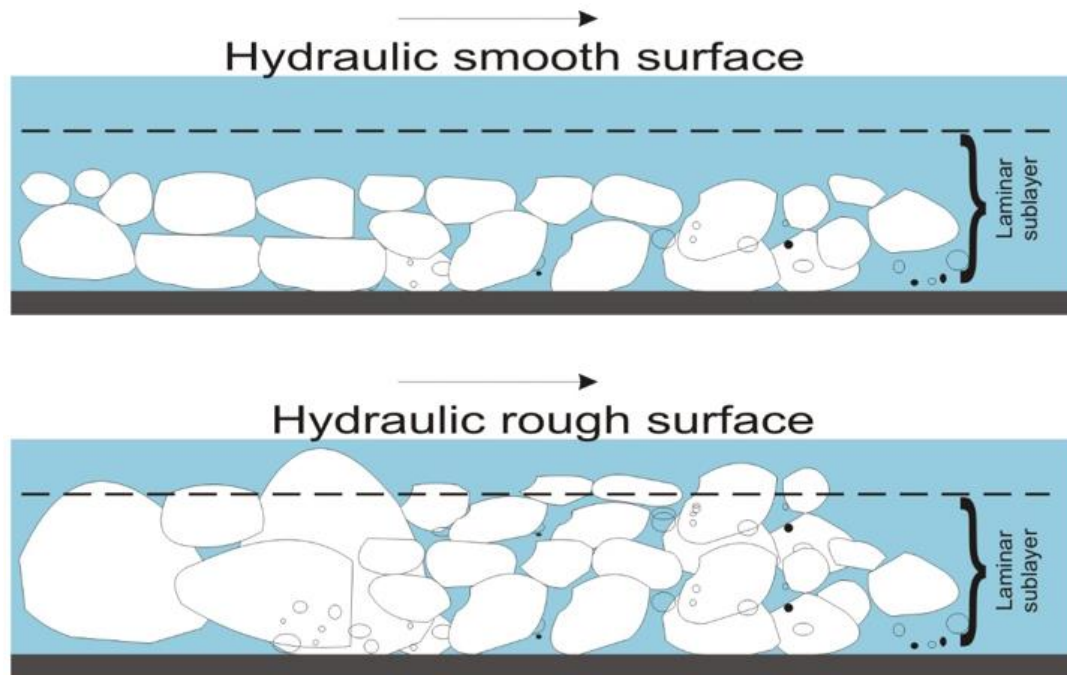


Figure 2.3a and b: Schematic diagram hydraulic smooth and rough surfaces

Form roughness on the other hand relates to the bedforms produced by sand ripples, biogenic mounds as well as benthic seagrasses. Nielsen (1981), Grant and Madsen (1982) carried out extensive research on flow boundary roughness. Also, there are a few published

studies conducted to evaluate the boundary roughness of sediment grain saltation in flows (You and Nielsen, 1997; Raudkivi, 1998).

Currently, estimates of bed roughness with biogenic mounds on sea beds is empirically carried out from photo images of the seabed (Grant et al., 1984; Wheatcroft, 1994) and as a result, it is a huge challenge to estimate the total roughness of sediment grain which constitute the irregular sand ripples, biogenic mounds, benthic seagrasses and sediment saltation in the field. Alternatively, therefore, the total bed roughness is now directly determined by fitting measured velocity current profiles to the logarithmic distribution, using the von Karman–Prandtl velocity equation. The roughness length generally, is taken as the distance above the bed of the position at which the extrapolation of the logarithmic profile has zero velocity (Burchard et al., 2008).

From Von Karman’s turbulence model, z_0 represents the surface roughness length or height, where the instantaneous velocity equals to zero. Raudkivi (1998), provided a relationship between z_0 and the size of the elements producing the roughness, in the form

$$z_0 = \frac{x}{30.2} \quad (3.10)$$

where x represents the size of the roughness elements (equivalent sand roughness which provides indication of the grain diameter).

Hence, rougher floors should have higher values of z_0 .

The natural enhancement of turbulence in flows by bed forms and bed floor roughness has been discussed by (Nelson et al., 1993; 1995). Their findings, however, complimented Bagnold (1966), theory by considering how bed form variation and bed roughness significantly impact on turbulence generation especially in natural flows with erodible beds. Their studies also indicated that, in addition to bed shear stress, sediment transport was a function of the near-bed turbulence which could have been impacted by the bed roughness

with a strong correlation between the sediment flow velocity and the observed near-bed velocity fluctuations.

2.6 Settling velocity of sediment grains

The transport of sediment grains in water settling or fall velocity of sediment grains is one of the fundamental variables in the study and modelling of sediment grain transport which is significant for understanding how sediment grains are suspended, deposited as well as the mixing and exchange processes in a flow (Zhiyao et al., 2008). A sediment grain which is under the influence of gravity and falling in a stationary body of water will continue to accelerate until the gravitational force is exactly balanced by the resisting force such as the drag force (Gabbitto and Tsouris, 2008). Thus, the Settling velocity is the velocity so attained when a sediment grain finally settles in a flow with the drag force being exactly equal to the downward gravitational force (Winterwerp and Van Kesteren, 2004; Mantovanelli and Ridd, 2006; Ha and Maa, 2010). It is a function of sediment grain properties (especially grain size, density and shape), the grains concentration as well as the character of the ambient fluid medium (density and viscosity).

In the estimation of sediment grain settling velocity, Nielsen (1992) had advocated equating gravity and drag forces using an appropriate drag coefficient for both cohesive and non-cohesive sediment grains. Similar recommendations for sand grains, in particular, was made by Fredsøe and Deigaard (1992).

Previous study of settling velocity of natural sediment grains dates back to 1851, when Stokes first developed the quantitative equation for non-cohesive spherical sediment grains (that are not subject to aggregation) in stationary fluids of low Reynolds number (Stokes, 1851; Dyer, 1989; Le Roux, 1992; Cartwright et al., 2011; Cartwright et al., 2013). Therefore, non-cohesive sediment grains with a specific gravity greater than that of water should settle

under the action of gravity, after certain initial acceleration with constant velocity and depend however, on the flow viscosity and density.

From Stokes (1851), the setting velocity of a spherical grain in a low Reynolds number still fluid, is estimated from the mathematical expression below;

$$\omega_s = \frac{(\rho_1 - \rho)gd_g^2}{(18\mu)} \quad (2.12)$$

Where ω_s is the settling velocity, ρ_1 is the density of grain, ρ is the fluid density, g is the gravitational acceleration, d_g is diameter of grain and μ viscosity of fluid.

There are now several new equations that have been derived and proposed to estimate the settling velocity of natural sediment grains applicable to all sediment grains irrespective of shape as well as for a wide range of Reynolds numbers such as Dietrich (1982), Graf (1984), Van Rijn (1993), Ahrens (2000), Ahrens (2003), Camenen (2007) and Zhiyao et al. (2008). The assumption of a sphere, according to Jiménez and Madsen (2003), have some consequences in which case, the settling velocity will be lower than that of a sphere with a nominal diameter.

The determination of the settling velocity for cohesive sediments, on the other hand, has been seen as a rather complicated process in contrast to non-cohesive sediment grains. According to Manning et al. (2011), the interactions factors such as the organic content, degree of flocculation, suspended sediment concentration, mineralogy and properties of the ambient fluid make the prediction very challenging. Therefore, suggestions of carrying out estimates of settling velocity for cohesive sediments in situ in the field due to the flocs sampling and transport issues have become popular (Winterwerp and Van Kesteren, 2004).

Finally, just as the settling velocity of sediment grains is important in flow and sediment grains transport, processes that equally affect or impede the settling of individual sediment grains in a natural flow are also known to exist and have been a subject of investigation. This

process is referred to as hindered settling of grains and will be briefly discussed in the next section below.

2.7 Hindered settling

The settling of sediment grains in a flow is influenced not only by the size of the grains and the surrounding ambient fluid, but also by the presence of a high concentration of other fine grains held in suspension. Hindered settling is the reduced sedimentation rate and/or inability of sediment grains to be deposited or settle on the bed floor due to increasing grain concentration in the flow (Tomkins et al., 2005). Previous studies by Winterwerp (2002), Dankers and Winterwerp (2007), described hindered settling of grains as a process which occurs when there is an over-population of fine sediment grains in a flow, resulting in greater grain-grain interactions and collisions as well as interference which makes the fine grains able to fill-up spaces in the flow. The effect is the considerable reduction of the settling velocity of the sediment grains, facilitating their suspension in the flow and the creation of a slower-moving mixture culminating in the hindered motion the grains. Hindered settling has also been known to greatly suppress the turbulence structure of a flow (Bagnold, 1954).

2.8 Sediment grain transport

Sediment grains are transported in fluvial, coastal and aeolian sedimentary environments. In natural water flows such as rivers, Einstein (1950) and Vanoni (1975), based on the grain characteristics such as size, shape and density as well as the viscosity of the transporting medium, clearly identified and distinguished the modes of sediment transport as the bedload and suspension load. In bed load sediment transport, the grains normally move by rolling, sliding or hopping (saltate) along the bed and usually have velocity significantly different from that of the flow. In suspended load transport, sediment grains are supported above the bed by the turbulent forces in the water and can travel far distances without coming directly in

contact with the bed as well as have velocity similar to the flow velocity. A third mode, identified as the wash load (which are usually clay-dominated and are $>8\mu\text{m}$ in size) are generally considered part of the suspended load.

An estimated volume of over 10 billion tons of sediments is reported to be transported yearly by rivers to continental shelves and further delivered to the oceans and seas (Milliman and Syvitski, 1992; McCool and Parsons, 2004). Bed load transport, however, account for up to 60% of the total sediments transported in rivers, oceans, lakes, seas as well as other bodies of water with most having gravelly base (Métivier et al., 2004; Meunier et al., 2006; Liu et al., 2008; Lajeunesse et al., 2010).

The movement of sediment grains appear to be simple, but the process is a rather more complex phenomenon. To fully understand the motion of sediment grains, several investigations on the mechanisms had led to theories proposed and developed more than half a century ago by Shields (1936); Einstein (1950) and Bagnold (1956, 1966, 1973) with later significant contributions from Graf (1984), Raudkivi (1998) Wilcock (2001), Wilcock and Crowe (2003), Parker (2008), Lajeunesse et al. (2010), Hurther and Thorne (2011), Buscombe and Conley (2012), Schmeeckle (2014) and Hill et al. (2017) among several others. In particular, Bagnold (1956, 1966) derived quantitative relations for the transport of sediment grains as bed load and suspended load based on the Energetics-based theory, with the assumption that a fixed fraction of the stream power of a flow is used to move sediment grains as bed load while the remaining is used to move the suspended load.

The flow stream power, P , is given by

$$P = \tau \bar{u} = \rho g h S \bar{u} \quad (2.13)$$

Where P is the total stream power, g is the acceleration due to gravity, h is flow depth, S is slope, τ is the basal shear stress and \bar{u} is mean flow velocity.

An outline of Bagnold's arguments is that sediment grains entrained in a flow are either

- supported by the upward diffusion of turbulence from the bed boundary (implying that the weight of the sediment grain is balanced by the upward component of the flow momentum transferred to it) or
- supported by the vertical upward component of forces due to the transfer of momentum from grain to grain and grain to bed (Raudkivi, 1998).

Flows laden with sediment grains has also been known to generate turbulence due to shear at the bed and consequently hinders the downward settling of grains moving them higher above the bed in the flow. A review of the mechanism of the two principal modes of sediment transport is discussed below.

2.8.1 Bed load sediment transport

Bed load transport is characterised by movement of sediments with grain sizes above 0.10mm (sand and gravel), and are in frequent contact with the bed. Bagnold (1956), explained that apart from the sediment grains being in successive contacts with the bed, they are also limited by the effect of gravity. Einstein (1950), in addition, was of the opinion that bed load sediment grains transport takes place within the thin two grain diameters thick layer above the bed. It is known that within the bed layer, mixing due to turbulence is very minimal and thus cannot support the suspension of grains.

It is well established that bed load grains travelling along the bed in a flow is facilitated by sliding, rolling and saltation resulting largely due to the shear stress exerted on the bed by the flowing water. Saltation (jumping of grains over the bed) has been identified as the most common pattern, with the other two, rolling and sliding (movement of the grains in continuous contact with the bed (Gao et al., 2005), which rarely occur and does so slowly at low sediment-transport rates and at the verge of the grain entrainment in the flow as well as between saltating jumps (Bridge and Dominic, 1984). An increase in the flow velocity could induce a relative increase in the speed of the rolling or sliding grains until saltating motion

begins. The key mechanism of saltating bed load grains especially at a relatively higher sediment transport rate may be attributed to the grain collision enhancement which results in the transfer of momentum between grains.

The mechanism of bedload sediment grain transport has been well explained by Bagnold, (1956, 1966, 1973). Bed load grains move relatively slower than the surrounding fluids due to grain-grain collisions and with the bed. Collisions of the moving grains with the bed layer exert both a tangential and normal stress on the bed surface. According to Bagnold (1966, 1973), for a steady maintenance of bed load sediment grains transport, there must be an upward dispersive stress balanced by an equal immersed weight of the grains in motion. Also, for low bed grain concentrations, the turbulent bed shear stress at the base of flow is expected to balance the critical bed shear stress of the fluid component at the threshold of sediment grain movement.

Recently, bed load sediment grain transport has been seen not only being influenced by fluid shear from above but also by the granular creep on the bed surface (Houssais et al., 2015). It is worth noting that the continuous contact of bed load grains with the immobile bed usually result in a resistance to grain motion. According to Bridge and Dominic (1984), this resisting force, could be overcome when the fluid exerts a mean downstream force.

On a sloping bed for instance, this downstream force, parallel to the bed is expressed as

$$\tau_0 + w' \sin \beta = T + \tau_1 \quad (2.14)$$

Where τ_0 represent the bed shear stress applied by the fluid, $w' \sin \beta$ is the downslope weight component of moving grains per unit bed area, T is the shear resistance due to the moving bed load and τ_1 is the residual shear stress carried by the mobile bed.

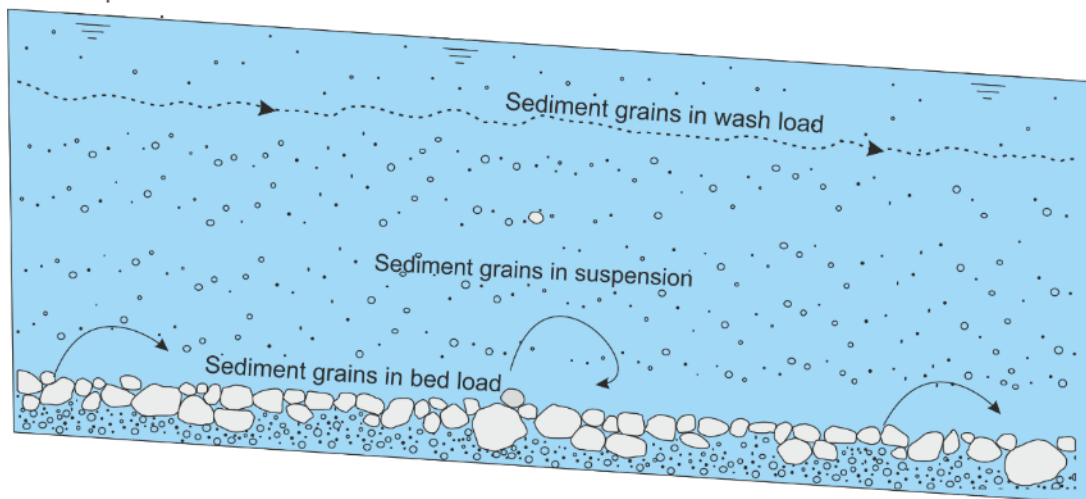


Figure 2.4: Sketch of modes of sediment grain transport

Most of the derived equations on bedload transport rely upon the data from laboratory or in-situ field data in river channel beds and are later tested.

Durafour et al. (2015), had observed that bedload sediment transport in the coastal areas is affected by the heterogeneity (in terms of the grain size, shape and density) of the sediment and the hydrodynamic forcings (such as the waves and currents) in the flow. As in other transport regimes, the shields parameter is critical in the initiation of sediment grain motion. Thus, when the dimensionless shear stress exceeds the critical value, grains movement begins.

2.8.2 Suspended load transport

Theoretically, sediment grains can be moved by suspension irrespective of size as long as the flow current is strong enough. Parsons et al. (2015), described suspended sediment transport to include the transport of fine sediments such as fine sand, silt and clays supported by turbulent eddies whose magnitude exceeds the fall velocities of the grains. Due to the relative absence of grain collisions with the bed layer, the sediment grains move at almost the same velocity as that of the flow. However, to maintain these sediment grains in

suspension, there must be a disparity between the upward-trending lifting forces associated with the flow turbulent eddies and the fall velocities causing the sediment grains to fall and settle towards the bottom of the flow or bed. Bagnold (1966) had postulated that sediment grains are able to remain in suspension when the upward-trending fluctuating velocity associated with turbulence is greater on average than the downward fluctuations.

Thus, in natural flowing waters, sediment grains transport by suspension is facilitated with the support of the turbulence shear stress which prevents the grain from falling to the flow bottom. Shields (1936) had emphasised that suspension of sediment grains occur when the local bottom shear exceeds the critical value. Thus, suspension will occur when the ratio $V'_{\text{rms.max}}/\overline{U_s} \geq 1$, where $V'_{\text{rms.max}}$ is the maximum root mean square velocity and $\overline{U_s}$ is the average flow velocity (Leeder et al., 2005).

Naturally, Sediment grains with density greater than water is expected to fall through a standing body of water since the gravitational forces acting on the grains are unopposed by the flow-induced lifting forces. Bagnold (1966) had emphasised that the residual vertical momentum flux prevents sediment grains from falling into the flow under gravity. Therefore, a sediment grain will be transported by suspension in a flow with the support of the turbulence field of the flowing water (Komar, 1980). The flow shear velocity will always be greater than the fall or settling velocity before gravitational force acting on the sediment grain will facilitate the grains falling back to the bed.

2.9 Chapter summary

The key points of this chapter are:

- Sediment grain properties (especially grain size, density and shape) the grains concentration as well as the character of the ambient fluid medium (density and viscosity) significantly influence a sediment grain's transport and its settling velocity.
- Sediment grains transported by turbulent fluid motion are predominantly in the form of suspended load, in which case, grains are usually relatively finer while the grain-grain contact with the bed or bedload motion is usually characterised by very coarse grains that are usually less significant.
- Cohesion of sediment grains may significantly affect grains resistance to shear and influence its suspension in a flow during transport.
- A sediment grain which is under the influence of gravity and falling in a stationary body of water will continue to accelerate until the gravitational force is exactly balanced by the resisting force such as the drag force. Thus, the Settling velocity is the velocity so attained when a sediment grain finally settles in a flow with the drag force being exactly equal to the downward gravitational force.
- Hindered settling of grains in natural flows occurs when there is high amount of suspended fines above a defined threshold value in a flow.
- Sediment grains are suspended in a flow when the rms amplitude of the vertical velocity fluctuation exceeds the grain's fall velocity.

3 Chapter Three; Character and Behaviour of turbulent flows

Review of governing equations.

3.1 Introduction; Key terms

This chapter provides background key concepts that relates to the character and behaviour of turbulent flows as well as the governing equations for understanding the turbulent suspension theory with respect to movement of sediment grains in a flow. It should be noted that this work considers unidirectional flows that move only along one direction such as turbidity current flows. In figure 3.1 below, a turbulent flow moving in a channel is represented, where the x -direction is taken as parallel to the channel slope, y is across the channel and z as perpendicular to the channel floor. These will be used later in the thesis.

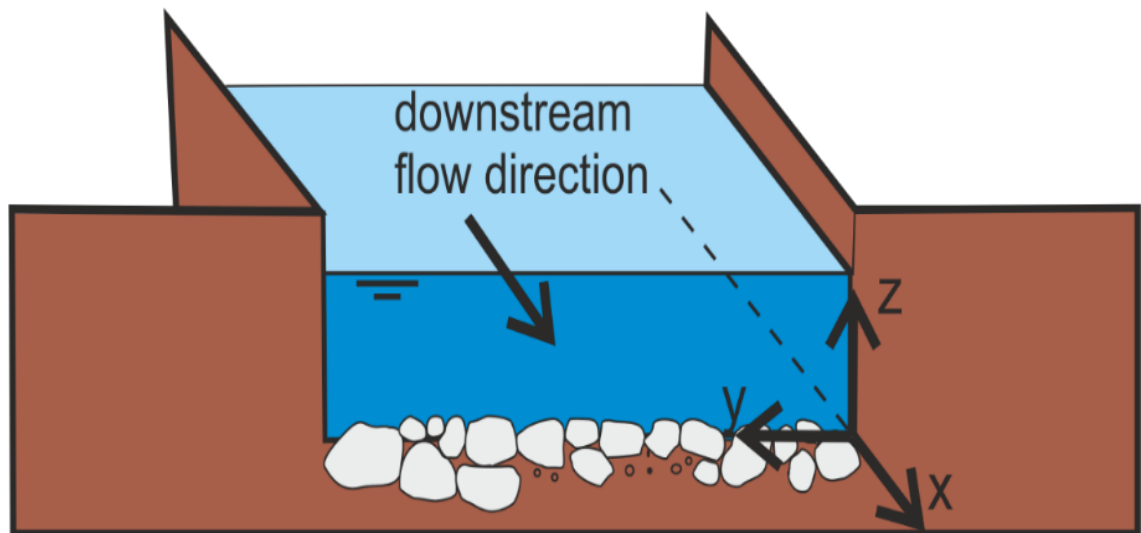


Figure 3.1: Sketch diagram of a unidirectional flow

3.2 Laminar and Turbulent Flow Regimes; Reynolds number

A flow can be either laminar or turbulent depending on the viscosity and inertia. Most water flows exhibit laminar character when moving at low velocities or relatively shallow water depths while turbulent flows are characterised by swirling motions of fluid particles.

Both laminar and turbulent flow regimes may occur in a single natural turbidity current flow as described in Bouma's (1962) depositional model, in which case only the T_a division represented deposition from suspension while the other three divisions, T_b , T_c , T_d were

described as products of mostly traction (laminar flow) or combined traction and suspension (turbulence). Sanders (1965) also suggested that turbulent suspension and laminar flow simultaneously exist in moving sand grains, but the laminar flow is mostly observed in the final stages of sand deposition, as the sand go through tractional ranges. Figure 3.2 below is a schematic diagram describing the two types of flows.

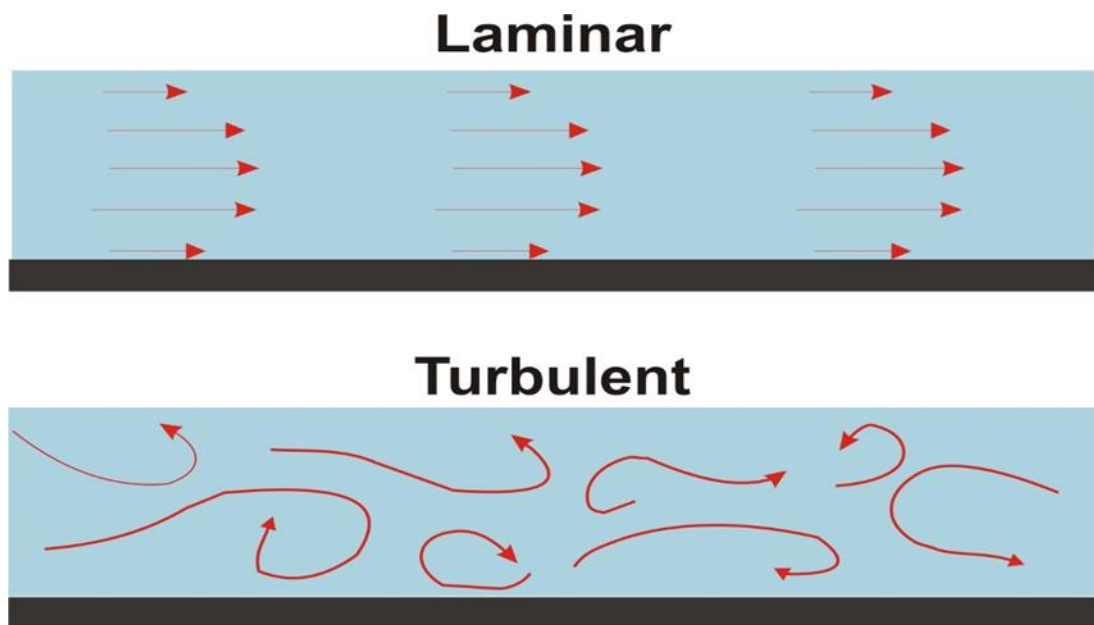


Figure 3.2: Sketch diagram showing the character of laminar and turbulent flows

The Reynolds number (R_e), named after Osborne Reynolds, is used to distinguish between laminar and turbulent flows. It has been widely used since 1883, after a classical experiment to demonstrate the behaviour of flows with changing velocity, using a thread of dye through a glass tube.

Equations 3.1 and 3.2 below provides the relationship between inertia and viscous forces in flows.

$$R_e = \frac{\text{inertia (inviscid) forces}}{\text{viscous forces}} \quad (3.1)$$

Flow is generally considered fully turbulent at flow Reynolds numbers of 2000 or above (e.g. Massey, 1989) and laminar when R_e is less than 2000,

$$R_e = \frac{\rho u D}{\mu} \quad (3.2)$$

where, ρ is the density of fluid, u is the velocity of the flow, D is the flow depth and μ is the flow dynamic viscosity.

3.3 Behaviour of turbulent flows

3.3.1 The flow boundary layer

Turbulent flows moving over or near a solid boundary such as the sea bed are usually retarded arising from viscous effects which are significantly prominent on the bed boundary. The concept of boundary layer was first discovered by Prandtl (1904), who noted the boundary layer to be characterised by a no-slip condition, velocity shear and where most erosion of sediment grains takes place. The flow boundary layer is the region of flow that is influenced by its proximity to the bed surface. Theoretically, if there is no motion of sediment grains on the bed, the thin layer of water having direct contact with the bed usually have a zero velocity and increases with the perpendicular distance away from the boundary due to a decrease in the effects of friction.

According to Nezu (1993), the structure of the turbulent boundary layer or bed (fig 3.3), is comprised of the following parts namely,

- A thin laminar viscous sublayer (usually less than 1.0mm to several mm thick) characterised by very slow viscous flow at the base (due to friction) and this layer tends to dampen any form of mixing and turbulence. It is a very important layer because grains are protected from large turbulent shear stresses above. Here the flow velocity increases linearly with the flow height.

- A transitional turbulent or buffer layer above the base characterised by a flow structure that is intermediate between laminar and turbulent.
- The Logarithmic boundary layer which is fully turbulent, and which obeys the “Law of the wall”, called the logarithmic layer. Here, the time-averaged velocity is often observed to increase logarithmically with flow height above the bed.
- As well as upper turbulent region, which no longer obeys the “law of the wall” and may be referred to as the free stream layer.

A velocity gradient and profile would resemble figure 3.1 below.

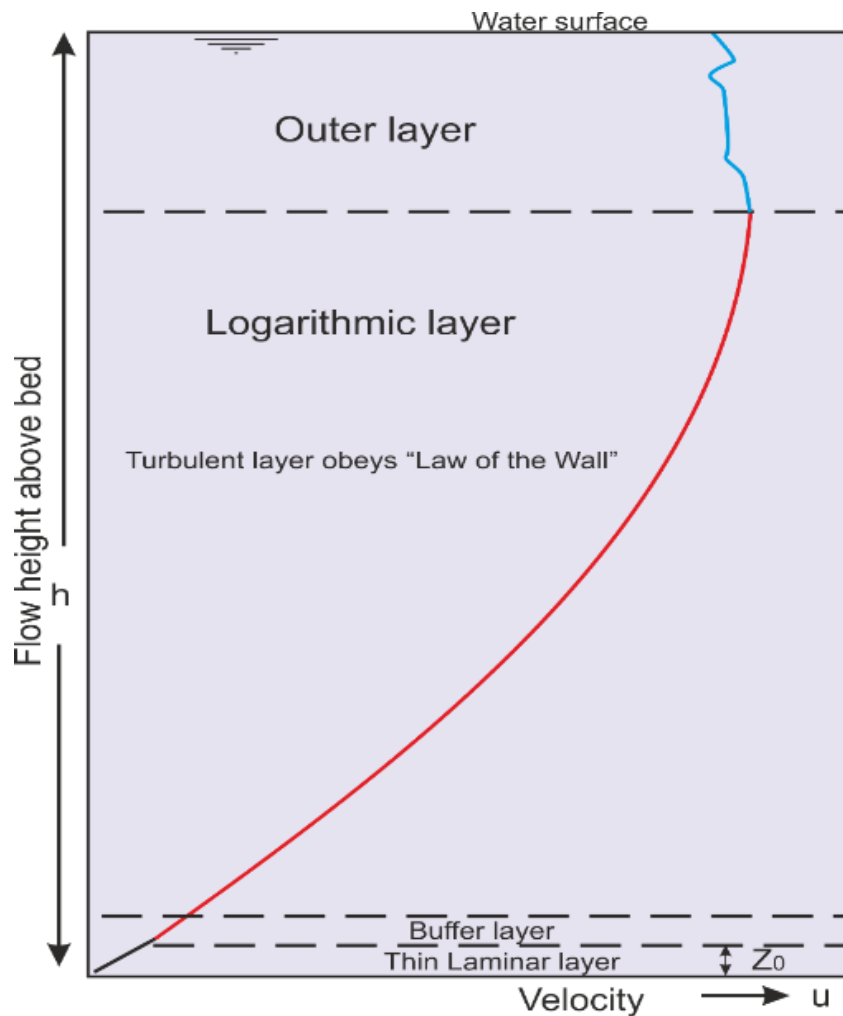


Figure 3.3 : Velocity profile and boundary layers for turbulent flow (modified from Soulsby, 1983)

It should be noted that the top of each “layer” of water is acted upon by a shear stress, which is a frictional force due to the layer above (because of the faster moving flow and drag) as well as by a shear stress due to the layer below (that moves slowly and tends to drag it back).

The next section will describe two key terms used in this thesis and their relevance.

3.3.2 Steady and Unsteady Flows

Steady flows refer to flows in which the water velocity and thickness (height) do not change with respect to time. Thus,

$$\frac{\partial v}{\partial t} = 0 \quad (3.3)$$

Where v , represent flow velocity and could be any other flow variable such as height

However, where there are changes in the flow velocity, in which case they differ from point to point along the flow over time, such a flow is described as unsteady.

$$\frac{\partial v}{\partial t} \neq 0 \quad (3.4)$$

Most natural flows such as rivers are turbulent as the water particles move in swirling motions (turbulent eddies) and are remarkably unsteady in nature. Examples include turbidity currents as well as flows along river channels.

3.3.3 Uniform and non-uniform Flows

Uniform flows are flows whose velocity and depth do not change in space at any point of the flow. Due to changes in the cross-section along the channel path, uniform flow conditions rarely occur in either natural flows or laboratory flume. Thus, uniform flow exists only when there is constant flow depth (thickness), roughness and slope in the direction of flow.

Non-uniform flows are usually characterised by spatial variation in flow velocity and cross sectional area. Non-uniform flows are common in most natural flows such as rivers, where

the flow speed near the bed is usually zero. Also, in river flows, variation in bed slope could cause the depth and velocity to vary in which case the water surface is not parallel to the bed. Non-uniform decelerating flows are usually associated with deposition while the accelerating flows are erosive.

3.3.4 Froude Number

Froude number expresses the ratio of inertial forces to gravitational forces. It was named after an English Engineer, William Froude (1810-1879), to essentially indicate the flow state and resistance of an object moving through water. The greater the Froude number, the greater the resistance. Froude number for a turbidity current can be mathematically expressed as below:

$$F_r = \frac{U_{head}}{\sqrt{\left(\frac{\rho_t}{\rho} - 1\right)gh}} \quad (3.5)$$

Where U_{head} is the mean velocity of the turbid flow, g , is gravitational acceleration, ρ is density of ambient water, ρ_t is density of grains in suspension and h is the hydraulic depth.

Table 3.1: Froude number and the states of flow

Flow type	Froude Number	Qualitative flow description
Supercritical flow	$F_r > 1$	Fast and shallow
Critical flow	$F_r = 1$	Intermediate
Subcritical flow	$F_r < 1$	Slow and deep

As summarised in table 3.1 three states of flow is described using the Froude number and these are the subcritical flow, where $F_r < 1$ (such a flow is tranquil); the supercritical flow, where $F_r > 1$ (flow is rapid and there is considerable mixing of flow with ambient). Turbidity currents can be either subcritical or supercritical depending on the bed slope, bed roughness and the magnitude of suspended concentration. Supercritical flows due to their fast nature can entrain more fluids from the ambient fluid above, with their maximum velocity very proximal to the bed relative to the flow interface. The subcritical turbidity current flow is

characterised by a negligible entrainment from the ambient fluid above and the velocity maximum is near the flow interface. Sequeiros (2012) from his experiment, and analysis of available flow data confirmed that the steeper the slope, the smoother the bed, and the heavier the suspended material are, the higher the Froude number is.

3.3.5 The Rouse Number

Rouse (1937), provided a criterion for characterising the mode of transport of sediment grains in a shear flow. It is expressed as the ratio of sediment grain settling velocity to the shear velocity of the flow.

$$R_N = \kappa \frac{\omega_s}{u_*} \quad (3.6)$$

Where κ , is von Karman's constant.

Rouse number can be an effective criterion for suspension of sediment grains. According to Allen (2009b), as presented on table 3.2, a Rouse number of 2.5 corresponds to the criterion that the settling velocity is equal to the shear velocity and this implies a rough criterion for sediment grain suspension.

Table 3.2: Froude number and the states of flow

Rouse Number	Mode of Sediment transport
$R_N > 2.5$	Bedload
$R_N \leq 2.5$	Suspension
$R_N < 0.8$	Washload

3.4 Shear Stress and Shear Velocity

The bed shear stress of a flow, τ_0 , is the flow force per unit area parallel to the bed which is available to move sediment grains in moving turbulent water against the bed of a flow channel. It represents the resistance of a bed to flows above it (Zhang et al., 2016).

Bed shear stress is a function of the flow depth, h , the bed slope, s and indirectly a function of the flow velocity. The shear stress exerted by a moving turbulent flow is proportional to the square of the velocity of flow. However, in addition to frictional drag, the motion of sediment grains is usually subjected to the lift force by the moving turbulent flow.

According to Bagherimiyab and Lemmin (2013), the bed shear stress is an “important turbulence scaling parameter in river studies as it relates to scour and channel changes”. Bed shear stress is also related to the near-bed velocity gradient, which increases with the steepness of the gradient and it is affected by the roughness of the channel bed. Also, because flow velocity increases systematically with distance from the bed, the rate of increase has been used to determine the shear stress at the bed as measuring it directly has been very challenging in natural systems (such as rivers and coastal water bodies) as well as in the laboratory. Hence practically, it is inferred from the shear velocity estimates, u_* .

According to Rowiński et al. (2005), Shear velocity is a measure of the bed shear stress having a dimension of velocity. It is the degree of variation of the velocity fluctuation due to turbulence around a point near the bed boundary. At the bed boundary, the shear velocity is known to reduce to zero (called the no-slip condition) due to the opposing frictional forces to flow. Shear velocity, therefore is a measure of the rate of change of the velocity of flow with distance from the bed boundary. The shear velocity, u_* is defined as

$$u_* = \sqrt{\tau_0 / \rho} \quad (3.7)$$

Also,

$$\tau_0 = \mu \frac{\partial u}{\partial z} \quad (3.8)$$

$$\text{By substitution, } u_* = \sqrt{\frac{\mu}{\rho} \frac{\partial u}{\partial z}} \quad (3.9)$$

Where τ_0 , is the bed shear stress, μ is the dynamic viscosity of the fluid, $\frac{\partial u}{\partial z}$ is the vertical velocity gradient (rate of change of velocity with depth) and ρ is water density.

In the absence of adequate measuring equipment, direct measurements of $\partial u/\partial z$ and u_* are difficult to quantify but has been carried out with acceptable error (Ortiz and Klompmaker, 2015). Generally, shear velocity is a derived quantity from the gradient of the velocity profile related to the bed shear stress, τ_0 , (Bagnold, 1966; Middleton and Southard, 1984; Komar, 1985; Garcia and Parker, 1993; Leeder, 2012). Sediment grains on the bed (fig 1.1) only begins motion when the bed shear stress, τ_0 , becomes sufficiently great enough to overcome the frictional and gravitational forces holding the grains on the bed (Critical shear stress).

3.5 Estimating Shear Stress

Several methods exist in the literature for estimating bed shear stress and these include Bergeron and Abrahams (1992), Wilcock (1996), Kim et al. (2000), Biron et al. (2004), Rowiński et al. (2005), Pope et al. (2006), Sherwood et al. (2006), Sime et al. (2007), Bagherimiyab and Lemmin (2013), Liu and Wu (2015), Lee and Baas (2016), Shivpure et al. (2016), and Zhang et al. (2016). Figure 3.4 shows the pictorial diagram illustrating the main methods used in bed shear stress estimation.

3.5.1 Bed Slope Method

Under defined conditions of flow, shear stress can be estimated based on the force balance over a control section of an open-channel which is used as a reference. This method makes use of bed slope data, S_0 and flow section characteristics (Graf, 1998; Rowiński et al., 2005).

Equation 3.23 and 3.25 expresses how estimation of shear velocity is done based on the bed slope method.

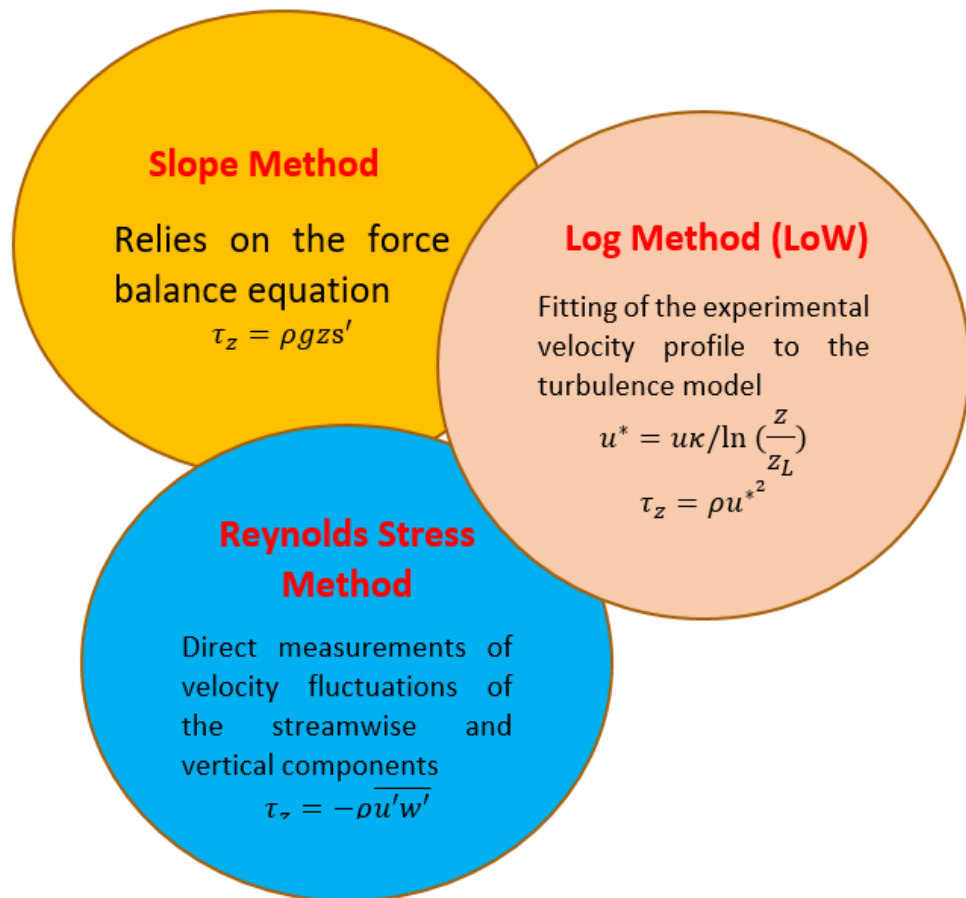


Figure 3.4: Basal shear stress estimation methods

However, according to Biron et al. (2004), this method may not be appropriate for local, small-scale estimates of the variation in shear stress and is prone to large uncertainty.

3.5.2 The Logarithmic Profile Method

This method has been commonly referred to as the Law-of-the-Wall or von Karman'-Prandtl law of vertical velocity distribution equation (Shivpure et al., 2016). The equation, derived

from the von Karman-Prandtl mixing length theory expresses the logarithmic relation between the shear velocity and the variation of mean velocity with height.

The von Karman-Prandtl mixing length theory has been expressed in equations 3.10-3.11 and are used in conjunction with equation (3.12) to estimate the shear stress of a bed. Estimates of basal shear stress can be carried out by fitting the measured experimental velocity profiles to equation 3.10.

By expanding equation 3.10, we can have a more simplified expression;

$$\bar{u} = \left(\frac{u_*}{\kappa}\right) \ln(z) - \left(\frac{u_*}{\kappa}\right) \ln(z_0) \quad (3.10)$$

Hence, when velocities at different flow heights or depths are plotted, the best fit line through the plot (such as u vs $\ln(z)$) will have a gradient of (u^*/κ) and an intercept of $(u^*/\kappa) \ln(z_0)$. Where, κ is the von Karman constant. Thus,

$$u_* = \kappa \cdot \text{Gradient} \quad (3.11)$$

and

$$z_0 = \exp\left(\frac{\text{intercept}}{\text{Gradient}}\right) \quad (3.12)$$

The fitting procedure involves an ordinary least square regression to the profile and calculating the values of u_* and z_0 from the slope and intercept of the computed regression equation. The logarithmic law method requires that the level of profile origin ($z=0$) is known in computing the flow parameters.

For a uniform flow where there is no sediment transport (clear water experiment), it has been established that von Karman's constant κ varies from 0.16 to 0.41. For example, Wang and Larsen (1994), $\kappa = 0.16$; Einstein and Chien (1955), $\kappa = 0.168-0.406$; Vanoni and Nomicos (1960); $\kappa = 0.209-0.384$; Gust and Southard (1983), $\kappa = 0.28$. All these values are substantially

smaller than the frequently assumed value of 0.4 – 0.41 (Felix et al., 2006; Darby and Peakall, 2012; Dorrell et al., 2014; Yin et al., 2016).

This method has been widely used for open-channel flows and river studies (Nezu and Nakagawa, 1993).

3.5.3 Reynolds Stress Method

This method relies on the theory that in a fully turbulent flow, shear stresses are related to the rate of momentum exchange between adjacent levels in a flow (Duncan, 1960) from which follows that;

$$u_* = \sqrt{\overline{-u'\omega'}} \quad (3.13)$$

where u' and ω' are the velocity fluctuations of the streamwise and vertical components respectively and the overbar denotes time-averaged values (Pope, 2001; Babaeyan-Koopaei et al., 2002).

Reynold stresses may be represented by the fluctuations in instantaneous velocity values measured by an appropriate velocity sampling instrument such as the Acoustic Doppler Velocimeter. To obtain the basal shear stress, the time-averaged product of the streamwise and vertical fluctuations at the flow base is required. This is usually practically carried out by linear extrapolation from the heights at which the product of the streamwise and vertical fluctuating velocities could be determined. The velocity fluctuations are estimated from the deviation above the mean velocity value from the direct measurements that is taken at the base of flow.

Reynolds stresses has been observed to vary linearly from the base of flow to the free surface, and in particular where there is significantly rough-beds underlying steady open channel flows. The linearity is used to extrapolate the total fluid stress acting on the bed.

Nikora and Goring (2000) had advocated extrapolating the Reynolds stress profile to the bed in estimating the shear velocity.

$$u_* = \sqrt{(-\overline{u' \omega'})} \quad z \rightarrow 0 \quad (3.14)$$

3.5.4 Uncertainty in Shear stress estimation

Shear stress estimation from velocity profiles could be plagued with uncertainty which affect the reliability of the results generated. Specifically, Bauer et al. (1992) identified three potential sources of uncertainty in the log profile method and these are listed below;

1. Instrument Error; Imprecision of measuring instruments such as the ADV and flow velocity meters could introduce errors during measurement.
2. Inappropriate application of velocity profiles equation under conditions that may be essentially different from those assumed when derived.
3. Errors from the statistical analysis while determining shear velocity and roughness length.

Also, using Reynolds shear stress methods, uncertainty mainly arises from instrument positioning and reading as well as in the statistical analysis of generated data.

3.6 Review of Governing Equations

The governing equations for a turbulent flow are the conservation of mass, the momentum as well as the mass of the sediment. Detailed derivation is in Parker et al., (1986) and Waltham et al., (2008). Sections below reviews aspects of these equations in relation to this research.

3.6.1 Basal Reynolds Shear Stress

Kneller et al. (1997), described Reynolds stress as representing the rate at which eddies transfer flow momentum towards the bed boundary. Thus, Reynolds stresses measure the amount of turbulent energy within a turbulent flow.

In the experiments performed that will be reported in the next chapter, it assumes that flow used in the flume-tank is quasi-steady, i.e. there are short term fluctuations in velocity due to turbulence but, on sufficiently long-time scales, it is meaningful to describe it about steady average velocities.

With this assumption, the instantaneous velocity can be decomposed into a steady part plus a fluctuating part, i.e. \bar{u} is the steady part while u' is the fluctuating part.

Throughout this report, an overbar ($\bar{}$), implies a time averaged velocity and so primed quantities are the instantaneous deviations from the average velocity. Thus,

$$u = \bar{u} + u' \quad (3.15)$$

$$v = \bar{v} + v' \quad (3.15)$$

$$w = \bar{w} + w' \quad (3.16)$$

where u is the x -component, v the y -component and w the z -component.

This expression is not limited, however to velocity fluctuations in flows but also pertains to other quantities (Φ) (e. g. pressure, temperature) affected by the turbulent flow field such that,

$$\Phi = \bar{\Phi} + \Phi' \quad (3.17)$$

In turbulent flows, Reynolds stresses are much larger than viscous stresses and the Reynolds' averaged Navier Stokes (RANS) equation in the x -direction takes the form as below;

$$\bar{u} \frac{\partial \bar{u}}{\partial x} + \bar{v} \frac{\partial \bar{u}}{\partial y} + \bar{w} \frac{\partial \bar{u}}{\partial z} = -\frac{\partial p}{\partial x} - g_s' - \left[\frac{\partial \overline{u'^2}}{\partial x} + \frac{\partial \overline{u'v'}}{\partial y} + \frac{\partial \overline{u'w'}}{\partial z} \right]. \quad (3.18)$$

(Tennekes and Lumley, 1972; Hinze, 1975; McComb, 1990; Foias et al., 2001).

where P is pressure, g is the acceleration due to gravity and s' is the tank slope.

The continuity equation, after substituting equations (3.15)-(3.17) and taking a time average, gives (Bridge and Demicco, 2008):

$$\frac{\partial \bar{u}}{\partial x} + \frac{\partial \bar{v}}{\partial y} + \frac{\partial \bar{w}}{\partial z} = 0 \quad (3.19)$$

and, since x and y derivatives are zero, this equation implies that \bar{w} does not change with height. But $\bar{w}=0$ at the tank floor and so $\bar{w}=0$ everywhere. Hence, the left-hand side of equation (3.18) disappears (for a uniform in x flow) and the right-hand side simplifies to

$$0 = -gs' - \frac{\partial \overline{u'w'}}{\partial z}. \quad (3.20)$$

Equation (3.20) states that the gradient of $\overline{u'w'}$ is $-gs'$ and this property will be used later to test whether the flows are really uniform in the x -direction. Equation (3.20) also allows calculations of the shear stress at the base of the flow i.e.

$$\tau_{xz} = -\rho \overline{u'w'} \quad \text{at } z=0 \quad (3.21)$$

by linearly extrapolating $\overline{u'w'}$ down to $z=0$.

This equation above will be the primary measurement against which other estimates of basal shear stress will be compared.

3.6.2 Slope Calculated Basal Stress

This thesis assumes a steady uniform flow in calculating the basal shear stress. Also, assumptions of the weight of the flow being balanced by friction at the flow base is significant. This leads immediately to the expression

$$\tau_{xz} = \rho g h s' \quad \text{at } z=0 \quad (3.22)$$

where h is the flow thickness. However, this expression will not be correct in the case of a narrow flume (such as the one that is available and used in this experiment which is approximately 30cm in width) due to likely additional frictional forces on the flume side-walls. Hence equation (3.22) can only provide an upper limit to the basal shear stress and therefore needful to be rewritten as

$$\tau_{xz} \leq \rho g h s' \quad \text{at } z=0. \quad (3.23)$$

3.6.3 Mixing Length Theory; Basal Shear Stress

The mixing length theory of turbulence provides the log-law for mean velocity distribution in turbulent flows. A major objective of this research is to evaluate the accuracy and robustness of mixing-length theory-based estimates of basal shear stress. The key prediction of the theory is that the depth profile of velocity is logarithmic (the law of the wall), i.e.

$$\bar{u} = \frac{u_*}{k} \ln \left(\frac{h}{z_0} \right) \quad (3.24)$$

where the “shearing velocity”, u_* , is related to basal shear stress by

$$\tau_{xz} = -\rho u_*^2 \quad (3.25)$$

and k is von Kármán’s constant.

An important parameter, z_0 , is the height where flow velocity is predicted to be zero, although, in practice, at this very small distance from the flow base the flow has become laminar and follows a simple linear profile. These small heights are not measured in this work and, hence, the failure of the law of the wall in that zone is not of primary interest. The resulting estimate of basal shear stress is independent of that obtained by equation (3.22) and so equation (3.22) can be used to evaluate the accuracy of equation (3.25).

From a practical point of view, equation (3.22)'s estimate of basal shear stress can be related to the average velocity, v_{av} , in the flume

$$\tau_{xz} = -\rho C_d v_{av}^2 \quad (3.26)$$

where C_d is a Chezy coefficient of friction.

3.6.4 Flow Average Velocity

As outlined in table 3.4, several instruments are available for measuring the instantaneous velocity of flow in a both in the field and laboratory. However, in the experiments undertaken, the Nortek II acoustic Doppler velocimeter (ADV) was used to measure the flow velocity. Also, of mention is the fact that due to the narrow nature of the flume, these instantaneous flow velocity measurements could not account for the effect of flume side-wall friction, on the flow hence the need to find alternate ways to estimate the flow average velocity. From personal interaction with Dave Waltham, the flow average velocity, v_{av} , could be estimated using the Law-of-the-Wall equation to check any side wall frictional effect.

Thus, From the Law-of-the-Wall,

$$v_{av} = \frac{u_*}{\kappa} \ln \left(\frac{H}{z_0} \right) = \frac{u_*}{\kappa} \ln(H) - \frac{u_*}{\kappa} \ln(z_0) \quad (3.27)$$

$$v_{av} = \frac{\int_{z_0}^H u \delta H}{\int_{z_0}^h \kappa H} = \frac{\frac{u_*}{\kappa}}{H-z_0} \left(\int_{z_0}^H \ln(H) \delta H - \ln(z_0) \int_{z_0}^H \delta Z \right) \quad (3.28)$$

$$= \frac{\frac{u_*}{\kappa}}{H-z_0} \left([H \ln H - h]_{z_0}^H - \ln(z_0) [z]_{z_0}^H \right) \quad (3.29)$$

$$= \frac{u_*}{\kappa} \left(\frac{H \ln H - H}{H-z_0} - \frac{z_0 \ln z_0 - z_0}{H-z_0} - \ln(z_0) \right) \quad (3.30)$$

$$\sim \frac{u_*}{\kappa} (\ln H - H) - \frac{u_*}{\kappa} (z_0) \quad (3.31)$$

$$= m(\ln\{H\} - H) + c \quad (3.32)$$

Therefore, the average velocity estimate from flume centre line will be done using the relation as in equation 3.30 above;

$$v_{av} = m * (\ln (h) - 1) + c \quad (3.33)$$

Where m is gradient, h is the flow thickness and c is the intercept.

3.6.5 Chezy equation

This equation relates uniform turbulent flow to bed resistance. It was formulated in 1775 by the French engineer, Chezy. The equation was first used to determine the relationship between the average velocity of steady uniform open-channel flow to channel slope, s , radius, r_h (hydraulic) and a coefficient which expresses the boundary roughness.

$$u = C\sqrt{r_h s} \quad (3.34)$$

Where C is the Chezy coefficient of friction

3.6.6 Turbulent suspension of sediment grains

Bagnold (1966), developed a mathematical equation for sediment grain suspension in flows which primarily centred on the criteria for fluids to oppose the gravitational settling of sediment grains as in autosuspension. However, the process was believed to be flawed with high uncertainty with respect to the criteria set for the turbulent suspension. (Pantin, 1979; Southard and Mackintosh, 1981), and this led to further investigations in various aspects of turbulent suspension of sediment grains, including researches by Leeder (1983); Wei and Willmarth (1991); Kneller et al. (1997); Bennett et al. (1998) and Leeder et al. (2005).

This current research will attempt to determine the maximum grain-size that could be potentially be transported in suspension in a turbulent flow based on the assumption that

grains will only be suspended if the rms amplitude of vertical fluctuations is greater than the grain fall-velocity in natural flows. This underlying theory was first proposed by Bagnold (1966) and expressed as in equation (3.35) below:

$$\sqrt{\overline{w'^2}} > \omega_s \quad (3.35)$$

Where the fall velocity, ω_s can be estimated from relationships such as Stokes' law (Stokes, 1851).

Also, Kneller et al. (1997), adopted a Suspension criterion of,

$$\omega_s = bu_* \quad (3.36)$$

Where b was taken as a constant value of 0.8

However, going back to Bagnold (1966), suspension criterion, in practice, $\overline{w'^2}$ is not usually measured and hence a further assumption is made that it can be replaced by u_*^2 as in equation (3.36), so that the suspension criterion becomes

$$u_* = \sqrt{\frac{\tau_0}{\rho}} > \omega_s \quad (3.37)$$

$$u_* = \sqrt{\frac{\tau_{xz}}{\rho}} > \omega_s \quad (3.38)$$

Our flume tank experiments allow this assumption to be directly tested.

However, in an un-instrumented flow, the rms velocity fluctuations are not known and therefore a further assumption is made that turbulence is approximately

$$\overline{w'^2} \approx \overline{u'w'} \quad (3.39)$$

The accuracy of this relationship will be determined later in this work.

Table 3.3: Some Flow Velocity measuring equipment

Technology	Operating Principles	Advantages	Disadvantages
Hot-wire Anemometry	Essentially a thermal method, based on the convective heat transfer from a heated sensor element to a relatively cold surrounding fluid which varies with the flow rate	<ul style="list-style-type: none"> • Cost is relatively very cheap • Small measurement volume • Low SNR • Good spatial and temporal resolution 	<ul style="list-style-type: none"> • It is an intrusive technique which can modify the local flow field • Contamination from deposition of impurities on sensor • Probe could easily break • Needs calibration
Laser-Doppler Velocimetry	Based on the Doppler shift effect. The difference in the frequency between the original beam and the moving particle known as the Doppler shift is proportional to the velocity of the moving particle.	<ul style="list-style-type: none"> • Does not require pre-calibration • Negligible probe interference • Can measure a wide range of flow velocities (eg from 0.0001 to 1000m/s) • High resolution as probe volume as small as 10^{-6} size can be obtained 	<ul style="list-style-type: none"> • Relatively very expensive • Need for eye protection against the direct laser beam • Flows ceases to be single phase flow as soon as particles are introduced into flow • Not very suitable for 3D flows
Acoustic-Doppler Velocimetry	Based on the principle of the Doppler shift effect.	<ul style="list-style-type: none"> • Non-intrusive and relatively cheap • 3D flow measurements • Relatively high SNR • No calibration required • Rugged and convenient to use in difficult to reach areas • Measures very low velocity 	<ul style="list-style-type: none"> • Signals affected by velocity shear across the sampling volume and nearness to boundary • Requires post-processing
Particle-image Velocimetry	Photographic recording of tracer particle motion in a fluid which are usually well illuminated. Image processing determines the flow velocity from the recording	<ul style="list-style-type: none"> • Non-intrusive • Captures velocity data in multiple points in the flow • High spatial resolution 	<ul style="list-style-type: none"> • Expensive • Size of area need to be small for greater accuracy

3.7 Chapter Summary

The key conclusions of this chapter are

- Most natural unidirectional flows such as rivers and streams are non-uniform, unsteady turbulent flows as the water particles move in swirling irregular pattern (turbulent eddies) and are characterised by physical quantities having random variation in time and space.
- Turbulence creates eddies that facilitates mixing and momentum exchange in a flow as amply demonstrated by the mixing-length theory of Prandtl-von Karman.
- The turbulent boundary layer is characterised by three parts, a thin laminar layer, the logarithmic layer and an outer layer. While the Logarithmic layer obeys the “law of the wall” in which the mean flow velocity increases logarithmically with flow height, the laminar viscous layer is characterised by very slow motion due to friction and mean flow velocity increases linearly with flow height.
- Both laminar and turbulent flow regimes may occur in a single natural turbidity current flow as described in Bouma’s (1962) depositional model.
- Bed roughness imparts on turbulence generation in flows
- Basal shear stress is related to the flow shear velocity and estimates can be carried out using the slope, log profile and Reynolds stress methods.

4 Chapter Four; Experimental Set-up, Instrumentation and Procedure

4.1 Introduction

This chapter describes the experimental methods used in this thesis. As previously discussed in chapter one, this research seeks to, among others, understand the role of turbulence in supporting sediment grains transport in long run-out turbidity current flows. However, designing scaled-flume experiments for this purpose poses a huge challenge as it is quite difficult to adequately simulate natural long run-out turbidity currents in the laboratory. Scaling of natural turbidity currents such as size of current is limited by the available laboratory facilities and hampers its recreation. Other scaling issues such as the time of propagation cannot be integrated into the experimental model. Because of this, experiments were designed as clear water open channel flows in order to generate instantaneous and fluctuating flow velocity data that will be used to validate the mixing-length theory of turbulent suspension.

The sections below describe the experimental design, set-up and procedure as well as instrumentation.

All flume experiments described here was carried out in collaboration with the School of Earth & Environmental Sciences of the University of Leeds, at the Sorby Fluid Dynamics Laboratory where the flume experimental facility is located.

4.2 Design and set-up of experiment

As explained in the previous section (4.1), the experiments were designed to make use of clear water in turbulent open channel flows. The set-up of the experiment includes using a slightly tilting (0.001° - 0.002°) re-circulating rectangular glass-sided flume, measuring approximately 8.5m long, 0.3m deep and 0.3m wide and instrumented with a three-dimensional (3-D) Acoustic Doppler Velocimeter measuring system. The re-circulating flume tank was used to ensure a steady uniform flow in the tank. The clear glass-sided walls

provided clear views of the flow and allowed for measurement of flow properties. The test section was located at the centre of the flume, about 4.2m from the downstream end and all instantaneous velocity sampling were taken at this point, since it is within the test section that we should expect a fully developed turbulent flow regime.

A Hidrostal centrifugal pump was fitted to the flume tank to drive clear water into the flume which was recirculated through the flume via a return PVC pipe of 0.20 m diameter. The recirculating flume was necessary to maintain uniform flow of water circulation in the flume. The flow discharge rate into the flume tank was monitored using an ABB electromagnetic flow meter which was controlled via an inverter control unit. A pack of stainless steel pipes of 25 mm radius was placed at the upstream end of the flume tank to reduce vortex flow. Water temperature was kept at $20\pm 2^{\circ}\text{C}$.

A schematic diagram showing the set-up of the experimental flume is shown in figure 4.1 while Figure 4.3 shows a photograph of the measurement and observation section as well as the ADV instrumentation and PC for recording signals.

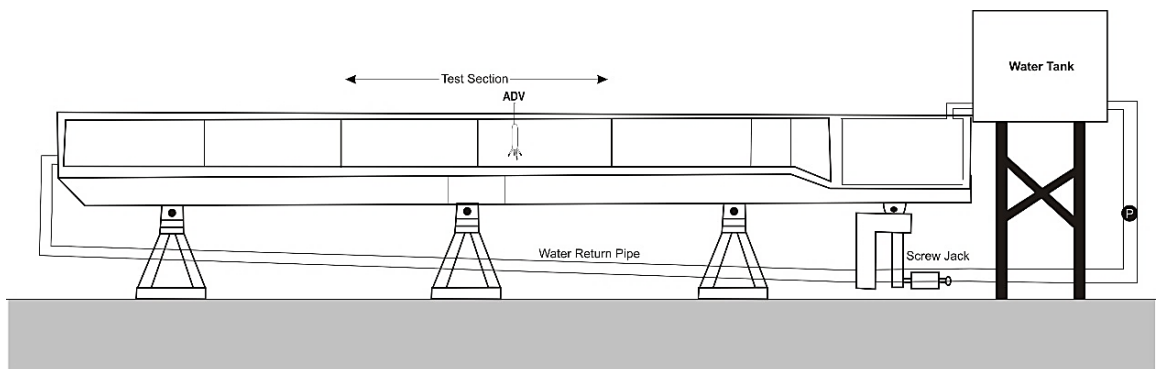


Figure 4.1: Sketch diagram of the laboratory flume tank used in this research

The experiments were conducted in six series, labelled as cases 1-6, characterised by parameters as listed in table 4.1. Experiments investigating the effect of bed roughness on flow turbulence was designed by comparing flows over smooth concrete ($D_{50} < 0.5\text{mm}$) as in

flow cases 1 and 2 (smooth floor; figure 4.2) and rough gravelly floors (D_{50} approx. 3.0mm) for flow cases 3-6, made of gravelly slabs (figure 4.3).

All six experimental flow cases (1-6) comprised of a total of forty-five flow runs with the measuring ADV instrument set at defined depth intervals. However, prior to the commencement of each experiment the metal flume tank floor was covered with slabs of either concrete or gravel to fit the entire floor to check interference of the floor with the ADV measuring instrument.



Figure 4.2: Photograph of concrete slab floor of flume tank, flow cases 1 and 2

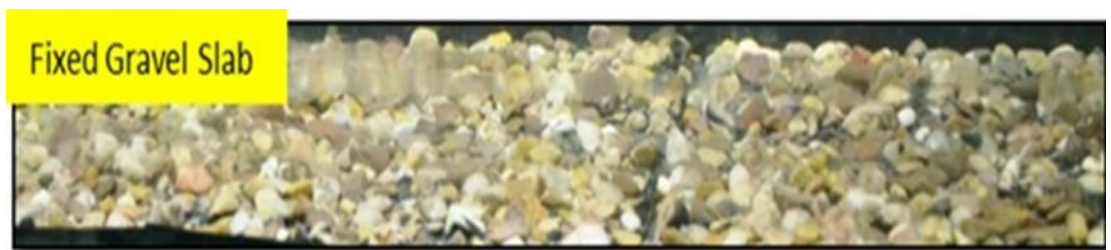


Figure 4.3: Photograph of gravel slab floor of flume tank, flow cases 3-6

Table 4.1: Summary flow character for the six cases

Experiment	Flow Character
Case 1	Flow thickness =0.192m; Mean discharge rate= 0.023m ³ /s; Fixed Concrete slab floor
Case 2	Flow thickness =0.180m; Mean discharge rate= 0.040m ³ /s; fixed Concrete slab floor
Case 3	Flow thickness =0.192m Mean discharge rate= 0.025m ³ /s; Fixed gravel slab floor
Case 4	Flow thickness =0.192m; Mean discharge rate= 0.031m ³ /s; Fixed gravel slab floor
Case 5	Flow thickness =0.140m, Mean discharge rate= 0.022m ³ /s; Fixed gravel slab floor
Case 6	Flow thickness =0.140m; Mean discharge rate= 0.033m ³ /s; Fixed gravel slab floor

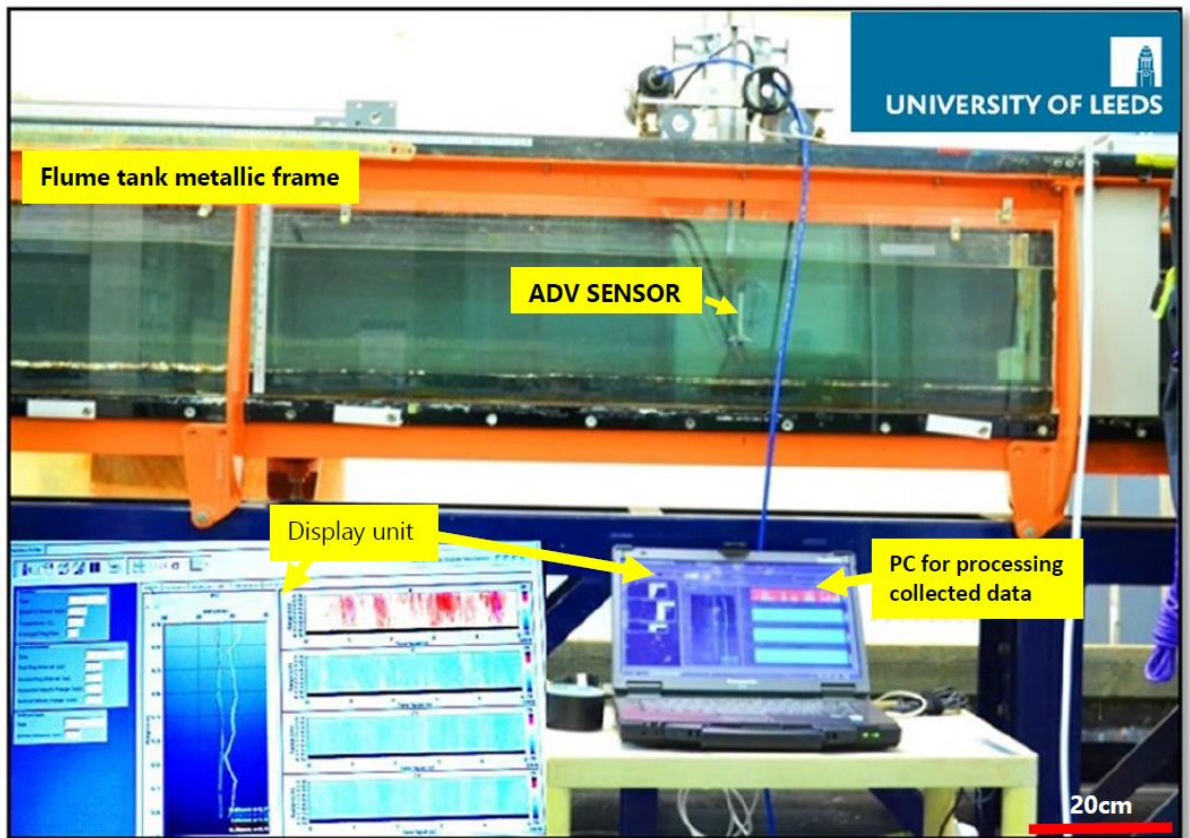


Figure 4.4: Photograph of the Flume (Measurement and Observation section)

4.3 Instrumentation

Among the several flow velocity measuring devices earlier outlined in Table 3.4 of this thesis, the Acoustic Doppler Velocimeter is more popular and widely used. This is due to its relatively simplicity, portability, easy-operated and use without any calibration.

In this study, the flume experiment made use of the Nortek Vectrino II Acoustic Doppler Velocimeter for measuring the flow fluctuating velocity. It is briefly described in the section below.

4.3.1 The Acoustic Doppler Velocimetry

The Acoustic Doppler Velocimeter (ADV) is a well-established modern technique for sampling instantaneous flow velocity and turbulence measurements using the principle of Doppler shift effects to measure instantaneous flow velocity in a small volume. It measures the Doppler shift of any moving particles to determine their speed. A key assumption in the use of Acoustic Doppler Velocimetry is that the scattering particles in the water have the same velocity as the flow velocity itself. Measurements are obtained by sending out a beam of acoustic waves at a fixed frequency from the centre transducer to the sampling volume. The reflection from the mobile suspended particles within the sampling volume causes a Doppler shift which is received by the receivers (3 or 4, depending on the specification) positioned at x , y , z_1 and z_2 directions. Details of the operation of the ADV is in Kim et al. (2000), Biron et al. (2004), García et al. (2005), Liu and Wu (2015), Shivpure et al. (2016) as well as the Vectrino Velocimeter User guide (Nortek, 2004).

The Acoustic Doppler Velocimeter consists of a probe, connected by a cable or a fixed term to the housing where the transmitter resides. Although the ADV is an intrusive device, with

the probe dipping into the flow, it has a sampling volume located about 50mm below the probe which helps to minimise the interference of the probe with the flow.

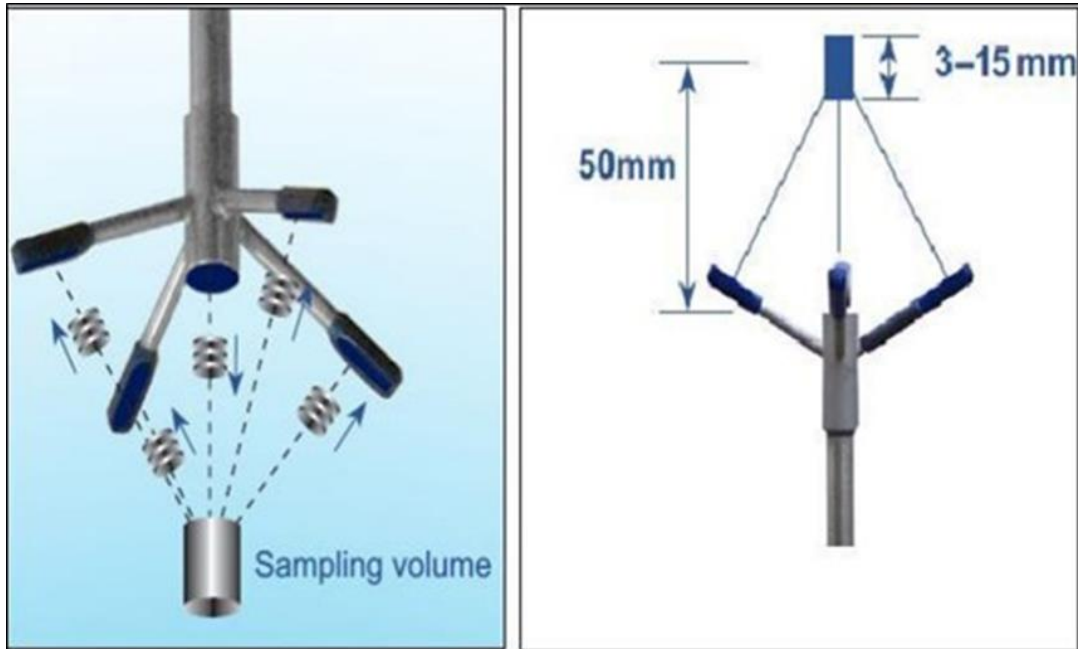


Figure 4.5: Nortek ADV probe with transducer, receiver, and sampling volume

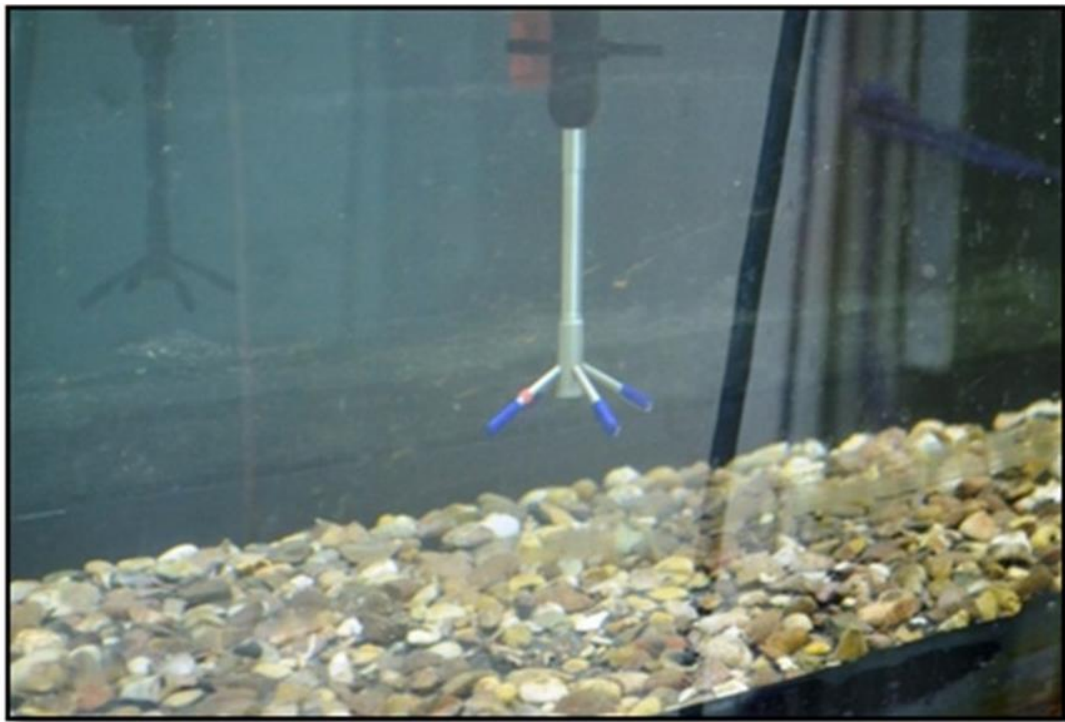


Figure 4.6: The Four signal receiving beams of an ADV

There have been significant improvements in modern single point ADVs unlike previous generation velocimeters where the measurements are done about 10.0mm from the bed boundary to obtain reliable results. The ADV (Nortek Vectrino II Profiler) in use today now have 4 receivers as in figure 4.4 and 4.5, (e.g. Lohrmann et al. (1994), Lane et al. (1998), Doroudian et al. (2010), Khorsandi et al. (2012), Durgesh et al. (2014)) which enhance its sampling capability. Two of the beams, 1 and 3 predominantly contributes to the downstream velocity, (u) and one vertical (w_1) measurement of velocity, and beams 2 and 4 predominantly contributing to the cross stream (v) and second vertical (w_2) measurement of velocity. The addition of the 4th receiver and the collection of two independent measurements of vertical velocity permit a method for estimating the contributions of instrument and Doppler noise to estimates of Reynolds normal and shear stresses (e.g. Hurther and Lemmin (2001)). Furthermore, the Vectrino Profiler permits the simultaneous measurement of velocities within 35 one-millimetre-high sampling bins, yielding a 34 mm-high profile from 40 to 74 mm below the transmitter (Craig et al., 2011). However, this research only reports measurements collected in a 1 mm-high bin at the focal point of all four beams and the transmitter (i.e. at a height of 50 mm below the transmitter, for highest data quality since it is at the intersection).

It is worthy to note that the experiment made use of the latest version of the Vectrino profiler ADV (Vectrino II), which was configured to simultaneously measure flow velocities at 17 different distances from the transmitter at each of the chosen probe position as set with the trolley which was vertically beneath the transducer (oriented perpendicular to the flume bed). The 17 multiple positions were performed to generate multiple overlapping vertical profiles so that a single time-averaged profile encompassing most of the water column could be formed.

The velocity profiles were constructed by moving the Vectrino profiler in 10 mm increments from 50 mm above each bed surface until the water surface began to interfere with the transmitter. At each location, velocities were sampled at 100 Hz for 300 seconds. According to Chanson et al. (2007), raw ADV velocity data do not represent true flow turbulence unless it has been post-processed to remove spikes, Doppler noise and any filtering effects arising from the ADV sampling method. In the experiments, the acquired flow velocity data were post-processed in-house by the University of Leeds Sorby Laboratory team using an intelligent correlation threshold filter comprising of a phase unwrapping algorithm and the phase space threshold spike filter (see Thomas and McLelland (2015) for more details).

Errors arising from the use of the ADV which have been identified by earlier researchers to include mainly the Doppler noise and velocity gradient errors but these have also been observed not to have any significant effect on the turbulence analysis such as shear stress estimation (Lohrmann et al., 1994; Voulgaris and Trowbridge, 1998). However, precautions were taken to minimise instrument associated errors by following the suggestions of McLelland and Nicholas (2000), García et al. (2005) that measuring errors of the ADV can be controlled by the probe orientation, sampling frequency, instrument velocity range, and local flow properties.

4.4 Experimental Procedure

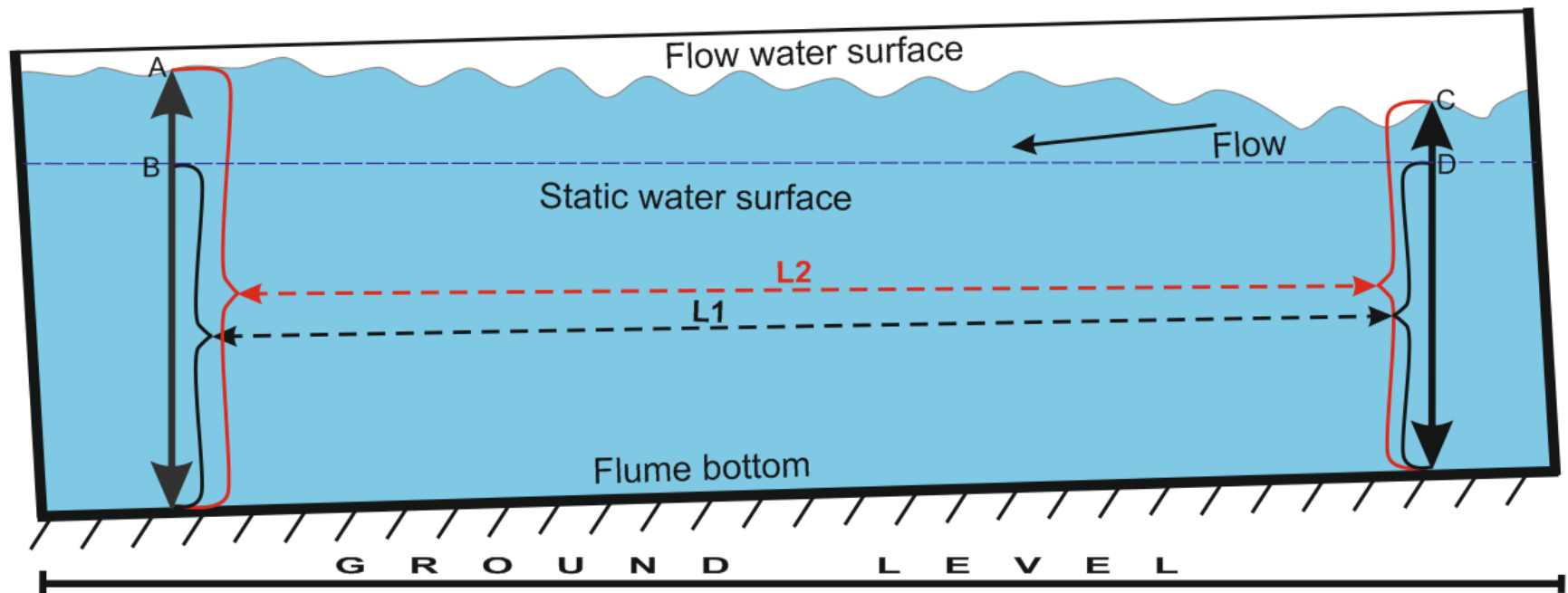
Soon after the flume was set up, clear water was pumped from an overhead tank into the flume and allowed to recirculate until a steady flow was achieved. The water level was carefully adjusted by varying the discharge rate until the water depth (flow thickness) in the flume tank was up to the desired flow height.

The slope of the flow surface was determined as shown in figure 4.6. The flume slope was adjusted using a hydraulic jack beneath the flume. This was done to check that the water surface slope was parallel to the flume tank floor. A manual estimation of the flow slope was done by measuring the height of the upstream and downstream ends of the water flow surface as well as their horizontal distance apart. The water depth was measured in two steps, first by taking the static water surface depth level which served as a reference (see figure 4.6). After the pump was switched on, the water levels at the same positions were measured again and the change in heights, since the static flow measurements gives the estimate of the flow slope.

It was not possible, to fully achieve a steady uniform flow in the experiments (as there were minor variations of about 0.5-1.0 mm in the flow depth across the flume). Care was always exercised to avoid hydraulic jump/vortex flow occurring along the flow path and especially at the upstream end of the flume by maintaining a discharge rate of $0.030 \pm 0.010 \text{ m}^3/\text{s}$. The initial flow speed was calculated from the volumetric discharge with respect to the cross-sectional area. This was varied for the different experimental flow cases (see table 5.1).

The instantaneous flow velocities were sampled using the Vetrino II three-dimensional, down-looking ADV profiler mounted on a transverse boom so that it can easily be moved between the sampling points in the flow. The first flow velocity sampling by the ADV Vetrino profiler was done at 50 mm above the flume floor (slab surface) and subsequently moved higher at 10mm interval in the flow until it became too shallow as the water surface interfered with the transmitter. For each run and instrument position, instantaneous velocities were sampled at 100 Hz for 300 seconds.

Each flow velocity profile consisted of six to thirteen sampling positions with over 30,000 velocity data obtained at each sampling point. The monitored signals were first transferred to a computer and later analysed by the Vetrino II software (see figure 4.3).



- A- Downstream flow height
- B- Downstream static height
- C- Upstream flow height
- D- Upstream static height
- L1 = Distance between upstream and downstream static surface
- L2 = Distance between upstream and downstream flow surface

Figure 4.7: Sketch diagram of how slope of flow was measured

4.5 Constraints of Experiment

This flume experiment was set up to investigate turbulence generation and the local influence of boundary conditions such as roughness on sediment grain transport. Overall objective, however, was to generate enough velocity fluctuating data that would be used to test the current mixing length theory of turbulence using a clear water flow.

However, it is known that an improperly designed flume could impede turbulence generation which could impact on the realisation of set objectives. There were unavoidable constraints encountered in the course of the experiments.

First, the dimensions of the available flume tank used for this experiment was approximately 8.5m long, 0.4 deep and 0.3m wide. This falls short of the recommendation by experts including Williams (1970), who advocated that as a general rule, “the width of the flume should be at least 4 times the water depth”. The implication of using a smaller size flume may be far reaching as there could be a high level of wall interference and complications which may affect the velocity distribution result generated. In addition, the flume tank height limited the volume of water that it could contain, and this directly affected the number of velocity profiles that could be produced from a single flow with the array of flow velocity measurements. This issue was however checked by positioning the ADV probe at least 50mm away from the flume tank floor when taking measurements, though the specifications of the ADV Nortek II equipment recommended 10.0mm from the tank floor and at least 5.0cm below the upper water surface (Rusello and Allard, 2012).

As reported in section 4.2.3, the flume tank had a metallic floor. This type of flume floor is expected to impact on the accuracy of velocity measurements from the ADV.

Hence there was the need to provide alternative non-metallic materials to cover the floors and in this case, concrete and gravelly slabs were used. The actual roughness level of the fixed gravel and concrete slabs used to cover the flume tank floor could not be determined as there was no equipment to adequately carry out such measurement at the time of investigation. Also, constraints of using only two types of bed floor simulated roughness conditions was a limiting factor in the research. The research would have been more robust with slabs having some bedforms features such as ripple marks and perhaps slabs that could simulate a ripple-bed floor condition to enable us to make more useful comparison on the effect of floor roughness on turbulence intensity generation.

With regards to measuring the flume tank and water surface slope, it was very challenging conducting iterative adjustments between the flume slope (using the hydraulic jack) and the discharge level to get a good water surface slope.

4.6 Chapter Summary

The major conclusions that can be drawn from this chapter are as follows:

1. Clear water flow experiments were carried out in a slightly tilting rectangular glass-sided laboratory flume, approximately 8.5m long, 0.3m deep and 0.3m wide instrumented with a three dimensional (3-C) Acoustic Doppler Velocimeter (ADV) to investigate turbulence in a quasi-steady flow.
2. The experiments comprised of six flow cases of 45 flow runs carried out under defined flow conditions with over 30,001 flow velocity measurements taken for each run.
3. To avoid any unnecessary interference between the flume tank and the measuring instrument (the ADV), slabs made of smooth concrete and rough gravel was used to cover the flume tank bottom.
4. The influence of bed floor roughness on turbulence in natural flows was investigated using fixed concrete slabs and fixed gravel slabs respectively.

5 Chapter Five; Results

Presentation of Raw Results and Data Analysis.

5.1 Introduction

This chapter presents the results of the flume experiment and analyses the large dataset comprising instantaneous flow velocities measured against flow height using a modern 3-C Acoustic Doppler Velocimeter in clear turbulent flow experiments from 45 flow runs in six different flow cases. The huge amount of velocity data generated from the flume experiment will be analysed and used for the first time to validate the Mixing-length theory of turbulent suspension.

5.2 Flow Velocity Measurements

5.2.1 Experimental Conditions

All the flume experiments were grouped into six flow cases with each flow case characterised by a set of flow conditions earlier described in the preceding chapter. Table 5.1 provides a summary of flume and hydraulic data that was used in this research such as the flume tank floor character, flume tank slope, the mean discharge rate of clear water entering the flume tank as well as the flow height.

Table 5.1: Summary of flume hydraulic data for all six experimental cases

Flow conditions	Case 1	Case 2	Case 3	Case 4	Case 5	Case 6
Type of floor	Concrete	Concrete	Gravel	Gravel	Gravel	Gravel
Flow height to roughness (m)	0.92	0.18	0.192	0.192	0.14	0.14
Flow area (m ²)	0.058	0.054	0.058	0.058	0.042	0.042
Flume average slope	0.053	0.071	0.079	0.088	0.132	0.141
Mean discharge rate (l/s)	21.6	39.6	24.6	31.3	21.6	33.19
Mean discharge rate (m ³ /s)	0.022	0.04	0.025	0.031	0.022	0.033
Mean flow velocity (m/s)	0.36	0.551	0.333	0.512	0.443	0.616

5.2.2 Velocity-depth profiles

Velocity profiles for all six clear water flow cases as computed based on averaging of the instantaneous velocity measurements are presented in figure 5.1 below. The profiles show a velocity maximum near the water surface and a velocity minimum near the base of flow.

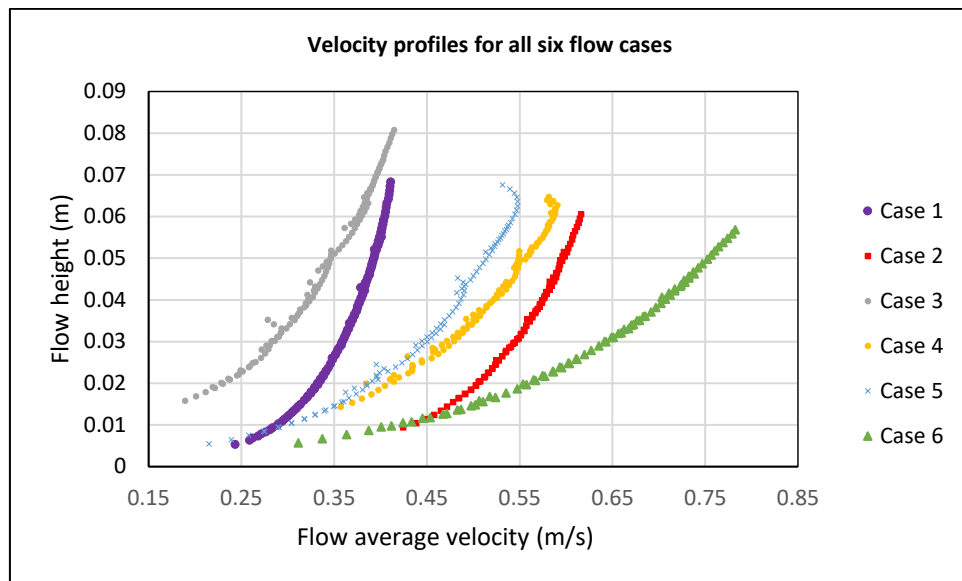


Figure 5.1: Vertical velocity profiles relative to flow height for flow cases 1-6

5.2.3 Instantaneous streamwise velocity- time series

Figures 5.2 and 5.3 show the instantaneous streamwise velocity-time series for both concrete and gravel floors for the flume experiments. The instantaneous streamwise velocity, here implies the sum of the time-averaged velocity and the fluctuating velocity components in the streamwise direction (see equation 3.17). Separate profiles correspond to different heights of the velocity sampling device (ADV) above the tank floor and different experimental flow conditions.

The quality of data generated was checked to ensure presence of less “spikes” or “blips” during initial processing. Spikes are artefacts occasioned by noise mainly

from the equipment proximity to the metallic floor of the flume. These “spikes” or “blips” were removed by increasing the cut-off values for real data from instrument configured value of 30% to 40 %. From figures 5.2 and 5.3, it is observed that the data spikes mostly occurred proximal to the base of flow. Further processing of velocity data was done in-house by the Sorby Fluid Dynamics team, University of Leeds. Table 5.2 below, provides the statistics of the velocity data showing how scattered (or consistent) the measured velocity is for all flow cases.

Table 5.2: Descriptive statistics of measured velocity for all six flow cases

Descriptive statistical data for all six flow cases investigated						
	Case 1	Case 2	Case 3	Case 4	Case 5	Case 6
Floor type	Concrete	Concrete	Gravel	Gravel	Gravel	Gravel
Flow thickness	0.234	0.222	0.234	0.234	0.182	0.182
Velocity analysis						
Mean velocity (m/s)	0.359945	0.551131	0.332889	0.511534	0.442539	0.616385
Standard Error	0.003887	0.005038	0.005402	0.006208	0.008732	0.013348
Mean velocity (m/s)	0.371767	0.562076	0.339471	0.5251	0.46449	0.642842
Standard Deviation	0.040957	0.046177	0.056918	0.061765	0.08511	0.118636
Variance	0.001678	0.002132	0.00324	0.003382	0.007244	0.014075
Kurtosis	-0.04681	-0.23866	-0.64554	-0.58372	-0.42589	-0.40918
Skewness	-0.89354	-0.72081	-0.53037	-0.63414	-0.70948	-0.67656
Range	0.167648	0.191836	0.22527	0.233562	0.332815	0.47102
Minimum	0.243438	0.424169	0.189146	0.356796	0.214919	0.311517
Maximum	0.411085	0.616005	0.414416	0.590358	0.547734	0.782536
Sum	39.95392	46.29499	36.95063	50.64188	42.04125	48.6944
Count	111	84	111	99	95	79

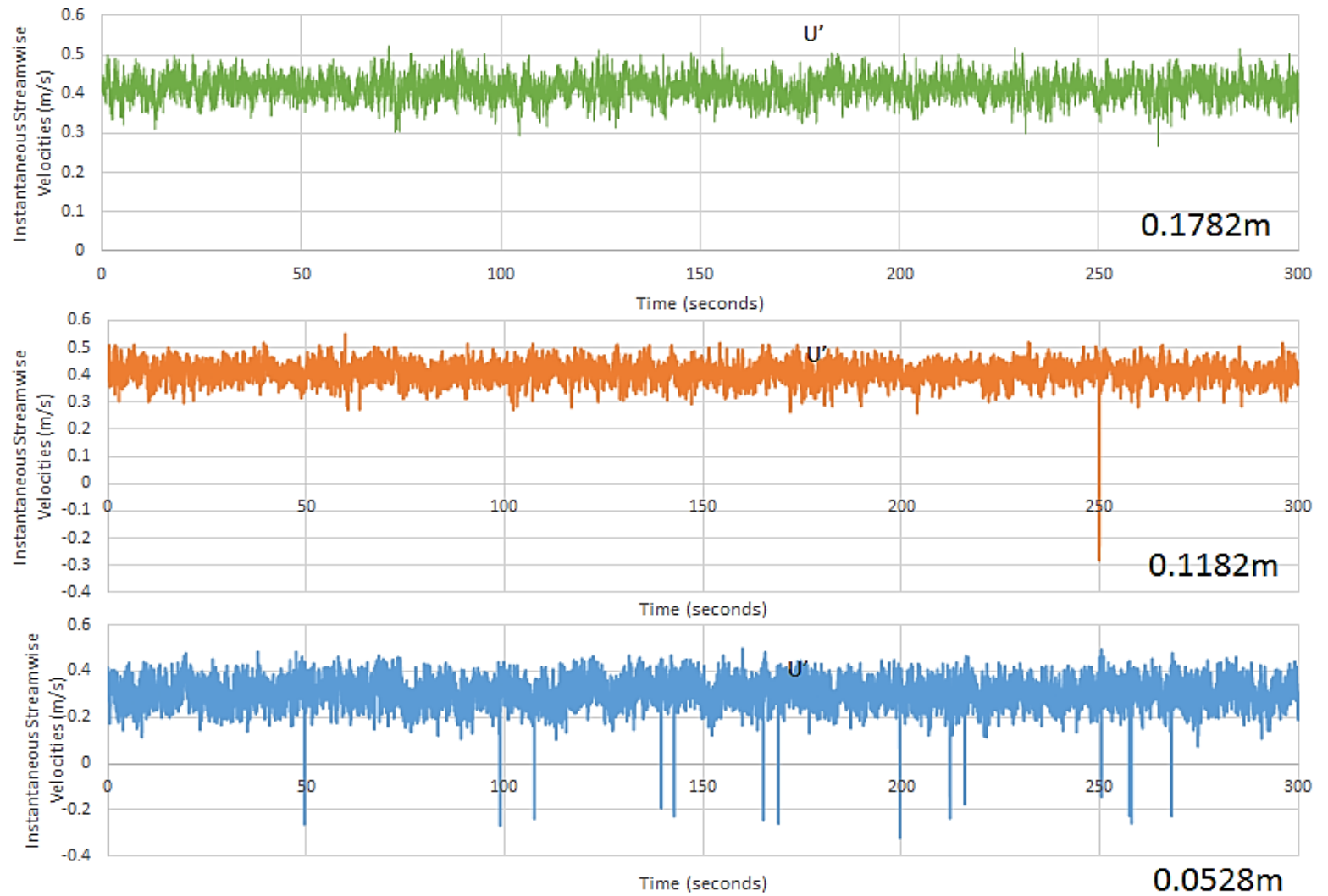


Figure 5.2: Instantaneous velocity –time series for case 1(Concrete floor)

Occasional “blips” in this data were removed during processing by increasing the cut-off values until the blips reduce. Bold numbers give height above tank floor at which measurements were taken. Note that the fluctuations around the mean show the degree of turbulence in the flow and that this is consistent at any given height. Also note that the mean velocity increases with height whilst the fluctuation strength drops with height.

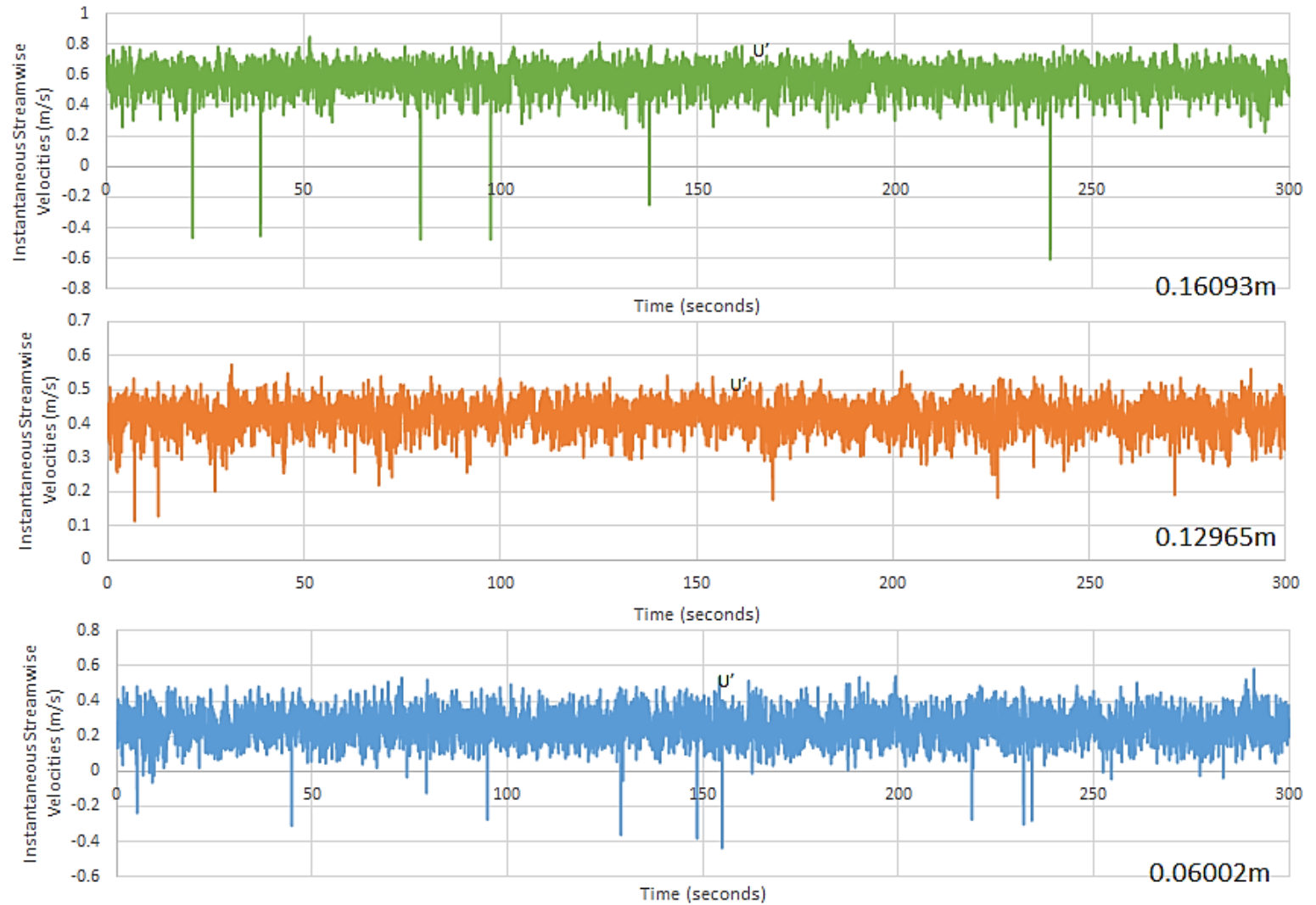


Figure 5.3: Instantaneous velocity –time series for case 1(Gravel floor)
 Occasional “blips” in this data were removed during processing by increasing the cut-off values until the blips reduce. Bold numbers give height above tank floor at which measurements were taken. Note that the fluctuations around the mean show the degree of turbulence in the flow and that this is consistent at any given height. Also note that the mean velocity increases with height whilst the fluctuation strength drops with height.

5.3 Shear Stress Estimates

Results of shear stresses obtained by traditional methods of bed slope, Law-of-the-Wall and Reynolds decomposition for the quasi-steady flow are presented below. These shear stress estimates will later be used to validate the mixing-length turbulence theory.

5.3.1 Bed slope method

With an assumed gravitational acceleration of 9.81, equation 3.24 and 3.25 (chapter three) is used to estimate the shear velocity. Shear stresses are further determined and are presented in table 5.1 below. An important observation is that the shear stresses increases with increase in bed slope.

Table 5.3: Shear stress estimates using the bed slope method

Flow Case	1	2	3	4	5	6
Flow thickness (m)	0.2340	0.2220	0.2340	0.2340	0.1820	0.1820
Bed slope, S (degree)	0.0006	0.0010	0.0016	0.0016	0.0021	0.0021
Shear Velocity, m/s	0.0371	0.0467	0.0546	0.0606	0.0612	0.0612
Shear stress (Pa)	1.3764	2.18089	2.9812	3.6723	3.7454	3.7454
Uncertainty	±0.00012	±0.000126	±0.0002	±0.0002	±0.0002	±0.0001

5.3.2 Reynolds Shear Stress Method

Table 5.9 is the summary of the results of shear stress estimates from the Reynolds stress methods. Equation 3. 21 (in chapter three) was used to estimate the Reynolds stresses at the base of flow. Figures 5.9 to 5.15 shows the plots of $\overline{u'w'}$ against flow height for all six cases investigated.

Table 5.4: Shear stress estimates using the Reynolds Stress method

Cases	Case 1	Case 2	Case 3	Case 4	Case 5	Case 6
Reynolds Basal Stress (Pa)	0.5185815	0.9480	0.88963	2.06748	1.41377	3.07707
Uncertainty	±0.017597	±0.027	±0.0165	±0.0591	±0.0237	±0.0726

Equation 3.21 predicts that the vertical profile of the Reynolds shear stress should be a straight line. Also, the corresponding values at $z = 0$, should give the Reynolds basal shear stress (Pa) at the base of flow ($\langle u'w' \rangle$). Figures 5.4 to 5.9 below significantly corroborates this.

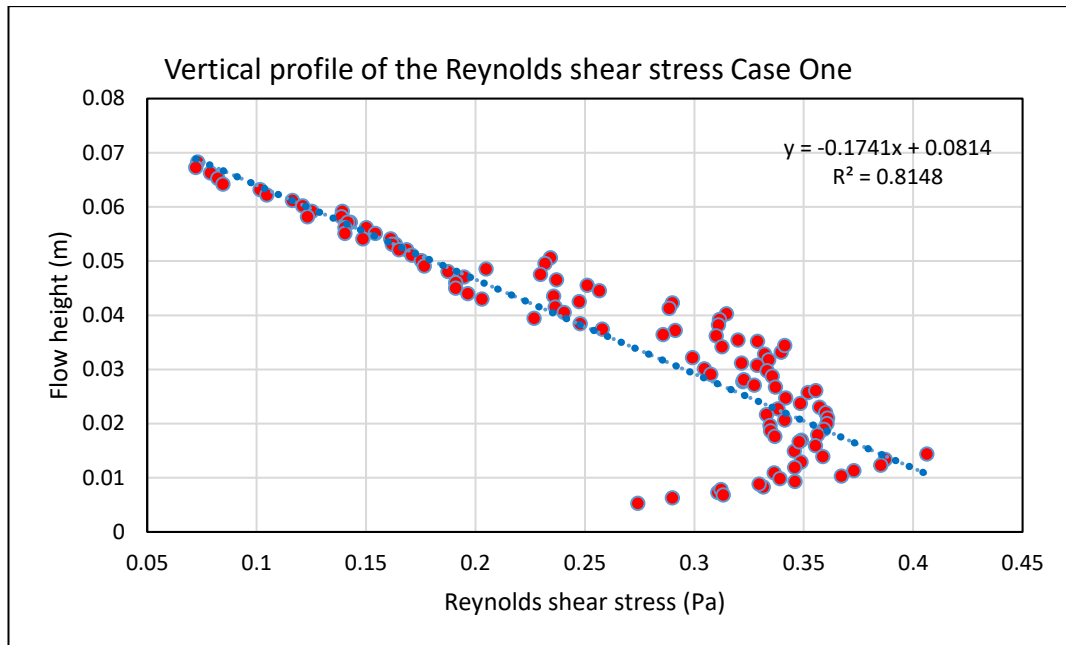


Figure 5.4: Vertical profile of the Reynolds shear stress, $\overline{u'w'}$, Case 1

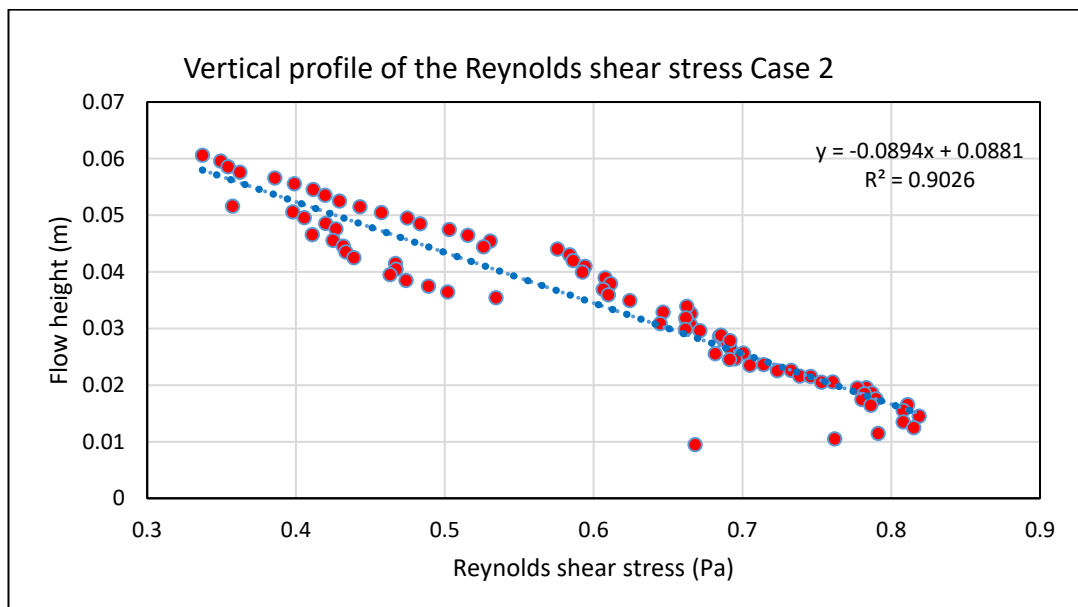


Figure 5.5: Vertical profile of the Reynolds shear stress, $\overline{u'w'}$, case 2.

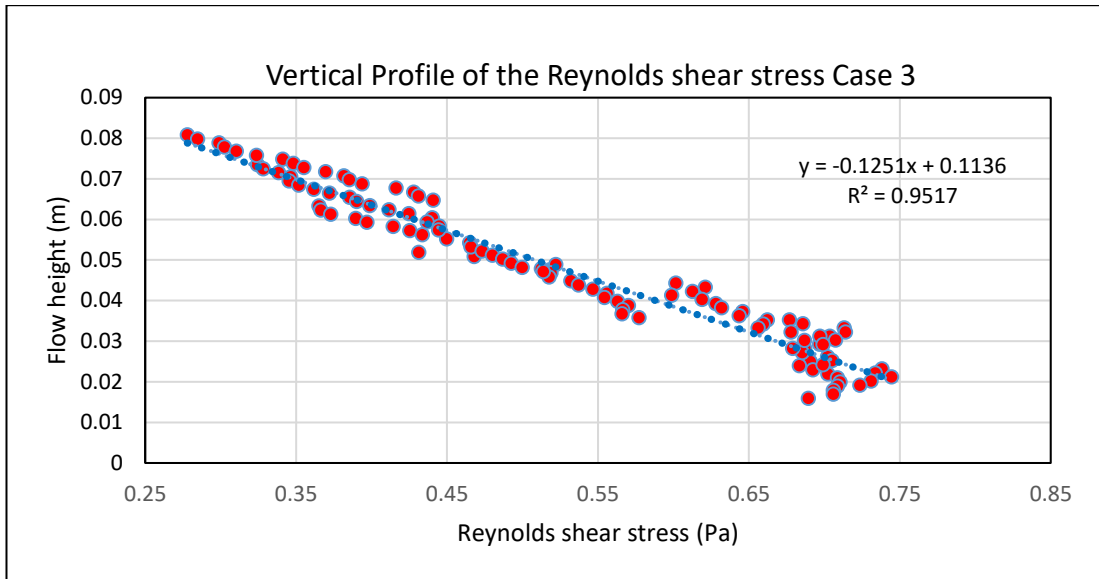


Figure 5.6: Vertical profile of the Reynolds shear stress, $\overline{u'w'}$, case 3

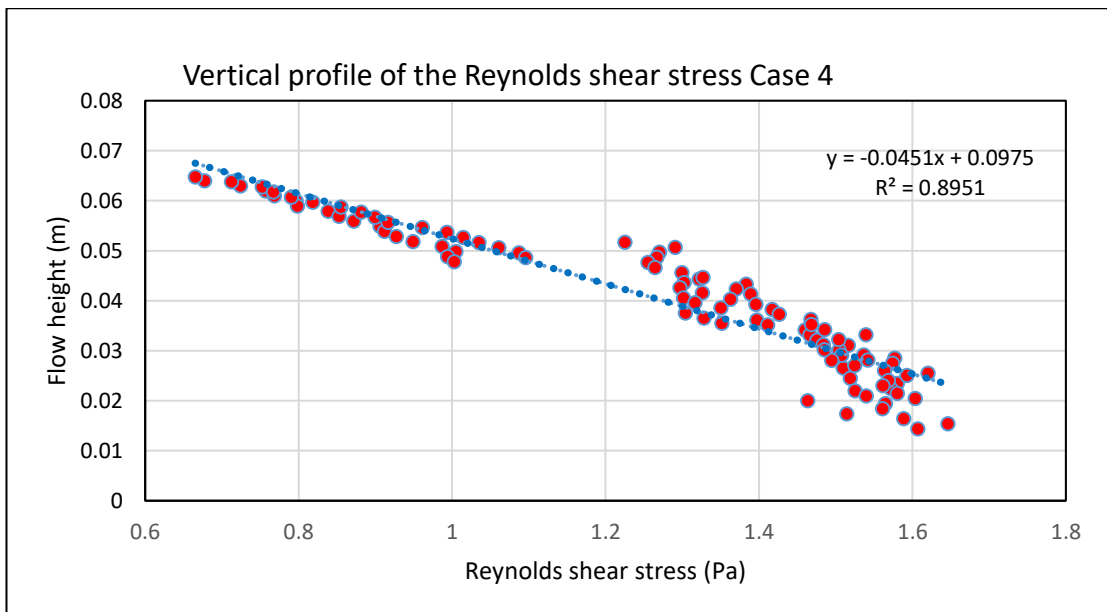


Figure 5.7: Vertical profile of the Reynolds shear stress, $\overline{u'w'}$, case 4

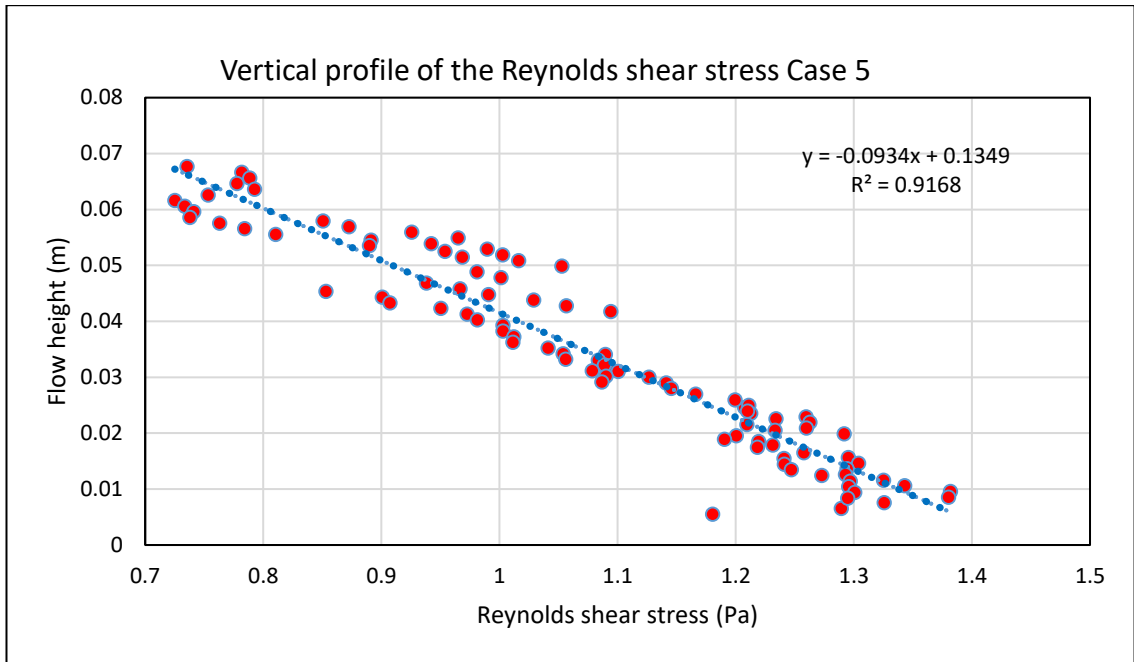


Figure 5.8: Vertical profile of the Reynolds shear stress, $\overline{u'w'}$, case 5

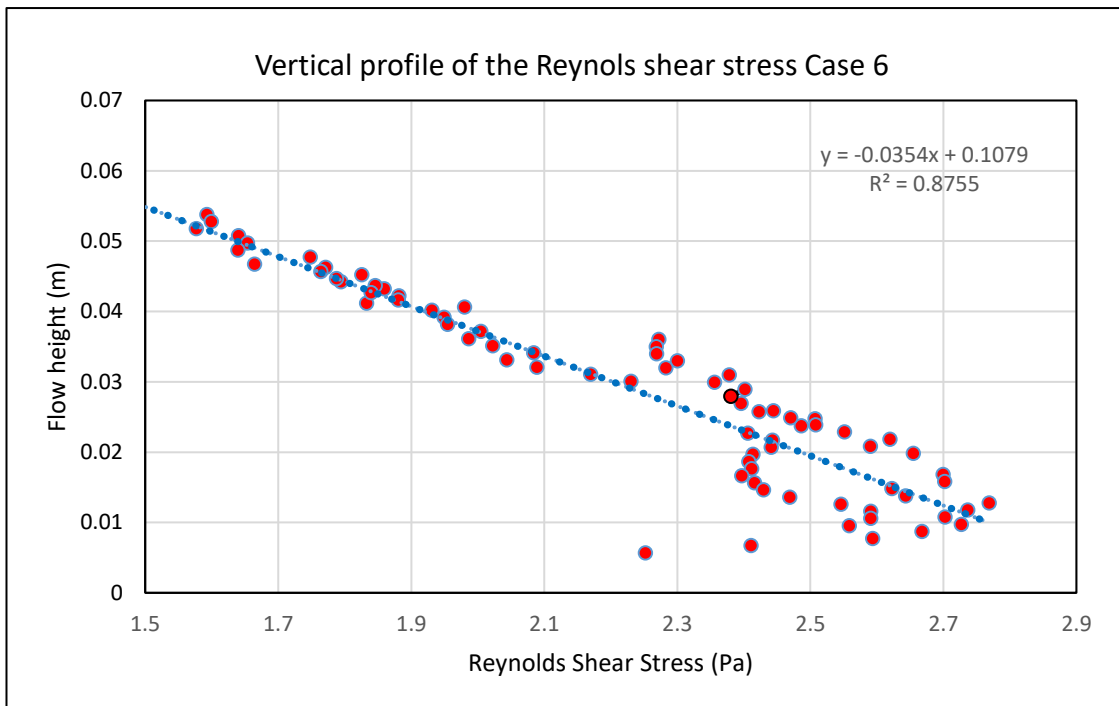


Figure 5.9: Vertical profile of the Reynolds shear stress, $\overline{u'w'}$, case 6

5.3.3 The Logarithmic Profile Method

Table 5.10 below, shows the analytical results of the shear stress estimates for all six flow cases using the log profile approach. More detailed analytical dataset comprising measured and modelled velocities as well as shear stresses for all six flow cases are presented in tables 9.3-9.8 (in Appendix).

A single graph of the velocity profiles for all six flow cases, produced by plotting \bar{u} against (z) was earlier presented in figure 5.1 above. All profiles show excellent curves signifying an increasing trend of \bar{u} with (z). For more clarity, Separate plots of velocity profiles for each flow case utilising both measured and modelled velocity are presented in figures 5.10 to 5.15 below.

Table 5.5: Shear stress estimates using the Logarithmic Profile

	Case 1	Case 2	Case 3	Case 4	Case 5	Case 6
Mean flow velocity (m/s)	0.359080	0.550810	0.332260	0.510980	0.441680	0.615150
u^*/k	0.065070	0.101417	0.132780	0.160400	0.134420	0.206920
Roughness height (z_0)	0.000120	0.000139	0.003574	0.001574	0.001096	0.001321
LoW basal shear stress (Pa)	0.033190	0.080630	1.382280	2.017030	1.416480	3.397750
Uncertainty	± 0.00286	± 0.01042	± 0.04384	± 0.07948	± 0.04112	± 0.04198

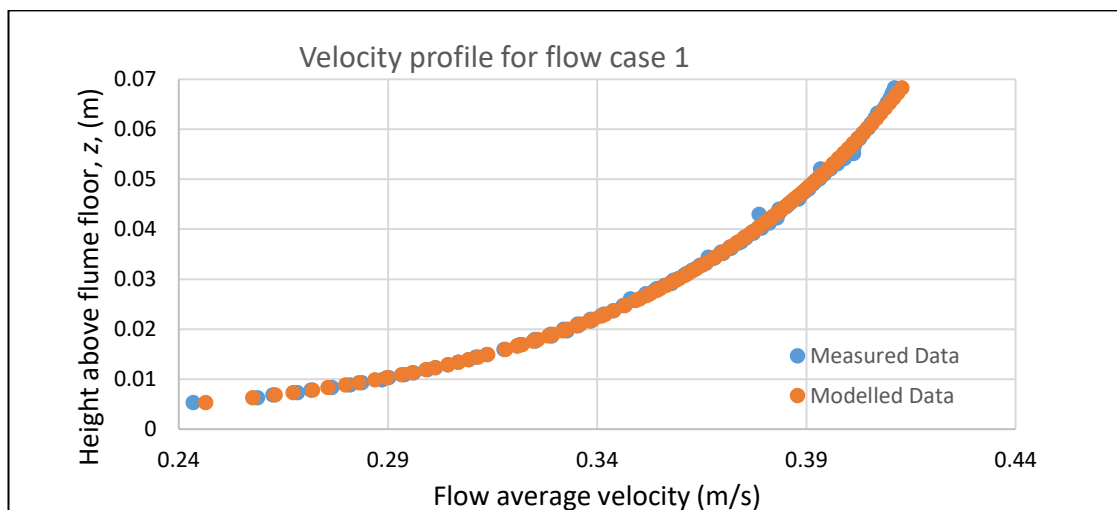


Figure 5.10: Velocity profile for flow case 1 (Measured vs Modelled dataset)

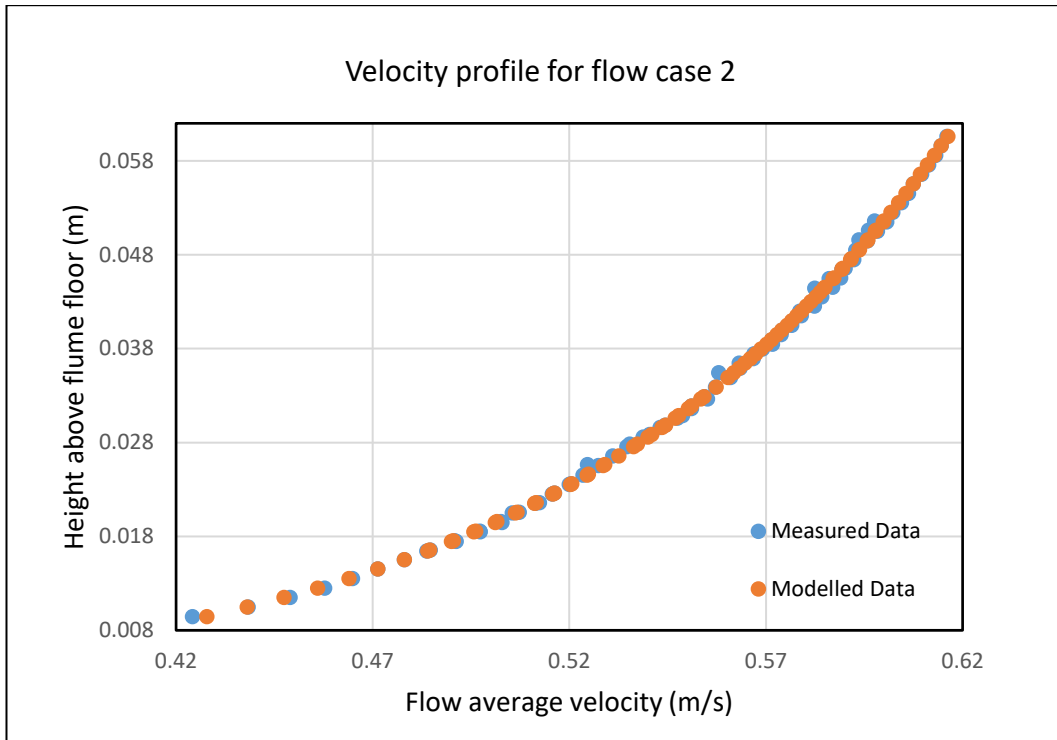


Figure 5.11: Velocity profile for flow case 2 (Measured vs Modelled dataset)

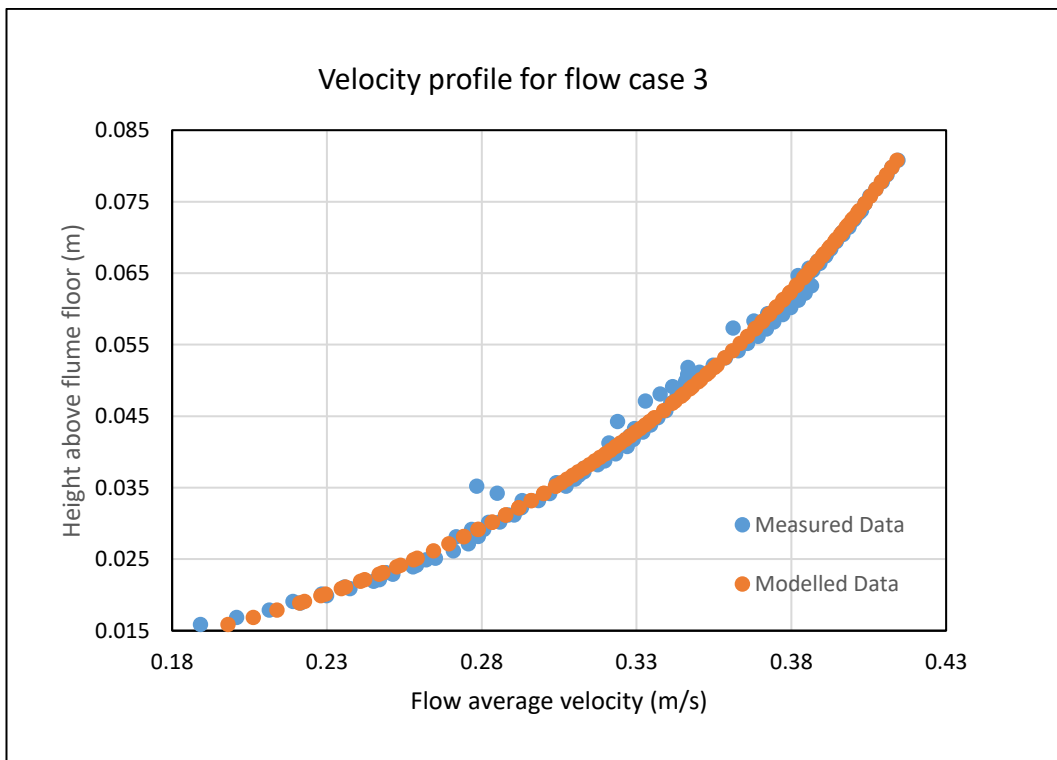


Figure 5.12: Velocity profile for flow case 3 (Measured vs Modelled dataset)

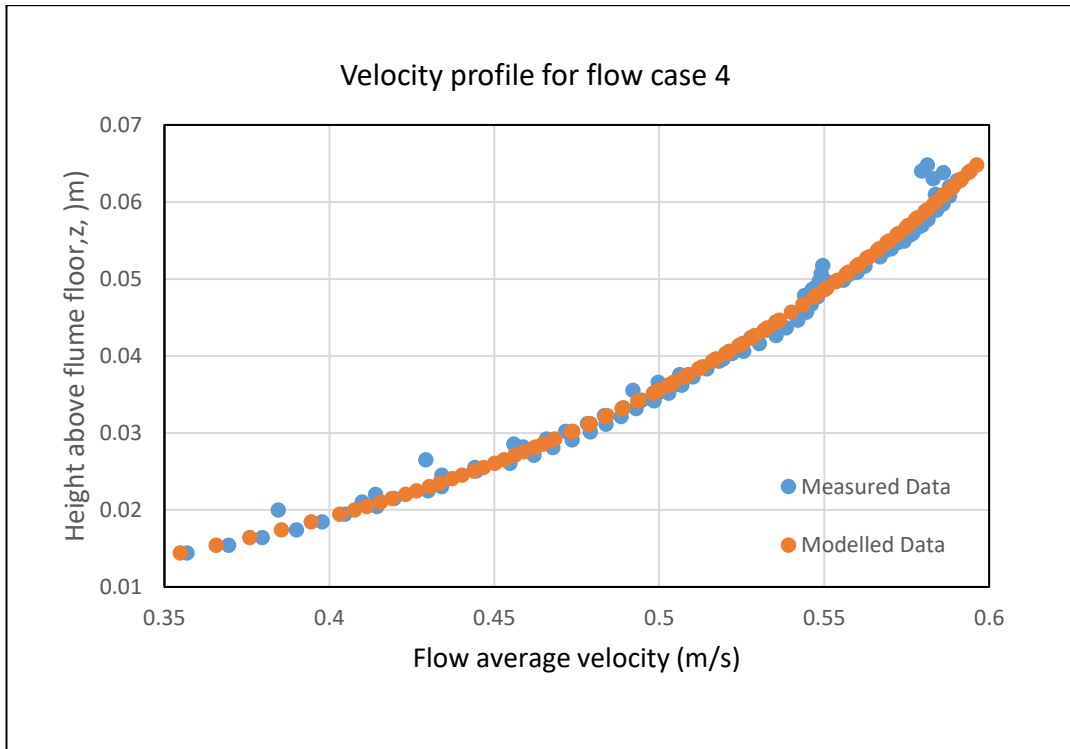


Figure 5.13: Velocity profile for flow case 4 (Measured vs Modelled dataset)

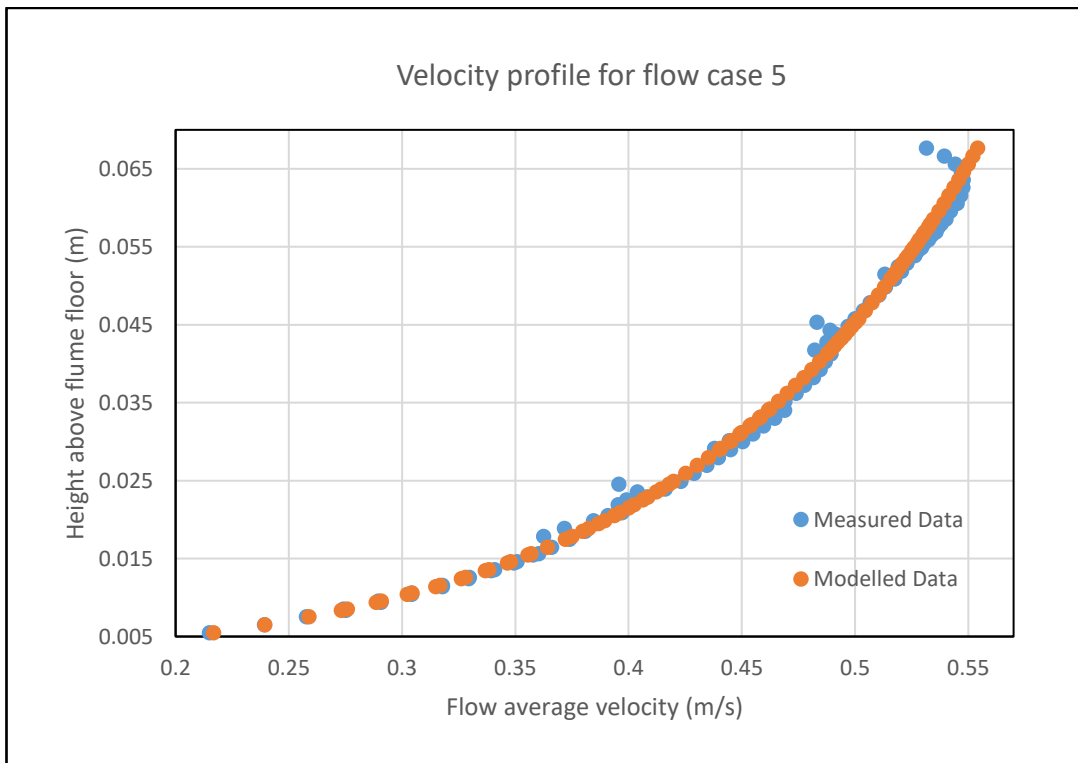


Figure 5.14: Velocity profile for flow case 5 (Measured vs Modelled dataset)

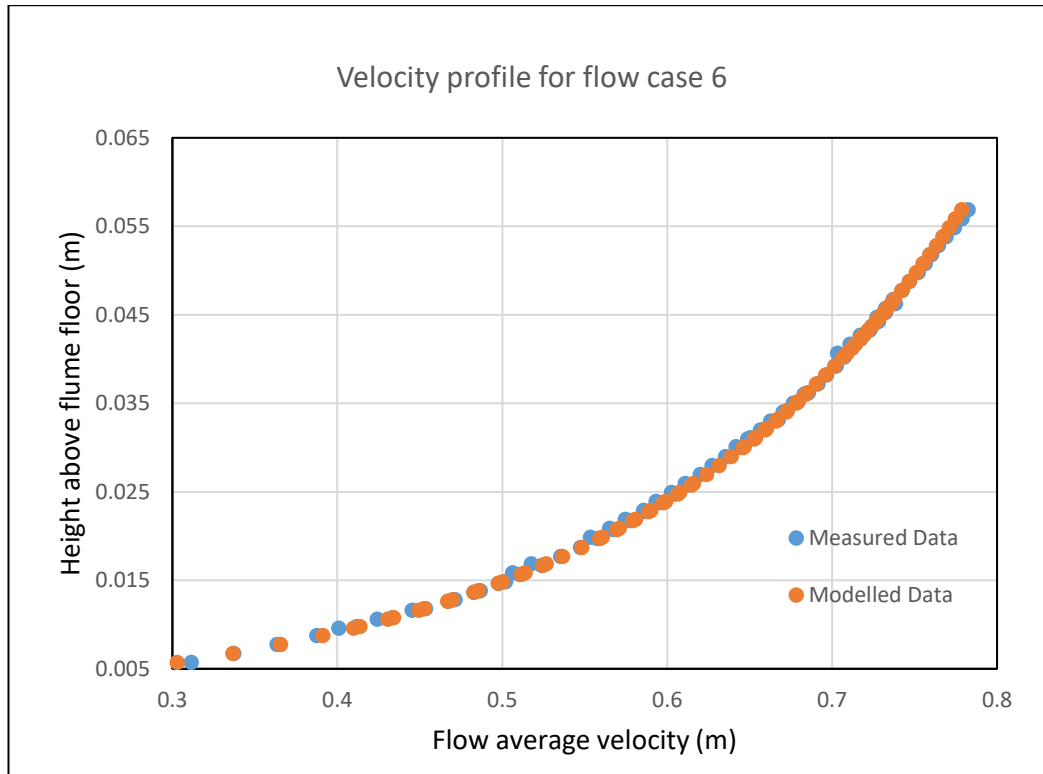


Figure 5.15: Velocity profile for flow case 6 (Measured vs Modelled dataset)

The gradient of the curves was used to determine the shear velocity, from which the basal shear stresses were estimated. Bed shear velocity was calculated by multiplying the slope of the straight line by the von Karman constant, κ . However, due to the large data involved, the *Regression* package in *Excel* was used to calculate the shear stress estimates. An assumed, κ value of 0.29 was used in the data analysis to minimise mismatch between the Law-of-the-Wall and Reynolds stresses.

Flow velocities at different depths were re-plotted against log of flow height ($\ln(z)$) as presented in figures 5.11 to 5.15, below. These plots show straight lines (see equation 3.10 – 3.11) and give the same information as earlier curves (figures 5.11-5.15). Also worthy of note in the figures is the observed significant agreement between measured and modelled velocities.

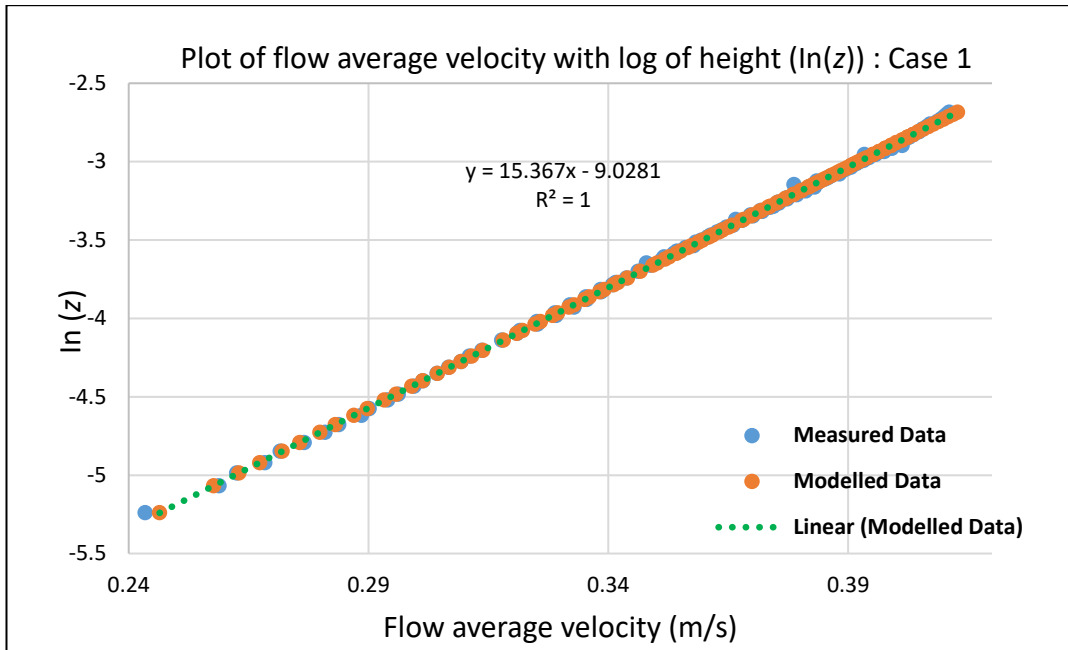


Figure 5.16: Plot of average velocity, \bar{u} vs log of height, $\ln(z)$, flow case 1

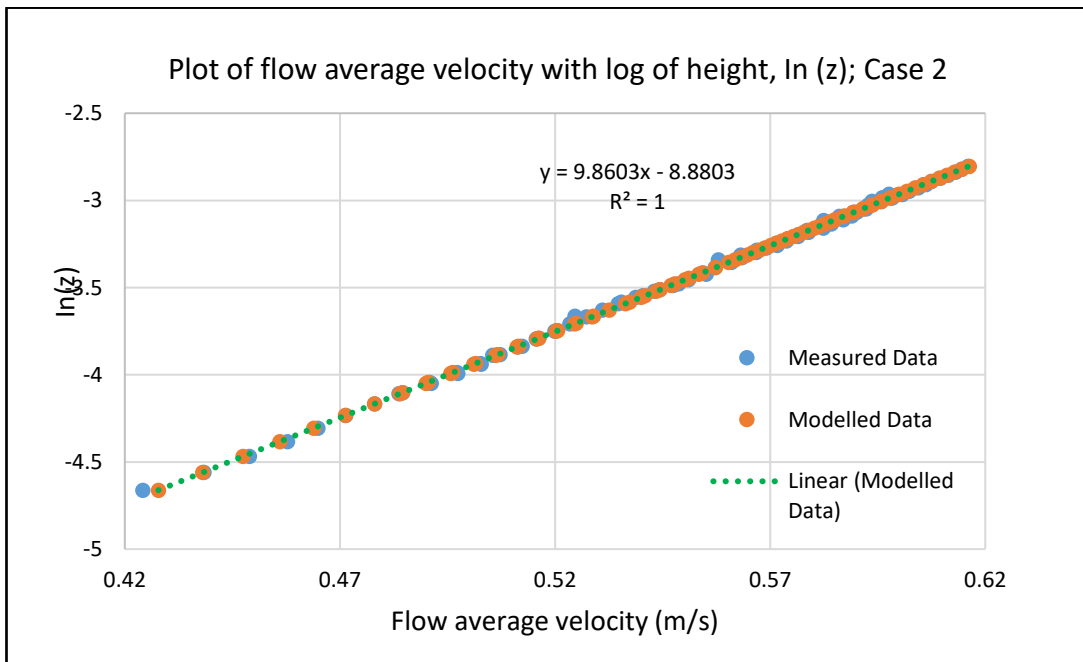


Figure 5.17: Plot of average velocity, \bar{u} vs log of height, $\ln(z)$, flow case 2

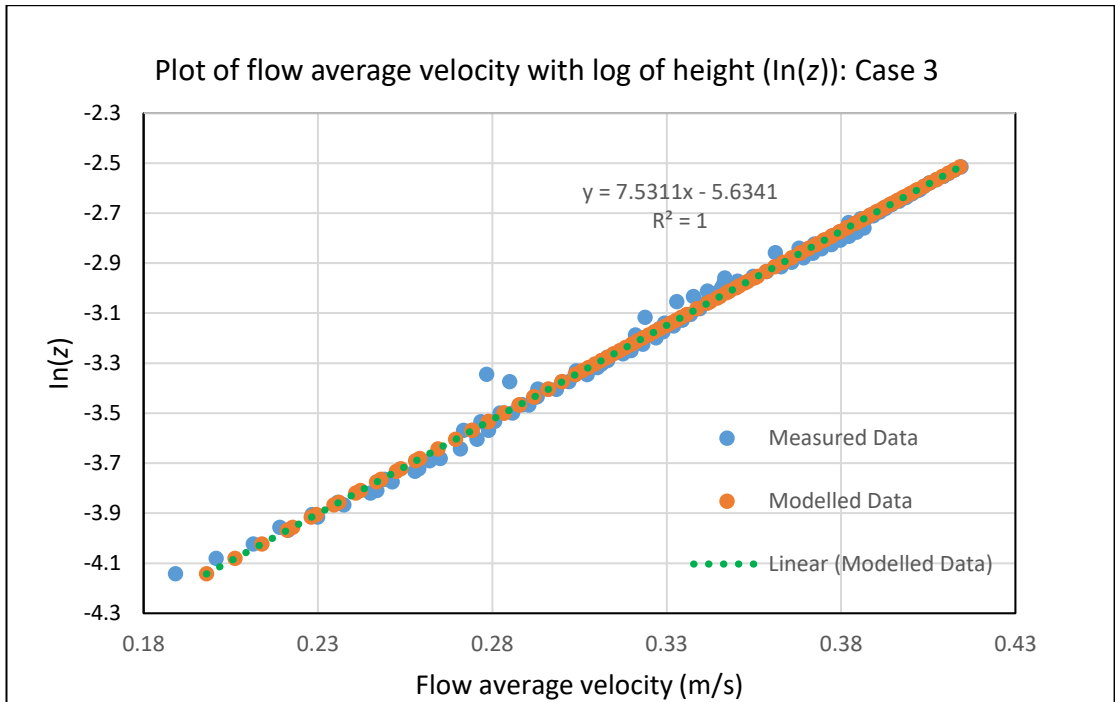


Figure 5.18: Plot of average velocity, \bar{u} vs log of height, ln (z), flow case 3

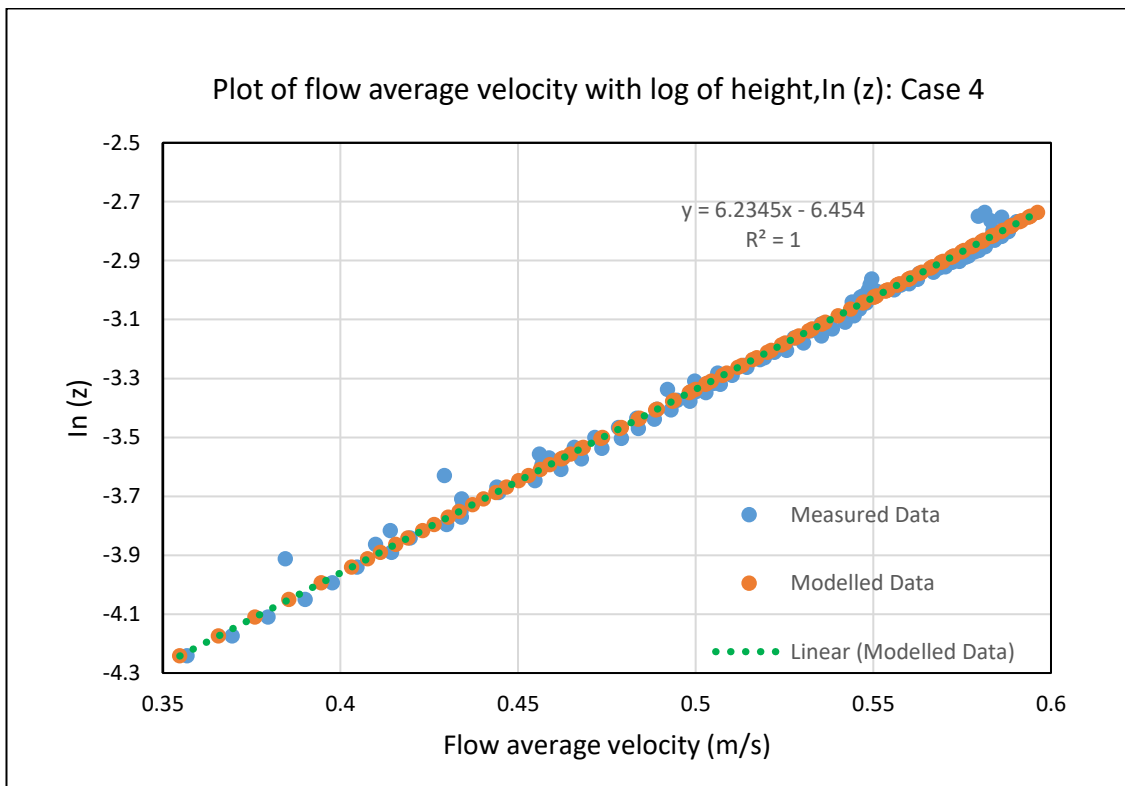


Figure 5.19: Plot of average velocity, \bar{u} vs log of height, ln (z), flow case 4

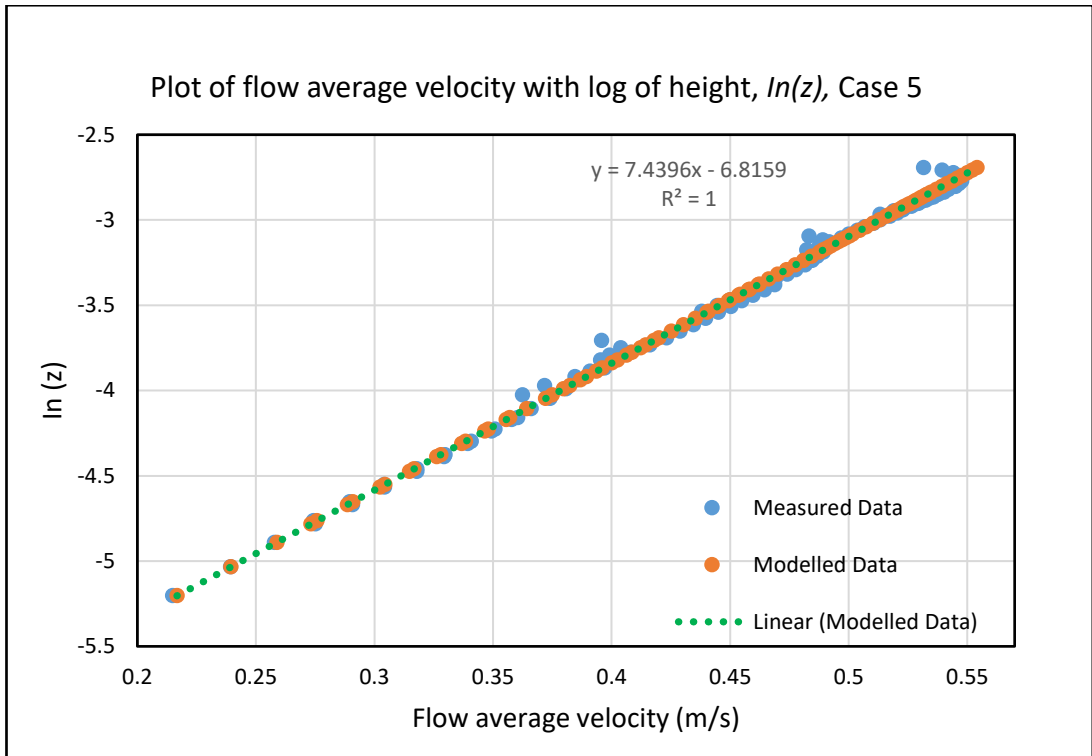


Figure 5.20: Plot of average velocity, \bar{u} vs log of height, $\ln(z)$, flow case 5

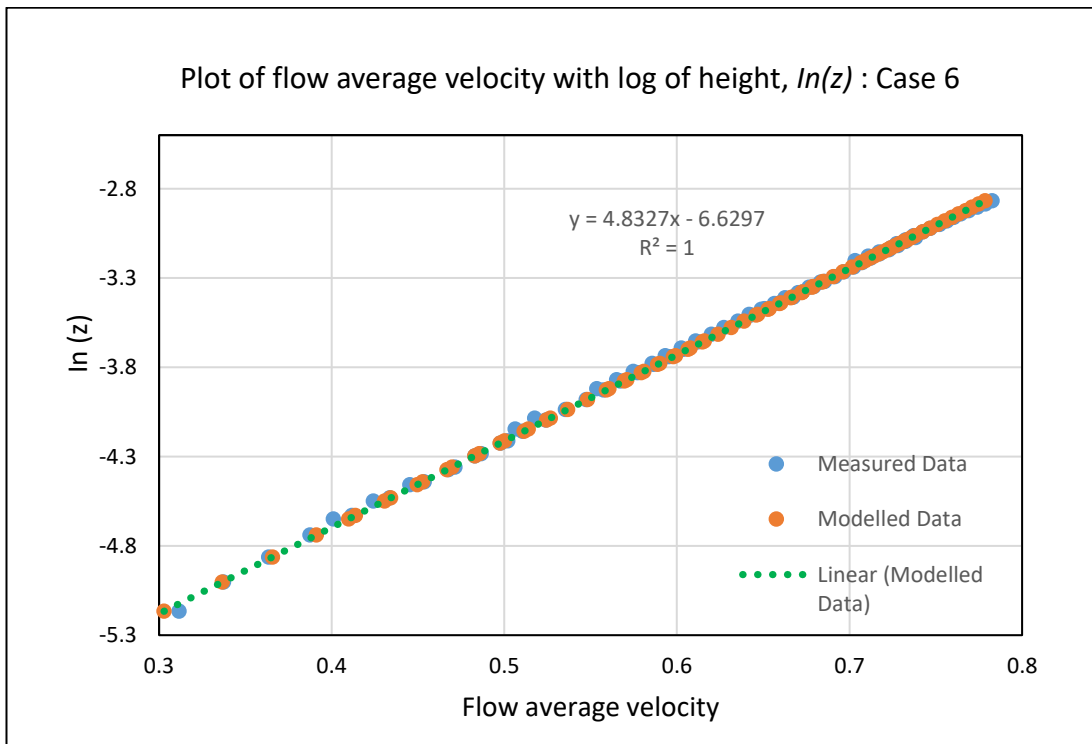


Figure 5.21: Plot of average velocity, \bar{u} vs log of height, $\ln(z)$, flow case 6

5.4 Comparing Measured Data with Model Predictions

5.4.1 Measured and Modelled Flow Velocities

Experimentally derived mean flow velocity data were matched with modelled velocities to determine how well both data agree as presented in figures 5.11 to 5.21. A regression statistical analysis using excel analytical tool confirmed a significant positive relationship between both velocities. Regression statistical analysis was further done including the R-squared and P-values for all six flow cases and results presented in table 5.6 below.

Table 5.6: Summary of Regression statistics of velocity data for all six cases

Summary of Regression statistics of velocity data for all six flow cases						
Regression statistics	Case 1	Case 2	Case 3	Case 4	Case 5	Case 6
Observations	112	85	112	110	96	80
Multiple R	0.99978	0.99962	0.997	0.995893	0.997855	0.999677
R-squared	0.99955	0.99925	0.99402	0.991802	0.995715	0.999354
Standard Error	0.00086	0.00127	0.00443	0.005615	0.005598	0.003029
P-value	3.10E-18	2.10E-131	3.80E-124	4.80E-104	4.10E-113	3.70E-126

The method used to derive estimates of modelled velocities was earlier explained in section 3.5. The approach is based on the Reynolds shear stress and Law-of-the-Wall or the von Karman-Prandtl mixing length theory. For example, using the Law-of-the-Wall approach, different measured velocities are plotted against flow height and then using the fitting procedure, estimates of shear velocities and roughness are derived from the slope and intercept of the computed regression equation. A Karman's constant of 0.29 was used in this thesis to get the best fit line

5.4.2 Reynolds Stress Validation

Equation (3.13 and 3.21) predicts that a plot of $\overline{u'w'}$ against height above base of flow should be a straight line with an intercept such that $\overline{u'w'}$ goes to zero. Figures 5.9 to 5.14 confirms this as the vertical profiles of the Reynolds shear stress, $\overline{u'w'}$ for each flow case align to a straight

line. The corresponding value @ $h=0$ also gives the Reynolds Basal Stress (Pa) at base of flow $\overline{u'w'}$.

Table 5.7 below shows the comparison of Reynolds shear stress estimates from both calculated and derived from as inferred from base of flow.

These results show similarity in the Reynolds stress calculated as well as that estimated from base of the flow as all data points align to a reasonable extent to a straight line as predicted by the theory.

Table 5.7: Comparison of calculated and predicted RSS estimates

Comparison of calculated and predicted Reynolds shear stress estimates						
Flow cases	Case 1	Case 2	Case 3	Case 4	Case 5	Case 6
Reynolds Basal Shear Stress (Pa) at base of flow($\langle u'w' \rangle$) @ $h=0$	0.48	0.9	0.88	2.02	1.39	3.1
Calculated Basal Reynolds Stress ($\langle u'w' \rangle$)	0.429	0.948	0.889	2.067	1.144	3.008

5.4.3 Law-of-the-Wall Validation

From equations (3.23), the Law-of-the-Wall predicts that a plot of \bar{u} against (z) should be a straight line. Figures 5.3(b) to 5.8 (b) shows very good agreement with this expectation. Also, as shown in the figures, model predictions such as the mean velocities are observed to be consistent with measured values as both are well aligned on the straight line. This good agreement between modelled and measured parameters confirms the validity of the Law-of-the-Wall in predicting flow parameters such as mean and shear velocity.

5.5 Hydraulic slope estimates from Reynolds Stress

Equations 3.26 and 3.27 (chapter 3) were used to determine the flow slope from Reynolds stress. The results are presented in the bar chart below (Figure 5.22). Comparison of slope estimates from Reynolds shear stress with directly measured slope estimates as in table 5.8, will be used to provide clues with regards to the flow conditions.

Table 5.8: Estimates of direct and Reynolds slope with their uncertainties

	Case 1	Case 2	Case 3	Case 4	Case 5	Case 6
Direct Slope	0.00061	0.001066	0.001176	0.001595	0.002121	0.002121
Uncertainty	0.00012	0.000126	0.000146	0.00016	0.00015	0.00012
Reynolds Slope	0.000477	0.00103	0.000775	0.002024	0.001	0.002692
Uncertainty	2.17E-05	3.71E-05	1.67E-05	7.00E-05	3.11E-05	0.0001074

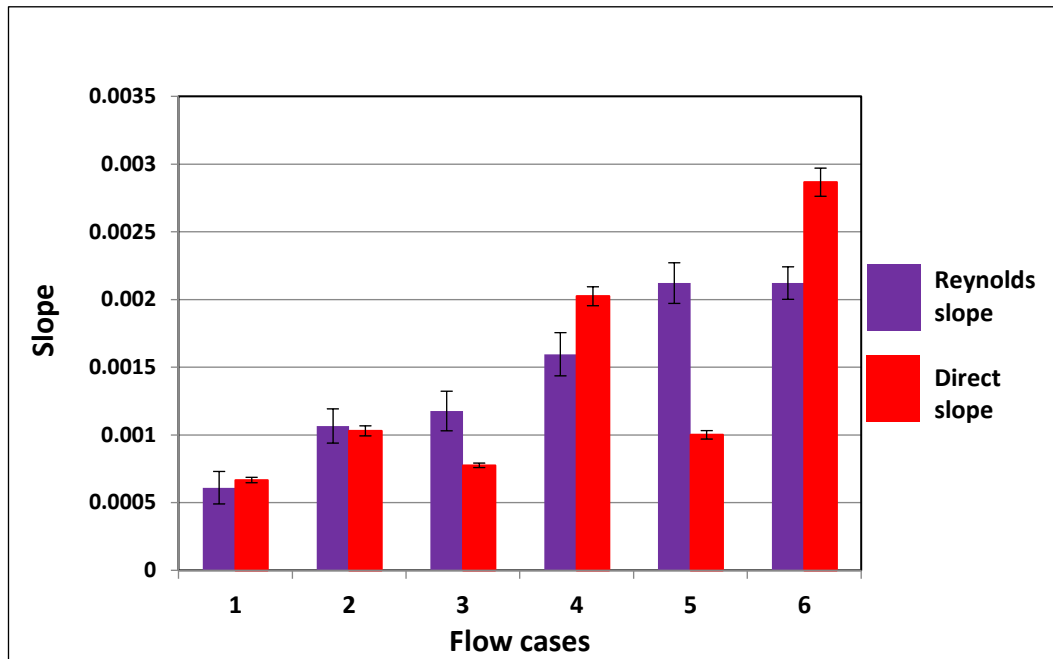


Figure 5.22: Comparison of direct slope with Reynolds slope estimates

5.6 Floor Surface Roughness and Drag coefficient

5.6.1 Surface Roughness

Bed roughness could significantly contribute to turbulence in a flow. The surface roughness height, z_0 , of the two types of slabs (concrete and gravel) used on the floor flume tank were, from the velocity profiles generated by the von Karman's turbulence model (described in chapter 3, section 3.2.2; see equation (3.25)). The roughness estimates and their uncertainties are presented in table 5.9 below.

Table 5.9: Estimates of roughness lengths for surfaces used in the experiment

	Case 1	Case 2	Case 3	Case 4	Case 5	Case 6
Floor type	Concrete	Concrete	Gravel	Gravel	Gravel	Gravel
Flow thickness (m)	0.19200	0.18000	0.19200	0.19200	0.14000	0.14000
Roughness (m)	0.00012	0.00014	0.00357	0.00157	0.00109	0.00132
Uncertainty	0.00003	0.00005	0.00023	0.00014	0.00008	0.00040

Also, Figure 5.23 below is a bar chart which shows the variation in roughness lengths between the concrete and gravel floors

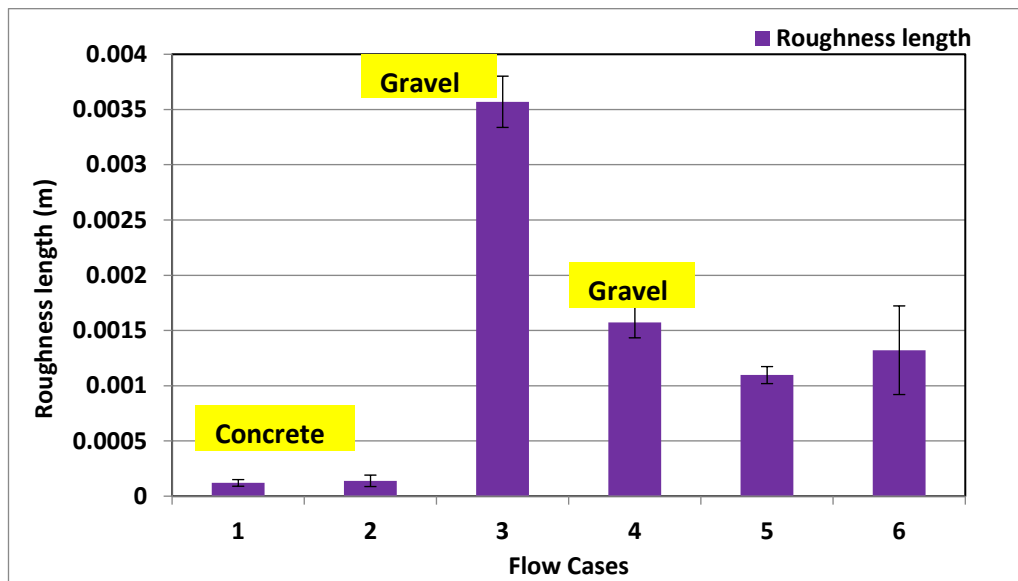


Figure 5.23: Comparison of roughness length (concrete and gravelly floors)

Note that bars 1 and 2 are the roughness lengths of concrete floors while bars 3 to 6 are for the gravelly floors

5.6.2 Drag coefficient

Equations 3.30 was used to estimate the drag coefficient, C_D , of the flows over both the concrete and rough gravel floor. Estimate of the basal shear stress (from the Law-of-the-Wall) was done by using the flume centre line average velocity due to effect of side-wall friction. (See equation 3.34). Table 5.10 below, shows the flume data and analytical results of the basal shear stress from both the Law-of-the-Wall and Reynolds Stress methods.

Table 5.10: Estimates of basal shear stress from LoW and RSS (flume center)

	Case 1	Case 2	Case 3	Case 4	Case 5	Case 6
Floor type	Concrete	Concrete	Gravel	Gravel	Gravel	Gravel
Ave. Velocity (m/s), from flume centre-line, V_{av}	0.415024	0.625290	0.396204	0.610113	0.517470	0.757540
Sq of Ave. Velocity from flume centre-line $(V_{av})^2$	0.172245	0.390876	0.156978	0.372238	0.267775	0.573867
LoW Basal shear stress (Pa)	0.331980	0.806370	1.382280	2.017020	1.416489	3.397750
Reynolds Basal shear stress (Pa)	0.429990	0.948060	0.889630	2.067480	1.413770	3.007960

Figures 5.24 and 5.25 show how the estimates of drag coefficient, C_D of the flows over smooth concrete and rough gravel floors were determined. Estimation was from the plots of the square of average velocity, V_{av} and the shear stress obtained from the Law-of-the-Wall (Log profile) as well the Reynolds shear stress methods respectively. However, consideration was on comparing the obtained results from the two methods as presented in table 5.11

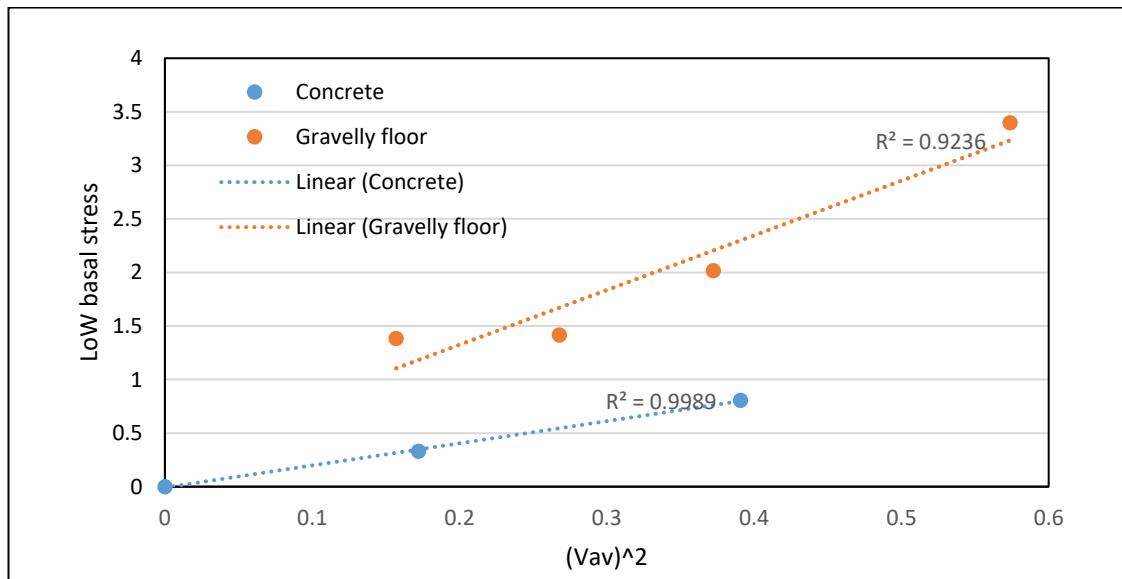


Figure 5.24: Drag Coefficient estimates from Law-of-the-Wall. The gradients of the straight line gives the estimate of C_D

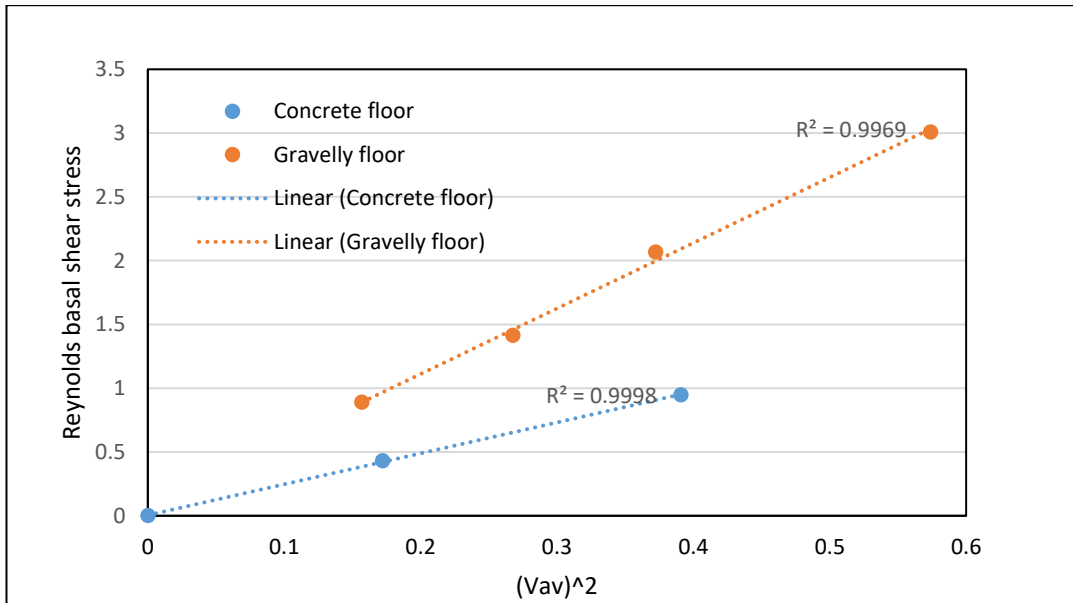


Figure 5.25: Drag coefficient estimates from Reynolds Stress

Table 5.11: Comparison of C_D estimates from LoW and Reynolds Stress

Drag Coefficient, C_D Estimates	Concrete base	Gravel base
Law-of-the-Wall	2.0405	5.8433
Reynolds Stress	2.4364	5.3418

5.7 Linking Turbulence and Sediment Grain Suspension

The foregoing experimental results all concern relationships between different estimates of turbulent fluctuation magnitude. However, in this section we focus on the capacity of a turbulent flow to maintain sediment particles suspension by turbulence. Turbulent suspension occurs when the vertical velocity fluctuations, near the flow base exceed the fall velocity (Bagnold, 1966). Characterizing these fluctuations by their root mean square (*rms*) value then gives a suspension criterion as in equation (3.37). Here, attempt is made here to test this suspension criterion and the result is presented in figure 5.26 below.

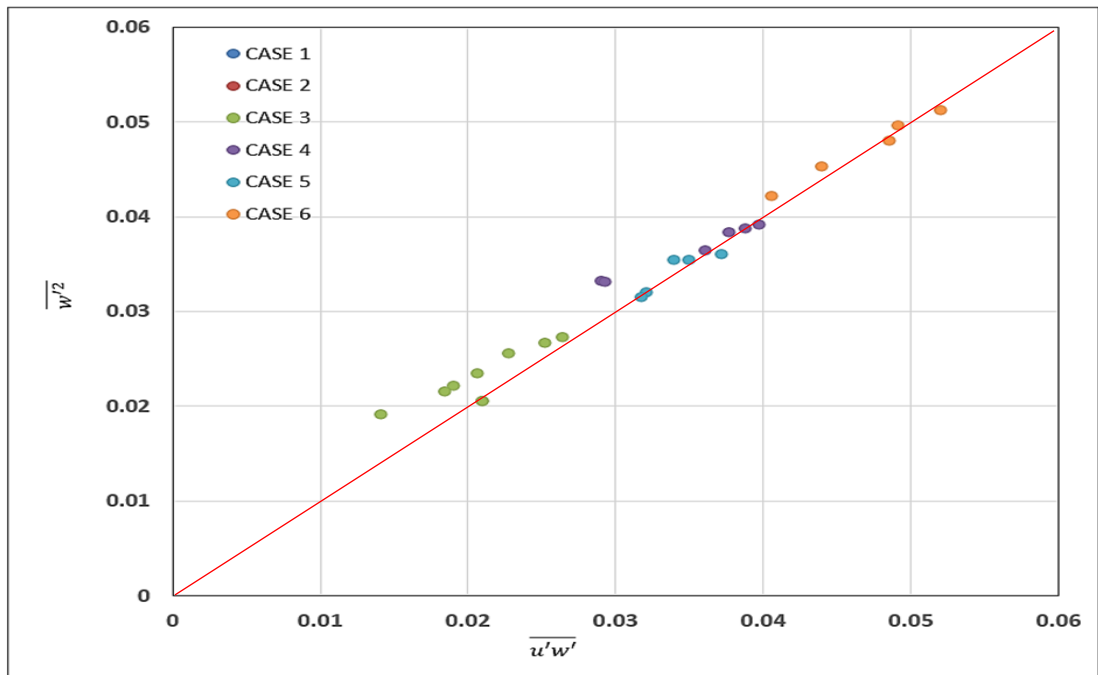


Figure 5.26: Comparison of vertical Reynolds normal stress, $\overline{w'^2}$, to $\overline{u'w'}$

Equation (3.41) implies that these should be equal and hence plot along the red line.

The key assumption of the theory therefore, is that equation (3.37) holds true (i.e., that the vertical rms velocity variations, $\overline{w'^2}$, are approximately the same as $\overline{u'w'}$ and that, therefore, the shearing velocity is an estimate of the maximum fall-velocity consistent with suspension).

This assumption was tested using data from the flume-tank experiment. Figure 5.26 shows a plot of $\overline{w'^2}$, against $\overline{u'w'}$ for the data from all six experimental set-ups. Figure 5.26 makes it clear that this is an excellent approximation and that, therefore, the suspension criterion of equation (3.37) is valid.

5.8 Chapter Summary

From the results analysed, the following key conclusions can be made:

- Modelled and measured flow velocities show a significant positive relationship with an statistical derived R-squared value of almost unity.
- Basal shear stress estimates obtained from the Law-of-the-Wall and Reynolds stress show reasonable agreement suggesting reliability of the Mixing Length turbulent suspension theory. Drag coefficient estimates obtained from both methods also show a significant correlation.
- The turbulent suspension theory has been supported by the good fits of measured data to predictions of the Law-of-Wall, good fits to the predictions of RANS as well as the good fits of $\text{stress} = C_d \cdot v^2$.
- Basal shear stress is attenuated by increased bed roughness
-

**Application of the Turbulent-Suspension Model to
Turbidity Current Flows in Agadir Basin, NW Africa.**

6.1 Introduction

This chapter presents a novel attempt to understand controls on long run-out turbidity current flows transporting coarse grains and mainly supported by flow turbulence using both field-scale data and numerical modelling approach. The case study is the flow that deposited Bed A5 in Agadir basin, offshore Morocco, where sands were reportedly transported and deposited by a relatively thin flow near the bed (Talling et al., 2007; Stevenson et al., 2014). It is unclear if it is possible for a thin flow to transport sand across the over 250 km wide Agadir basin from the far Moroccan margin without its settling. Flows moving sediment grains near the bed are mainly controlled by the size of grains in the flow, terminal settling velocities, flow thickness and turbulent accelerations (Bagnold, 1966; La Porta et al., 2001).

This work seeks to re-create the flows transporting sediment grains into the Agadir basin and establish if turbulence can singly act to suppress the settling of sand grains in the turbidity current flow, although suggestions of multiple support mechanisms such as grain-to-grain interaction (as in debris flow origin, Talling et al., 2007) has been proposed. Since there is apparent lack of debris flow deposit features (giant scours and minimal deposition) in Bed A5 deposits and evidence of fast flow velocities, sands are expected to be mainly supported by turbulence. This study applies a simple 2-D depth-averaged analytical model, developed by Waltham et al., (2008), using algorithms of Reynolds-Averaged Navier Stokes (RANS) as well as the Chezy equations, based solely on turbulence-suspension theory to carry out this novel investigation.

The following goals and questions will be addressed by this research:

- To understand, firstly, whether unusually detailed field measurements of long run-out turbidity currents can be replicated by a numerical model?

To a first order, is it possible to re-create the extent, thickness and grain size trends of long run-out turbidity current flows that extend beyond the continental slope using a depth-averaged numerical flow model?

- To quantitatively determine the maximum suspended grain size moved by a flow using a turbulence- suspension theory

Can we infer flow properties of long run-out oceanic turbidity currents based on relatively simple inputs?

The next section below, provides a brief description of the Agadir basin, offshore Morocco.

6.2 The late Quaternary Agadir Basin, Offshore NW African Margin

6.2.1 Introduction

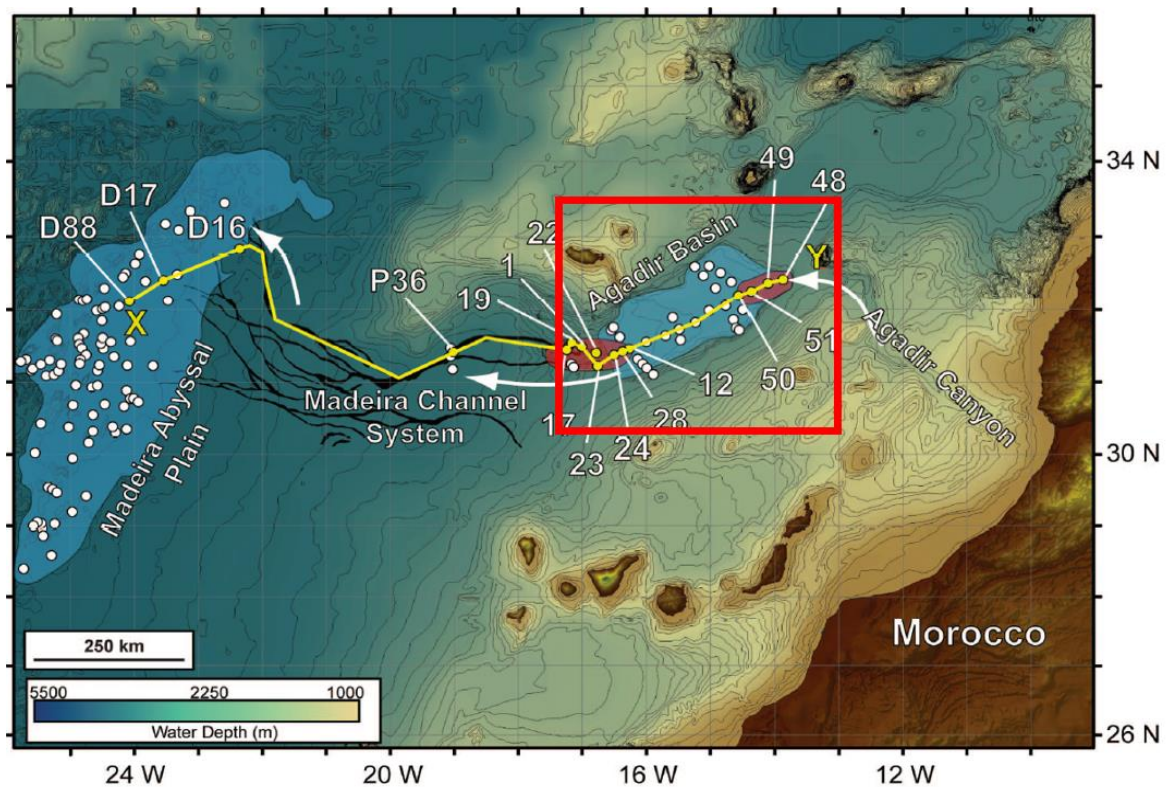


Figure 6.1: Location map of Agadir Basin showing the pathway of Bed A5 flow. White dots are recovered core locations used by Stevenson et al., (2014) study. Red outline indicates the position of Agadir basin in relation to other basins within the Moroccan Turbidite System.

The Agadir basin is situated offshore Morocco in North-western Africa (Wynn et al., 2002) (see figure 6.1). It is part of a triple- member interlinked Moroccan Turbidite System (MTS), and is centrally located with regards to the relative position with the other two; the Seine Abyssal Plain (SAP) and the Madeira Abyssal plain (MAP), that are located to the northeast and to the western

most extent of the system respectively. The basin covers an estimated total area of about 35000km², with water depths in the range of 4300m to 4500m (Wynn et al., 2002).

Flows responsible for the transport and deposition of sediments into Agadir basin were mainly from the Moroccan Margin (siliclastic flows); Canary Islands (volcanoclastic flows) as well as from localised seamount collapses which supply the carbonate-rich flows (Weaver et al., 1992; Wynn et al., 2002b). These flows, averaging 30 to 120 m in thickness extend across the entire width of the basin with the highest amount of sand transported by flows about 5 to 14 m thick with sand transported in the lower 5 to 7 m of the flows (Stevenson et al., (2014).

The Agadir basin unlike other deep-water basins, presently provides the only location where sediment cores of turbidity current deposits taken from the modern sea floor have been mapped out across distances of over 250km wide in exceptional details.

6.2.2 Bathymetry

The Agadir basin has been described as a large intraslope basin, with an almost flat topography, having an ENE-WSW slope gradient ranging between 0.010- 0.030. There is an intrabasinal sill of over 100m height above the basin floor, which separates the basin from the Seine Abyssal Plain in the north-east while the western end is marked by a series of distributary channels with much lower gradients (Wynn et al., 2002). Stevenson et al., 2014 used the GEBCO dataset to generate the slope maps of the basin.

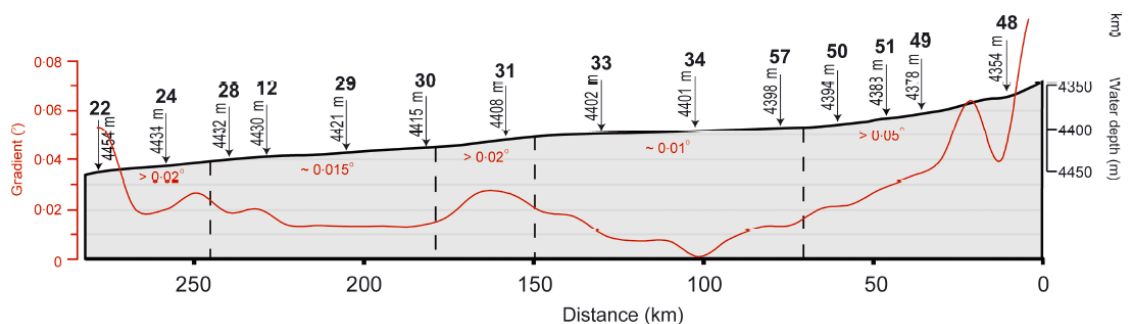


Figure 6.2: Change in seafloor gradient (red line) along the axis of Agadir basin
Adapted from Talling (2013).

The seafloor slope was estimated from the spot depths, followed by a general smoothing within a 3.0km² grid (see figure 6.2). GEBCO grid (General Bathymetric Chart of the Oceans) is a continuous terrain model for ocean and land with a spatial resolution of 30-arc-seconds. This level of detail is expected to aid the capture of any small-scale roughness of the seabed. The GEBCO grid was generated by combining quality-controlled ship depth soundings with interpolation between sounding points aided by satellite gravity data.

The Agadir basin act as a bypass and/or area for deposition for both confined and unconfined turbidity current sediments conveyed through the Agadir Canyon (fig 6.1 A). According to Ercilla et al. (2003), between the Oligocene and Lower Miocene, the basin was a bypass area and flows entering the basin came through the channels that runs along the basin and the flow pathway was essentially controlled by the paleotopography. However, later, during the Miocene and Upper Quaternary, the basin became a site for turbidite deposition (such as the channel-fills, overbank and lobe deposits).

6.2.3 Agadir basin sedimentary facies

Wynn and Cronin (2005), Talling et al., (2007), Wynn et al., (2012) and Stevenson et al., (2014) reported their findings of studying shallow *ca* 12m piston of over fifty sediment cores from the Agadir basin (core locations are shown in figure 6.1A). Two distinct sedimentary facies associations dominate the sedimentary sequence of Agadir basin and these are the hemipelagic muds and submarine flow deposit sands and muds. Using the facies scheme of Sumner et. al., (2012), these facies have been further described to include the *structureless sand* (no sedimentary structures but has mud contents between 5-10%); *mud-rich structureless sand* (mud rich of up to 40 - 50% and found within bed 5 across the basin, largely ungraded and directly overlie the relatively clean structureless sand); *Laminated sand* (which include the planar laminated sand occurring at the base of the deposits, Ripple cross laminated sand

occurring at the upper part of the deposits or at the base if the deposit is thin, usually graded and have a higher mud content of up to 20% compared with the planar laminated sands) and the *Contorted laminated sand* intervals (which also occur at mid-height in the beds with up to 25 % mud content and characterised by normal and/ or inverse grading).

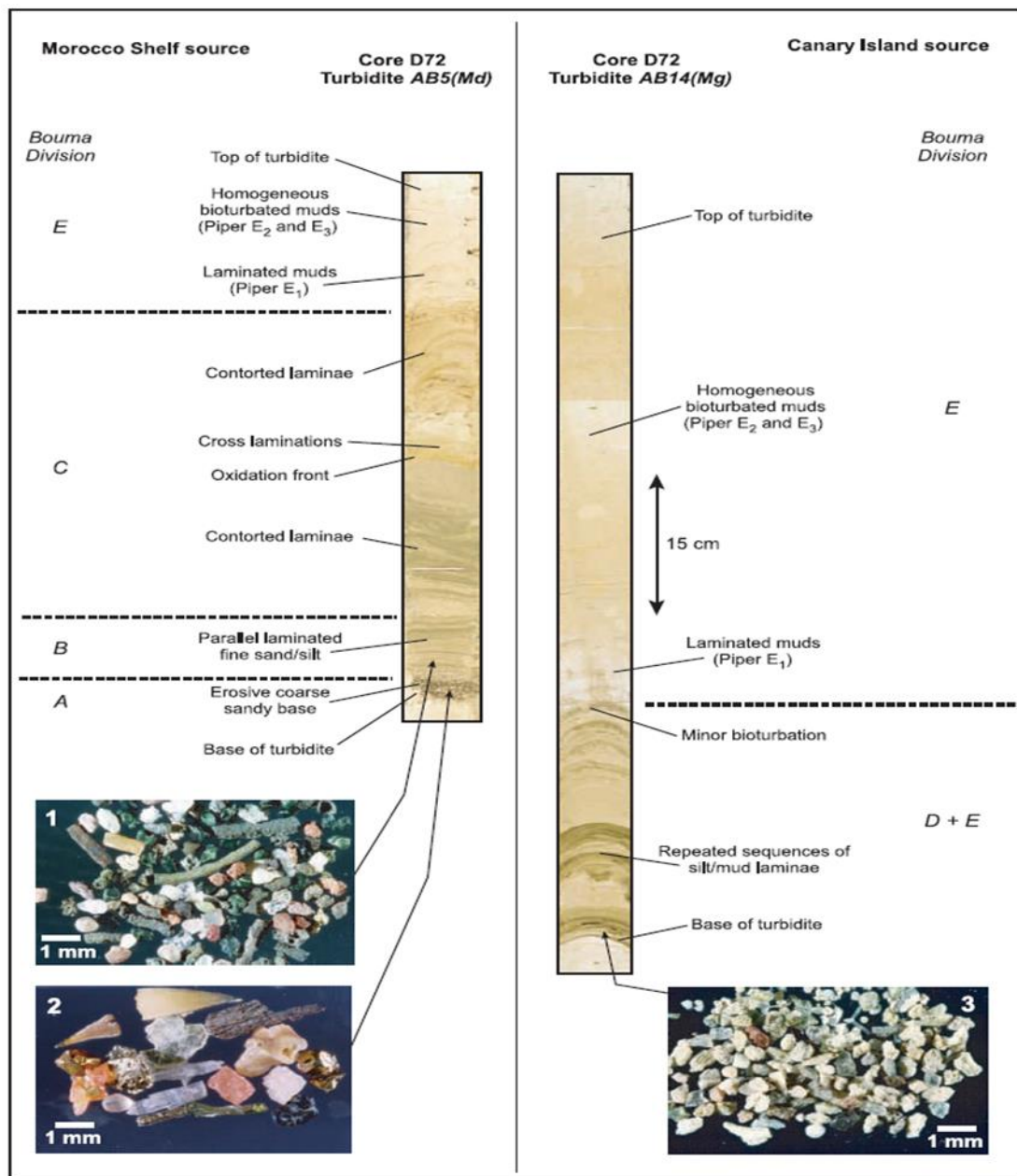


Figure 6.3 Core photograph of turbidites from the Agadir basin
Inset 1-3 are the sand fraction mineralogy. Figure adapted from Wynn et al., (2002).

Finally, there are *Turbidite muddy facies* which are volumetrically, the most abundant facies in the Agadir basin. Turbidite muds contains up to 70% smectite and illite with less than 40 % kaolinite and chlorite.

They normally grade into ungraded structureless mud with silt: clay ratio of ca 1:1. Five beds, namely A3, A5, A7, A11 and A12 extend laterally throughout the basin with sand having distinctive mineralogy generally occurring at the base (Fig 6.2). These beds are well described, interpreted and documented in Stevenson et al., (2014). However, Bed A5 will be focus of this chapter, being the product of a high-volume flow with the highest sand fraction observed a few metres above the basal part of the cored sequences.

6.2.4 Why study Bed A5 flows?

Bed A5 is one of the flow deposits of the Agadir basin, NW Africa, previously studied by Talling et al., 2007; Stevenson et al., 2014 from shallow sediment cores. Results suggest that the flow that deposited Bed A5, is from transformation, following a landslide on the Moroccan Margin. Field evidence and analysis of sediment cores show that the flow contained over 120 kg³ of sediment (approximately 22.5×10^{13} kg of sediment, assuming a density of 1800kgm⁻³). Therefore, the flow that deposited Bed A5 is considerably very large as it is apparently ten times more voluminous than the annual flux contributed by all rivers of the world (river flows hardly transport sediments in excess of 10^9 - 10^{11} kg to the ocean, even at very high floods and the annual flux of sediments from all world rivers to the oceans is approximately 2×10^{13} kg (Khripounoff et al., 2003)).

Bed A5 is also documented to contain the highest proportion of sand (ca 40%) and drapes 24 to 33m up the basin margins, with sand suspended just a few meters (5.0-7.0m) from the bed, making it the thinnest flow that transport sand-sized sediment grains (Stevenson et al., 2014). The basin-wide extent of the sandy facies in Bed A5 suggest that the flow maintained high concentration state throughout the length of the basin (fig. 6.3).

However, the thickness of flows that deposited bed A5 in Agadir basin, NW Africa was inferred from the deposit height as it drape-up basin margin and documented to be *ca* 120m thick, with the highest fraction of sand deposited less than 5 to 7 m above the bed floor. The relationship between flow thickness and grain size has been well elucidated in Rouse, 1937; Bowen et al 1984; Normark et al., 2009, with fine-grained flows tending to be relatively thicker. Also, variation in flow thickness have been suggested to influence the run-out distances and the size of the resulting deposits (Kneller and Branney, 1995; Kneller et al., 1997; Kneller and McCaffrey, 1999).

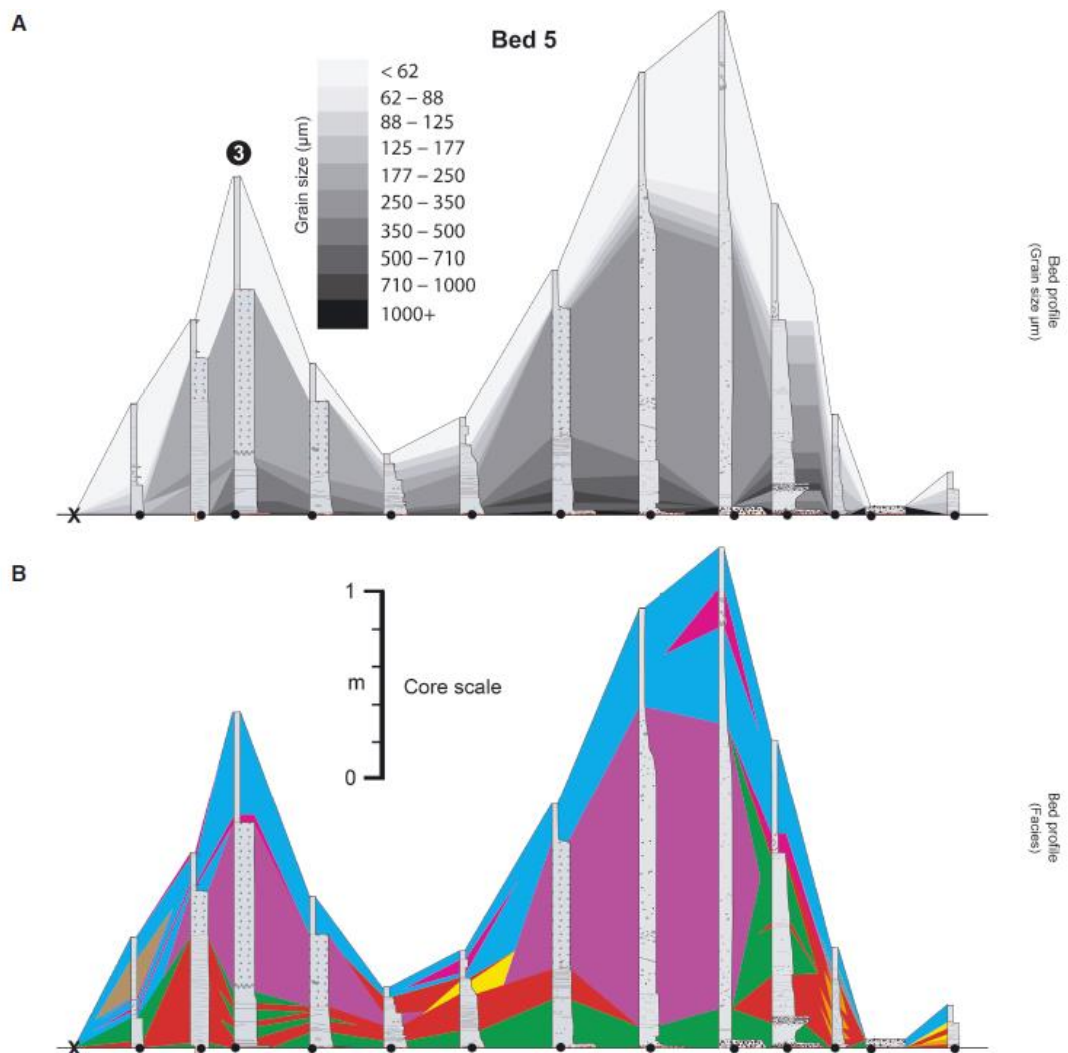


Figure 6.4: Bed A5 interpreted facies profile (from Stevenson et al., 2014).
 (A) Vertical and spatial distribution of grain size. Positions (B) Color denotes interpreted facies.

Models of turbidity current flows suggest that thin turbidity current flows dissipate fast on low slopes (Kneller et al., 2016), and therefore, the persistence travel of thin flows that deposited bed A5 across the Agadir basin is very unclear. The key question is how thin flows (of about 5-7 m) is able to suspend sand through a long run-out distance of over 250km wide Agadir basin, Northwest Africa?

6.3 The Numerical flow model

The numerical flow model used in this thesis is a simple two-dimensional depth-averaged flow model that can be used to understand sediment grain transport supported by turbulence as well as predict flow properties. The model assumes no vertical change in velocity, concentration and grain size distribution and adopts the von Karman-Prandtl mixing length turbulence-suspension theory to predict bed shear stress and velocity profiles of oceanic turbidity current flows. It was developed by Waltham et al., (2008a) using algorithms of Reynolds-Averaged Navier Stokes (RANS) as well as the Chezy equations earlier discussed in chapter three of this thesis. A detailed discussion of the governing equations of the flow model is in Waltham *et al.*, (2008). The main reason for choosing this 2D depth averaged flow model is because it is computationally fast to run and its use of few input parameters. More advanced models such as the DNS are computationally very expensive, slow to run and would require a lot of initial input parameters. However, this 2D depth-averaged flow model like other depth-averaged models have its own limitations especially in the procedure of vertical integration. For instance, it is unable to simulate vertical changes in velocity, concentration and grain size distribution. It does not also recognise erosion or any form of mixing and basal entrainment into flow. It is only applicable to turbulence-supported flows transporting sediment grains in long run-out distances therefore Laminar flows are not particularly suited to be captured by the flow model and may not adequately be used to understand debris flows. The numerical flow model is also unable to model flows that are essentially laminar and with particle concentration greater than 10%.

Finally, the flow model may not be able to capture the vertical density stratification such as reported by Stevenson et al., (2014) for flows in Agadir basin, offshore NW Africa, being strongly stratified by the facies characterisation.

Despite these limitations, the 2D depth-averaged numerical flow model seems sensible for this thesis given the large area to be accessed. Moreover, as it can only simulate turbulence-supported transport processes, the flow model will be used to investigate the likely origin of the large-volume (over 100kg³) long run-out flow that deposited Bed A5 of the Agadir basin and isolate its grain support mechanism. Field data from Stevenson et al., (2014) will be used as input parameters to further determine the possibility of this large-volume flows suspending sand only a few meters from the bed. This observation contradicts many models whereby thick flows could transport sand across very long distances.

6.3.1 Model inputs

Model input includes parameters such as grain size data (comprising both the coarse and fine fractions), flow thickness and particles concentration (comprising both coarse and fine concentration). Other inputs were based on the seafloor topography, using regional bathymetric data adopted from GEBCO, (see fig 6.1C), Canyon width, inflow time, run width and the Chezy coefficient. Table 6.1 outlines all the parameters used in the flow model with their default values.

These default input parameters and their values such as particle concentration are for a typical turbidity current while others are assumed field data of Agadir basin reported in Talling et al (2007) and Stevenson et al., (2014). However, to ensure quality assurance of the model output, it was necessary to first carry out sensitivity analysis of the input parameters as it affects the predictions of the model.

Table 6.1: Input variables used in the flow model.

<i>Quantified observations from Bed A5 (Talling et al., 2007; Stevenson et al., 2014)</i>		
Parameter	Description	Default values
1. Grain size (μm) coarse diameter	The diameter of individual coarse grains carried by the flow	250 μm
2. Grain size (μm) fine diameter	The diameter of fine grain fraction carried by the flow	50 μm
3. Flow thickness (m)	Approximates the size of flow entering the basin through the canyon	200.0m
<i>Estimated Parameters</i>		
1. Concentration (coarse) %	The amount of fine particles in the flow	1.5%
2. Concentration (fine) %	The amount of fine particles in the flow	3.5%
3. Inflow width (km)	The width of the Canyon conveying flow into the basin	15.0km
4. Inflow time (hrs)	The total time it takes for the flow to enter the basin	7.0 hrs
5. Chezy coefficient	The drag on the flow controlled by the seafloor roughness	0.004 (set by Talling et al., 2007)
6. Run time (hrs)	The total time allowed for the Model to run	50.0hrs

6.4 Method: *Sensitivity Analysis*

Sensitivity analysis was carried out to identify those input parameters that significantly influence the flow model output or alternatively those that are less influential in re-creating the desired flow model output and to establish whether model predictions are robust to the variations in the input parameters. Figures 6.5 – 6.16 below, shows the model output arising from doubling the default values to determine their sensitivity.

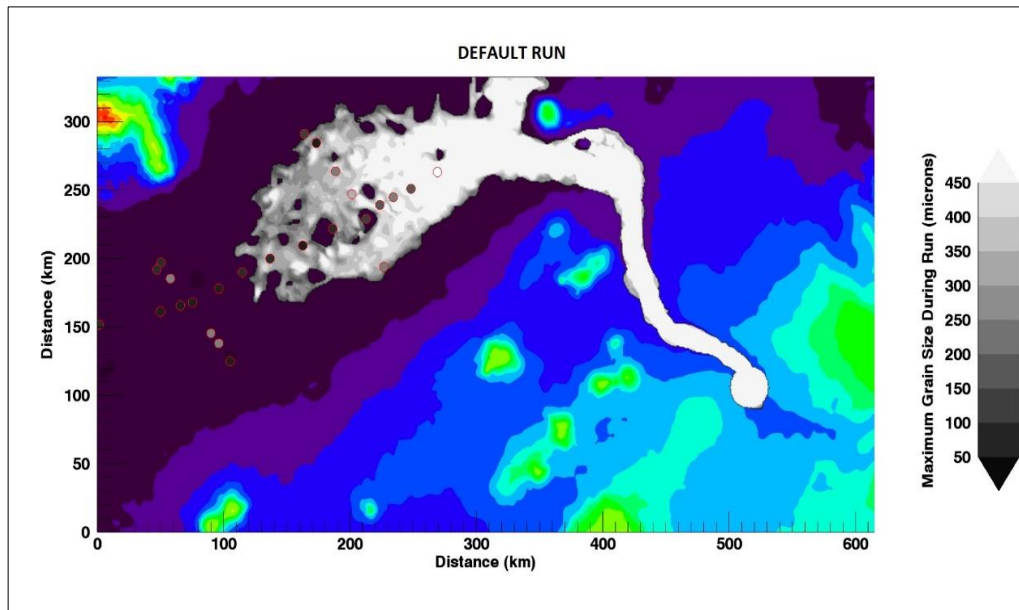


Figure 6.5: Default run of the Numerical flow model

6.4.1 The default run

Figure 6.5 shows the default run of the modelled prototype flow based on the default data presented in Table 6.1. Note the tiny red circular dots in the map which are the sediment core sampling locations used in the study as reported in Stevenson et al (2014). This default run shows a flow with a run-out distance of about 200.0 km which was unable to reach the distal part of the basin. Sediment grains held in the flow were deposited in the middle of the basin after about 50.0hours run time. The default model also showed that the flow could transport a large amount of sand-sized sediments carried through the canyon to the proximal and mid part of the basin.

6.4.2 Coarse diameter doubled

The effect of doubling the coarse diameter of grains (to 500 μm) is presented in Figure 6.6 below. it was observed that such increase does not significantly affect the model's output. The reason is that the modelled flow is dominated by the fine-grains and, hence, doubling the coarse grain diameter is insignificant. The flow run-out distance is essentially the same.

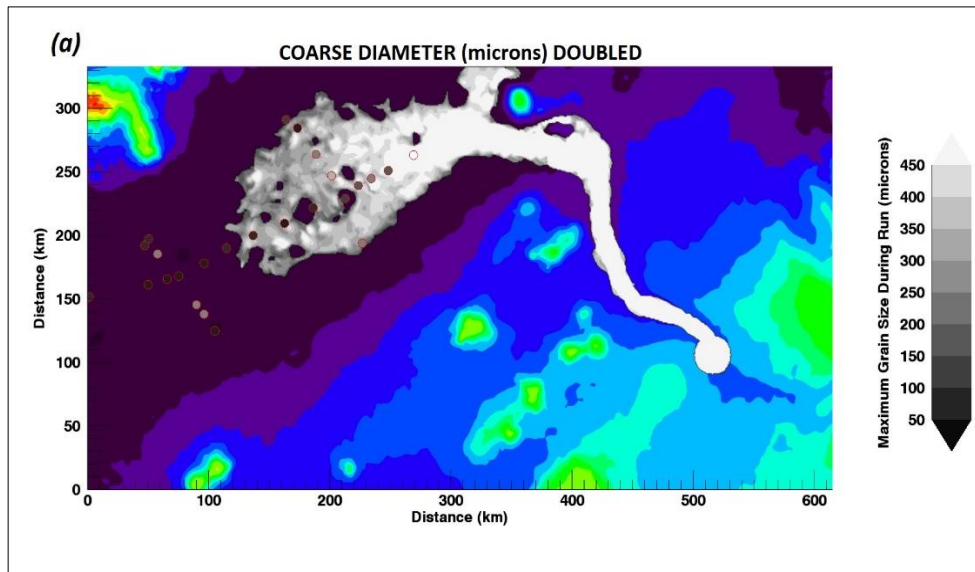


Figure 6.6: Effect of increasing grains coarse diameter to $500\mu\text{m}$
Flow model is not sensitive to such increase

6.4.3 Fine diameter doubled

Increase in the fine diameter from the default value of $50\mu\text{m}$ to $100\mu\text{m}$ may have led to an early settling of sediment grains from the flow into the basin. This may be attributed to the fine grains being now larger than they were and settle out more quickly. From Fig 6.7, it is evident that the run-out distance is now reduced.

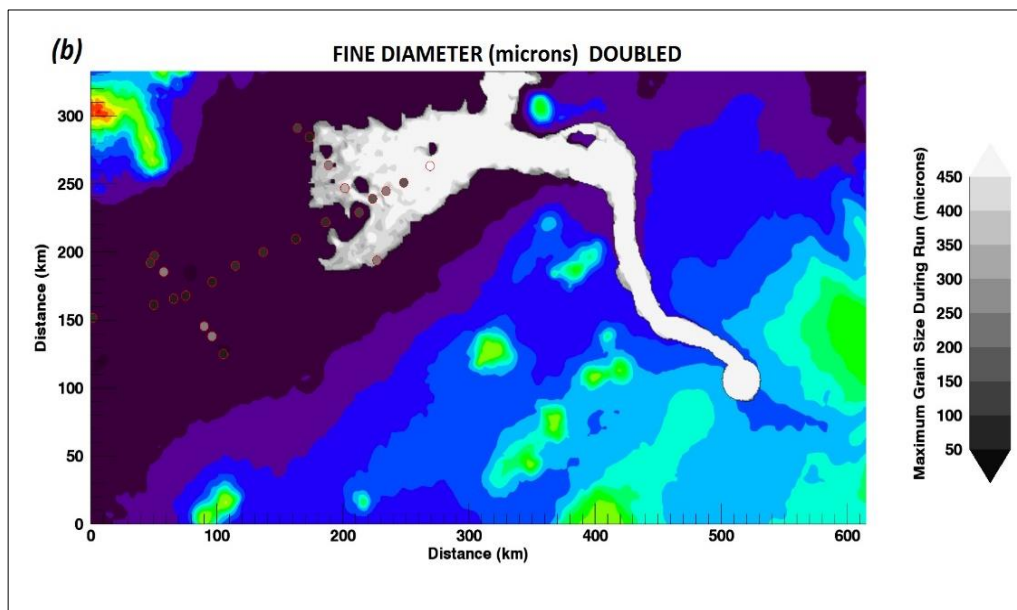


Figure 6.7: Effect of increasing the fine diameter to $100\mu\text{m}$
Flow model is sensitive to the increase as the flow run-out distance decreases

6.4.4 Coarse concentration doubled

Increase in the coarse concentration from the default value of 1.5 to up to 3.0% do not show a clear difference when compared to the default run as flow behaviour is dominated by the fine-grains. The flow is essentially the same (See fig 6.8).

6.4.5 Fine concentration doubled

Here, with the fine concentration doubled from 3.5 % to 7.0%, there is a clearly observed increase in the flow's run-out distance. The flow is able to propagate further into the distal part of the basin (see fig 6.9). The increased flow density allows the flow to travel further and faster.

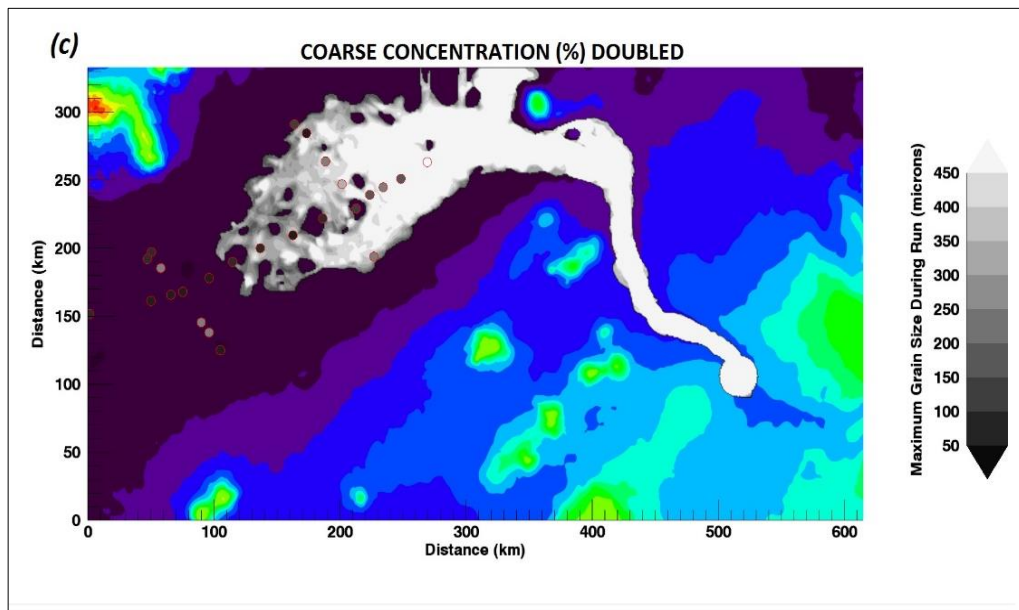


Figure 6.8: Effect of increasing the coarse concentration to 3.0%. Flow model is sensitive to the increase as the flow run-out distance increased marginally

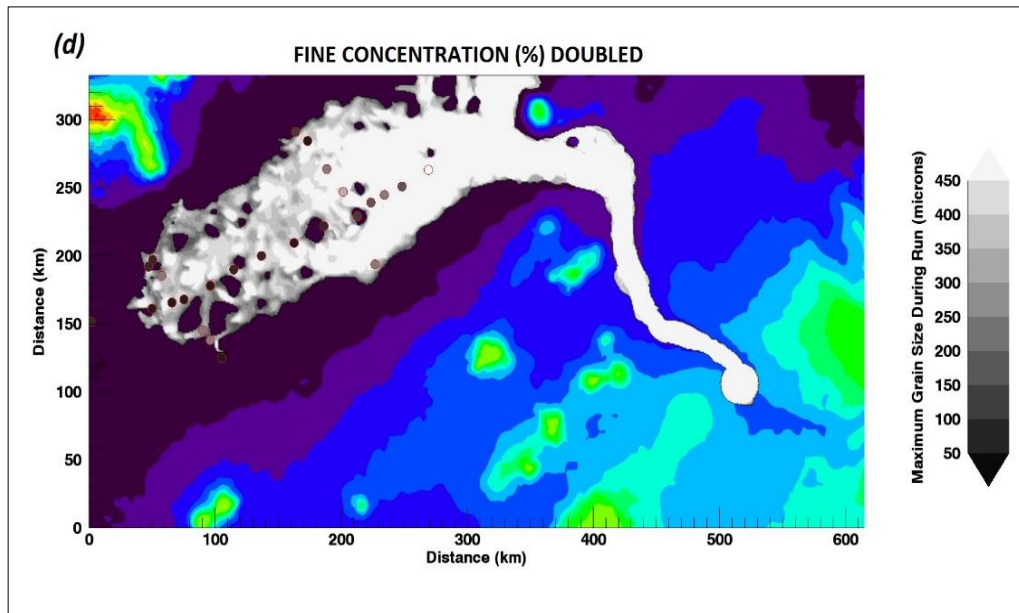


Figure 6.9: Effect of increasing the fine concentration to 7.0%.
Flow model is sensitive to the increase as the flow run-out distance increases

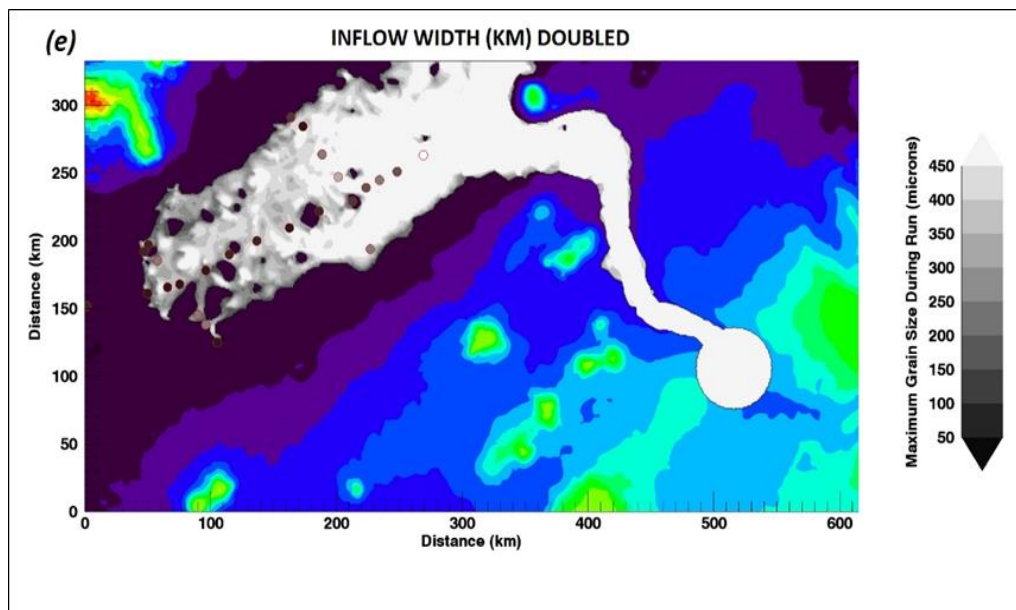


Figure 6.10: Effect of flow width of the canyon to 30.0km
Flow model is sensitive to the increase as the flow run-out distance increases. The diameter of the flow channel or canyon also determines the amount of flow being delivered into the basin

6.4.6 Inflow width doubled

Increase in inflow width from a default value of 15.0km to 30.0 km showed a significant increase in the run-out distance of the flow. The increase in inflow width allowed greater volume of flow

into the basin, thus enhancing the ability of the flow to propagate more into the distal margin of the basin (see fig 6.10).

6.4.7 Flow thickness doubled

As observed in figure 6.11, doubling the flow thickness in the flow model to 400m showed a significant influence on the flow ability to propagate far into the basin. From the figure, it is noted that the flow run-out distance increased considerably when compared to the run distance of the default run and the flow could get to the distal basin margin and even beyond. Also, a thicker flow should contain a wide range of sediment grain sizes and more sand-sized grains are able to be moved up in suspension by the flow. Thicker flows will have relatively higher grain density than thin flows and so the momentum of such a flow should be higher, which makes it able to travel far.

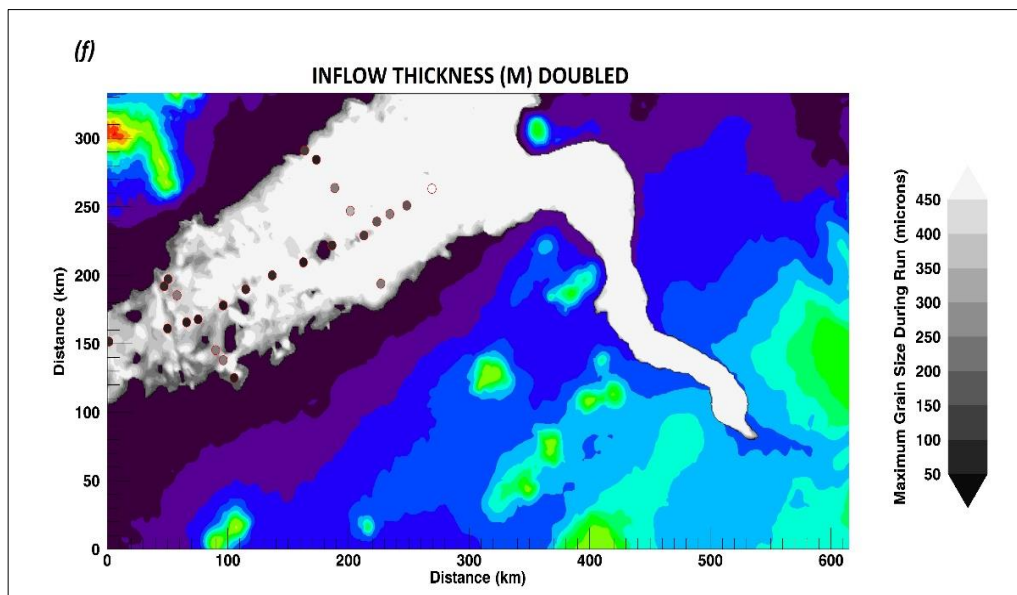


Figure 6.11: Effect of increasing the flow thickness to 400.0m
Flow model is sensitive to the increase as the flow run-out distance increases even beyond the basin margin

6.4.8 Chezy coefficient doubled

With every other parameter in default state apart from the Chezy coefficient which is increased by a factor of two, it is clearly observed from the output, (fig 6.12), that the flow travelled less far distance when compared to the default run (fig 6.5). Here, there is early deposition of sediment grains near the middle of the basin as a result of increased friction.

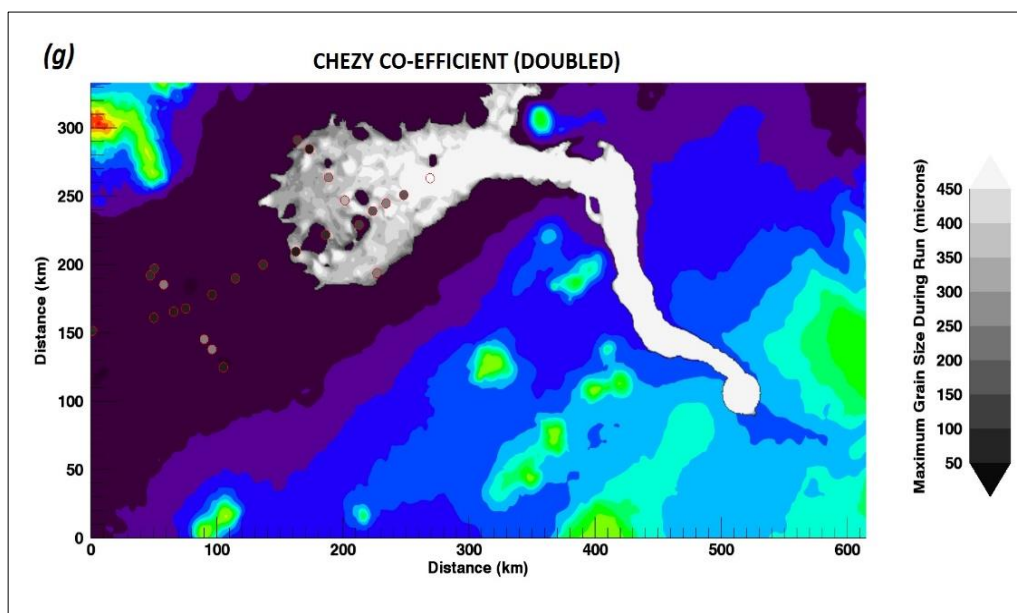


Figure 6.12: Effect of increasing Chezy co-efficient by a factor of two
Output flow model shows a higher drag of flow and flow seems retarded leading to early deposition of grains occurring in the middle of basin

6.4.9 Model run time doubled

Doubling the model run time, shows a significant increase in the run-out distance of the flow (see figure 6.13 below). This confirms time as a very important factor in flow modelling. When compared to the default run, it is clearly observed that the flow could move further down the basin with relatively more fine sediment grains in suspension. Hence, the default run-time is not sufficient to capture the full flow behaviour and simulations will have to be run for longer.

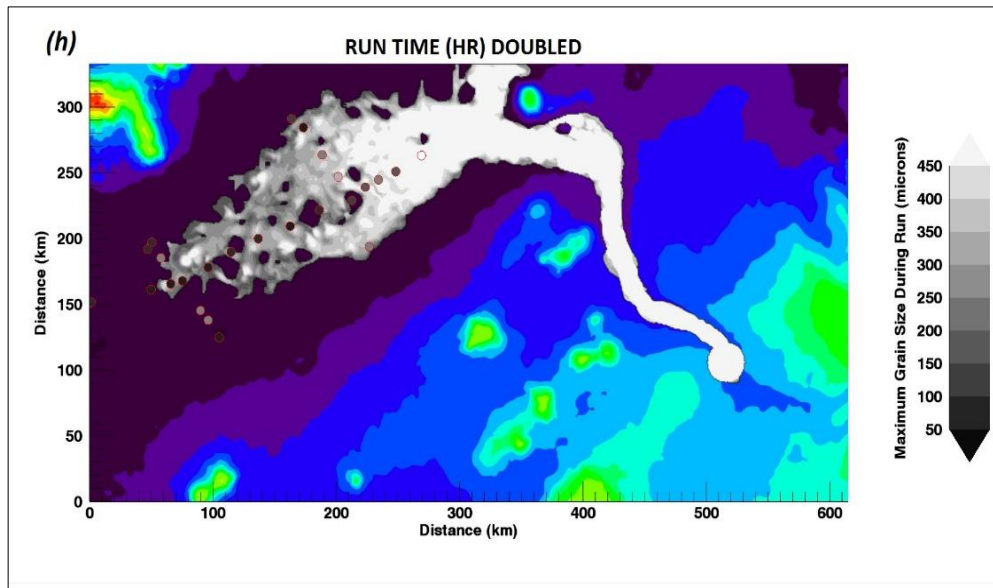


Figure 6.13: Effect of increasing model run time by a factor of two
Flow model is sensitive to doubling the model run time as the flow run-out distance increases

6.4.10 Inflow time doubled

In the default run, the total time it takes the flow to enter the basin through the channel or canyon was assumed to be 7.0hrs. However, when this was doubled, it was observed that the flow volume is higher and the run-out distance of flow have increased too. The model output is shown in figure 6.14 below.

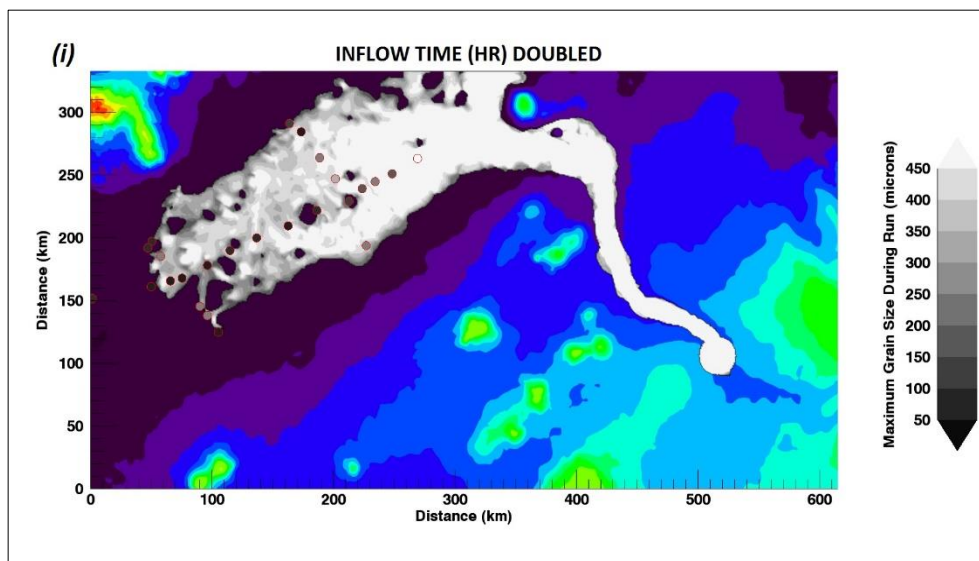


Figure 6.14: Effect of increasing inflow time by a factor of two

Flow model is sensitive to doubling inflow time as flow volume and the flow run-out distance tend to have increased considerably

6.5 Model output

6.5.1 Modelled bathymetry and flow evolution of Agadir basin

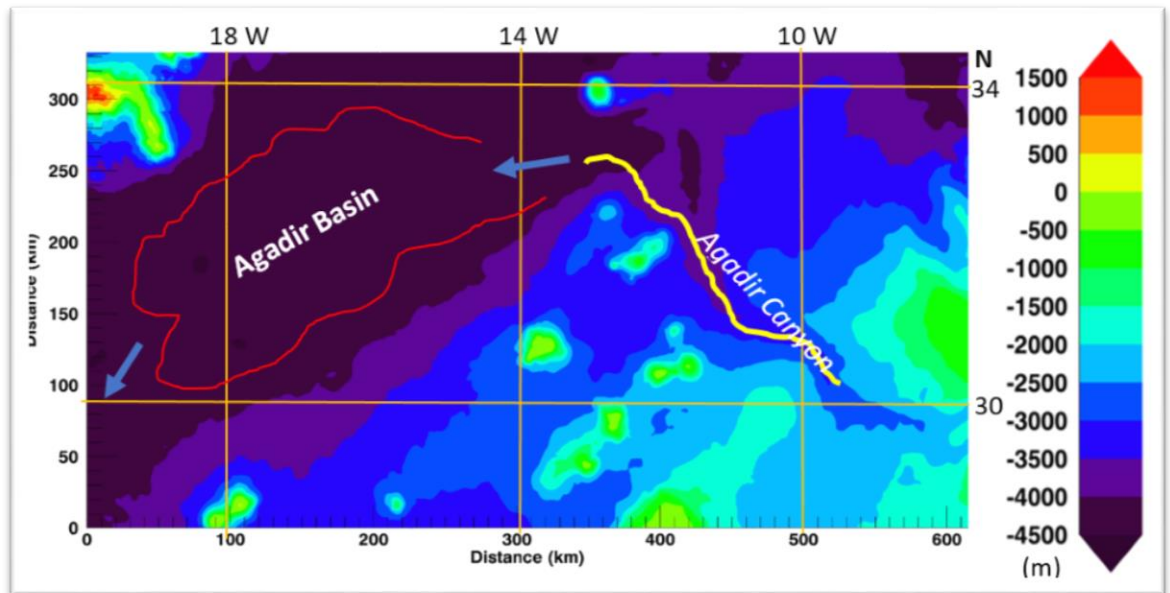


Figure 6.15: Modelled Bathymetric map of Agadir basin

Red outline (not to scale) represent the location of the study area. The yellow curve indicates the Agadir canyon while arrows show flow direction.

Figure 6.15 above is the modelled bathymetry of the Agadir basin using input parameters from Talling et al., (2007), Wynn et al., (2012) and Stevenson et al., (2014). Flow into the Agadir basin comes from the Moroccan margin through the Agadir canyon.

Based on a series of simulations of turbidity currents flow in the basin, the evolution of the Agadir flow is presented in Fig 6.16 (A-H). This justifies the capacity of the flow model to simulate field-scale turbidity current. From the flow model (fig 6.16A and B), it is observed that within the first five hours run time, flow emanating from the Moroccan margin was channelized with no evidence of spill in adjacent overbank areas, and it continued to maintain its course within the Agadir canyon.

At 10.0hour, the flow is observed to continue in its northward direction until it made a sharp 90° bend (fig 6.15C) to begin its course into the basin.

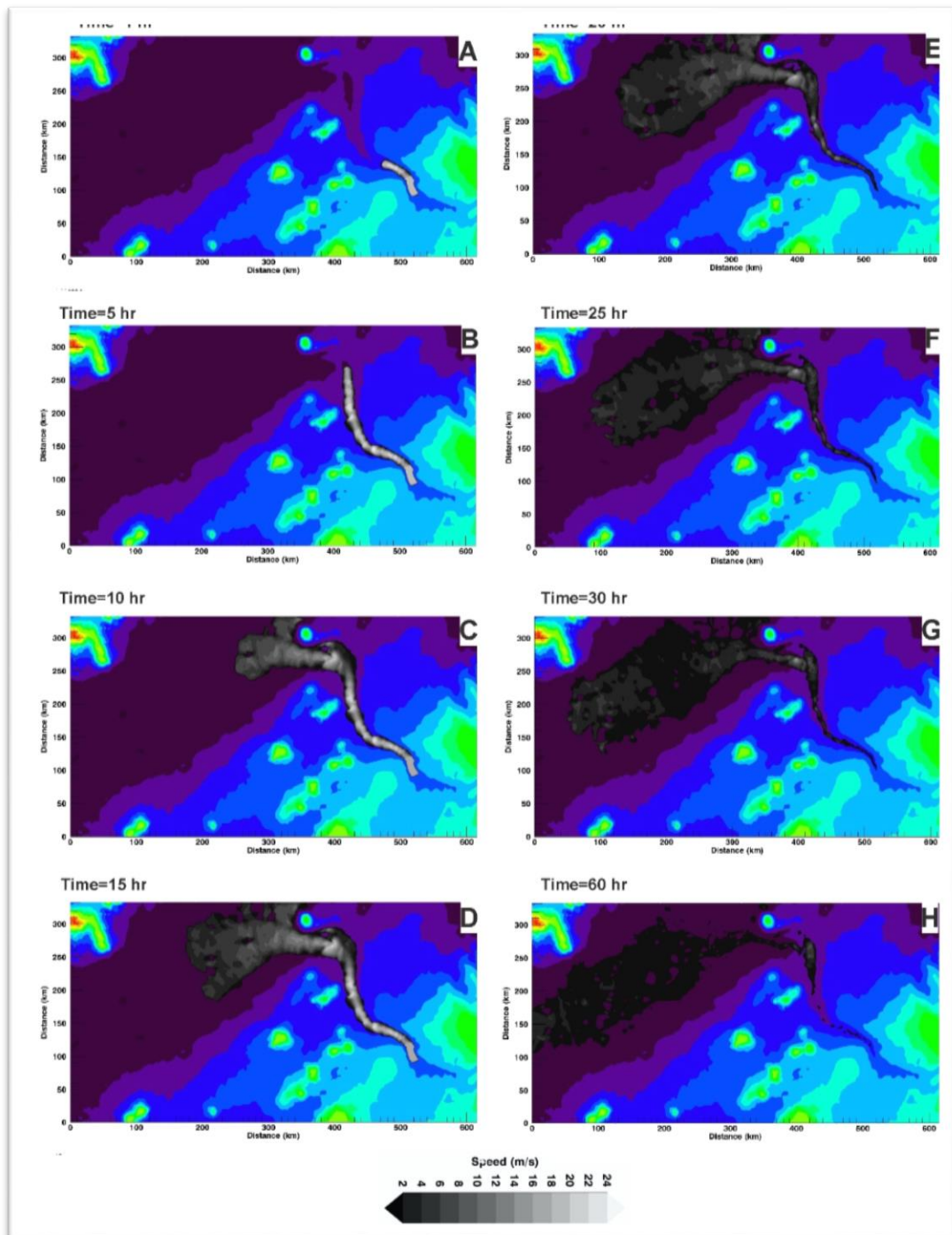


Figure 6.16: Modelled flow evolution of Agadir basin

Recall, the flow model does not allow for basal entrainment, or erosion and if Stevenson et al., (2014) observation is true, the flows in Agadir basin is largely non-erosive so the flow velocity should gradually reduce due to the dissipation of the flow energy. At about 15.0 hr of the flow,

its average speed gradually reduced to about 10.0m/s, and the flow further propagated downstream into the basin developing submarine fans (Fig 6.16D).

At 20.0 hr propagation of the turbidity current flow continue to increase down the gentle sloping basin sea floor and maintained its momentum following an increase in the flow thickness (Fig. 6.16E). At 25.0hrs, the flow speed reduced to about 8.0m/s due to weakening of the current (Fig 6.16 F). The flow continued its downstream motion and subsequent deposition of its load in the basin gradually began due to further waning of current speed (Fig 6.16F and G). Figure 6.16H shows that at 60hr, the flow's thickness has drastically reduced to less than 2.0m/s and deposition of the suspended sediments within the basin is almost complete.

6.5.2 Approximate fit to data; comparison to field evidence

Based on the outcome of the model sensitivity analysis, the main input parameters influencing run-out distance and competence of the subaqueous flows are the thickness, volume of fine concentration, model run time as well as the inflow time. This agrees with existing models such as Rouse, (1937); Bowen et al (1984); Kneller and Buckee, 2000 and Normark et al., (2009).

Using field data of Bed A5 flow deposit as input parameters of the 2D depth-averaged numerical flow model, attempt is made here to investigate the findings of Stevenson et al., (2014) on how the large- volume Bed A5 flows with very long run-out capacity could only suspended sand-sized grains just a few meters from the bed.

Here, the flow model output is compared with field observations to see how well the model and the data fits.

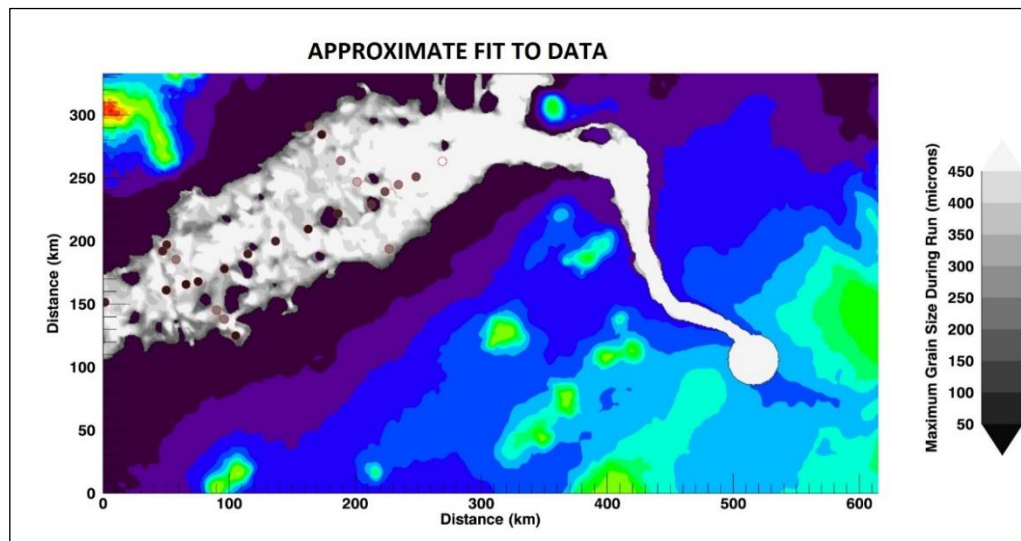


Figure 6.17: Flow model with approximate fit to data

Note the dark grey colour tone expressed in the red circular dots (the sediment core sampling points in the basin), is suggestive of fine grains. However, white colour predominates in greater part of the flow in basin, suggesting more of coarse sediment grains deposition.

This flow model confirms that flows coming from the Moroccan margin through the Agadir channel are able to deposit its suspended load in Agadir basin after a long-distance travel. From the flow model, it was observed that the flow model is mostly dominated by coarse grains transported by flow with an average thickness of approximately 100.0m into the basin.

As previously noted, the flow model transport sediment grains that are relatively coarse and to be able to propagate farther into the basin, (to attain a long run-out flow), the flows thick be thick. Fig 6.16 above, supports this explanation. But these model observations contradict Stevenson et al., (2014) field observation.

It will be naturally expected that turbidity current flows as thick as the one prescribed in the flow model, could attain a long run-out distance, far across the basin and will be able to laterally advect a range of sediment grain sizes including the coarse sand grains identified. However, the flow model is unable to account for the possibility of thin flows carrying these coarse sediments far into basin without deposition and therefore reproducibility of field observations in Agadir basin is not achievable by this model.

6.5.3 Resulting maximum flow thickness; comparison to field evidence

Figure 6.17 shows the model output of flow thickness in relation to the distance moved by the flow. It is observed from the flow model that maximum thickness of flow occurs at proximal part of the basin due to reduced deposition and high turbulence, but the flow subsequently spread out, carrying a range of sediment grain sizes coarse sediments in suspension and move farther into the basin. According to Talling et al. (2007), a thick flow will be able to carry most of its sediment load well above the flow bed and could deposit only a small percentage on the bed at any point in time during transport. In the analogy to field evidence by Stevenson et al. (2014), suggestions of thinner flows transporting sand size sediment grains across over 250 km wide Agadir basin cannot be substantiated by the flow model. Thin flows unless heavily turbulent and characterised by high concentration of fines, encourage rapid settling of sediment grains as the flow momentum could easily get dissipated.

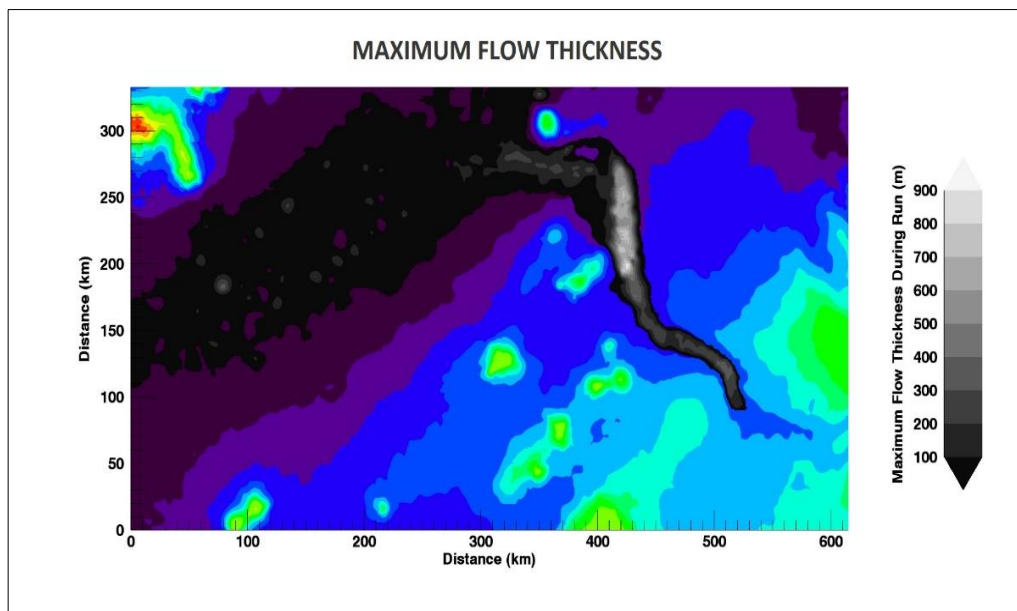


Figure 6.18: Flow model showing the flow thicknesses with distance

The dark colour tone suggests flow thicknesses of about 200.0 meters transporting sediment grains across the basin. The lighter colour tone observed in the canyon suggest initial thicker flows which subsequently spreads and gets thinner with distance across the basin

6.5.4 Maximum suspended grain size in Bed A5 flow

The size of a sediment grain exerts a first order control on its suspension and subsequent transport in a flow. In near bed zones, other parameters apart from grain size such as terminal settling velocities, flow thickness and turbulent accelerations which should be greater than the gravitational force are the main controls (Bagnold, 1966; La Porta et al., 2001).

For sediment grains transported in the region far above the bed, turbulent diffusion and vertical settling are the dominant competing processes which determine the particle concentration and transport process.

Here, a novel attempt is made to quantitatively determine the maximum grain size that can be suspended and moved by a turbidity current flow using Bed A5 flow of the Agadir basin, offshore Morocco as a case study. This research follows inferences from earlier work by Talling et al., 2007; Wynn et al., 2012 and Stevenson et al., 2014, suggesting that the flows that deposited sand in the voluminous bed A5 is less than 7.0m thick.

It is unclear if Bed A5 flow can generate enough turbulence to sustain sand grains suspension throughout its long-distance transport from the Moroccan Continental margin, which is the primary source of the siliclastic sediments. Essentially, it is expected that coarse siliclastic grains such as sand grains transported by a thin turbidity current flow should settle faster under the action of gravity and moved within relatively short distances from source. But the reverse seems the case here, as it was reported that sands (about 250 μm) were transported for well over 250km by thin flows resulting in the deposition of Bed A5 in Agadir basin. This could only be justified if sands were suspended and transported in flows higher up from the bed, where turbulence predominates, and vertical settling is insignificant.

Table 6.2 (A and B) below, show the key assumptions as well as the field data of Bed A5 flow from published work of Stevenson et al., (2014).

Table 6.2A: Key Bed A5 field data from Stevenson et al., (2014)

Flow bed	Lithology	Bed geometry downslope	Grain diameter (μm)	Flow height with sand fraction (m)	Basin slope (degrees)
A5	Clean sands Mud-rich sands	tubular lenticular	200	5.0	0.02-0.05

Table 6.2B: Key assumptions for estimating Max. Suspended grains in bed A5 flow

Particle volume concentration (%)	0.1	For very dilute flow
	10.0	Maximum concentration in flow at the base of flow
Density of water (kg/m^3)	1000	

Using the mathematical expressions provided by Waltham (2008), the basal shear stress re-expressed as shearing velocity (see equation 3.7 of chapter 3) was estimated using the data provided in tables 6.2A and B above. Also, the mean velocity (Eqn 6.1) was estimated from the mixing-length theory (Duncan et al., 1960) with full details also in Waltham (2008), where it is shown that

$$\tau_0 = -\rho \left(\frac{\kappa \bar{u}}{b \ln\left(\frac{Hf}{z_0}\right)} \right) \quad (6.1)$$

Where κ is Karman's constant, \bar{u} is the mean velocity of flow, f is the turbulent bed-layer fractional thickness (approx. 0.05, from Kneller et al., 1999) and b is a constant (order of one).

The drag coefficient was equally estimated using the expression (Eqn 6.2) below:

$$C_d = \left[\frac{\kappa}{b \ln(fh/z_0)} \right]^2 \quad (6.2)$$

Finally, the depth averaged velocity was then calculated from the expression (Eqn 6.3) below:

$$\bar{u} = \sqrt{-\frac{g' h s'}{C_d}} \quad (6.3)$$

In estimating the maximum suspended grain size, the formulae from Stokes's Law was adequate. For the grain diameter modelling. Five different scenarios were modelled, and maximum grain

size diameter estimated. Table 6.3 below shows the estimates of the maximum grain sizes for bed A5 flows for 5.0m thick flow on the gentle sloping (0.02) Agadir basin.

The results affirm that we can infer flow properties of long run-out oceanic turbidity currents based on relatively simple inputs and it is possible to quantitatively determine the maximum suspended grain size moved by a flow using the Mixing-length turbulence- suspension theory

Table 6.3: Estimates of maximum suspended grain size for bed A5 flow

Parameter	Case 1	Case 2	Case 3	Case 4	Case 5
Reduced gravity, g'	0.0161865	0.080933	0.161865	0.809325	1.61865
Drag coefficient	0.025	0.025	0.025	0.025	0.025
density of flow (kg/m ³)	1001.65	1008.25	1016.5	1082.5	1165
Density of water (kg/m ³)	1000	1000	1000	1000	1000
density excess (T.C)	1.65	8.25	16.5	82.5	65
Bed roughness, z_0	0.01477	0.00457	0.00457	0.00457	0.00457
Concentration (%)	0.1	0.5	1.0	5.0	10.0
Mean Velocity	0.08046489	1.7992494	2.544523	5.689727	8.046489
Shear Velocity	0.040232	0.089962	0.127226	0.284486	0.402324
Max. Suspended grain size (m)	0.000211	0.000316	0.000376	0.000563	0.000669

These estimates show that apart from the flow thickness and assuming all other flow parameters such as particle volume concentration are within the limits that can drive the flow, the maximum grain size that can be suspended by bed A5 is well influenced by the flow velocity. The results of this modelling show that as the flow velocity increases, the 5.0 m thick flow is able to suspend and transport increasing and larger sediment grain sizes. For example, the five different scenarios or cases show that a flow travelling with velocities of 0.080m/s (case 1), 1.799m/s (case 2), 2.54m/s (case 3), 5.69m/s(case 4) and 8.05m/s (case 5) can suspend and transport sediment grain sizes of 211 μ m, 316 μ m, 376 μ m, 563 μ m and 669 μ m respectively.

Therefore, it is possible for the 5.0m thick flow to suspend and transport sand across the 250km long Agadir basin. However, turbulence alone may not be the only grain support mechanism in the flow as observed from the 2-D analytical model.

6.6 Chapter summary

The following are the key points of this chapter:

- The simple 2D depth-averaged numerical flow model has been unable to reproduce the observed real-world long run-out thin turbidity current flows observed in Agadir basin. The flow model output is thick and observed to suspend mainly coarse grains.
- Suggestions of thin flows transporting sand grains across over 250 km wide Agadir basin cannot be substantiated by the flow model. Thin flows unless heavily turbulent and characterised by high concentration of fines, encourage rapid settling of sediment grains as the flow momentum could easily get dissipated.
- Initial sensitivity analysis of model flows suggests that input parameters influencing run-out distance and competence of the subaqueous flows are the thickness, volume of fine concentration, model run time as well as the inflow time. This agrees with existing models such as Rouse, (1937); Bowen et al (1984); Kneller and Buckee, 2000 and Normark et al., (2009).

7 Chapter Seven

Discussion/Implications of Study

7.1 Validation of the turbulence-suspension theory

7.1.1 Comparison of bed shear stress estimates

Bed shear stress determined by the three traditional approaches are expected to give similar estimates but in reality, they are hardly the same and no particular trend in estimates can be predicted. In this work, the *slope method*, *Law-of-the-wall or Logarithmic profile method* as well as the *Reynolds stress method* were all applied in estimating the basal shear stress.

As described in chapter three, the *slope method*, requires measurement of the flow slope, density and thickness, but limited as it only provides an upper limit value of the shear stress estimate. The *Reynolds stress method*, on the other hand, requires measurement of velocity-fluctuations and extrapolating the linear distribution of $\overline{u'w'}$ to the base of the turbulent flow. The third approach, called the *Law-of-the-wall or Logarithmic profile method* involves the extrapolation of the mean flow velocity to the base of the flow.

These three methods are expected to yield similar estimates if the von Karman-Prandtl turbulence suspension theory is to remain valid with respect to sediment transport.

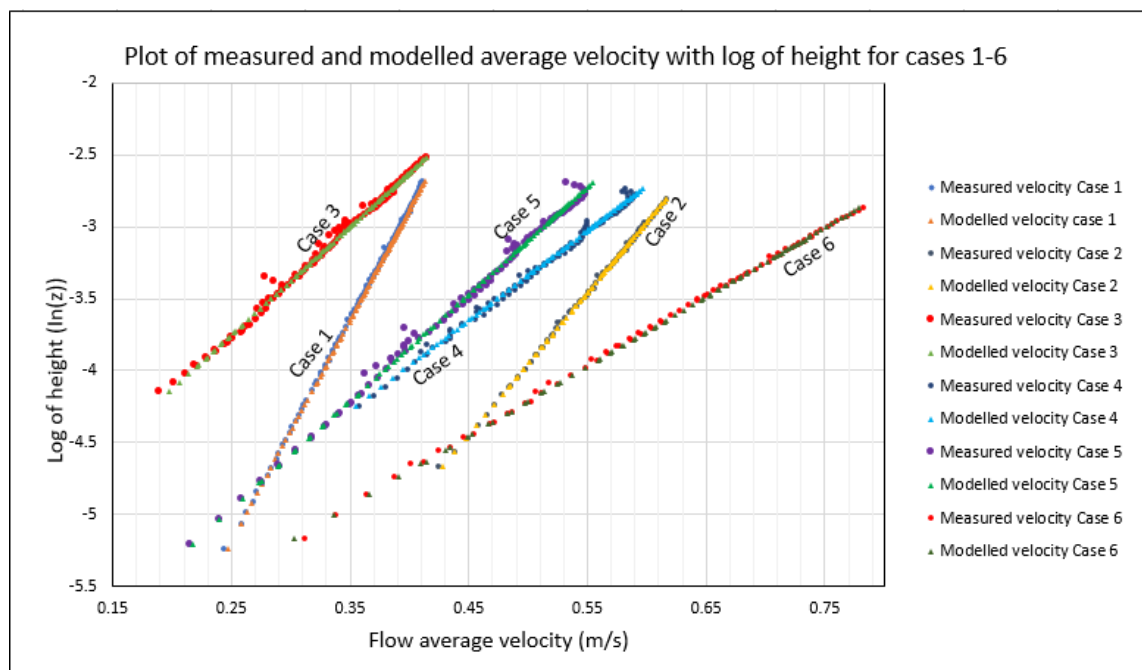


Figure 7.1: Agreement between measured and modelled dataset

Figures 7.1 and 7.2 shows the comparison of the velocity profiles obtained from modelled and measured dataset. Both profiles can be said to show a significant degree of agreement. All six experimental flow cases show similar trend in similarity with an R-squared value of approximately 0.99.

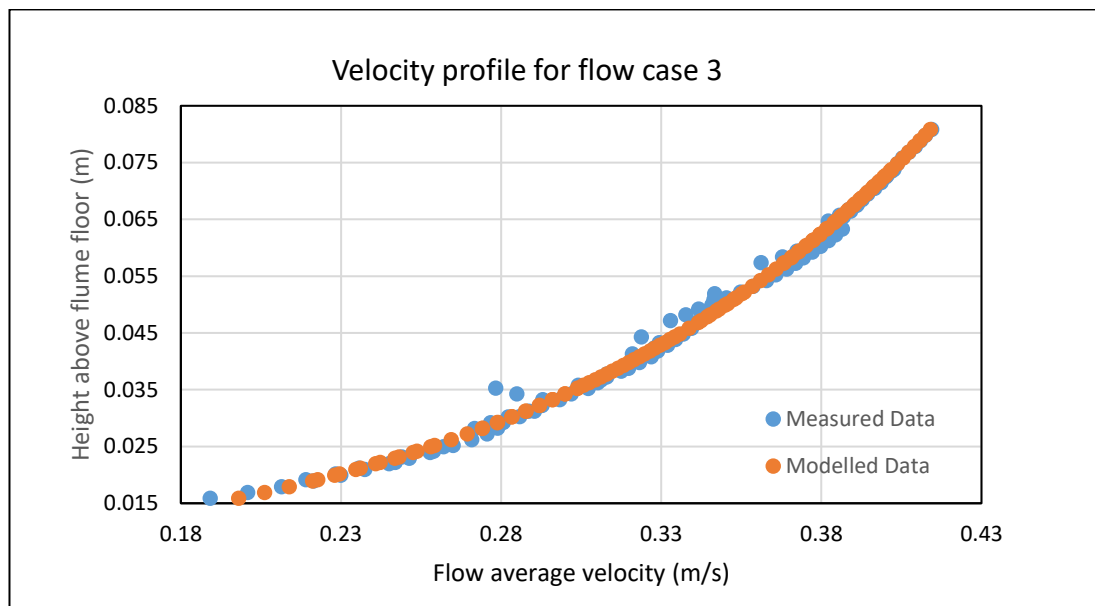


Figure 7.2: Similarity of velocity profile from measured and modelled dataset

Also, figure 7.1 provides a graphical representation of the estimates for all six flow cases which demonstrates how well the shear stress estimates from the Law-of-the-wall or Logarithmic profile and Reynolds stress methods agree with each other.

The key observation from figure 7.1 above, is that the basal shear stress estimates from both the Law-of-Wall and Reynolds stress methods significantly agree although the estimates do not exactly match as the Law-of-the-Wall estimates were comparatively higher in two of the six flow cases (3 and 6). For example, bed shear estimates in cases 3 and 6 were higher with about 40.0% and 15.6 % respectively. Other researchers such as Kim et al., (2000), Biron et al., (2004) and Sherwood et al., (2006) in their respective works also noted higher Law-of-the-Wall estimates in comparison to Reynolds Shear stress derived estimates. Also, Wilcock (1996), flow experiments

showed that four out of the nine flow experiments had estimates from the logarithmic profile higher than estimates from other methods.

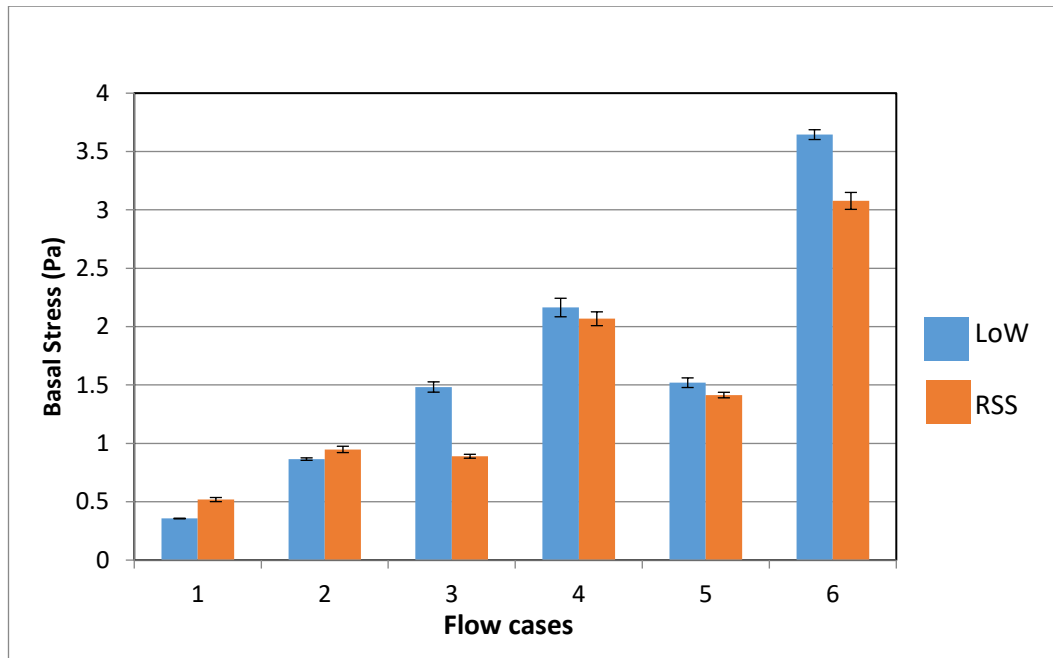


Figure 7.3: Comparing basal shear stress estimates from LoW and RSS

Similarly, Rowinski et al., (2005), also noted higher values of shear stress estimates from logarithmic profile method in their flow experiments. Following these observed comparatively lower Reynolds stress estimates, arguments attributing potential source of error and uncertainties has been traced to instrument sensitivity as the Reynolds stress method is very sensitive to sensor alignment, which make the Reynolds stress estimates liable errors arising from improper instrument positioning. A very important observation is that the higher estimates from logarithmic profile method were all from flows over rough floor surfaces. It is unclear why the estimates from the logarithmic profile method, in particular, were consistently higher in all the flows over rough floors. The other two flow cases (1 and 2) were flows over smooth concrete surface and have comparatively lower estimate values when compared to the Reynolds stress methods (Cases 1 (-45.6 %) and 2 (-9.6 %)). Flow cases 1, 2, 4 and 5, show good correlation as

they have very similar shear stress estimates (difference of less than 9.7% in estimate). The choice of $\kappa = 0.29$ in this work as earlier explained in the methodology, arrived by manual adjustment had contributed largely to minimising the difference between the Law-of-the-Wall and the Reynolds stresses. Clearly, on an overall scale, and as expected, the fit between the Law-of-the-Wall and Reynolds Shear Stress estimates is not perfect but can be regarded as acceptably good for a theory which only approximates the complex, true behaviour of turbulent flows. Hence, the shear stress estimates by any of the two methods should be a reasonable, first approximation to the eddy stresses at the base of the flow.

7.1.2 Comparison of direct slope with Reynolds slope

Slope derived from Reynolds shear stress could provide clues to the flow regime from laboratory flume experiment. For example, comparing the directly measured slope with that estimated from the Reynolds stress could provide clue on whether the flow was uniform or non-uniform. It is expected that in uniform flows, both slope estimates should agree while in non-uniform flows there could be some disparity in the estimates.

Figure 7.4 below shows a comparison of directly measured slope estimates with the Reynolds derived slope estimates for each of the six experimental flow cases reported in this thesis. It can be observed from the figure, that flow cases 1 and 2 show reasonable agreement between directly measured slope and estimates from the Reynolds shear stress methods. It can be inferred that these flows (cases 1 and 2) are uniform flows. Also, flow cases 3, 4, 5 and 6 whose estimates do not agree are inferred to signify non-uniform turbulent flows.

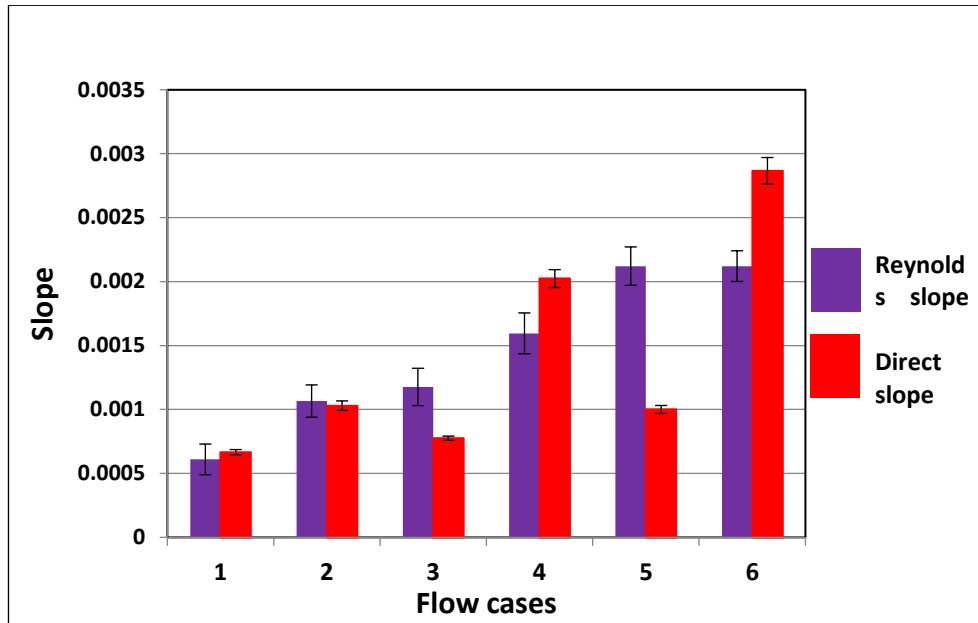


Figure 7.4: Comparing direct slope estimates with that from Reynolds Stress

7.1.3 Influence of roughness

Bed roughness can be produced by bed forms (ripples and mega ripples) as well as by individual sediment grains. From the turbulence model, z_0 represents the surface roughness length or height, where the instantaneous velocity equals to zero. In this work, the value of roughness length, z_0 , was derived from the fitting of the velocity profiles. The relationship between z_0 and the size of the roughness element which provides a measure of the bed grain size as derived by Raudkivi (1998) is presented in equation (3.10).

It is expected that rougher floors should have higher values of z_0 and consequently, greater turbulence. To test this, the roughness length, z_0 , was estimated from the log-profile method, through a best fit and by adjusting κ to a value of 0.29 (to minimise the difference between the basal stress from Law-of-the-Wall and the Reynolds stress (see table 5.12 and figure 5.16)). Clearly, from the results, gravel has a higher z_0 than concrete and there is a clear dichotomy between the gravel cases with $z_0 \sim 0.002$ m and the concrete-base case with $z_0 \sim 0.0001$ m. However, these results also show that roughness elements, χ , is greater than the roughness length, z_0 , which interestingly confirms Raudkivi (1998).

The drag coefficient, C_D , of the flows was estimated using expression provided by Waltham (2008). Table 5.11 (Chapter five) provides the estimates as well as the comparison of drag coefficient, C_D , of the flows over concrete and rough floors from the Law-of-the-Wall and the Reynolds shear stress methods. It is clear from the results as well as figures 5.17 and 5.18 (Chapter five) that both methods produce similar estimates of drag coefficient, C_D , and are thus reliable. A key observation from these figures confirms that the estimates of the drag coefficients for the rough gravel surfaces are higher than that of the smooth concrete surface. Table 5.10 also shows that that the basal shear stress of the rough gravelly floor is higher than that of the smooth concrete floor. This confirmed earlier works of Poggi et al. (2003), suggesting that shear stress should increase with bed roughness. Chen and Chiew (2003), in their experiment also found that shear velocity in marble bed was higher compared to sand bed due to the relative roughness of the marble bed. The implication is that rough beds create more flow turbulence and facilitate sediment grain suspension. Mazumder et al. (2005), from investigation, also revealed that higher bed roughness significantly controls the size distribution of suspended load and accounts for keeping sand-size sediment grains in suspension.

7.2 Bed A5 flow: comparing flow model with field-scale data

7.2.1 Areal extent of deposit

Figure 7.5 (A) shows the modelled areal extent of bed A5 flow deposit (using field scale input data from Talling et al., (2007); Stevenson et al., (2014)). It is observed from the figure that the modelled flow deposit was unable to get to the distal part of the basin and thus do not reflect exactly, the extensive nature of the flow given by the field description of Stevenson et al., (2014). The modelled flow had a thickness of 120.0 m and was deposited mid-way into the basin (see figure 7.5 B). The inability of the flow to reach the distal end of the basin may be attributed to the size of the flow as well as the fine sediment concentration. However, Talling et al., (2007), Wynn et al., (2012) and Stevenson et al., (2014) from field study, had reported basin-wide

occurrence of Bed A5 deposited from a large volume far-travelling turbidity current flow (figure 7.4B). Comparatively, both deposits, (fig 7.5 A and B), do not exactly match in areal extent with regards to their run-out distances. Estimating the actual size of deposits is outside the scope of this thesis.

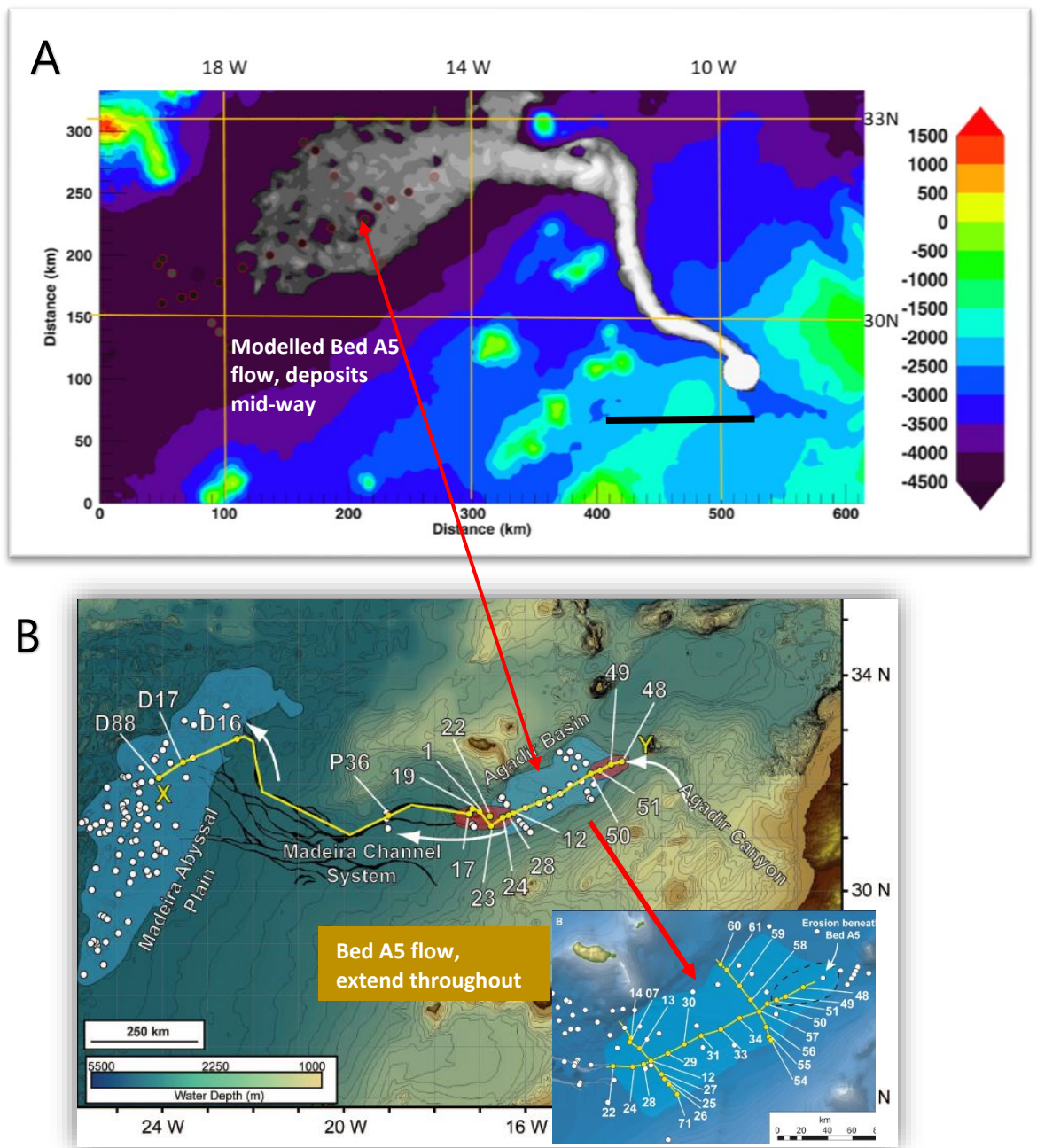


Figure 7.5: Areal extent of modelled (A) and mapped flow deposit (B)

7.2.2 Downstream grain-size trends

Spatial changes in grain size parameters of natural sediments in a flow usually vary with sampling locations due mainly to the sediment grain transport process such as abrasion and mixing of bed materials derived from multiple sources. Existing theories and empirical evidence suggest that grain sizes gradually fine downstream with distance, thus allowing prediction of sediment transport directions.

In this study, the grain size trends for sediments transported by bed A5 flow was assessed with a 2-D numerical model using input field data from 11 shallow sediment cores of Agadir basin, offshore Morocco, (fig. 7.6) reported by Stevenson et al., (2014).

Results showed no systematic change in grain size as it conforms to expected grain size distribution prediction, in which coarser grain sizes are at the proximal part of the basin near the canyon and marginally fining downstream further down the distal part of the basin (Fig. 7.7A). The observed downstream marginal grain size fining in Bed A5 deposit may be attributed to intense abrasion due to the grain-grain interaction in the flow and a possible decrease in mean flow velocity as the flow moves downslope.

Grain sizes ranged between 155 μm to 265 μm , with the lowest values recorded for core location 22 at the distal part of the basin. It was however, difficult to undertake a quantitative correlation of both modelled and measured grain size trends due to limitations of the model used but generally, both appear to have similar D_{50} grain size ranges (Fig. 7.7A and B).

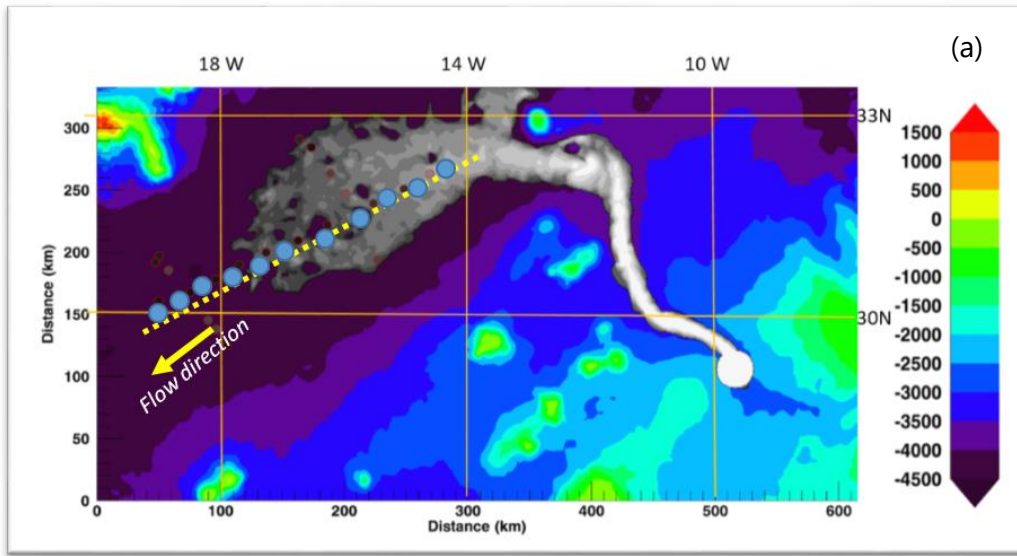
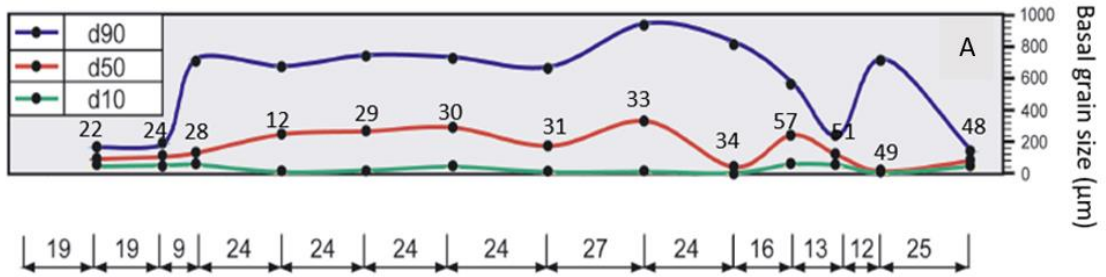


Figure 7.6: Downstream core locations (blue circles) for this study



Modelled D_{50} grain size trend bed A5 Agadir basin. (B)

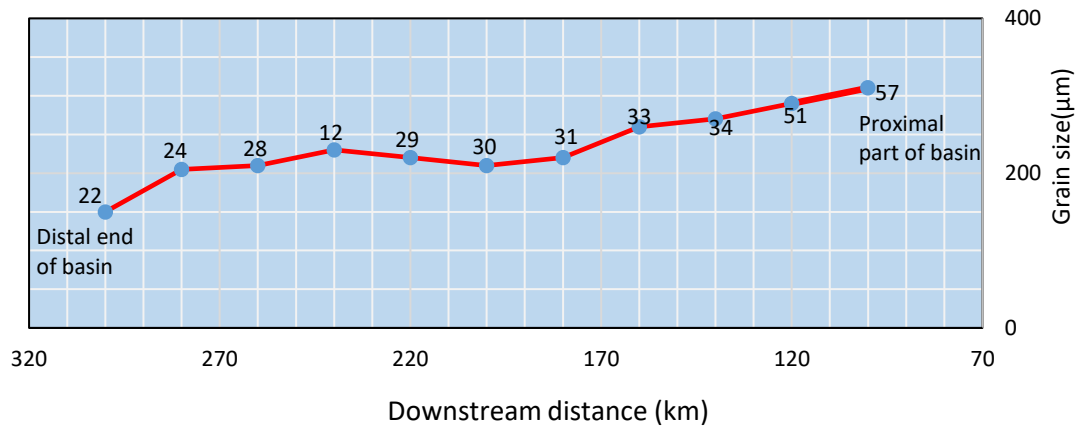


Figure 7.7(A & B): Comparison of measured (b) and modelled (a) D_{50} grain sizes (Figure 7.7A from Stevenson et al., 2014).

7.3 Variation of flow thickness

The thicknesses of turbidity current flows have been suggested to control the flow's run-out distances, its deposit size as well as how it interacts with topography (Kneller and Branney, 1995; Kneller et al., 1997; Kneller and McCaffrey, 1999). Flow thicknesses of turbidity currents can be determined from the heights to which the flow deposits drape-up channel or basin margins (Bowen et al., 1984; Kneller and Buckee, 2000). Alternative method such as using the channel topography and overbank levee deposits analysis has been applied in several other studies such as the Monterey Canyon, (Komar, 1969) and the Amazon Channel (Hiscott, 1997; Pirmez and Imran, 2003). In the Agadir basin, Stevenson et al., (2014) inferred thicknesses of turbidity current flows from the height to which the flows extend the margin topography. This method seems more sensible as the height provides the maximum estimate of the flow thickness as well as thickness of the depositional part of the flow.

In demonstrating the relationship between flow thickness and the run-out distances, numerical simulations on varied flow thickness using iterative values of 50.0m, 100.0m, 150.0m and 200.0m in the flow model produced outputs as presented in figures 7.8 (A-D). It is obvious from the figures that the thicker the turbidity current flow, the greater the distance the flow can travel, assuming all other flow parameters are constant. Kneller et al., (2016), from numerical evidence and field data also observed that turbidity currents propensity to travel long distances depends mainly on its thickness.

From figure 7.8A-D, the flow thickness of 50.0 m could not get the flow to reach the distal end of the depositional basin unlike the thickness of about 200.0m which propagate far into the distal part of the basin.

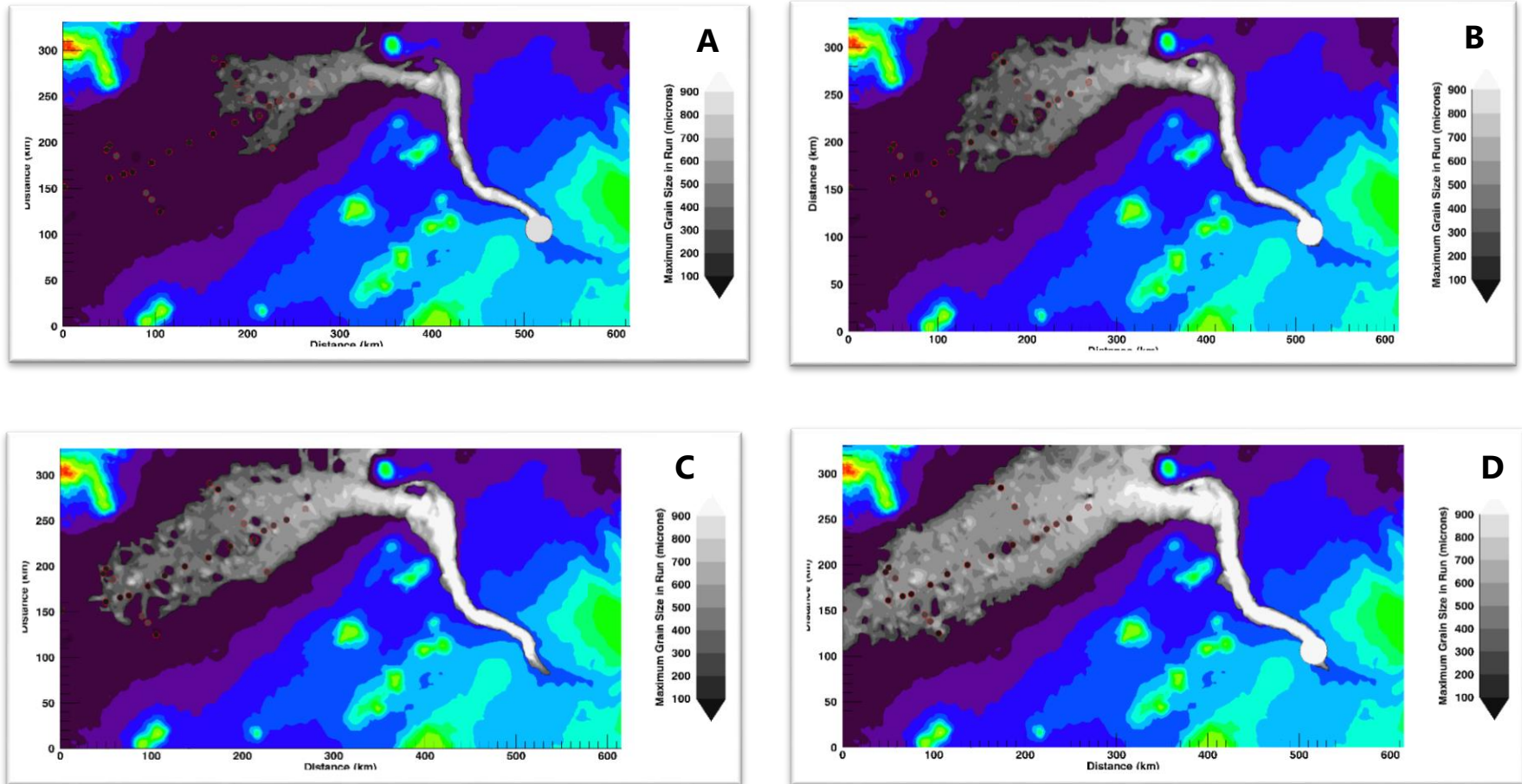


Figure 7.8: Variation of flow thickness with run-out distances (A= 50.0m thick; B =100.0m thick; C= 150.0m thick; D= 200.0m thick;)

7.4 Evolution of Bed A5 flow

The results of the numerical flow modelling (simulations), show that the flows that deposited Bed A5 do not exactly match with the field-scale dataset presented by Stevenson et al., (2014). The modelled flow deposit shows a flow thickness of approximately 60.0m suspending sand grains (*ca* 400 μ m) but not travelling far into the distal end of the basin. This is at odds with Talling et al., (2007) and Stevenson et al., (2014) observation of thin long run-out flows (of <5.0-7.0m), suspending sand grains just above the flow bed.

As previously explained the numerical flow model applied simply works on the assumption that turbulence alone facilitates the suspension of sediment grains in the turbidity current flow.

The series of initial simulations of the turbulence flow model showed that among other model input parameters, the thickness of the flow is a key factor that influence the competence and run-out distance of turbidity current flow. It was demonstrated in fig 6.11 that increasing the average flow thickness to 200.0m, the flow can adequately support the transport of coarse sediment grains to distal parts of the offshore basin. The implication is that thin flows are unable to generate enough turbulence to suspend sand grains over long distances. However, the question of how large volume long run-out flows suspended sand only a few meters (thin flows) from bed A5 in Agadir basin, raises more questions than answers. Are there alternative grain support mechanisms (such as hindered settling/ grain-grain collisions/matrix strength), apart from turbulence that keep the grains the flow? Similarly, do the physical properties of the non-Newtonian turbulent flow such as viscosity play any major role in precluding the settling of sand grains to allow its continuous propagation to the distal end of the basin?

The competence of a turbidity current flow and its run-out distances have been examined by several authors including Komar, (1970); Hiscott (1994); Gladstone et al., (1998), Felix (2002), and Kneller et al., (2016). It has long been speculated that fine grained sediments such as clays and silts are essential elements in turbidity currents which aid the transport of sand over long

distances. From experimental modelling of turbidity currents, bottom gradient and grain size have also been recognised as invaluable in the long-distance transport of sand. Thus, flows on low gradient and transporting a lot of fine sediments in suspension were observed to achieve long run-out distances (Reading and Richards, 1994). This was equally corroborated by Gladstone et al., (1998) laboratory experiments which indicated that despite the presence of a small fraction of fine-grained sediment in a turbidity current flow, its run-out distance is usually substantially increased.

The sedimentary facies of Bed A5 as earlier interpreted by Talling et al., (2007b), comprise simply of sand overlain by mud showing convincing evidence of stratification, dense near-bed layers and muddy debris flows. However, not all the facies identified in Bed A5 provide evidence of dilute, well mixed turbulent flow. Unfortunately, the numerical turbulent flow model can only be used to understand flow processes associated with turbulent suspension of sediment grains. Therefore, suggestions of bed A5 resulting from a higher-concentration mud-rich flow, described as a cohesive debris flow, documented in Talling et al., 2007 (a and b; Sumner et al., 2012; Stevenson et al., 2014) will come into more focus. In addition, Talling et al., (2007, 2013) inferred Bed A5 to be a linked-debrite (see figure 7.9 (a) and (b)) that particularly demonstrates flow transformation along their course, in which case there is the possibility of a switching from turbulence supported flows to muddy debris flows that are dominated by a laminar flow regime (which then switch back again). In the figure below, Talling et al., (2007) explained two perspectives of the likely evolution of Bed A5 flow (fig.7.9 provides a schematic description and evolution of bed A5 flow from two distinct perspectives for generating debris flows.

Generally, Talling et al., (2007) and Stevenson et al., (2014) showed that the flow that deposited Bed A5 may have been generated by a landslide on the Moroccan continental margin, proximal to the head of the Agadir Canyon, which produced a debris flow. This debris flow according to Talling et al., 2007, was transformed into a turbidity current at the base of the exit ramp located

at the mouth of the Agadir Canyon (See Figure 7.9 a). Within the Agadir basin, there was another transformation to debris and turbidity current leaving the coarse sands at the base of the flow and near to the bed.

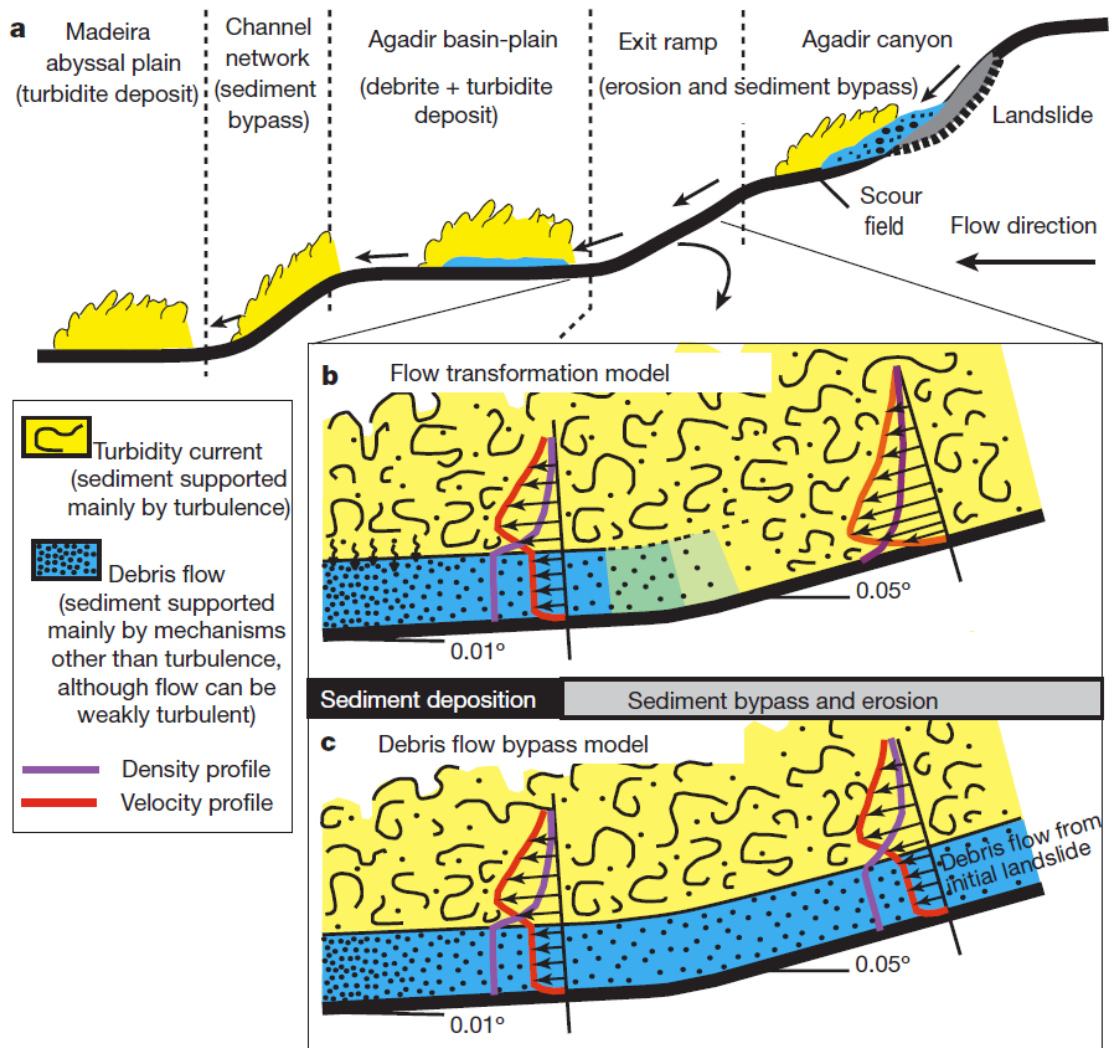


Figure 7.9: Possible mechanisms for deposition of Bed A5

(a) Evolution of the entire flow event from Agadir canyon to Agadir basin and beyond.

(b) Debris flow forms owing to flow transformation from turbidity current beyond the break in slope

(c) Debris flows may form by disintegration of initial landslide in the Upper Canyon (From Talling et al., 2007b).

This idea of a likely cohesive debris flow origin from the Moroccan margin landslide, for flow Bed A5 may well be the reason why the 2D depth- averaged flow model failed to reproduce the turbidity current flow as the grain support mechanism in a debris flow is quite at different from that of a turbidity current flow. Shanmugam (1997) exhaustively discussed the differences between a turbidity current and debris flows. The most interesting of these differences, as it relates to the theme of this thesis, is that turbidity current flow is considered a two-phase turbulent flow (water and solid) while debris flow is a one-phase laminar flow in which the whole mass undergoes large and continuous deformation (Coussot and Meunier,1886). Also, sediment grains transport by turbidity currents are held in suspension by the fluid turbulence (Middleton and Hampton, 1973), while in debris flows, it is supported essentially by multiple support mechanisms including matrix strength, dispersive pressure and buoyancy (Middleton, 1993). It has been observed from field evidence, that turbidity currents transport only fine-grained sediments (due to turbulence) whereas debris flows could transport sediments of all sizes (due to the multiple grain support mechanisms).

The 2-D depth averaged flow model used in this thesis has been able to confirm that the flows transporting sand that led to the deposition of Bed A5 is not necessarily supported by turbulence alone but a likely multiplicity of mechanisms including grain-grain interaction and matrix strength.

7.5 Implications of study

The results of the flume experiments and analysis presented in this thesis demonstrates the validity of the turbulence-suspension theory and therefore advocates its continuous relevance in sedimentology, particularly in solving sediment transport challenges.

This work reviewed the theoretical link between turbulence and sediment grain suspension which is yet to be fully understood. Although early researchers have developed different criteria for sediment grain entrainment into suspension (Bagnold (1966), Engelund (1965a, b) van Rijn (1984), Leeder (2005)), a common assumption among them remains the significant influence of turbulence of the flow. Ideally, for sediment grain to be entrained into suspension in a turbulent flow, the vertical flow velocity, w , must exceed the grain settling velocity, ω_s , (Bagnold 1966). However, a suspension criterion validated from the experimental data and based on the assumption that sediment grains will be suspended if the rms amplitude of vertical fluctuations, $\overline{w'^2}$, is greater than the grain settling-velocity in flowing water. Since $\overline{w'^2}$ is not usually measured, a further assumption made was for $\overline{w'^2}$ to be replaced by the shear velocity, u_*^2 . The vertical rms velocity variations $\overline{w'^2}$, was found to be approximately equal to $\overline{u'w'}$ and that, therefore, the shearing velocity u_*^2 , gives the same magnitude as the maximum fall-velocity that is consistent with suspension. More work will be needed, however, to further confirm this criterion.

Over the years, the turbulent-suspension theory has been fundamentally related to a steady, uniform flow such as the body of a turbidity current where the width, gradient and direction are almost constant or vary slowly. However, from the experimental results, by comparing direct slope with Reynolds slope, the theory can be applied to flows that are non-uniform. This is a very important result as the theory is valid in natural flows such as rivers and streams, which are almost never uniform.

Bedforms produced from flows over erodible beds have been known to attenuate turbulence in flows which subsequently facilitate sediment grain suspension. In the absence of bedforms, turbulence is controlled by the roughness at the flow base and the size of this coefficient can be predicted from the turbulence-suspension theory. This work has been able to demonstrate further that drag due to friction on gravelly surfaces exceeds that of the smooth floor.

There are many other obvious implications of the results of this work. First, based on the turbulence-suspension theory, it has been demonstrated that flow thickness of turbidity currents exerts a first order control on the flow's run-out distances. For example, thicker flows are relatively able to achieve long run-out distances as they have higher grain density and momentum compared to thinner flows. Secondly, thicker flows can advect a range of sediment grain sizes including coarse grains due to the increased turbulence in the flow. Thirdly, the continued suspension of fines in the flow is suggestive of the non-Newtonian behaviour of the likely muddy water in the flow (due to increased viscosity) and this drives the flow further in the basin. Fourth, it was noted that the flow model being based solely on turbulence suspension mechanism, suggest additional mechanisms may have contributed to Agadir's thin flow achieving a long run-out distance and being able to suspend sand sized sediment grains.

The numerical flow model used in this thesis discriminates only flows supported by turbulent-suspension, and unable to recognise any other additional grain support mechanisms not originally incorporated in the model. Thus, suggestions of flows evolving from a likely debris laminar flow which seem a possibility, cannot be captured by the flow model. This however, does not preclude the possibility of additional mechanisms supporting the transport of sand near the bed in the long run-out large volume flows.

Several field and laboratory evidence has been documented, supporting long run-out behaviour of turbidity current flows on flat basin floors (Komar, 1977; Underwood and Norville, 1986; Kneller et al., 2016). However, arguments for multiple support mechanisms facilitating the

suspension of sediment grains within a single flow at any one time is therefore proffered. These additional suspension mechanisms may include dispersive pressure, *hindered settling* and/or *grain-grain collisions* (Pickering and Hiscott, 2015). Hindered settling of sediment grains in turbidity current flow is due to increased concentration of fine grains leading to a greater grain-grain interaction that precludes the early settling of sediment grains in turbidity current flows (Tomkins et al., 2005; Dankers and Winterwerp, 2007), and also enhance its long distance travel. Therefore, the combination of flow turbulence, grain-grain collisions and hindered settling are the likely support mechanisms for the transport of sand in turbidity current flows that deposited Bed A5 in Agadir basin.

8 Chapter Eight: Summary

Summary and Conclusions

8.1 Summary and Conclusion

Nobody pretends that mixing-length (turbulence-suspension) theory is a precise model of flow turbulence. Instead, the contention has been how sufficiently well it approximates turbulence to be useful. This thesis has validated this for turbidity current flows under assumed uniform and non-uniform conditions at a level of detail not previously attempted. The outcome of this investigation demonstrate that the underlying approximations are indeed reasonably good and that, therefore, sedimentologists can continue to apply mixing-length theories and estimates of basal shear velocities to provide insights into the transport of suspended sediments. Using the combined experimental and numerical modelling investigative approach, the following key conclusions can be drawn from this study:

1. Modern measurements of flow turbulence confirm that shear stresses within a steady, uniform water flow are balanced by eddy stresses of the kind predicted by Reynolds (1896).
2. Mixing-length theory of turbulent suspension of sediment grains work well within a steady, uniform flow and, hence, the law of the wall provides a good model of the vertical velocity profile. However, the results of this study have also demonstrated that the theory is applicable to unsteady, non-uniform flows such as rivers.
3. Time-averaged velocity versus height is well approximated by the Von Karman turbulence model. This is well illustrated by Figures 5.16- 5.21.
4. Reports, from earlier studies, that von Karman's constant, is not after all universal but varies and can be significantly smaller than the widely accepted value of 0.41, are strongly supported. Based on the clear water flow experiments, a κ value of 0.29 is recommend for low concentration flows. Low values for κ have been reported by several other researchers and so the derived κ value of 0.29 in this research is not unreasonable.
5. Basal shear stress calculated from the Von-Karman turbulence model agree with the Reynold's estimates provided a von Karman constant of 0.29 is used.

6. Modelled and measured flow velocities show a significant positive relationship with an R-squared value of almost unity.
7. Basal shear stress estimates obtained from the Law-of-the-Wall and Reynolds stress show reasonable agreement confirming the reliability of the Mixing Length turbulent suspension theory. Drag coefficient estimates obtained from both methods also show a significant correlation.
8. The turbulent suspension theory has been supported by the good fits of measured data to predictions of the Law-of-the-Wall, good fits to the predictions of RANS as well as the good fits of $\text{stress} = C_d \cdot v^2$.
9. Flow turbulence is controlled by the roughness at the flow base and the size of this coefficient is greater than the roughness element, z_0 , which interestingly confirms Raudkivi (1998). Drag coefficient estimated from Waltham (2008) also confirms that drag due to friction on gravelly surfaces exceeds that of the smooth floor used in the flume experiment.
10. A numerical flow model developed by Waltham et al., (2008) using algorithms of Reynolds-Averaged Navier Stokes (RANS) as well as the Chezy equations was used to understand sediment grain transport in Agadir basin, NW Africa, supported by turbulence only as well as predict flow properties.
11. Streamwise grain size trend from modelled and field data suggest a systematic change in grain size across the Agadir basin with relatively coarse grain sizes more dominant at the proximal part of the basin, near to the Agadir canyon and gradually grades to finer grain sizes in the central and distal areas of the basin.
12. Bed A5, which is one of the flow deposits of the Agadir basin, and a focus of this investigation is generally assumed to have evolved from flows generated by a landslide on the Moroccan margin which transported sands few meters from the base of the bed.

13. Recreating Bed A5 flow deposit using a 2-d depth averaged numerical model and comparing with field-scale data inputs was not very successful as the model output could not exactly match due to differences in the run-out distances and the grains suspended by the flow.
14. However, suggestions of Bed A5 flows evolving from a likely debris laminar flow, by earlier researchers seem a possibility, as the 2-D model used in this study was limited to capturing turbulent suspension of grains only.
15. Therefore, the reported evolution of Bed A5 from an initial landslide followed by flow transformation to turbidity current as proposed by Tailing et al., 2007 and Stevenson et al., 2014, remains the only acceptable plausibility for now until a more advanced model capable of capturing multiple sediment grain support mechanisms with a wide range of sediment grain sizes is applied to test the field inferences.

8.2 Future work

There is no doubt, from the results of this work, that the turbulence-suspension theory is still very valid. However, there are a few identified areas that will be of interest for future research and these are:

- 1) More research will be needed to investigate fine-grained suspension mechanisms. Possibilities are effect of grain collisions, increased viscosity of muddy waters as well as the non-Newtonian behaviour of muddy water.
- 2) More work is needed in confirming the theoretical link between turbulence and suspension.
- 3) The numerical flow model applied can be improved upon by including modelling of bed-load sediment grains with additional support mechanism such as grain-grain interaction as well as incorporating varied grain sizes (more than 2 grain sizes).













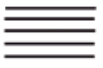







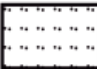








APPENDIX

A1. Glossary of notations

A	Cross sectional area of the flow channel
β	Bed slope angle
C_L	Lift coefficient
C_D	Drag coefficient
D_g	Grain diameter
D_w	Sediment grain fall diameter in cm
D_v	Sediment grain sieve diameter in cm
D_{50}	Grain median size (50th percentile)
D_{90}	Grain size at 90th percentile
F_D	Drag Force
F_G, g	Force due to gravity
F_L	Lift Force
δ_{sub}	Thickness of the laminar sublayer
h	Flow depth
K	Permeability
L	Distance over which flow moves
P	Total stream power
Q	Flow discharge rate
R_e	Fluid Reynolds Number
R_e^*	Grain Reynolds number
\emptyset	Porosity
\emptyset_0	Frictional angle (grain angle of repose)
s	Channel or sediment bed slope
T	Shear resistance due to the moving bed load
ρ	Density of fluid
ρ_s	Density of grain
$\Delta\rho$	Excess flow density
ν	Kinetic viscosity

κ	von Karman constant
μ	Dynamic viscosity
\bar{u}	Depth averaged flow velocity
u^*	Shear velocity
ω_s	Settling velocity
τ_0	Bed or basal shear stress
θ_{crit}	Dimensionless Critical Bed Shear Stress
τ_{crit}	Critical Bed or Basal shear stress
g	Acceleration due to gravity
$W' \sin \beta$	Downslope weight of moving sediment load
z_0	Surface roughness length
v_{pore}	Volume of all pores
v_{bulk}	Volume of sediment sample
v_{solid}	Volume of solid grain

A2. Key to graphic log on Bed A5 facies, Agadir basin (Fig 6.4)

Grain size (μm)		Sedimentary structures			
	D90	Graphic 	Label	Colour	Description
	D50		ST		Structureless gravel sized particles, often with shell fragments
	D10		ST		Clean and structureless
	Sorting <i>(after Folk & Ward, 1957)</i>		ST		Mud-rich and structureless
Symbols					
	Grain-size break overlain with finer sediment		ST _D		Mud-rich with clasts
	Grain-size break overlain with coarser sediment		PL		Parallel lamination
	Sharp and/or erosive boundary		LXL		Low-angle cross- lamination
	Turbidite sediment		RXL		Ripple cross- lamination
	Hemipelagic mud		CL		Contorted lamination
	Turbidite pinch-out		L		Mud/silt lamination
			CM		Contorted mud
			M		Structureless mud

A3. Measured and modelled flow velocity data Case 1

Flow height h (m)	Ln (h)	Measured <u>	<u'w'>	Turbulent stress (Pa)	shift	Model <u>	sq error
0.014395	-4.24085	0.311025	-0.00041	0.406187	-9.5413E-05	0.311520	2.44726E-07
0.009295	-4.67823	0.283796	-0.00035	0.345943		0.283058	5.45313E-07
0.008295	-4.79205	0.276597	-0.00033	0.331460		0.275651	8.9364E-07
0.007295	-4.92051	0.268396	-0.00031	0.310756		0.267292	1.21774E-06
0.006295	-5.06793	0.258854	-0.00029	0.289932		0.257699	1.33385E-06
0.005295	-5.24091	0.243438	-0.00027	0.274156		0.246442	9.02935E-06
0.023001	-3.77223	0.341531	-0.00036	0.357275	0.00152216	0.342014	2.33452E-07
0.019969	-3.91359	0.331983	-0.00036	0.360549		0.332815	6.92461E-07
0.018958	-3.96553	0.328824	-0.00036	0.359081		0.329436	3.74498E-07
0.032796	-3.41746	0.364591	-0.00033	0.332112	0.00151371	0.365100	2.59632E-07
0.031785	-3.44876	0.362650	-0.00033	0.333984		0.363063	1.70368E-07
0.030774	-3.48108	0.360681	-0.00033	0.328766		0.360960	7.78905E-08
0.029764	-3.51447	0.358201	-0.00033	0.333278		0.358787	3.43299E-07
0.028753	-3.54902	0.356072	-0.00034	0.335604		0.356539	2.18491E-07
0.022689	-3.78589	0.340886	-0.00034	0.338291		0.341125	5.75339E-08
0.021678	-3.83146	0.338549	-0.00033	0.333025		0.338160	1.5113E-07
0.020667	-3.8792	0.335505	-0.00034	0.341356		0.335053	2.03775E-07
0.042263	-3.16385	0.382979	-0.00029	0.289934	0.00238809	0.381604	1.89255E-06
0.041252	-3.18806	0.381146	-0.00029	0.288539		0.380028	1.2506E-06
0.040241	-3.21288	0.379297	-0.00031	0.314658		0.378413	7.81074E-07
0.039229	-3.23833	0.377304	-0.00031	0.311469		0.376757	2.98981E-07
0.038218	-3.26444	0.375584	-0.00031	0.310965		0.375058	2.76531E-07
0.037207	-3.29125	0.373732	-0.00029	0.291243		0.373313	1.75901E-07
0.030130	-3.50225	0.359376	-0.0003	0.304647		0.359583	4.29152E-08
0.029118	-3.53638	0.357807	-0.00031	0.307539		0.357361	1.98696E-07
0.028107	-3.57173	0.354259	-0.00032	0.322624		0.355062	6.44864E-07
0.027096	-3.60836	0.351593	-0.00033	0.327355		0.352678	1.17627E-06
0.026085	-3.64639	0.347920	-0.00036	0.355504		0.350203	5.21242E-06
0.050586	-2.98409	0.393520	-0.00023	0.234200	0.00387949	0.393301	4.77701E-08
0.049575	-3.00428	0.392206	-0.00023	0.231700		0.391987	4.78245E-08
0.048564	-3.02488	0.390773	-0.0002	0.204800		0.390646	1.61287E-08
0.047552	-3.04592	0.389647	-0.00023	0.229700		0.389277	1.36602E-07
0.046541	-3.06741	0.388385	-0.00024	0.237000		0.387879	2.55943E-07
0.045530	-3.08938	0.386508	-0.00025	0.251000		0.386449	3.43147E-09
0.044519	-3.11184	0.385205	-0.00026	0.256600		0.384988	4.72016E-08
0.043508	-3.13481	0.383695	-0.00024	0.235700		0.383493	4.06226E-08
0.059169	-2.82736	0.403596	-0.00014	0.139200	0.00507245	0.403500	9.37665E-09
0.058158	-2.8446	0.402613	-0.00014	0.138800		0.402378	5.53492E-08
0.057146	-2.86214	0.401655	-0.00014	0.142800		0.401237	1.7525E-07
0.056135	-2.87999	0.400405	-0.00015	0.150100		0.400075	1.08661E-07
0.055124	-2.89817	0.399153	-0.00015	0.154300		0.398892	6.78319E-08
0.054113	-2.91668	0.397792	-0.00016	0.161200		0.397688	1.09664E-08
0.053102	-2.93554	0.396740	-0.00016	0.163500		0.396460	7.85505E-08
0.052091	-2.95477	0.395737	-0.00017	0.168500		0.395209	2.78613E-07
0.051080	-2.97437	0.394344	-0.00017	0.170900		0.393934	1.68236E-07
0.050069	-2.99436	0.393195	-0.00018	0.175300		0.392633	3.16682E-07
0.049058	-3.01476	0.391663	-0.00018	0.176600		0.391305	1.28191E-07
0.068272	-2.68426	0.411085	-7.3E-05	0.073100	0.00592345	0.412812	2.98179E-06
0.067261	-2.69918	0.410546	-7.2E-05	0.072240		0.411841	1.6785E-06
0.062205	-2.77732	0.406402	-0.0001	0.104600		0.406756	1.25823E-07
0.061194	-2.7937	0.405492	-0.00012	0.116400		0.405690	3.90603E-08
0.060183	-2.81036	0.404774	-0.00012	0.121000		0.404606	2.82697E-08
0.059172	-2.82731	0.403564	-0.00013	0.125300		0.403503	3.63008E-09

A4. Measured and modelled flow velocity data Case 2

Flow height, h(m)	Ln (h)	Measured <u>	<u'w'>	Turbulent stress (Pa)	shift	Modelled <u>	sq error
0.025618739	-3.66443	0.524617	-0.0007008	0.700760	0.000381	0.528977993	1.9E-05
0.024608046	-3.70468	0.524336	-0.000695	0.695035		0.524895889	3.13E-07
0.023597352	-3.74662	0.520397	-0.0007142	0.714241		0.520642558	6.02E-08
0.022586658	-3.7904	0.516191	-0.0007327	0.732662		0.516203008	1.48E-10
0.021575965	-3.83618	0.512380	-0.0007385	0.738483		0.511560188	6.73E-07
0.032607559	-3.42321	0.555133	-0.0006655	0.665460	0.002992	0.553441853	2.86E-06
0.031596866	-3.4547	0.551030	-0.0006621	0.662079		0.550248612	6.11E-07
0.030586172	-3.48721	0.547490	-0.0006652	0.665244		0.546951546	2.9E-07
0.029575478	-3.52081	0.543059	-0.0006715	0.671460		0.543543681	2.35E-07
0.028564785	-3.55558	0.538806	-0.0006845	0.684475		0.540017314	1.47E-06
0.027554091	-3.5916	0.534643	-0.0006897	0.689688		0.536363897	2.96E-06
0.043990292	-3.12379	0.584067	-0.0005757	0.575703	0.00201	0.583808677	6.65E-08
0.042979599	-3.14703	0.581633	-0.0005838	0.583812		0.581451396	3.3E-08
0.041968905	-3.17083	0.578540	-0.0005862	0.586181		0.579038014	2.48E-07
0.040958211	-3.1952	0.576709	-0.0005942	0.594160		0.576565799	2.05E-08
0.039947518	-3.22019	0.574112	-0.0005926	0.592572		0.574031814	6.45E-09
0.038936824	-3.24581	0.571497	-0.0006077	0.607668		0.571432886	4.06E-09
0.037926131	-3.27211	0.569142	-0.0006115	0.611492		0.568765605	1.42E-07
0.036915437	-3.29913	0.566767	-0.0006065	0.606540		0.566026273	5.48E-07
0.035904743	-3.32689	0.563462	-0.0006098	0.609838		0.56321089	6.29E-08
0.03489405	-3.35544	0.560997	-0.0006244	0.624370		0.560315117	4.65E-07
0.033883356	-3.38483	0.557202	-0.0006625	0.662504		0.557334222	1.75E-08
0.032872663	-3.41511	0.554373	-0.0006467	0.646731		0.554263054	1.21E-08
0.031861969	-3.44634	0.551098	-0.0006621	0.662064		0.551095968	5.62E-12
0.030851275	-3.47858	0.548768	-0.0006449	0.644851		0.547826782	8.87E-07
0.029840582	-3.51189	0.544388	-0.0006618	0.661784		0.544448698	3.63E-09
0.028829888	-3.54634	0.540422	-0.0006856	0.685627		0.540954201	2.83E-07
0.027819194	-3.58203	0.535389	-0.0006916	0.691570		0.537334985	3.79E-06
0.051592266	-2.96438	0.597593	-0.0003573	0.357301	0.004408	0.599974862	5.68E-06
0.050581573	-2.98417	0.596088	-0.0003977	0.397720		0.59796838	3.53E-06
0.049570879	-3.00435	0.593650	-0.0004055	0.405465		0.595921396	5.16E-06
0.048560185	-3.02495	0.593233	-0.0004199	0.419909		0.593832244	3.59E-07
0.047549492	-3.04598	0.591927	-0.0004269	0.426882		0.591699151	5.18E-08
0.046538798	-3.06747	0.590150	-0.000411	0.410957		0.589520226	3.97E-07
0.045528105	-3.08943	0.588996	-0.0004249	0.424945		0.587293459	2.9E-06
0.039463943	-3.23237	0.573822	-0.0004632	0.463236		0.572796642	1.05E-06
0.038453249	-3.25831	0.571651	-0.0004739	0.473946		0.570165452	2.21E-06
0.037442556	-3.28495	0.566920	-0.0004891	0.489079		0.567464177	2.96E-07
0.036431862	-3.31231	0.563155	-0.0005019	0.501928		0.564688977	2.35E-06
0.035421168	-3.34045	0.557952	-0.0005343	0.534299		0.561835694	1.51E-05
0.060592019	-2.80359	0.616005	-0.0003371	0.337106	0.005408	0.616281874	7.68E-08
0.059581326	-2.82041	0.614517	-0.0003493	0.349312		0.614575937	3.43E-09
0.058570632	-2.83752	0.613153	-0.0003543	0.354319		0.612840812	9.75E-08
0.057559938	-2.85493	0.611415	-0.0003624	0.362351		0.611075483	1.15E-07
0.056549245	-2.87264	0.609572	-0.0003857	0.385675		0.609278882	8.59E-08
0.055538551	-2.89068	0.607483	-0.0003989	0.398939		0.607449878	1.12E-09
0.054527858	-2.90904	0.606276	-0.0004115	0.411488		0.605587284	4.74E-07
0.053517164	-2.92775	0.604462	-0.0004196	0.419609		0.603689839	5.96E-07
0.05250647	-2.94682	0.602286	-0.0004292	0.429229		0.601756216	2.81E-07
0.051495777	-2.96626	0.600724	-0.000443	0.443049		0.599785012	8.81E-07
0.050485083	-2.98608	0.598332	-0.0004574	0.457379		0.59777473	3.11E-07
0.04947439	-3.0063	0.595815	-0.0004748	0.474760		0.595723797	8.35E-09

A5. Measured and modelled flow velocity data Case 3

Flow height,h (m)	Ln (h)	Measured <u>(m/s)	<u'w'>	Turbulent stress (Pa)	shift	Modelled <u>	Sq error
0.024943	-3.69118	0.262056	-0.000691	0.690655	-0.00891	0.257988	1.65E-05
0.023936	-3.73239	0.257783	-0.000683	0.683439		0.252516	2.77E-05
0.022928	-3.77538	0.251288	-0.000692	0.692436		0.246809	2.01E-05
0.021921	-3.82029	0.245057	-0.000702	0.702415		0.240845	1.77E-05
0.020914	-3.86732	0.237450	-0.000709	0.708586		0.234600	8.12E-06
0.035244	-3.34545	0.278349	-0.000677	0.676843	-0.00917	0.303895	0.000653
0.034237	-3.37445	0.284943	-0.000686	0.685731		0.300044	0.000228
0.033229	-3.40432	0.293022	-0.000713	0.713034		0.296078	9.34E-06
0.032222	-3.43511	0.292835	-0.000714	0.714046		0.291990	7.14E-07
0.031214	-3.46688	0.288617	-0.000704	0.703507		0.287772	7.14E-07
0.030207	-3.49968	0.285820	-0.000707	0.707454		0.283415	5.78E-06
0.029199	-3.5336	0.280683	-0.000697	0.696804		0.278911	3.14E-06
0.028192	-3.56872	0.278904	-0.000687	0.687113		0.274249	2.17E-05
0.027185	-3.60511	0.275648	-0.000685	0.685405		0.269417	3.88E-05
0.026177	-3.64287	0.270864	-0.000702	0.702151		0.264403	4.17E-05
0.044285	-3.11712	0.323817	-0.000602	0.601521	-0.00867	0.334214	0.000108
0.043277	-3.14013	0.329365	-0.000621	0.621132		0.331158	3.21E-06
0.042270	-3.16368	0.327828	-0.000613	0.612538		0.328031	4.11E-08
0.041262	-3.18781	0.321034	-0.000599	0.598903		0.324827	1.44E-05
0.040255	-3.21252	0.322077	-0.000619	0.618916		0.321545	2.83E-07
0.028165	-3.56966	0.271738	-0.000679	0.679030		0.274123	5.69E-06
0.051852	-2.95935	0.346641	-0.000431	0.431348	-0.00548	0.355162	7.26E-05
0.046815	-3.06155	0.340982	-0.000519	0.518810		0.341592	3.72E-07
0.045808	-3.0833	0.339471	-0.000518	0.517647		0.338703	5.89E-07
0.044800	-3.10554	0.336871	-0.000532	0.531947		0.335750	1.26E-06
0.043793	-3.12829	0.334472	-0.000537	0.537115		0.332730	3.03E-06
0.039763	-3.22482	0.323200	-0.000563	0.563042		0.319912	1.08E-05
0.038755	-3.25049	0.319763	-0.000570	0.570187		0.316505	1.06E-05
0.037748	-3.27682	0.312966	-0.000566	0.566392		0.313007	1.73E-09
0.036740	-3.30388	0.311348	-0.000566	0.565909		0.309415	3.74E-06
0.035733	-3.33168	0.304109	-0.000577	0.577164		0.305723	2.61E-06
0.063256	-2.76056	0.386560	-0.000365	0.365015	-0.0069	0.381558	2.5E-05
0.062249	-2.77662	0.384457	-0.000366	0.366310		0.379426	2.53E-05
0.061241	-2.79294	0.382313	-0.000373	0.372880		0.377259	2.55E-05
0.060234	-2.80952	0.379782	-0.000389	0.389446		0.375057	2.23E-05
0.059226	-2.82639	0.377195	-0.000397	0.396979		0.372817	1.92E-05
0.058219	-2.84355	0.374372	-0.000414	0.414342		0.370539	1.47E-05
0.057211	-2.861	0.371936	-0.000425	0.425359		0.368221	1.38E-05
0.056204	-2.87877	0.369210	-0.000434	0.433616		0.365862	1.12E-05
0.047137	-3.0547	0.332890	-0.000514	0.513702		0.342501	9.24E-05
0.073467	-2.61093	0.401964	-0.000324	0.324308	-0.00757	0.401427	2.88E-07
0.072459	-2.62474	0.400202	-0.000328	0.328165		0.399593	3.71E-07
0.071451	-2.63875	0.398651	-0.000338	0.338412		0.397733	8.44E-07
0.059356	-2.8242	0.372395	-0.000437	0.436804		0.373108	5.09E-07
0.058348	-2.84132	0.367908	-0.000445	0.444785		0.370834	8.56E-06
0.057341	-2.85875	0.361147	-0.000444	0.444357		0.368521	5.44E-05
0.080816	-2.51558	0.414416	-0.000278	0.277946	-0.00417	0.414087	1.08E-07
0.079808	-2.52813	0.412518	-0.000285	0.284721		0.412421	9.51E-09
0.078800	-2.54084	0.410908	-0.000299	0.298891		0.410733	3.05E-08
0.077792	-2.55371	0.409375	-0.000302	0.302498		0.409024	1.23E-07
0.076785	-2.56675	0.407347	-0.000310	0.310448		0.407292	3.02E-09
0.065698	-2.72269	0.385706	-0.000431	0.431030		0.386587	7.76E-07
0.064690	-2.73815	0.382192	-0.000441	0.440708		0.384534	5.49E-06

A6. Measured and modelled flow velocity data Case 4

Flow height, h(m)	Ln (h)	Measured <u> (m/s)	<u'w'>	Turbulent Stress (Pa)	shift	Modelled <u>	Sq error
0.028532	-3.55674	0.455964	-0.00158	1.576911	-0.00236	0.464716	7.66E-05
0.027521	-3.59282	0.456715	-0.00157	1.573998		0.458928	4.9E-06
0.026509	-3.63025	0.429201	-0.00151	1.509985		0.452924	0.000563
0.025498	-3.66914	0.444066	-0.00162	1.620324		0.446687	6.87E-06
0.024487	-3.7096	0.434100	-0.00152	1.519082		0.440197	3.72E-05
0.036165	-3.31967	0.506896	-0.0014	1.397202	0	0.502741	1.73E-05
0.035154	-3.34803	0.502844	-0.00141	1.411514		0.498193	2.16E-05
0.034143	-3.37721	0.498375	-0.00146	1.460242		0.493512	2.37E-05
0.033131	-3.40727	0.493017	-0.00147	1.466384		0.488690	1.87E-05
0.032120	-3.43827	0.488390	-0.00148	1.475405		0.483719	2.18E-05
0.031109	-3.47025	0.483851	-0.00152	1.516572		0.478588	2.77E-05
0.030098	-3.50329	0.479084	-0.0015	1.504350		0.473288	3.36E-05
0.029087	-3.53746	0.473588	-0.00151	1.507870		0.467808	3.34E-05
0.028076	-3.57284	0.467803	-0.00149	1.494628		0.462133	3.21E-05
0.044352	-3.1156	0.535273	-0.00132	1.322112	0.001596	0.535473	4.01E-08
0.043340	-3.13867	0.532366	-0.00138	1.383282		0.531773	3.52E-07
0.042329	-3.16229	0.527714	-0.00137	1.370265		0.527985	7.35E-08
0.041317	-3.18647	0.525210	-0.00139	1.389002		0.524105	1.22E-06
0.040306	-3.21126	0.522118	-0.00136	1.362878		0.520130	3.95E-06
0.039294	-3.23668	0.518080	-0.0014	1.395876		0.516053	4.11E-06
0.038283	-3.26276	0.514401	-0.00142	1.417144		0.511870	6.4E-06
0.037271	-3.28953	0.510212	-0.00143	1.426477		0.507575	6.96E-06
0.036260	-3.31705	0.505104	-0.00147	1.467691		0.503162	3.77E-06
0.035248	-3.34534	0.500106	-0.00147	1.468403		0.498623	2.2E-06
0.034237	-3.37446	0.494714	-0.00149	1.485741		0.493953	5.79E-07
0.033225	-3.40445	0.489082	-0.00154	1.539265		0.489143	3.74E-09
0.032214	-3.43537	0.483366	-0.0015	1.503830		0.484184	6.69E-07
0.031202	-3.46727	0.478267	-0.00148	1.483983		0.479066	6.39E-07
0.030191	-3.50022	0.471601	-0.00149	1.485168		0.473781	4.75E-06
0.029179	-3.5343	0.465799	-0.00154	1.536324		0.468314	6.33E-06
0.028168	-3.56958	0.458693	-0.00154	1.542012	0.003738	0.462655	1.57E-05
0.051709	-2.96213	0.549514	-0.00123	1.225096		0.560089	0.000112
0.050697	-2.98189	0.549043	-0.00129	1.290747		0.556921	6.21E-05
0.049686	-3.00204	0.548534	-0.00127	1.270198		0.553688	2.66E-05
0.044628	-3.10939	0.542027	-0.00133	1.327219		0.536469	3.09E-05
0.043616	-3.13232	0.538472	-0.0013	1.302242		0.532791	3.23E-05
0.035524	-3.33754	0.492010	-0.00135	1.351792		0.499875	6.19E-05
0.063987	-2.74907	0.579533	-0.00068	0.677320	0.001566	0.594263	0.000217
0.062976	-2.76501	0.583039	-0.00072	0.724243		0.591707	7.51E-05
0.061964	-2.7812	0.587993	-0.00076	0.757219		0.589110	1.25E-06
0.060953	-2.79766	0.583686	-0.00077	0.768476		0.586470	7.75E-06
0.059941	-2.81439	0.585644	-0.0008	0.796759		0.583786	3.45E-06
0.058930	-2.83141	0.584102	-0.0008	0.798309		0.581056	9.27E-06
0.057918	-2.84873	0.580187	-0.00084	0.838358		0.578279	3.64E-06
0.056907	-2.86635	0.579676	-0.00085	0.852498		0.575453	1.78E-05
0.055895	-2.88428	0.576844	-0.00087	0.871898		0.572576	1.82E-05
0.054883	-2.90254	0.574206	-0.00091	0.906268		0.569647	2.08E-05
0.053872	-2.92114	0.570300	-0.00091	0.911743		0.566663	1.32E-05
0.064786	-2.73667	0.581306	-0.00067	0.665164	0.000744	0.596253	0.000223
0.063774	-2.75241	0.586107	-0.00071	0.712374		0.593728	5.81E-05
0.062762	-2.7684	0.590358	-0.00075	0.752731		0.591163	6.48E-07
0.061750	-2.78466	0.588624	-0.00077	0.767287		0.588555	4.73E-09
0.060738	-2.80118	0.588006	-0.00079	0.790571		0.585905	4.41E-06
0.059726	-2.81798	0.586079	-0.00082	0.818437		0.583210	8.23E-06

A7. Measured and modelled flow velocity data Case 5

Flow height,h(m) (m)	Ln (h)	Measured <u> (m/s) (m/s)	<u'w'> (m/s)	Turbulent Stress (Pa) (Pa)	shift	Modelled <u> (m/s)	Sq error
0.015608	-4.15999	0.360346	-0.0013	1.295239	0.00012	0.356995	1.12E-05
0.014597	-4.22696	0.350806	-0.0013	1.304134		0.347993	7.91E-06
0.013586	-4.29875	0.340888	-0.00129	1.294325		0.338344	6.47E-06
0.012574	-4.37609	0.329762	-0.00129	1.292806		0.327948	3.29E-06
0.024546	-3.70719	0.395723	-0.00121	1.207451	0.001281	0.417858	0.00049
0.023535	-3.74926	0.403886	-0.00121	1.212729		0.412204	6.92E-05
0.022524	-3.79317	0.399142	-0.00123	1.234042		0.406301	5.13E-05
0.021513	-3.8391	0.395791	-0.00121	1.209445		0.400128	1.88E-05
0.034023	-3.38073	0.468845	-0.00109	1.089735	0.002231	0.461740	5.05E-05
0.033012	-3.4109	0.464490	-0.00108	1.083802		0.457685	4.63E-05
0.032001	-3.442	0.459573	-0.00109	1.092373		0.453503	3.68E-05
0.030989	-3.47411	0.454944	-0.0011	1.100440		0.449188	3.31E-05
0.029978	-3.50728	0.450337	-0.00113	1.126417		0.444729	3.14E-05
0.028967	-3.54159	0.445052	-0.00114	1.141126		0.440117	2.44E-05
0.027956	-3.57712	0.439659	-0.00115	1.145575		0.435342	1.86E-05
0.026945	-3.61396	0.434572	-0.00117	1.166038		0.430390	1.75E-05
0.025934	-3.6522	0.428882	-0.0012	1.199359		0.425249	1.32E-05
0.024923	-3.69197	0.423157	-0.00121	1.211156		0.419904	1.06E-05
0.023912	-3.73339	0.416171	-0.00121	1.209871		0.414337	3.37E-06
0.022901	-3.77659	0.408068	-0.00126	1.259490		0.408529	2.13E-07
0.021889	-3.82175	0.395397	-0.00126	1.262951		0.402460	4.99E-05
0.045301	-3.09443	0.483199	-0.00085	0.853119	0.001709	0.500223	0.00029
0.044290	-3.117	0.488997	-0.0009	0.900853		0.497189	6.71E-05
0.043279	-3.14009	0.490023	-0.00091	0.907308		0.494085	1.65E-05
0.042268	-3.16373	0.490458	-0.00095	0.950342		0.490907	2.01E-07
0.037212	-3.29112	0.477693	-0.00101	1.012176		0.473784	1.53E-05
0.036201	-3.31867	0.474009	-0.00101	1.011337		0.470081	1.54E-05
0.035190	-3.347	0.469081	-0.00104	1.041060		0.466274	7.88E-06
0.034179	-3.37615	0.464964	-0.00105	1.053742		0.462355	6.81E-06
0.033168	-3.40618	0.460430	-0.00106	1.056032		0.458319	4.46E-06
0.032157	-3.43714	0.455669	-0.00109	1.088958		0.454157	2.28E-06
0.031146	-3.46909	0.450073	-0.00108	1.078607		0.449863	4.41E-08
0.030134	-3.50209	0.444483	-0.00109	1.090131		0.445427	8.91E-07
0.029123	-3.53622	0.437971	-0.00109	1.086674		0.440840	8.23E-06
0.057918	-2.84872	0.537964	-0.00085	0.850623	-0.00114	0.533249	2.22E-05
0.056907	-2.86633	0.535718	-0.00087	0.872462		0.530882	2.34E-05
0.055896	-2.88426	0.532493	-0.00093	0.925801		0.528472	1.62E-05
0.046796	-3.06196	0.503697	-0.00094	0.938017		0.504588	7.94E-07
0.045785	-3.0838	0.500040	-0.00097	0.966594		0.501651	2.6E-06
0.044774	-3.10613	0.496915	-0.00099	0.990610		0.498650	3.01E-06
0.043763	-3.12897	0.491704	-0.00103	1.029056		0.495580	1.5E-05
0.042752	-3.15235	0.487540	-0.00106	1.056594		0.492438	2.4E-05
0.041741	-3.17628	0.482257	-0.00109	1.094317		0.489220	4.85E-05
0.067640	-2.69356	0.531540	-0.00074	0.735501	-0.00034	0.554106	0.000509
0.066629	-2.70862	0.539371	-0.00078	0.781782		0.552081	0.000162
0.065618	-2.72391	0.544184	-0.00079	0.788397		0.550026	3.41E-05
0.064607	-2.73944	0.546972	-0.00078	0.777729		0.547939	9.34E-07
0.063595	-2.75521	0.547734	-0.00079	0.792651		0.545818	3.67E-06
0.062584	-2.77124	0.547604	-0.00075	0.753263		0.543664	1.55E-05
0.061573	-2.78753	0.546576	-0.00073	0.725048		0.541475	2.6E-05
0.060562	-2.80409	0.545035	-0.00073	0.733417		0.539249	3.35E-05
0.059551	-2.82092	0.542085	-0.00074	0.741224		0.536986	2.6E-05
0.058540	-2.83805	0.540161	-0.00074	0.737746		0.534684	3E-05
0.057529	-2.85547	0.536780	-0.00076	0.762939		0.532342	1.97E-05

A8. Measured and modelled flow velocity data Case 6

Flow height,h (m)	Ln (h)	Measured <u>(m/s)	<u'w'>	Turbulent Stress (Pa)	shift	Modelled <u>	Sq error
0.016834	-4.084338	0.517591	-0.002700	2.699706	-0.00023	0.526694727	8.29E-05
0.015823	-4.146306	0.506347	-0.002702	2.701978		0.513872172	5.66E-05
0.014811	-4.212368	0.502031	-0.002622	2.622389		0.500202287	3.35E-06
0.013800	-4.283107	0.486621	-0.002643	2.643112		0.485565002	1.12E-06
0.025761	-3.658904	0.611993	-0.002423	2.422619	0	0.614726595	7.47E-06
0.024749	-3.698978	0.603696	-0.002507	2.507282		0.606434338	7.5E-06
0.023737	-3.740725	0.595325	-0.002486	2.486433		0.597795844	6.1E-06
0.022725	-3.784292	0.586298	-0.002406	2.406104		0.588780917	6.16E-06
0.021713	-3.829843	0.577121	-0.002443	2.442864		0.579355315	4.99E-06
0.020701	-3.877569	0.567169	-0.002441	2.440999		0.569479779	5.34E-06
0.019689	-3.927688	0.557474	-0.002414	2.413688		0.559109168	2.67E-06
0.018677	-3.980451	0.547520	-0.002408	2.407638		0.548191292	4.5E-07
0.017665	-4.036154	0.535323	-0.002412	2.411537		0.536665099	1.8E-06
0.016653	-4.095143	0.523994	-0.002397	2.396925		0.524458805	2.16E-07
0.015641	-4.157832	0.510623	-0.002416	2.416182		0.511487076	7.47E-07
0.014629	-4.224716	0.497835	-0.002429	2.429404		0.497647384	3.53E-08
0.036030	-3.323397	0.683198	-0.002272	2.272410	0	0.68415048	9.08E-07
0.035018	-3.351884	0.676445	-0.002268	2.268219		0.678255771	3.28E-06
0.034006	-3.381207	0.670202	-0.002269	2.268910		0.672188194	3.94E-06
0.032994	-3.411416	0.662680	-0.002300	2.299943		0.665937291	1.06E-05
0.031983	-3.442566	0.656436	-0.002283	2.282890		0.659491682	9.34E-06
0.030971	-3.474718	0.648836	-0.002378	2.378024		0.652838814	1.6E-05
0.029959	-3.507937	0.642842	-0.002356	2.356028		0.6459649	9.75E-06
0.028947	-3.542299	0.635277	-0.002402	2.401864		0.638854794	1.28E-05
0.027935	-3.577883	0.627228	-0.002381	2.380508		0.631491649	1.82E-05
0.026923	-3.614780	0.619959	-0.002396	2.395980		0.623856803	1.52E-05
0.025911	-3.653091	0.610873	-0.002445	2.444695		0.615929417	2.56E-05
0.024899	-3.692928	0.602480	-0.002471	2.470568		0.60768616	2.71E-05
0.023887	-3.734419	0.593177	-0.002508	2.508075		0.599100873	3.51E-05
0.022875	-3.777705	0.585625	-0.002551	2.551379		0.590143894	2.04E-05
0.021863	-3.822951	0.574619	-0.002620	2.619535		0.580781558	3.8E-05
0.020851	-3.870341	0.565139	-0.002591	2.590500		0.570975499	3.41E-05
0.019839	-3.920089	0.553501	-0.002655	2.654870		0.560681511	5.16E-05
0.046271	-3.073247	0.738340	-0.001771	1.771426	-0.0002	0.735912122	5.89E-06
0.045258	-3.095367	0.732476	-0.001826	1.825728		0.731334985	1.3E-06
0.044246	-3.117988	0.728142	-0.001794	1.794378		0.726654288	2.21E-06
0.043234	-3.141132	0.722864	-0.001859	1.859410		0.721865256	9.97E-07
0.034123	-3.377773	0.672701	-0.002084	2.083895		0.6728989	3.91E-08
0.033111	-3.407887	0.667391	-0.002043	2.043393		0.666667637	5.23E-07
0.032099	-3.438936	0.659604	-0.002089	2.088648		0.660242857	4.09E-07
0.031087	-3.470980	0.650762	-0.002170	2.169913		0.653612184	8.12E-06
0.030074	-3.504085	0.641756	-0.002230	2.230127		0.646762009	2.51E-05
0.056844	-2.867443	0.782536	-0.001408	1.407832	-0.00048	0.778497641	1.63E-05
0.055832	-2.885411	0.778779	-0.001428	1.427840		0.774779586	1.6E-05
0.054820	-2.903708	0.774156	-0.001485	1.484664		0.770993485	1E-05
0.053807	-2.922346	0.769135	-0.001592	1.592480		0.767136816	3.99E-06
0.052795	-2.941339	0.764491	-0.001600	1.599525		0.763206913	1.65E-06
0.051783	-2.960698	0.760262	-0.001577	1.576764		0.759200925	1.13E-06
0.050770	-2.980441	0.756468	-0.001641	1.640576		0.755115833	1.83E-06
0.049758	-3.000580	0.752229	-0.001654	1.653871		0.750948464	1.64E-06
0.048746	-3.021134	0.746869	-0.001639	1.639351		0.746695455	3.01E-08
0.047734	-3.042119	0.742462	-0.001748	1.747999		0.742353194	1.18E-08
0.040648	-3.202813	0.703228	-0.001980	1.980028		0.70910203	3.45E-05

REFERENCES

- Ahrens, J. P., 2000, A fall-velocity equation: *Journal of waterway, port, coastal, and ocean engineering*, v. 126, no. 2, p. 99-102.
- Ahrens, J. P., 2003, Simple equations to calculate fall velocity and sediment scale parameter: *Journal of waterway, port, coastal, and ocean engineering*, v. 129, no. 3, p. 146-150.
- Albrecht, H.-E., Damaschke, N., Borys, M., and Tropea, C., 2013, *Laser Doppler and phase Doppler measurement techniques*, Springer Science & Business Media.
- Allen, J., 1984, Experiments on the settling, overturning and entrainment of bivalve shells and related models: *Sedimentology*, v. 31, no. 2, p. 227-250.
- Allen, P. A., 2009, *Earth surface processes*, John Wiley & Sons.
- Allen, T., 2013, *Particle size measurement*, Springer.
- Altuhafi, F., O'sullivan, C., and Cavarretta, I., 2012, Analysis of an image-based method to quantify the size and shape of sand particles: *Journal of Geotechnical and Geoenvironmental Engineering*, v. 139, no. 8, p. 1290-1307.
- An, S., Julien, P. Y., and Venayagamoorthy, S. K., 2012, Numerical simulation of particle-driven gravity currents: *Environmental fluid mechanics*, p. 1-19.
- Azpiroz-Zabala, M., Cartigny, M.J., Talling, P.J., Parsons, D.R., Sumner, E. J., Clare, M.A., Cooper C, Pope E.I., 2017, Newly recognised turbidity currents structure can explain prolonged flushing of submarine canyons. *Science advances*, 3(10), p.e 1700200
- Baas, J. H., Best, J. L., and Peakall, J., 2011, Depositional processes, bedform development and hybrid bed formation in rapidly decelerated cohesive (mud-sand) sediment flows: *Sedimentology*, v. 58, no. 7, p. 1953-1987.
- Baas, J. H., Best, J. L., Peakall, J., and Wang, M., 2009, A phase diagram for turbulent, transitional, and laminar clay suspension flows: *Journal of Sedimentary Research*, v. 79, no. 4, p. 162-183.
- Babaeyan-Koopaei, K., Ervine, D., Carling, P., and Cao, Z., 2002, Velocity and turbulence measurements for two overbank flow events in River Severn: *Journal of Hydraulic Engineering*, v. 128, no. 10, p. 891-900.
- Bagherimiyab, F., and Lemmin, U., 2013, Shear velocity estimates in rough-bed open-channel flow: *Earth surface processes and landforms*, v. 38, no. 14, p. 1714-1724.
- Bagnold, R., 1954, Experiments on a gravity-free dispersion of large solid spheres in a Newtonian fluid under shear, *in Proceedings of the Royal Society of London A: Mathematical, Physical and Engineering Sciences*, Volume 225, The Royal Society, p. 49-63.
- Bagnold, R., 1966, *An approach to the sediment transport problem: General Physics Geological Survey*, Prof. paper.
- Bagnold, R. A., 1956, The flow of cohesionless grains in fluids: *Philosophical Transactions of the Royal Society of London A: Mathematical, Physical and Engineering Sciences*, v. 249, no. 964, p. 235-297.
- Balachandar, S. and Eaton, J.K. (2010) Turbulent dispersed multiphase flow. *Annual Review of Fluid Mechanics* 42, 111–133.
- Bauer, B. O., Sherman, D. J., and Wolcott, J. F., 1992, Sources of uncertainty in shear stress and roughness length estimates derived from velocity profiles: *The Professional Geographer*, v. 44, no. 4, p. 453-464.
- Beal, M. A., and Shepard, F. P., 1956, A use of roundness to determine depositional environments: *Journal of Sedimentary Research*, v. 26, no. 1.
- Beheshti, A., and Ataie-Ashtiani, B., 2008, Analysis of threshold and incipient conditions for sediment movement: *Coastal Engineering*, v. 55, no. 5, p. 423-430.
- Bennett, S. J., Bridge, J. S., and Best, J. L., 1998, Fluid and sediment dynamics of upper stage plane beds: *Journal of Geophysical Research: Oceans*, v. 103, no. C1, p. 1239-1274.

- Bennett SJ, Atkinson JF, Hou Y, Fay MJ, 2013. Turbulence modulation by suspended sediment in a zero mean-shear geophysical flow. In: Venditti JG, Best J, Church M, Hardy RJ (eds) *Coherent flow structures at the earth's surface*. Wiley, Chichester, pp 309–321. doi:10.1002/9781118527221.ch20
- Bergeron, N. E., and Abrahams, A. D., 1992, Estimating shear velocity and roughness length from velocity profiles: *Water Resources Research*, v. 28, no. 8, p. 2155-2158.
- Best, J., Kirkbride, A., and Peakall, J., 2001, Mean Flow and Turbulence Structure of Sediment-Laden Gravity Currents: New Insights using Ultrasonic Doppler Velocity Profiling: *Particulate gravity currents*, p. 157-172.
- Best, J.L., 2005b The fluid dynamics of river dunes: a review and some future research directions. *Journal of Geophysical Research, Earth Surface* 110
- Beuselinck, L., Govers, G., Poesen, J., Degraer, G., and Froyen, L., 1998, Grain-size analysis by laser diffractometry: comparison with the sieve-pipette method: *Catena*, v. 32, no. 3, p. 193-208.
- Biron, P. M., Robson, C., Lapointe, M. F., and Gaskin, S. J., 2004, Comparing different methods of bed shear stress estimates in simple and complex flow fields: *Earth Surface Processes and Landforms*, v. 29, no. 11, p. 1403-1415.
- Blanchette, F., Piche, V., Meiburg, E., and Strauss, M., 2006, Evaluation of a simplified approach for simulating gravity currents over slopes of varying angles: *Computers & fluids*, v. 35, no. 5, p. 492-500.
- Blott, S. J., Croft, D. J., Pye, K., Saye, S. E., and Wilson, H. E., 2004, Particle size analysis by laser diffraction: *Geological Society, London, Special Publications*, v. 232, no. 1, p. 63-73.
- Blott, S. J., and Pye, K., 2006, Particle size distribution analysis of sand-sized particles by laser diffraction: an experimental investigation of instrument sensitivity and the effects of particle shape: *Sedimentology*, v. 53, no. 3, p. 671-685.
- Blott, S. J., and Pye, K., 2008, Particle shape: a review and new methods of characterization and classification: *Sedimentology*, v. 55, no. 1, p. 31-63.
- , 2012, Particle size scales and classification of sediment types based on particle size distributions: Review and recommended procedures: *Sedimentology*, v. 59, no. 7, p. 2071-2096.
- Bogárdi, J., and Szilvássy, Z., 1974, *Sediment transport in alluvial streams*, Akadémiai Kiadó Budapest.
- Boggs, S., 2009, *Petrology of sedimentary rocks*, Cambridge University Press.
- Bonnecaze, R. T., Huppert, H. E., and Lister, J. R., 1993, Particle-driven gravity currents: *Journal of Fluid Mechanics*, v. 250, p. 339-369.
- Bouma, A. H., 1962, *Sedimentology of some flysch deposits: a graphic approach to facies interpretation*, Elsevier Pub. Co.
- Bridge, J., and Demicco, R., 2008, *Earth surface processes, landforms and sediment deposits*, Cambridge University Press.
- Bridge, J., and Dominic, D., 1984, Bed load grain velocities and sediment transport rates: *Water Resources Research*, v. 20, no. 4, p. 476-490.
- Bridge, J. S., and Bennett, S. J., 1992, A model for the entrainment and transport of sediment grains of mixed sizes, shapes, and densities: *Water Resources Research*, v. 28, no. 2, p. 337-363.
- Brune, J. N., Curray, J., Dorman, L., and Raitt, R., 1992, A proposed super-thick sedimentary basin, Bay of Bengal: *Geophysical research letters*, v. 19, no. 6, p. 565-568.
- Buffington, J. M., 1999, The legend of AF Shields: *Journal of Hydraulic Engineering*, v. 125, no. 4, p. 376-387.
- Buffington, J. M., and Montgomery, D. R., 1997, A systematic analysis of eight decades of incipient motion studies, with special reference to gravel-bedded rivers: *Water Resources Research*, v. 33, no. 8, p. 1993-2029.

- Burchard, H., Craig, P. D., Gemmrich, J. R., van Haren, H., Mathieu, P.-P., Meier, H. M., Smith, W. A. M. N., Prandke, H., Rippeth, T. P., and Skillingstad, E. D., 2008, Observational and numerical modeling methods for quantifying coastal ocean turbulence and mixing: *Progress in oceanography*, v. 76, no. 4, p. 399-442.
- Buscombe, D., and Conley, D., 2012, Effective shear stress of graded sediments: *Water Resources Research*, v. 48, no. 5.
- Buscombe, D., and Masselink, G., 2009, Grain-size information from the statistical properties of digital images of sediment: *Sedimentology*, v. 56, no. 2, p. 421-438.
- Camenen, B., 2007, Simple and general formula for the settling velocity of particles: *Journal of Hydraulic Engineering*, v. 133, no. 2, p. 229-233.
- Cantero, M. I., Balachandar, S., and Parker, G., 2009, Direct numerical simulation of stratification effects in a sediment-laden turbulent channel flow: *Journal of Turbulence*, no. 10, p. N27.
- Cantero, M. I., Shringarpure, M., and Balachandar, S., 2012, Towards a universal criteria for turbulence suppression in dilute turbidity currents with non-cohesive sediments: *Geophysical Research Letters*, v. 39, no. 14.
- Cao, Z., Li, J., Pender, G., and Liu, Q., 2014, Whole-process modeling of reservoir turbidity currents by a double layer-averaged model: *Journal of Hydraulic Engineering*, v. 141, no. 2, p. 04014069.
- Cao, Z., Pender, G., and Meng, J., 2006, Explicit formulation of the Shields diagram for incipient motion of sediment: *Journal of Hydraulic Engineering*, v. 132, no. 10, p. 1097-1099.
- Cartwright, G., Friedrichs, C., and Sanford, L., 2011, In situ characterization of estuarine suspended sediment in the presence of muddy flocs and pellets: *Proceedings of Coastal Sediments*, Miami, FL, USA, p. 2-6.
- Cartwright, G. M., Friedrichs, C. T., and Smith, S. J., 2013, A test of the ADV-based Reynolds flux method for in situ estimation of sediment settling velocity in a muddy estuary: *Geo-Marine Letters*, v. 33, no. 6, p. 477-484.
- Chanson, H., Trevethan, M., and Koch, C., 2007, Discussion of "Turbulence measurements with acoustic Doppler velocimeters" by Carlos M. Garcia, Mariano I. Cantero, Yarko Nino, and Marcelo H. Garcia: *Journal of Hydraulic Engineering*, v. 133, no. 11, p. 1283-1286.
- Chen, X., and Chiew, Y.-M., 2003, Response of velocity and turbulence to sudden change of bed roughness in open-channel flow: *Journal of Hydraulic Engineering*, v. 129, no. 1, p. 35-43.
- Cheng, N.-S., 2004, Analysis of bedload transport in laminar flows: *Advances in water resources*, v. 27, no. 9, p. 937-942.
- Chien, N., and Wan, Z., 1999, *Mechanics of sediment transport*.
- Cho, G.-C., Dodds, J., and Santamarina, J. C., 2007, Closure to "Particle Shape Effects on Packing Density, Stiffness, and Strength: Natural and Crushed Sands" by Gye-Chun Cho, Jake Dodds, and J. Carlos Santamarina: *Journal of geotechnical and geoenvironmental engineering*, v. 133, no. 11, p. 1474-1474.
- Clare, M. A., Clarke, J.H., Talling, P.J., Cartigny, M.J.B and Pratomo, D.G., 2016. Preconditioning and triggering of offshore slope failures and turbidity currents revealed by most detailed monitoring yet at a fjord-head delta. *Earth and Planetary Science Letters*, 450, pp. 208-220
- Clarke, H.J.E., 2016. First wide-angle view of channelized turbidity currents linking migrating cyclic steps to flow characteristics. *Nat. Commun.* 7, 118960. <http://dx.doi.org/10.1038/ncomms11896>
- Clarke, H.J.E, Brucker, S., Muggah, J., Church, I., Cartwright, D., Kuus, P., Eisan, B., 2012a . The Squarmish Prodelta, monitoring active landslides and turbidity currents. In: *Canadian Hydrographic Conference*.

- Clifford, N. J., and French, J.R., 1993 Monitoring and modelling turbulent flows: historical and contemporary perspectives. In: *Turbulence: Perspectives on Flow and Sediment transport*(Eds N.J.Clifford, J.R. French and J. Hardisty). pp, 1-34. John Willey and Sons Ltd, New York.
- Craig, R. G., Loadman, C., Clement, B., Rusello, P. J., and Siegel, E., Characterization and testing of a new bistatic profiling acoustic Doppler velocimeter: The Vectrino-II, *in Proceedings Current, Waves and Turbulence Measurements (CWTM)*, 2011 IEEE/OES 10th2011, IEEE, p. 246-252.
- Dade, W. B., and Huppert, H. E., 1995, A box model for non-entraining, suspension-driven gravity surges on horizontal surfaces: *Sedimentology*, v. 42, no. 3, p. 453-470.
- Dankers, P., and Winterwerp, J., 2007, Hindered settling of mud flocs: theory and validation: *Continental shelf research*, v. 27, no. 14, p. 1893-1907.
- Darby, S. E., and Peakall, J., 2012, Modelling the equilibrium bed topography of submarine meanders that exhibit reversed secondary flows: *Geomorphology*, v. 163, p. 99-109.
- Dashtgard, S. E., Gingras, M. K., and Pemberton, S. G., 2008, Grain-size controls on the occurrence of bioturbation: *Palaeogeography, Palaeoclimatology, Palaeoecology*, v. 257, no. 1, p. 224-243.
- Dewals, B.J., Rulot, F., Ercicun, S., Archambeau, P., and Pirotton, M. 2010b Long term sediment management for sustainable hydropower. *Comprehensive Renewable Energy*. Volume 6-Hydro Power, A Sayigh, ed., Elsevier, Oxford.
- Di Stefano, C., Ferro, V., and Mirabile, S., 2010, Comparison between grain-size analyses using laser diffraction and sedimentation methods: *Biosystems Engineering*, v. 106, no. 2, p. 205-215.
- Dietrich, W. E., 1982, Settling velocity of natural particles: *Water resources research*, v. 18, no. 6, p. 1615-1626.
- Doroudian, B., Bagherimiyab, F., and Lemmin, U., 2010, Improving the accuracy of four-receiver acoustic Doppler velocimeter (ADV) measurements in turbulent boundary layer flows: *Limnology and Oceanography: Methods*, v. 8, no. 11, p. 575-591.
- Dorrell, R., Darby, S., Peakall, J., Sumner, E., Parsons, D., and Wynn, R., 2014, The critical role of stratification in submarine channels: Implications for channelization and long runout of flows: *Journal of Geophysical Research: Oceans*, v. 119, no. 4, p. 2620-2641.
- Doyle, E., Hogg, A., Mader, H., and Sparks, R., 2010, A two-layer model for the evolution and propagation of dense and dilute regions of pyroclastic currents: *Journal of Volcanology and Geothermal Research*, v. 190, no. 3, p. 365-378.
- Droppo, I., Walling, D., and Ongley, E., 2000, Influence of floc size, density and porosity on sediment and contaminant transport: *IAHS Publication*(International Association of Hydrological Sciences), no. 263, p. 141-147.
- Duncan, W. J., 1960, *An elementary treatise on the mechanics of fluids*, Arnold.
- Durafour, M., Jarno, A., Le Bot, S., Lafite, R., and Marin, F., 2015, Bedload transport for heterogeneous sediments: *Environmental Fluid Mechanics*, v. 15, no. 4, p. 731-751.
- Durgesh, V., Thomson, J., Richmond, M. C., and Polagye, B. L., 2014, Noise correction of turbulent spectra obtained from acoustic doppler velocimeters: *Flow Measurement and Instrumentation*, v. 37, p. 29-41.
- Dyer, K., 1989, Sediment processes in estuaries: future research requirements: *Journal of Geophysical Research: Oceans*, v. 94, no. C10, p. 14327-14339.
- Eggenhuisen, J. T., Cartigny, M. J., and de Leeuw, J., 2017, Physical theory for near-bed turbulent particle suspension capacity: *Earth Surface Dynamics*, v. 5, no. 2, p. 269.
- Einstein, H., and Chien, N., 1955, Effects of heavy sediment concentration near the bed on velocity and sediment distribution, Rep. 8, Mo. River Div: US Army Corps of Eng., Omaha, Nebr.

- Einstein, H. A., 1950, The bed-load function for sediment transportation in open channel flows, US Department of Agriculture Washington DC.
- El-Gawad, S. A., Pirmez, C., Cantelli, A., Minisini, D., Sylvester, Z., and Imran, J., 2012, 3-D numerical simulation of turbidity currents in submarine canyons off the Niger Delta: *Marine Geology*, v. 326, p. 55-66.
- Elhakeem, M., and Imran, J., 2011, Density functions for entrainment and deposition rates of nonuniform sediment: *Journal of Hydraulic Engineering*, v. 138, no. 7, p. 591-609.
- Elhakeem, M., Papanicolaou, A. T., and Tsakiris, A. G., 2016, A probabilistic model for sediment entrainment: The role of bed irregularity: *International Journal of Sediment Research*.
- Elhakeem, M., and Sattar, A., 2015, An entrainment model for non-uniform sediment: *Earth Surface Processes and Landforms*, v. 40, no. 9, p. 1216-1226.
- Ercilla, G., Alonso, B., Baraza, J., Estrada, F., and Farran, M., 2003, Oligocene to recent processes on the Agadir Continental Margin and Basin (Central Eastern Atlantic), *European Margin Sediment Dynamics*, Springer, p. 283-287.
- Ercilla, G., Alonso, B., Perez-Belzuz, F., Estrada, F., Baraza, J., Farran, M., Canals, M., and Masson, D., 1998, Origin, sedimentary processes and depositional evolution of the Agadir turbidite system, central eastern Atlantic: *Journal of the Geological Society*, v. 155, no. 6, p. 929-939.
- Felix, M., Peakall, J., and McCaffrey, W., 2006, Relative importance of processes that govern the generation of particulate hyperpycnal flows: *Journal of Sedimentary Research*, v. 76, no. 2, p. 382-387.
- Foias, C., Manley, O., Rosa, R., and Temam, R., 2001, Navier-Stokes equations and turbulence, Cambridge University Press.
- Folk, R. L., 1980, Petrology of sedimentary rocks, Hemphill Publishing Company.
- Folk, R. L., and Ward, W. C., 1957, Brazos River bar: a study in the significance of grain size parameters: *Journal of Sedimentary Research*, v. 27, no. 1.
- Fredsøe, J., and Deigaard, R., 1992, Advanced series on ocean engineering: World Scientific, v. 3, p. 392.
- Frenz, M., Wynn, R. B., Georgiopoulou, A., Bender, V. B., Hough, G., Masson, D. G., Talling, P. J., and Cronin, B. T., 2009, Provenance and pathways of late Quaternary turbidites in the deep-water Agadir Basin, northwest African margin: *International Journal of Earth Sciences*, v. 98, no. 4, p. 721-733.
- Frey, P and Church, M. 2009. How sediments move. *Science*, 325 (5947), pp1509-1510.
- Fukuda, M. K., and Lick, W., 1980, The entrainment of cohesive sediments in freshwater: *Journal of Geophysical Research: Oceans*, v. 85, no. C5, p. 2813-2824.
- Gabitto, J., and Tsouris, C., 2008, Drag coefficient and settling velocity for particles of cylindrical shape: *Powder Technology*, v. 183, no. 2, p. 314-322.
- Gao, N., Wang, S., Ubhi, H., and Starink, M., 2005, A comparison of grain size determination by light microscopy and EBSD analysis: *Journal of materials science*, v. 40, no. 18, p. 4971-4974.
- García, C. M., Cantero, M. I., Niño, Y., and García, M. H., 2005, Turbulence measurements with acoustic Doppler velocimeters: *Journal of Hydraulic Engineering*, v. 131, no. 12, p. 1062-1073.
- Garcia, M., and Parker, G., 1991, Entrainment of bed sediment into suspension: *Journal of Hydraulic Engineering*, v. 117, no. 4, p. 414-435.
- , 1993, Experiments on the entrainment of sediment into suspension by a dense bottom current: *Journal of Geophysical Research: Oceans*, v. 98, no. C3, p. 4793-4807.
- Goossens, D., 2008, Techniques to measure grain-size distributions of loamy sediments: a comparative study of ten instruments for wet analysis: *Sedimentology*, v. 55, no. 1, p. 65-96.

- Gore, R., and Crowe, C. T., 1989, Effect of particle size on modulating turbulent intensity: *International Journal of Multiphase Flow*, v. 15, no. 2, p. 279-285.
- Grabowski, R. C., Droppo, I. G., and Wharton, G., 2011, Erodibility of cohesive sediment: the importance of sediment properties: *Earth-Science Reviews*, v. 105, no. 3, p. 101-120.
- Graf, W. H., 1984, *Hydraulics of sediment transport*, Water Resources Publication.
- Graf, W. H. A., 1998, *Fluvial hydraulics: Flow and transport processes in channels of simple geometry*, v. 551.483 G7.
- Grant, W. D., and Madsen, O. S., 1982, Movable bed roughness in unsteady oscillatory flow: *Journal of Geophysical Research: Oceans*, v. 87, no. C1, p. 469-481.
- Grant, W. D., Williams III, A. J., and Glenn, S. M., 1984, Bottom stress estimates and their prediction on the northern California continental shelf during CODE-1: the importance of wave-current interaction: *Journal of Physical Oceanography*, v. 14, no. 3, p. 506-527.
- Gray, T.E., Alexander, J. and Leeder, M.R., 2006. Longitudinal flow evolution and turbulence structure of dynamically similar, sustained, saline density and turbidity currents. *Journal of Geophysical Research: Oceans*, 111(C8).
- Griffiths, J. C., 1967, *Scientific method in analysis of sediments*.
- Gust, G., and Southard, J. B., 1983, Effects of weak bed load on the universal law of the wall: *Journal of Geophysical Research: Oceans*, v. 88, no. C10, p. 5939-5952.
- Gutiérrez-Pastor, J., Nelson, C. H., Goldfinger, C., and Escutia, C., 2013, Sedimentology of seismo-turbidites off the Cascadia and northern California active tectonic continental margins, northwest Pacific Ocean: *Marine Geology*, v. 336, p. 99-119.
- Ha, H. K., and Maa, J. P.-Y., 2010, Effects of suspended sediment concentration and turbulence on settling velocity of cohesive sediment: *Geosciences Journal*, v. 14, no. 2, p. 163-171.
- Hager, W. H., and Oliveto, G., 2002, Shields' entrainment criterion in bridge hydraulics: *Journal of Hydraulic Engineering*, v. 128, no. 5, p. 538-542.
- Halsey, T.C., Kumar, A., and Perillo, M.M., Sedimentological regimes for turbidity currents: Depth-averaged theory. *Journal of GEOPHYSICAL research: Oceans*, 122(7), pp. 5260-5285
- Harris, T. C., Hogg, A. J., and Huppert, H. E., 2002, Polydisperse particle-driven gravity currents: *Journal of Fluid Mechanics*, v. 472, p. 333-371.
- Heimsund, S., 2007, Numerical simulation of turbidity currents: a new perspective for small-and large-scale sedimentological experiments: The University of Bergen.
- Hill, K. M., Gaffney, J., Baumgardner, S., Wilcock, P., and Paola, C., 2017, Experimental study of the effect of grain sizes in a bimodal mixture on bed slope, bed texture, and the transition to washload: *Water Resources Research*, v. 53, no. 1, p. 923-941.
- Hinze, J., 1975, *Turbulence* McGraw-Hill: New York, v. 218.
- Hjulstrom, F., 1935, Studies of the morphological activity of rivers as illustrated by the River Fyris, *Bulletin: Geological Institute Upsalsa*, v. 25, p. 221-527.
- Ho, V. L., Dorrell, R., Keevil, G., Burns, A., and McCaffrey, W., 2017, Pulse propagation in turbidity currents: *Sedimentology*.
- Hofland, B., and Battjes, J. A., 2006, Probability density function of instantaneous drag forces and shear stresses on a bed: *Journal of Hydraulic Engineering*, v. 132, no. 11, p. 1169-1175.
- Houssais, M., Ortiz, C. P., Durian, D. J., and Jerolmack, D. J., 2015, Onset of sediment transport is a continuous transition driven by fluid shear and granular creep: *Nature communications*, v. 6.
- Hu, P., Cao, Z., Pender, G., and Tan, G., 2012, Numerical modelling of turbidity currents in the Xiaolangdi reservoir, Yellow River, China: *Journal of hydrology*, v. 464, p. 41-53.
- Huang, H., Imran, J., and Pirmez, C., 2005, Numerical model of turbidity currents with a deforming bottom boundary: *Journal of Hydraulic Engineering*, v. 131, no. 4, p. 283-293.

- Hubbard, S. M., Covault, J. A., Fildani, A., and Romans, B. W., 2014, Sediment transfer and deposition in slope channels: deciphering the record of enigmatic deep-sea processes from outcrop: *Geological Society of America Bulletin*, v. 126, no. 5-6, p. 857-871.
- Hunt, J. E., Wynn, R. B., Talling, P. J., and Masson, D. G., 2013, Frequency and timing of landslide-triggered turbidity currents within the Agadir Basin, offshore NW Africa: Are there associations with climate change, sea level change and slope sedimentation rates?: *Marine Geology*, v. 346, p. 274-291.
- Hunter, T., Peakall, J., and Biggs, S., 2011, Ultrasonic velocimetry for the in situ characterisation of particulate settling and sedimentation: *Minerals Engineering*, v. 24, no. 5, p. 416-423.
- Huppert, H. E., 1998, Quantitative modelling of granular suspension flows: *PHILOSOPHICAL Transactions-Royal Society Of London Series A Mathematical Physical And Engineering Sciences*, p. 2471-2496.
- Hurther, D., and Lemmin, U., 2001, A correction method for turbulence measurements with a 3D acoustic Doppler velocity profiler: *Journal of Atmospheric and Oceanic Technology*, v. 18, no. 3, p. 446-458.
- , 2008, Improved turbulence profiling with field-adapted acoustic Doppler velocimeters using a bifrequency Doppler noise suppression method: *Journal of Atmospheric and Oceanic Technology*, v. 25, no. 3, p. 452-463.
- Hurther, D., and Thorne, P. D., 2011, Suspension and near-bed load sediment transport processes above a migrating, sand-rippled bed under shoaling waves: *Journal of Geophysical Research: Oceans*, v. 116, no. C7.
- Imran, J., Khan, S. M., Pirmez, C., and Parker, G., 2017, Froude scaling limitations in modeling of turbidity currents: *Environmental Fluid Mechanics*, v. 17, no. 1, p. 159-186.
- Jaafar, W., Fischer, S., and Bekkour, K., 2009, Velocity and turbulence measurements by ultrasound pulse Doppler velocimetry: *Measurement*, v. 42, no. 2, p. 175-182.
- Jain, R. K., and Kothiyari, U. C., 2009, Cohesion influences on erosion and bed load transport: *Water resources research*, v. 45, no. 6.
- Janocko, M., Cartigny, M., Nemec, W., and Hansen, E., 2013, Turbidity current hydraulics and sediment deposition in erodible sinuous channels: laboratory experiments and numerical simulations: *Marine and Petroleum Geology*, v. 41, p. 222-249.
- Jiménez, J. A., and Madsen, O. S., 2003, A simple formula to estimate settling velocity of natural sediments: *Journal of waterway, port, coastal, and ocean engineering*, v. 129, no. 2, p. 70-78.
- Jobe, R.Z., Howes, N., Romans B.W. and Covault J.A., 2018, Volume and recurrence of submarine-fan-building turbidity currents. *The depositional Record*.
- Kaitna, R., Dietrich, W.E. and Hsu, L., 2014. Surface slopes, velocity profiles and fluid pressures in coarse grained debris flows saturated with water and mud. *Journal of Fluid Mechanics*, 741, pp. 377-403.
- Khorsandi, B., Mydlarski, L., and Gaskin, S., 2012, Noise in turbulence measurements using acoustic Doppler velocimetry: *Journal of Hydraulic Engineering*, v. 138, no. 10, p. 829-838.
- Khripounoff, A., Vangriesheim, A., Babonneau, N., Crassous, P., Dennielou, B., and Savoye, B., 2003, Direct observation of intense turbidity current activity in the Zaire submarine valley at 4000 m water depth: *Marine Geology*, v. 194, no. 3, p. 151-158.
- Kim, S.-C., Friedrichs, C., Maa, J.-Y., and Wright, L., 2000, Estimating bottom stress in tidal boundary layer from acoustic Doppler velocimeter data: *Journal of Hydraulic Engineering*, v. 126, no. 6, p. 399-406.
- Kleesment, A., 2009, Roundness and surface features of quartz grains in Middle Devonian deposits of the East Baltic and their palaeogeographical implications: *Estonian Journal of Earth Sciences*, v. 58, no. 1.

- Kneller, B., Bennett, S., and McCaffrey, W., 1997, Velocity and turbulence structure of density currents and internal solitary waves: potential sediment transport and the formation of wave ripples in deep water: *Sedimentary Geology*, v. 112, no. 3-4, p. 235-250.
- Kneller, B., and Buckee, C., 2000, The structure and fluid mechanics of turbidity currents: a review of some recent studies and their geological implications: *Sedimentology*, v. 47, no. s1, p. 62-94.
- Kneller, B., Nasr-Azadani, M. M., Radhakrishnan, S., and Meiburg, E., 2016, Long-range sediment transport in the world's oceans by stably stratified turbidity currents: *Journal of Geophysical Research: Oceans*.
- Kneller, B. C., Bennett, S. J., and McCaffrey, W. D., 1999, Velocity structure, turbulence and fluid stresses in experimental gravity currents: *Journal of Geophysical Research: Oceans*, v. 104, no. C3, p. 5381-5391.
- Kneller, B. C., and McCaffrey, W. D., 2003, The interpretation of vertical sequences in turbidite beds: the influence of longitudinal flow structure: *Journal of Sedimentary Research*, v. 73, no. 5, p. 706-713.
- Komar, P. D., 1977, Computer simulation of turbidity current flow and the study of deep-sea channels and fan sedimentation: *The sea*, v. 6, p. 603-621.
- , 1980, Modes of sediment transport in channelized water flows with ramifications to the erosion of the Martian outflow channels: *Icarus*, v. 42, no. 3, p. 317-329.
- , 1985, The hydraulic interpretation of turbidites from their grain sizes and sedimentary structures: *Sedimentology*, v. 32, no. 3, p. 395-407.
- Komar, P. D., and Li, Z., 1986, Pivoting analyses of the selective entrainment of sediments by shape and size with application to gravel threshold: *Sedimentology*, v. 33, no. 3, p. 425-436.
- Konsoer, K., Zinger, J. and Parker, G., 2013. Bankfull hydraulic geometry of submarine channels created by turbidity currents: relations between bankfull channel characteristics and formative flow discharge. *Journal of Geophysical Research: Earth Surface*, 118(1), pp.216-228.
- Kramer, H., Sand mixtures and sand movements in fluvial models, *in Proceedings Proceedings of the American Society of Civil Engineers* 1934, Volume 60, ASCE, p. 443-484.
- Krastel, S., Wynn, R. B., Feldens, P., Schürer, A., Böttner, C., Stevenson, C., Cartigny, M. J., Hühnerbach, V., and Unverricht, D., 2016, Flow behaviour of a giant landslide and debris flow entering Agadir Canyon, NW Africa, *Submarine Mass Movements and their Consequences*, Springer, p. 145-154.
- Krumbein, W. C., and Pettijohn, F. J., 1938, *Manual of sedimentary petrography: I. Sampling, preparation for analysis, mechanical analysis and statistical analysis*, Appleton-Century-Crofts.
- Krumbein, W. C., and Tisdell, F. W., 1940, Size distribution of source rocks of sediments: *American Journal of Science*, v. 238, no. 4, p. 296-305.
- Kuenen, P. H., 1951, Properties of turbidity currents of high density.
- Lajeunesse, E., Malverti, L., and Charru, F., 2010, Bed load transport in turbulent flow at the grain scale: Experiments and modeling: *Journal of Geophysical Research: Earth Surface*, v. 115, no. F4.
- La Porta, A., Voth, G. A., Crawford, A. M., Alexander, J., and Bodenschatz, E. 2001 Fluid particle accelerations in fully developed turbulence, *Nature*, 970, 1017–1019.
- Lamb, M. P., Dietrich, W. E., and Venditti, J. G., 2008, Is the critical Shields stress for incipient sediment motion dependent on channel-bed slope?: *Journal of Geophysical Research: Earth Surface*, v. 113, no. F2.
- Lane, S., Biron, P., Bradbrook, K., Butler, J., Chandler, J., Crowell, M., McLelland, S., Richards, K., and Roy, A., 1998, Three-dimensional measurement of river channel flow processes

- using acoustic Doppler velocimetry: *Earth Surface Processes and Landforms*, v. 23, no. 13, p. 1247-1267.
- LAPIONITE, M., 1992, Burst-like sediment suspension events in a sand bed river. *Earth Surface Processes and Landforms*, 17, 253-270.
- Le Roux, J., 1992, Settling velocity of spheres: a new approach: *Sedimentary Geology*, v. 81, no. 1-2, p. 11-16.
- , 2005, Grains in motion: A review: *Sedimentary Geology*, v. 178, no. 3, p. 285-313.
- Lee, Z. S., and Baas, A. C., 2012, Streamline correction for the analysis of boundary layer turbulence: *Geomorphology*, v. 171, p. 69-82.
- , 2016, Variable and conflicting shear stress estimates inside a boundary layer with sediment transport: *Earth Surface Processes and Landforms*, v. 41, no. 4, p. 435-445.
- Leeder, M., 1983, On the dynamics of sediment suspension by residual Reynolds stresses—confirmation of Bagnold's theory: *Sedimentology*, v. 30, no. 4, p. 485-491.
- Leeder, M. R., 2012, *Sedimentology: process and product*, Springer Science & Business Media.
- Leeder, M. R., Gray, T. E., and Alexander, J., 2005, Sediment suspension dynamics and a new criterion for the maintenance of turbulent suspensions: *Sedimentology*, v. 52, no. 4, p. 683-691.
- Liu, H., and Wu, J.-x., 2015, Estimation of bed shear stresses in the pearl river estuary: *China Ocean Engineering*, v. 29, p. 133-142.
- Liu, J. T., Kao, S.-J., Huh, C.-A., and Hung, C.-C., 2013, Gravity flows associated with flood events and carbon burial: Taiwan as instructional source area: *Annual review of marine science*, v. 5, p. 47-68.
- Liu, Y., Métivier, F., Lajeunesse, É., Lancien, P., Narteau, C., Ye, B., and Meunier, P., 2008, Measuring bedload in gravel-bed mountain rivers: averaging methods and sampling strategies: *Geodinamica Acta*, v. 21, no. 1-2, p. 81-92.
- Lohrmann, A., Cabrera, R., and Kraus, N. C., Acoustic-Doppler velocimeter (ADV) for laboratory use, *in Proceedings Fundamentals and advancements in hydraulic measurements and experimentation 1994*, ASCE, p. 351-365.
- Lopez, M., 2001, Architecture and depositional pattern of the Quaternary deep-sea fan of the Amazon: *Marine and Petroleum Geology*, v. 18, no. 4, p. 479-486.
- Luchi, R., Balanchandar, S., Seminara, G. and Parker, G., 2018, Turbidity currents with equilibrium basal driving layers: A mechanism for long run-out. *Geophysical Research Letters*, 45(3), PP. 1518-1526.
- Manica, R., 2012. Sediment gravity flows: study based on experimental simulations. In *Hydrodynamics-Natural Water Bodies*. InTech.
- Manning, A., Baugh, J., Soulsby, R., Spearman, J., and Whitehouse, R., 2011, Cohesive sediment flocculation and the application to settling flux modelling, *Sediment Transport*, InTech.
- Mantovanelli, A., and Ridd, P. V., 2006, Devices to measure settling velocities of cohesive sediment aggregates: A review of the in situ technology: *Journal of Sea Research*, v. 56, no. 3, p. 199-226.
- Mantz, P. A., 1977, Incipient transport of fine grains and flakes by fluids-extended shield diagram: *Journal of the Hydraulics division*, v. 103, no. ASCE 12992.
- Massey, B. S. (1989). *Mechanics of fluids*. London: Chapman&Hall, p. 599
- Mazumder, B., Ghoshal, K., and Dalal, D., 2005, Influence of bed roughness on sediment suspension: experimental and theoretical studies: *Journal of Hydraulic Research*, v. 43, no. 3, p. 245-257.
- McCave, I., Hall, I. R., and Bianchi, G. G., 2006, Laser vs. settling velocity differences in silt grain size measurements: estimation of palaeocurrent vigour: *Sedimentology*, v. 53, no. 4, p. 919-928.
- McCave, I., and Syvitski, J. P., 1991, *Principles and methods of geological particle size analysis: Principles, methods and application of particle size analysis*, p. 3-21.

- McComb, W. D., 1990, The physics of fluid turbulence: Chemical Physics.
- McCool, W. W., and Parsons, J. D., 2004, Sedimentation from buoyant fine-grained suspensions: *Continental Shelf Research*, v. 24, no. 10, p. 1129-1142.
- McLelland, S. J., and Nicholas, A. P., 2000, A new method for evaluating errors in high-frequency ADV measurements: *Hydrological Processes*, v. 14, no. 2, p. 351-366.
- Meiburg, E., and Kneller, B., 2010, Turbidity currents and their deposits: *Annual Review of Fluid Mechanics*, v. 42, p. 135-156.
- Meiburg, E., Radhakrishnan, S., and Nasr-Azadani, M., 2015, Modeling gravity and turbidity currents: computational approaches and challenges: *Applied Mechanics Reviews*, v. 67, no. 4, p. 040802.
- Métivier, F., Meunier, P., Moreira, M., Crave, A., Chaduteau, C., Ye, B., and Liu, G., Transport dynamics and morphology of a high mountain stream during the peak flow season: The Ürümqi River (Chinese Tian Shan), *in Proceedings River Flow2004*, Volume 1, p. 761-777.
- Meunier, P., Métivier, F., Lajeunesse, E., Meriaux, A., and Faure, J., 2006, Flow pattern and sediment transport in a braided river: The "torrent de St Pierre" (French Alps): *Journal of Hydrology*, v. 330, no. 3, p. 496-505.
- Miall, A., 2013, *Principles of sedimentary basin analysis*, Springer Science & Business Media.
- Middleton, G. V., and Southard, J. B., 1984, *Mechanics of sediment movement*, SEPM.
- Migeon, S., Mulder, T., Savoye, B., and Sage, F., 2012, Hydrodynamic processes, velocity structure and stratification in natural turbidity currents: results inferred from field data in the Var Turbidite System: *Sedimentary Geology*, v. 245, p. 48-62.
- Miller, M., McCave, I., and Komar, P. D., 1977, Threshold of sediment motion under unidirectional currents: *Sedimentology*, v. 24, no. 4, p. 507-527.
- Milliman, J. D., and Syvitski, J. P., 1992, Geomorphic/tectonic control of sediment discharge to the ocean: the importance of small mountainous rivers: *The Journal of Geology*, v. 100, no. 5, p. 525-544.
- Mulder, T., and Alexander, J., 2001, The physical character of subaqueous sedimentary density flows and their deposits: *Sedimentology*, v. 48, no. 2, p. 269-299.
- Mulder, T., Ducassou, E., Eberli, G., Hanquiez, V., Gonthier, E., Kindler, P., Principaud, M., Fournier, F., Léonide, P., and Billeaud, I., 2012, New insights into the morphology and sedimentary processes along the western slope of Great Bahama Bank: *Geology*, v. 40, no. 7, p. 603-606.
- Mulder, T., Savoye, B., and Syvitski, J., 1997, Numerical modelling of a mid-sized gravity flow: the 1979 Nice turbidity current (dynamics, processes, sediment budget and seafloor impact): *Sedimentology*, v. 44, no. 2, p. 305-326.
- Muste, M., Hauet, A., Fujita, I., Legout, C., and Ho, H.-C., 2014, Capabilities of Large-scale Particle Image Velocimetry to characterize shallow free-surface flows: *Advances in Water Resources*, v. 70, p. 160-171.
- Muste, M., Kim, D., and Merwade, V., 2012, Modern digital instruments and techniques for hydrodynamic and morphologic characterization of river channels: *Gravel-Bed Rivers: Processes, Tools, Environments*, p. 315-341.
- Neill, C., 1967, Mean-velocity criterion for scour of coarse uniform bed-material.
- Nelson, J. M., McLean, S. R., and Wolfe, S. R., 1993, Mean flow and turbulence fields over two-dimensional bed forms: *Water Resources Research*, v. 29, no. 12, p. 3935-3953.
- Nelson, J. M., Shreve, R. L., McLean, S. R., and Drake, T. G., 1995, Role of near-bed turbulence structure in bed load transport and bed form mechanics: *Water Resources Research*, v. 31, no. 8, p. 2071-2086.
- Nezu, I. a. N. H., 1993, *Turbulence in open-channel flows*.
- Nichols, G., 2009, *Sedimentology and stratigraphy*, John Wiley & Sons.
- Nielsen, P., 1981, Dynamics and geometry of wave-generated ripples: *Journal of Geophysical Research: Oceans*, v. 86, no. C7, p. 6467-6472.

- , 1992, Coastal bottom boundary layers and sediment transport, World Scientific Publishing Co Inc.
- Nikora, V., and Goring, D., 2000, Flow turbulence over fixed and weakly mobile gravel beds: *Journal of Hydraulic Engineering*, v. 126, no. 9, p. 679-690.
- Normark, W. R., Posamentier, H., and Mutti, E., 1993, Turbidite systems: state of the art and future directions: *Reviews of Geophysics*, v. 31, no. 2, p. 91-116.
- Nortek, A., 2004, VECTRINO velocimeter user guide (Rev. C), Norway.
- Noss, C., Salzmann, T., and Storchenegger, I., 2010, Turbulent and advective momentum fluxes in streams: *Water Resources Research*, v. 46, no. 12.
- O'Brien, M. P. 1933 Review of the theory of turbulent flow and its relation to sediment-transportation. *Eos, Transactions American Geophysical Union* 14(1), pp. 487-491.
- Ortiz, J. D., and Klompaker, A. A., 2015, Turbidity Currents: Comparing Theory and Observation in the Lab: *Oceanography*, v. 28, no. 3, p. 220-227.
- Owens, P., Batalla, R., Collins, A., Gomez, B., Hicks, D., Horowitz, A., Kondolf, G., Marden, M., Page, M., and Peacock, D., 2005, Fine-grained sediment in river systems: environmental significance and management issues: *River research and applications*, v. 21, no. 7, p. 693-717.
- Pantin, H., 1979, Interaction between velocity and effective density in turbidity flow: phase-plane analysis, with criteria for autosuspension: *Marine Geology*, v. 31, no. 1-2, p. 59-99.
- Papanicolaou, A. N., Knapp, D., and Strom, K., Bedload predictions by using the concept of particle velocity: Applications, *in Proceedings Hydraulic Measurements and Experimental Methods 2002*, p. 1-10.
- Paphitis, D., 2001, Sediment movement under unidirectional flows: an assessment of empirical threshold curves: *Coastal Engineering*, v. 43, no. 3, p. 227-245.
- Parker, G., 1990, Surface-based bedload transport relation for gravel rivers: *Journal of hydraulic research*, v. 28, no. 4, p. 417-436.
- , 2008, Transport of gravel and sediment mixtures: *Sedimentation Engineering: Processes, Measurements, Modeling, and Practice*, v. 110, p. 165-252.
- Parker, G., Fukushima, Y., and Pantin, H. M., 1986, Self-accelerating turbidity currents: *Journal of Fluid Mechanics*, v. 171, p. 145-181.
- Partheniades, E., 2009, *Cohesive Sediments in Open Channels: Erosion, Transport and Deposition*, Butterworth-Heinemann.
- Patil, V. A., and Liburdy, J. A., 2013, Turbulent flow characteristics in a randomly packed porous bed based on particle image velocimetry measurements: *Physics of Fluids*, v. 25, no. 4, p. 043304.
- Peters, E. J., 2012, *Advanced Petrophysics: Volume 1: Geology, Porosity, Absolute Permeability, Heterogeneity and Geostatistics*: Live Oak Book Co, Austin, Texas.
- Pettijohn, F., 1975, *Sedimentary Rocks*. Harper and Row Publishers: New York.
- Pickering, K., and Hiscott, R., 2015, *Deep Marine Systems: Processes, Deposits, Environments, Tectonic and Sedimentation*, John Wiley & Sons.
- Piper, D. J., Cochonat, P., and Morrison, M. L., 1999, The sequence of events around the epicentre of the 1929 Grand Banks earthquake: initiation of debris flows and turbidity current inferred from sidescan sonar: *Sedimentology*, v. 46, no. 1, p. 79-97.
- Pirmez, C., 1994, Growth of a submarine meandering channel-levee system on the Amazon Fan: Columbia University New York, USA.
- Poggi, D., Porporato, A., and Ridolfi, L., 2003, Analysis of the small-scale structure of turbulence on smooth and rough walls: *Physics of Fluids*, v. 15, no. 1, p. 35-46.
- Polakowski, C., Sochan, A., Bieganski, A., Ryzak, M., Földényi, R., and Tóth, J., 2014, Influence of the sand particle shape on particle size distribution measured by laser diffraction method: *International Agrophysics*, v. 28, no. 2, p. 195-200.

- Pope, N., Widdows, J., and Brinsley, M., 2006, Estimation of bed shear stress using the turbulent kinetic energy approach—a comparison of annular flume and field data: *Continental Shelf Research*, v. 26, no. 8, p. 959-970.
- Pope, S. B., 2001, *Turbulent flows*, IOP Publishing.
- Prandtl, L., 1904, On fluid motions with very small friction: *Verhldg*, v. 3, p. 484-491.
- Prandtl L., 1925 Bericht uber untersuchungen zur ausgebildeten turbulenz. *Zeitschrift fur Angewandte Mathematik und Mechanik* 5 (2): 136-139
- Pye, K., 1994, *Sediment transport and depositional processes*, v. 551.3. 051 SED.
- Raudkivi, A. J., 1998, *Loose boundary hydraulics*, CRC Press.
- Recking, A., 2009, Theoretical development on the effects of changing flow hydraulics on incipient bed load motion: *Water Resources Research*, v. 45, no. 4.
- Reynolds, O., 1895 On the dynamical theory of incompressible viscous fluids and the determination of the criterion. *Philosophical Transactions of the Royal Society of London. A* 186, pp 123-164.
- Ribberink, J., 2011, *River Dynamics II: Transport Processes and Morphology*.
- Righetti, M., and Lucarelli, C., 2007, May the Shields theory be extended to cohesive and adhesive benthic sediments?: *Journal of Geophysical Research: Oceans*, v. 112, no. C5.
- Ristić, S. S., Ilić, J. T., Čantrak, Đ. S., Ristić, O. R., and Janković, N. Z., 2012, Estimation of laser-Doppler anemometry measuring volume displacement in cylindrical pipe flow: *Thermal Science*, v. 16, no. 4, p. 1027-1042.
- Rottman, J. W., and Simpson, J. E., 1983, Gravity currents produced by instantaneous releases of a heavy fluid in a rectangular channel: *Journal of Fluid Mechanics*, v. 135, p. 95-110.
- Rouse, H., 1937, Modern conceptions of the mechanics of fluid turbulence: *Transactions of the American Society of Civil Engineers*, v. 102, no. 1, p. 463-505.
- Rowiński, P., Aberle, J., and Mazurczyk, A., 2005, Shear velocity estimation in hydraulic research: *Acta Geophysica Polonica*, v. 53, no. 4, p. 567-583.
- Rusello, P., and Allard, M., Near boundary measurements with a profiling acoustic Doppler velocimeter, *in Proceedings Hydraulic Measurement and Experimental Methods Conference 2012*.
- Salarashayeri, A., and Siosemarde, M., 2012, Prediction of soil hydraulic conductivity from particle-size distribution: *World Acad. Sci. Eng. Technol*, v. 61, no. 61, p. 454-458.
- Sanders, J. E., 1960, Primary sedimentary structures formed by turbidity currents and related resedimentation mechanisms.
- Schmeeckle, M. W., 2014, Numerical simulation of turbulence and sediment transport of medium sand: *Journal of Geophysical Research: Earth Surface*, v. 119, no. 6, p. 1240-1262.
- Schmeeckle, M. W., Nelson, J. M., and Shreve, R. L., 2007, Forces on stationary particles in near-bed turbulent flows: *Journal of Geophysical Research: Earth Surface*, v. 112, no. F2.
- Selley, R. C., 2000, *Applied sedimentology*, Elsevier.
- Sherwood, C. R., Lacy, J. R., and Voulgaris, G., 2006, Shear velocity estimates on the inner shelf off Grays Harbor, Washington, USA: *Continental Shelf Research*, v. 26, no. 17, p. 1995-2018.
- Shields, A., 1936, *Anwendung der Aehnlichkeitsmechanik und der Turbulenzforschung auf die Geschiebebewegung*: PhD Thesis Technical University Berlin.
- Shivpure, V., Sharm, A., and Kumar, B., 2016, Comparison of bed shear stress in plane and curvilinear bed channel using multiple criteria: *Water resources*, v. 43, no. 1, p. 79-85.
- Shugar, D.H., Kostaschuk, R., Best, J.L, Parsons, D.R, Lane, S.N, Orefo, o AND Hardy, R.J, 2010. On the relationship between flow and suspended sediment transport over the crest of a sand dune, Rio Parana, Argentina. *Sedimentology*, 57(1), pp. 252-272.

- Shvidchenko, A. B., and Pender, G., 2000, Flume study of the effect of relative depth on the incipient motion of coarse uniform sediments: *Water Resources Research*, v. 36, no. 2, p. 619-628.
- Shvidchenko, A. B., Pender, G., and Hoey, T. B., 2001, Critical shear stress for incipient motion of sand/gravel streambeds: *Water Resources Research*, v. 37, no. 8, p. 2273-2283.
- Sime, L. C., Ferguson, R. I., and Church, M., 2007, Estimating shear stress from moving boat acoustic Doppler velocity measurements in a large gravel bed river: *Water Resources Research*, v. 43, no. 3.
- Simpson, J., 1999, *Gravity currents in Environment and Laboratory*. Cambridge University Press.
- Singer, J., Anderson, J., Ledbetter, M., McCave, I., Jones, K., and Wright, R., 1988, An assessment of analytical techniques for the size analysis of fine-grained sediments: *Journal of Sedimentary Research*, v. 58, no. 3.
- Smith, D. A., and Cheung, K. F., 2004, Initiation of motion of calcareous sand: *Journal of Hydraulic Engineering*, v. 130, no. 5, p. 467-472.
- Southard, J. B., and Mackintosh, M. E., 1981, Experimental test of autosuspension: *Earth Surface Processes and Landforms*, v. 6, no. 2, p. 103-111.
- Sperry, J. M., and Peirce, J. J., 1995, A model for estimating the hydraulic conductivity of granular material based on grain shape, grain size, and porosity: *Groundwater*, v. 33, no. 6, p. 892-898.
- Statham, I., 1977, *Earth surface sediment transport*, Clarendon Press.
- Stevenson, C. J., Talling, P. J., Sumner, E. J., Masson, D. G., Frenz, M., and Wynn, R. B., 2014, On how thin submarine flows transported large volumes of sand for hundreds of kilometres across a flat basin plain without eroding the sea floor: *Sedimentology*, v. 61, no. 7, p. 1982-2019.
- Stevenson, C.J., Jackson, C.A L., Hodgson, D.M., Hubbard, S.M., and Eggenhuisen, J.T., 2015 Deep-Water sediment bypass. *Journal of Sedimentary RESEARCH*, 85(9), pp. 1058-1081
- Soulsby R. L., 1983 The bottom boundary layer of shelf seas, In Elsevier oceanography series (vol 35. pp. 189-266)
- Stevenson, C.J., Feldens, P., Georgiopoulou, A., Schonke, M., Krastel, S., Piper, D.J., Lindhorst, K and Mosher, D., 2018, Reconstructing the sediment concentration of a giant submarine gravity flow. *Nature communications*, 9(1), p2616
- Soulsby, R.L and Damgaard, J.S 2005 Bedload sediment transport in coastal waters. *Coastal Engineering*, 52(8), pp 673-689
- Stokes, G. G., 1851, *On the effect of the internal friction of fluids on the motion of pendulums*, Pitt Press.
- Subhasish, D., 2016 *Fluvial Hydrodynamics: Hydrodynamics and Sediment Transport Phenomena*. Springer, Berlin, 2014 687 pages.
- Sun, D., Bloemendal, J., Rea, D., Vandenberghe, J., Jiang, F., An, Z., and Su, R., 2002, Grain-size distribution function of polymodal sediments in hydraulic and aeolian environments, and numerical partitioning of the sedimentary components: *Sedimentary Geology*, v. 152, no. 3, p. 263-277.
- Sutherland, A. J., 1967, Proposed mechanism for sediment entrainment by turbulent flows: *Journal of Geophysical Research*, v. 72, no. 24, p. 6183-6194.
- Sukhodolov, A., Thiele, M. and Bungatz, H., 1998. Turbulence structure in a river reach with sandbed. *Water Resources Research*, 34(5), pp.1317-1334.
- Symons, W. O., Sumner, E. J., Paull, C. K., Cartigny, M. J., Xu, J., Maier, K. L., Lorenson, T. D., and Talling, P. J., 2017, A new model for turbidity current behavior based on integration of flow monitoring and precision coring in a submarine canyon: *Geology*, v. 45, no. 4, p. 367-370.

- Syvitski, J., LeBlanc, K., and Asprey, K., 1991, Interlaboratory, interinstrument calibration experiment: Principles, Methods, and Application of Particle Size Analysis. JPM Syvitski (ed.). Cambridge University Press, New York, NY, p. 174-193.
- Syvitski, J. P., 2007, Principles, methods and application of particle size analysis, Cambridge University Press.
- Syvitski, J.P 2003. Supply and flux of sediment along hydrological pathways: research for the 21st Century. *Global and Planetary Change* 39(1-2), pp. 1-11
- Takeda, Y., 2012, Ultrasonic Doppler velocity profiler for fluid flow, Springer Science & Business Media.
- Talling, P. J., Allin, J., Armitage, D. A., Arnott, R. W., Cartigny, M. J., Clare, M. A., Felletti, F., Covault, J. A., Girardclos, S., and Hansen, E., 2015, Key future directions for research on turbidity currents and their deposits: *Journal of Sedimentary Research*, v. 85, no. 2, p. 153-169.
- Talling, P. J., Amy, L. A., and Wynn, R. B., 2007, New insight into the evolution of large-volume turbidity currents: comparison of turbidite shape and previous modelling results: *Sedimentology*, v. 54, no. 4, p. 737-769.
- Talling, P. J., Masson, D. G., Sumner, E. J., and Malgesini, G., 2012, Subaqueous sediment density flows: depositional processes and deposit types: *Sedimentology*, v. 59, no. 7, p. 1937-2003.
- Talling, P.J., Wynn, R.B., Masson, D.G., Frenz, M., Cronin, B.T., Schiebel, R., Akhmetzhanov, A.M., Dallmeier-Tiessen, S., Benetti, S., Weaver, P.P.E., Georgiopoulou, A., Zuñ Hlsdorff, C., And Amy, L.A., 2007, Onset of submarine debris flow deposition far from original giant landslide: *Nature*, v. 450, p. 541–544.
- Talling, P.J., 2013, Hybrid submarine flows comprising turbidity current and cohesive debris flow: deposits, theoretical and experimental analyses, and generalised models: *Geosphere*, v. 9, p. 460–488
- Talling, P.J., 2014, On the triggers, resulting flow types and frequency of subaqueous sediment density flows in different settings: *Marine Geology*, v. 352, p. 155–182
- Tennekes, H., and Lumley, J. L., 1972, *A first course in turbulence*, MIT press.
- Thomas, R. E., and McLelland, S. J., 2015, The impact of macroalgae on mean and turbulent flow fields: *Journal of Hydrodynamics, Ser. B*, v. 27, no. 3, p. 427-435.
- Tomkins, M. R., Baldock, T. E., and Nielsen, P., 2005, Hindered settling of sand grains: *Sedimentology*, v. 52, no. 6, p. 1425-1432.
- Tritton, D. J., 1988 A review of IUTAM Symposium on Fluid Mechanics in the Spirit. 315-317
- Tscharnuter, W., 2000, Photon correlation spectroscopy in particle sizing: *Encyclopedia of analytical chemistry*.
- Tucker, M. E., 2009, *Sedimentary petrology: an introduction to the origin of sedimentary rocks*, John Wiley & Sons.
- Underwood, M. B., and Norville, C. R., 1986, Deposition of sand in a trench-slope basin by unconfined turbidity currents: *Marine geology*, v. 71, no. 3-4, p. 383-392.
- Ungarish, M., 2009, *An introduction to gravity currents and intrusions*, CRC Press.
- Urlaub, M., Talling, P.J., And Masson, D.G., 2013, Timing and frequency of large submarine landslides: implications for understanding triggers and future geohazard: *Quaternary Science Reviews*, v. 72, p. 63–82.
- Van, L. A., and Van Bang, D. P., 2013, Hindered settling of sand–mud flocs mixtures: From model formulation to numerical validation: *Advances in Water Resources*, v. 53, p. 1-11.
- Van, Maren, D.S., Winterwerp, J.C., Wu, B.S and Zhou, J.J 2009. Modelling hyperconcentrated flow in the yellow River. *Earth Surface Processes and Landforms*, 34(4). pp. 596-612.
- Van Rijn, L. C., 1993, *Principles of sediment transport in rivers, estuaries and coastal seas*, Aqua publications Amsterdam.

- Van Rijn L. C., 2007 Unified view of Sediment Transport by Currents and Waves. I: Initiation of Motion, Bed Roughness and Bed-Load Transport. *Journal of Hydraulic Engineering*, 133(6), 649-667.
- Vanoni, V. A., 1964, Measurements of critical shear stress for entraining fine sediments in a boundary layer.
- Vanoni, V. A., 1975, River dynamics: *Advances in applied mechanics*, v. 15, p. 1-87.
- Vanoni, V. A., and Nomicos, G. N., 1960, Resistance properties of sediment-laden streams: *Transactions of the American Society of Civil Engineers*, v. 125, no. 1, p. 1140-1167.
- Voulgaris, G., and Trowbridge, J. H., 1998, Evaluation of the acoustic Doppler velocimeter (ADV) for turbulence measurements: *Journal of Atmospheric and Oceanic Technology*, v. 15, no. 1, p. 272-289.
- Waltham, D., Jeffrey, N., MacLean, S, and Zampetti, V., 2008a Stratigraphic Modelling of turbidite prospects to reduce exploration risk. *Petroleum Geoscience*, 14(3), pp. 273-280.
- Waltham, D., 2008b, Slope control on submarine channel widths. *Journal of Sedimentary Research*, 78(5), pp. 317-322.
- Waltham, D., Pickering, K., and Bray, V. 2008c, Particulate Gravity Currents on Venus. *Journal of Geophysical Research: Planets*, 113(E2).
- Wang, Z., and Larsen, P., 1994, Turbulent structure of water and clay suspensions with bed load: *Journal of Hydraulic Engineering*, v. 120, no. 5, p. 577-600.
- Wang and Andutta, F.P., 2013. Sediment transport dynamics in ports, estuaries and other coastal environments. In *Sediment Transport Processes and their Modelling Applications*. In Tech
- Warrick, J. A., Rubin, D. M., Ruggiero, P., Harney, J. N., Draut, A. E., and Buscombe, D., 2009, Cobble Cam: Grain-size measurements of sand to boulder from digital photographs and autocorrelation analyses: *Earth Surface Processes and Landforms*, v. 34, no. 13, p. 1811-1821.
- Weaver, P., Rothwell, R., Ebbing, J., Gunn, D., and Hunter, P., 1992, Correlation, frequency of emplacement and source directions of megaturbidites on the Madeira Abyssal Plain: *Marine Geology*, v. 109, no. 1-2, p. 1-20.
- Wei, T., and Willmarth, W., 1991, Examination of v-velocity fluctuations in a turbulent channel flow in the context of sediment transport: *Journal of Fluid Mechanics*, v. 223, p. 241-252.
- Wentworth, C. K., 1922, A scale of grade and class terms for clastic sediments: *The Journal of Geology*, v. 30, no. 5, p. 377-392.
- Wheatcroft, R. A., 1994, Temporal variation in bed configuration and one-dimensional bottom roughness at the mid-shelf STRESS site: *Continental Shelf Research*, v. 14, no. 10-11, p. 1167-1190.
- Wiberg, P. L., and Smith, J. D., 1987, Calculations of the critical shear stress for motion of uniform and heterogeneous sediments: *Water resources research*, v. 23, no. 8, p. 1471-1480.
- Wilcock, P. R., 1996, Estimating local bed shear stress from velocity observations: *Water Resources Research*, v. 32, no. 11, p. 3361-3366.
- Wilcock, P. R., 2001, Toward a practical method for estimating sediment-transport rates in gravel-bed rivers: *Earth Surface Processes and Landforms*, v. 26, no. 13, p. 1395-1408.
- Wilcock, P. R., and Crowe, J. C., 2003, Surface-based transport model for mixed-size sediment: *Journal of Hydraulic Engineering*, v. 129, no. 2, p. 120-128.
- Wilcock, P. R., and Kenworthy, S. T., 2002, A two-fraction model for the transport of sand/gravel mixtures: *Water Resources Research*, v. 38, no. 10.
- Williams, G. P., 1970, Flume width and water depth effects in sediment-transport experiments, *Citeseer*.

- Wilson, A. M., Huettel, M., and Klein, S., 2008, Grain size and depositional environment as predictors of permeability in coastal marine sands: *Estuarine, Coastal and Shelf Science*, v. 80, no. 1, p. 193-199.
- Winterwerp, J., 2002, On the flocculation and settling velocity of estuarine mud: *Continental shelf research*, v. 22, no. 9, p. 1339-1360.
- Winterwerp, J. C., and Van Kesteren, W. G., 2004, *Introduction to the physics of cohesive sediment dynamics in the marine environment*, Elsevier.
- Wright, S., and Parker, G., 2004a, Density stratification effects in sand-bed rivers: *Journal of Hydraulic Engineering*, v. 130, no. 8, p. 783-795.
- , 2004b, Flow resistance and suspended load in sand-bed rivers: simplified stratification model: *Journal of Hydraulic Engineering*, v. 130, no. 8, p. 796-805.
- Wynn, R. B., and Cronin, B., 2005, RRS" Charles Darwin" Cruise CD166, 29 Oct-22 Nov 2004. Sedimentary processes and deposits in the Agadir Basin and Gulf of Cadiz.
- Wynn, R. B., Weaver, P. P., Masson, D. G., and Stow, D. A., 2002, Turbidite depositional architecture across three interconnected deep-water basins on the north-west African margin: *Sedimentology*, v. 49, no. 4, p. 669-695.
- Xie, H.H 1981. *River Sediment Engineering*. Vol1. Water Resources Press, Beijing.
- Xu, J., 2010, Normalized velocity profiles of field-measured turbidity currents: *Geology*, v. 38, no. 6, p. 563-566.
- Xu, J., Noble, M., and Rosenfeld, L. K., 2004, In-situ measurements of velocity structure within turbidity currents: *Geophysical Research Letters*, v. 31, no. 9.
- Xu, J., Wright, L., and Boon, J., 1994, Estimation of bottom stress and roughness in Lower Chesapeake Bay by the inertial dissipation method: *Journal of Coastal Research*, p. 329-338.
- Yang, S. Q., and Chow, A. T., 2008, Turbulence structures in non-uniform flows. *Advances in Water resources*, 31(10), pp. 1344-1351
- Yalin, M. S., 1977, On the determination of ripple length: *Journal of the Hydraulics Division*, v. 103, no. 4, p. 439-442.
- Yalin, M. S., and Karahan, E., 1979, Inception of sediment transport: *Journal of the hydraulics division*, v. 105, no. 11, p. 1433-1443.
- Yin, D., Peakall, J., Parsons, D., Chen, Z., Averill, H. M., Wignall, P., and Best, J., 2016, Bedform genesis in bedrock substrates: Insights into formative processes from a new experimental approach and the importance of suspension-dominated abrasion: *Geomorphology*, v. 255, p. 26-38.
- You, Z.-J., and Nielsen, P., 1997, Movable bed roughness in the flow of irregular waves and currents over movable beds, *Coastal Engineering* 1996, p. 3495-3506.
- Zanke, U., 2003, On the influence of turbulence on the initiation of sediment motion: *International Journal of Sediment Research*, v. 18, no. 1, p. 17-31.
- Zhang, X.-F., Yang, W.-T., and Xia, J.-Q., 2016, Bed shear stress in non-uniform flow: *Environmental Fluid Mechanics*, v. 16, no. 4, p. 777-792.
- Zhiyao, S., Tingting, W., Fumin, X., and Ruijie, L., 2008, A simple formula for predicting settling velocity of sediment particles: *Water Science and Engineering*, v. 1, no. 1, p. 37-43.